



HAL
open science

Diagnosics and Prognostics of Uncertain Dynamical Systems in a Bond Graph Framework

Mayank Shekhar Jha

► **To cite this version:**

Mayank Shekhar Jha. Diagnosics and Prognostics of Uncertain Dynamical Systems in a Bond Graph Framework. Automatic. Ecole Centrale de Lille, 2015. English. NNT : 2015ECLI0027 . tel-01437139

HAL Id: tel-01437139

<https://theses.hal.science/tel-01437139>

Submitted on 17 Jan 2017

HAL is a multi-disciplinary open access archive for the deposit and dissemination of scientific research documents, whether they are published or not. The documents may come from teaching and research institutions in France or abroad, or from public or private research centers.

L'archive ouverte pluridisciplinaire **HAL**, est destinée au dépôt et à la diffusion de documents scientifiques de niveau recherche, publiés ou non, émanant des établissements d'enseignement et de recherche français ou étrangers, des laboratoires publics ou privés.

ECOLE CENTRALE DE LILLE

THESE

Présentée en vue
d'obtenir le grade de

DOCTEUR

En

Automatique, Génie Informatique, Traitement du Signal et des Images

Par

Mayank Shekhar JHA

DOCTORAT DELIVRE PAR L'ECOLE CENTRALE DE LILLE

Titre de la thèse :

Diagnostic et Pronostic de Systèmes Dynamiques Incertains dans un contexte Bond Graph

Diagnostics and Prognostics of Uncertain Dynamical Systems in a Bond Graph Framework

Soutenue le 8 Décembre 2015 devant le jury d'examen :

Président	M. Nouredine ZERHOUNI	Professeur, FEMTO-ST, Besançon, France
Rapporteur	M. Rafael GOURIVEAU	Maître de Conférences HDR, FEMTO-ST, France
Rapporteur	M. Wolfgang BORUTZKY	Professeur, University of Applied Sciences, Allemagne
Membre	M. Joseph Anand VAZ	Professeur, National Institute of Technology Jalandhar, Inde
Directeur de thèse	Mme. Geneviève DAUPHIN-TANGUY	Professeur, Ecole Centrale de Lille, France
Co-Directeur de thèse	M. Belkacem OULD-BOUAMAMA	Professeur, Polytech de Lille, France

Thèse préparée dans le **Centre de Recherche en Informatique, Signal et Automatique de Lille**
CRISTAL CNRS UMR 9189
Ecole Doctorale SPI 072
PRES Université Lille Nord-de-France

DEDICATION

To the Love and Support of My Dearest Papa and Mummy,

To the Grace of SWAMI,

To the Inspirations of My Dearest Grandfather,

For Love.

EPIGRAPH

This is not the end. It is not even the beginning of the end.

But it is, perhaps, the end of the beginning.

-Winston Churchill

It is through Love, with Love, and in the depths of Love that all answers are found.

-Mayank Shekhar JHA

ACKNOWLEDGEMENTS

In the completion of this dissertation, I would like to express my most sincere regards and heartfelt gratitude to my supervisor and my mentor **Mme. Prof. Geneviève Dauphin-Tanguy**, for her constant encouragement and guidance throughout the period of my stay & research here. Her motivations and insightful guidance are the main factors for the successful completion of this work. I am enormously thankful to her for boosting in me a strong enthusiasm and confidence for the research. I am grateful to her for spending endless time in discussions which made a huge impact on my approach towards the research objective. I will always cherish those immensely enlightening and brain-wrenching discussions in her office room. Her guidance have not only improved my scientific acumen, but also guided me in many important matters of life. Her confidence in me has been the greatest motivation throughout. Most importantly, I am grateful to her for inspiring me to achieve the things I could never think of, giving me the confidence to jump into the unknown. Big Thank you!

I am immensely grateful to my co-supervisor **Prof. Belkacem Ould-Bouamama** who always motivated me to obtain the best results. He has always been there whenever I needed his presence and made sure that I have right the guidance throughout. He also supported me strongly in acquiring the various required scientific skills, for the successful accomplishment of research objective.

I am also very grateful, and will remain indebted to **Prof. Joseph Anand Vaz**, who believed in me and kept his faith in the sincerity of my efforts towards the achievement of academic goals/pursuits.

I am grateful to **Prof. Wolfgang Borutzky** and **Prof. Rafael Gouriveau** for reviewing this thesis. Their suggestions and recommendations have been very helpful in improving the structure of this thesis.

My parents (**Prof. Manoj Kumar Jha & Dr. Mridula Mishra**) have been my greatest support all this while. Their love and care for me, knows no bounds. I am immensely grateful to them for everything, especially for compromising on their own priorities, so that I could complete my research on time. My Grandfather **Prof. Ramesh Jha**, has inspired me deeply for scientific pursuits, right from the childhood. I am immensely thankful to him for motivating me in the right and a noble direction.

Right from the first day in Lille, there have been many people who have blessed me with their time, support, help and guidance. I thank them all, few of them being: **Mme. Bukowski, Brigitte Menu, Christine Yvoz, Prof. Christophe Sueur, Prof. Rochdi Merzouki, M. Daniel Riviere** and **Prof. Jean-Yves Dauphin**.

This journey wouldn't have been the same or even possible, without the help, support and company of my dear friends. I would like to thank them all. In particular, I am thankful to: **Anna** for her love, care, support and motivation throughout this period; **Mohit**, for being an amazing friend and keeping the company with me in everything, helping me out tirelessly in conducting experiments; **Noe**, for always bearing with me patiently and helping me in experiments and many academic related matters; **Mathieu**, for being very helpful and optimistic about our work; **Pushpendra, Singla, Raghav, Debarun, Ajay, Samadhan**: for their amazing company and willingness to cook food whenever I went lazy (and starved!); **Koyal & François, Gerardo, Mohamed Kebdani, Antoine, Damien**: for the amazing times and celebrations!

Lastly, but truly, I am grateful to the Almighty for writing this story beautifully, so far.

Villeneuve d'Ascq, France

13.11.2015

Mayank Shekhar JHA

RESUME

Cette thèse a été préparée au sein de l'équipe de recherche « Méthodes et Outils pour la Conception Intégrée de Systèmes (MOCIS) » au Centre de Recherche en Informatique, Signal et Automatique de Lille (CRISTAL).

La thèse se concentre sur le développement d'approches pour le diagnostic et le pronostic des systèmes dynamiques incertains en utilisant la technique de modélisation Bond Graph (BG). La technique de modélisation BG implique une approche systématique vers une représentation graphique efficace, l'utilisation de la causalité et l'étude des propriétés structurelles et analytiques du modèle. Le travail réalisé ici étend et développe les avantages de l'approche BG pour le diagnostic et le pronostic de systèmes incertains multi-énergétiques.

L'équipe MOCIS a une grande expérience et une bonne expertise dans le domaine de la conception intégrée des systèmes multi-énergétiques, en utilisant la technique de modélisation BG. Dans ce contexte, la dernière décennie a vu des efforts importants déployés pour le développement des techniques de contrôle pour les systèmes industriels en utilisant l'approche BG. Il y a dans la littérature de nombreux travaux liés à la détection et l'isolation des défauts de systèmes complexes et incertains. En particulier, dans le contexte du diagnostic robuste de systèmes incertains, la construction d'un modèle BG-LFT (Linear Fractional Transformation) a été largement exploitée pour les systèmes incertains. Cependant peu de travaux portent sur l'étude et le développement de la méthode de génération de seuils de détection. L'un des objectifs de ce travail vise à intégrer les techniques basées sur les règles de l'arithmétique d'intervalle avec le modèle BG-LFT pour un diagnostic robuste aux incertitudes de modèle et efficace.

Tout d'abord, dans le Chapitre 2, une représentation par intervalles des incertitudes paramétriques et de mesures est intégrée à un modèle BG-LFT. Cela conduit à une dérivation systématique des Relations de Redondance Analytique exprimées en termes d'intervalles (I-ARRS) à partir du modèle BG incertain. Une méthode de détection robuste de défaut est développée en utilisant les règles de l'arithmétique d'intervalle pour la génération de seuils robustes et adaptatifs sur les résidus nominaux. Ainsi, les avantages de l'arithmétique d'intervalle et du BG sont intégrés pour un meilleur diagnostic des systèmes incertains. La méthode est validée et mise en œuvre en temps réel sur un système de générateur de vapeur.

D'autre part, le concept de maintenance en fonction de l'état (Condition Based Maintenance) ou maintenance prédictive n'a émergé que récemment, où les activités de maintenance ne sont effectuées que lorsqu'une condition de panne ou de défaillance est prévue. Il permet également d'assurer la sécurité, la fiabilité et l'optimisation des coûts globaux. Durant la dernière décennie, de nombreux travaux de recherche ont porté sur les stratégies de maintenance pro-actives. Celles-ci concernent essentiellement la surveillance des données pour fournir une évaluation précise de l'état de santé d'un composant / système.

Cela implique l'utilisation d'un système de surveillance en temps réel et le traitement des données. Afin de prédire la progression d'un mode de défaillance particulier depuis son commencement jusqu'au moment de la défaillance d'un composant. Bien que le pronostic soit en relation avec le diagnostic, il ne repose pas sur les mêmes approches. En outre, il nécessite la connaissance des modes de défaillance existants et les taux de détérioration, la relation entre les défaillances et leur taux de progression. Ainsi, le pronostic est fortement influencé par la nature des dégradations des paramètres du système et de ses composants.

Malgré le fait que le pronostic a été approché par diverses techniques, il reste encore peu exploré dans le cadre de la modélisation par BG. Il y a eu très peu de travaux effectifs en faveur du développement de procédures efficaces pour le pronostic.

La majorité des tentatives existantes dans le cadre de la modélisation par BG, considère la progression des dommages de nature déterministe, difficilement capable de s'adapter à la réelle progression des dommages et donc, la fiabilité des prédictions reste minime. En outre, les incertitudes liées aux mesures, aux conditions de fonctionnement, au bruit de processus, etc. ne sont pas prises en compte de manière efficace. Il en résulte la prédiction de la durée de vie résiduelle (RUL) sans intervalles de confiance associés. Cela rend les prédictions inutiles pour la certification industrielle et les applications critiques.

Les problèmes liés au pronostic mentionnés ci-dessus sont traités dans le Chapitre 3, dans lequel une nouvelle approche pour le pronostic hybride est développée en utilisant les Relations de Redondance Analytique déduites d'un modèle BG incertain et les Filtres Particulaires (PF). Un paramètre du système est identifié comme étant le candidat pour le pronostic. Le modèle de dégradation est supposé connu a priori. Le problème du pronostic est posé comme un problème commun état-estimation des paramètres, appelé approche pronostic hybride, dans lequel le modèle de défaut est construit en considérant le modèle de dégradation statistique du paramètre du système candidat pour le pronostic. Les mesures sont

obtenues à l'aide du résidu nominal déduit du BG sous la forme de Relations de Redondance Analytique évaluées par Intervalles (I-ARRs) développés dans le chapitre 2.

L'utilisation de filtres particuliers permet d'obtenir des estimations de l'état du paramètre du système candidat pour le pronostic sous l'effet de la dégradation (ainsi que les paramètres cachés associés qui influencent la progression des dommages du candidat au pronostic, appelés paramètres de progression de la dégradation (PPD)). Les estimations sont suivies pour obtenir l'état de dommages en termes probabilistes. Les estimations du candidat au pronostic et les PPD associés sont utilisés pour la prédiction de la durée de vie résiduelle (RUL) du système par rapport à ce paramètre. La prédiction de la RUL est atteinte en termes probabilistes. De plus une nouvelle méthodologie a été développée pour obtenir les observations de la variable d'état de la partie nominale des I-ARRs pour les processus d'estimation et de prédiction. Les incertitudes associées aux mesures bruitées, les conditions environnementales, etc. sont gérées efficacement. Cette méthodologie est appliquée sur un système mécatronique (un système à barre de torsion) et évaluée par simulation de la dégradation paramétrique. Les performances d'estimation et les performances de prédiction RUL sont calibrées par des métriques pronostiques appropriées. La méthodologie est également validée en temps réel. Pour ce dernier exemple, un montage de type levier mécanique a été fabriqué et ajouté au système mécatronique. Grâce à une charge variable, le couple exercé par le dispositif de levier est variable. Celui-ci est traité comme la variation d'un paramètre (coefficient de friction) du système. Les estimations de la dégradation et la prévision de la RUL sont obtenues en temps réel.

Dans le chapitre 4, la méthodologie de pronostic développée est convenablement exploitée pour la surveillance efficace de l'état de santé d'un composant / sous-système d'un grand système incertain. A cet effet, un modèle BG adapté pour le diagnostic et le pronostic d'une pile à combustible à membrane échangeuse de protons (PEMFC) industrielle est utilisé. Les parties électrique et électrochimique (EE) de PEMFC sont considérées incertaines. Un modèle BG-LFT de celles-ci est développé. La méthodologie pronostic hybride développée est mise en œuvre sur ces parties.

L'incertitude paramétrique sur la résistance électrique globale est considérée. En utilisant des algorithmes PF, l'estimation de l'état de santé (SOH) est obtenu. Cela est utilisé pour la prédiction de la durée de vie résiduelle (RUL) de la partie de l'EE de la PEMFC basée sur des

ensembles de données de dégradation réelles sous un courant de charge constante et dynamique.

La prédiction d'estimation de SOH et RUL est obtenue avec une grande précision et des intervalles de confiance précis. De plus, une nouvelle méthodologie a été développée pour obtenir les observations de la partie nominale de l'ARR incertaine (dérivée du modèle BG-LFT) pour les processus d'estimation et de prédiction. Les résultats obtenus montrent la haute efficacité, la précision et la fiabilité de l'approche proposée pour le pronostic des systèmes dynamiques incertains.

TABLE OF CONTENTS

List of Abbreviations	1
General Introduction	3
Objectives	4
Thesis Layout and Summary of Thesis	4
Contributions of the Thesis	6
1. Background, Tools and Techniques	9
1.1 Condition Based Maintenance	9
1.1.1 Diagnostics	12
1.1.2 Prognostics	13
1.2 Prognostics and Health Management	18
1.3 The Diagnostics-Prognostics Process	19
1.4 Diagnostics Approaches	20
1.4.1 Data-Driven Approaches	21
1.4.2 Model Based Approaches	23
1.4.3 Bond Graph Based Quantitative Diagnosis	26
1.4.4 Robustness in Model Based Diagnosis	34
1.5 Approaches of Prognostics	40
1.5.1 Experience based Approaches	41
1.5.2 Data-Driven Techniques	42
1.5.3 Model Based Prognostic Approaches	45
1.5.4 Hybrid Prognostics	48
1.5.5 Prognostics in BG Framework	49
1.6 Conclusions	50
2. Robust Fault Detection with Interval Valued Uncertainties	51
2.1 Assumptions	52

2.2	Interval Arithmetic: A Brief Discussion	52
2.3	Modelling Uncertainties as Intervals	55
2.3.1	System Parameter Uncertainty	55
2.3.2	Measurement Uncertainty	59
2.4	Interval Valued Analytical Redundancy Relations	64
2.5	Interval Valued Robust Thresholds	67
2.6	Application: Robust Fault Detection of Steam Generator System	71
2.6.1	Uncertain Steam Generator System	71
2.6.2	Interval Valued ARR generation	84
2.6.3	Experimental Results	87
2.6.4	Comparison with BG-LFT Robust FDI	92
2.6.5	BG-LFT Enabled Threshold Generation for Steam Generator System	96
2.7	Conclusions and Contribution	100
3.	A Methodology of Hybrid Prognostics	101
3.1	Assumptions and Objectives	101
3.2	Degradation Model	102
3.2.1	Obtaining Degradation model in BG Framework	103
3.3	Methodology for Hybrid Prognostics in BG Framework	104
3.3.1	Robust Detection of Degradation Beginning	104
3.3.2	Fault Model Construction	106
3.3.3	Estimation of the State of Degradation	108
3.3.4	Remaining Useful Life Prediction	114
3.4	Health monitoring of Prognostic Candidate	116
3.5	Evaluation Metrics	117
3.5.1	Estimation performance	117
3.5.2	Prediction performance	118
3.5.3	Prognostics performance	118

3.6	Case Study on Mechatronic System through Simulations	119
3.6.1	Nominal System	119
3.6.2	Inter valued ARR and Robust Thresholds	122
3.6.3	Nominal Conditions	124
3.6.4	Generation of Parametric degradation	125
3.6.5	Fault Model	125
3.6.6	Degradation Estimation	126
3.6.7	RUL Prediction	127
3.6.8	A Qualitative Analysis	127
3.6.9	Computational Complexity	132
3.7	Application: Health Monitoring of Mechanical Torsion Bar System	133
3.7.1	Case I: Linear Variation of Load	136
3.7.2	Case II: Exponential Variation of Load	140
3.8	Conclusions and Contributions	143
4.	Hybrid Prognostics of Proton Exchange Membrane Fuel Cell	145
4.1	Description of a PEMFC	146
4.2	Bond Graph Model of PEMFC	148
4.2.1	Hydrogen Inlet and Oxygen Inlet	148
4.2.2	Oxygen Inlet.	148
4.2.3	Chemical Part	149
4.2.4	Electrical and Electro-Chemical (EE) Part	150
4.2.5	Thermal Part	151
4.3	Generation of Deterministic ARR and Robust Thresholds	152
4.3.1	Derivation of Deterministic ARR of PMFC	152
4.3.2	Generation of Robust Adaptive Thresholds	153
4.4	Experimental Setup	155
4.4.1	Degradation Tests	156

4.4.2	Degradation Model	157
4.5	Prognostics of the Electrical-Electrochemical Part	161
4.5.1	Fault Model	161
4.5.2	State of Health Estimation and RUL Prediction	164
4.6	Conclusions and Contributions	172
4.7	Acknowledgements	174
5.	General Conclusions and Perspectives	175
Appendix A	Bond Graph Generalities	178
A.1.	Causality	182
Appendix B	Bond Graph in Linear Fractional Transformation	185
B.1.	BG-LFT based Robust Fault Detection	190
Appendix C	Non-Linear Bayesian Filtering using Particle Filters	192
C.1.	Particle Filters	194
C.2.	Importance Sampling	195
C.3.	Particle Degeneracy and Resampling	196
Appendix D	Matlab and Simulink Code	199
D.1.	Programation Code in Chapter 3	199
D.2.	Programation code in Chapter 4	206
References		211

List of Abbreviations

ARR	Analytical Redundancy Relations
BG	Bond Graph
BG-LFT	Bond Graph in Linear Fractional Transformation
DM	Degradation Model
DPP	Degradation Progression Parameter
EE	Electical-Electrochemical Part
EKF	Extended Kalman Filter
EOL	End of Life
FC1	Fuel Cell 1 (Under Constant Load Test)
FC2	Fuel Cell 2 (Under Variable Load Test)
i.i.d	independent and identically distributed
IA	Interval Arithmetic
I-ARR	Interval Valued Analytical Redundancy Relations
IEF	Interval Extension Function
NIE	Natural Interval Extension
OCV	Open Circuit Voltage
PDF	Probability Density Function
PEMFC	Proton Exchange Membrane Fuel Cell
PF	Particle Filters
RA	Relative Accuracy
RIF	Rational Interval Function
RMAD	Relative Median Absolute Deviation
RMSE	Root Mean Square Error

SIR	Sampling Importance Resampling
RUL	Remaining Useful Life
SOH	State of Health
URIF	Uncertain Residual Interval Function

General Introduction

This thesis is prepared within the research group "Methodes et Outils pour la Conception Integree de Systemes (MOCIS)" at Centre de Recherche en Informatique, Signal et Automatique de Lille (CRISTAL).

MOCIS exhibits an extensive amount of experience as well as expertise in the field of integrated design of multi-energetic systems, using the unifying modeling language of BG. In this context, the past decade has seen excessive efforts being made for the development of supervision techniques for industrial systems in BG framework. There are extensive amount of literature published related to Fault Detection and Isolation (FDI) of complex systems, uncertain multi physic systems, etc. However, development of supervision procedures has been mainly limited to FDI and related issues, where the primary objectives have been efficient diagnosis of the fault in the system. Specifically in the context of robust FDI of uncertain systems, BG in Linear Fractional Transformation (BG-LFT) has proven to be a very effective tool. It has been widely exploited for the uncertain systems belonging to various energy domains. Although, there has been a wide and successful implementation of the BG-LFT method for FDI in various domains of engineering, little efforts have been put for development of efficient methodology for threshold generation. As one of the objectives, this work intends to integrate interval arithmetic based techniques with BG-LFT technique for efficient robust diagnosis.

The concept of condition-based maintenance or predictive maintenance has emerged only recently, where maintenance activities are only performed when a fault or failure condition is expected. It also promises to ensure safety, reliability, and optimization of the overall costs. In last one decade, there has been a huge surge in the research and development of pro-active maintenance strategies which mainly involve monitoring of system data to provide an accurate assessment of the health, or state, of a component/system. It involves using real-time system monitoring and data processing. The term prognostics and health management (PHM) has emerged very recently, which describes systems that are developed to implement a CBM philosophy. Prognostics involves predicting the time progression of a specific failure mode from its incipience to the time of component failure. Although prognostics is related to diagnostics, it is not same as the latter. Moreover, it requires the knowledge of existing failure modes and deterioration rates, relationship between failures and

their progression rates, and is significantly influenced by the nature of the underlying degradations of system parameter/component.

Although prognostics of failure has been approached through various techniques, it still remains immature in the framework of BG modeling. There have been very few efficient efforts towards development of efficient prognostic procedures. Most of the previous attempts in BG framework consider damage progression deterministic in nature, incapable of adapting to the current damage progression and hence, reliability of predictions remains minimal. Moreover, uncertainties associated with measurements, operating conditions, process noise etc. have not been taken into account effectively. This results in prediction of RUL without any associated confidence bounds, rendering it useless for industrial certification and critical applications. Moreover, an efficient approach towards system level (and not merely component level) prognostics in BG modeling paradigm can be envisaged.

Objectives

At the commencement of this work, following objectives were envisaged:

- Amelioration of the robust diagnostics of uncertain systems through treatment of uncertain parameters as interval models. A suitable integration of interval arithmetic or set-based approaches, with the benefits of BG-LFT based approach was sought.
- Development of an efficient methodology for model based prognostics in the BG modeling framework was envisaged.
- An integrated and holistic solution towards the diagnostic and prognostic issues in BG framework.

The aforementioned objectives are achieved in this thesis.

Thesis Layout and Summary of Thesis

Chapter 1 introduces the concept of condition based maintenance, diagnostics and prognostics. Emphasis is laid upon the suitability and relation of prognostics with diagnostics techniques. Diagnostic approaches are reviewed and special emphasis is laid upon BG based diagnostic techniques, for which extensive literature review is provided. BG-LFT enabled robust diagnosis is discussed in a detailed manner and the associated limitations are also highlighted. Additionally, the bounding approaches and interval based approaches are

reviewed. This way, the motivations for integration of the benefits of BG LFT method and interval based approaches is highlighted. Thereafter, the concept of prognostics is discussed and an extensive review is provided for prognostics related works. In particular, model based prognostic approaches and hybrid prognostics are reviewed in detail. Prognostics based upon Bayesian techniques is discussed. Moreover, the existing approaches of prognostics in BG framework is provided and significant limitations are discussed. As such, the motivations for development of efficient prognostics in BG framework are highlighted and justified.

In Chapter 2, the issues related to diagnostic procedure are addressed. The properties of Interval arithmetic are used for modeling uncertain system parameters and uncertain measurements, as interval models. The various properties of BG-LFT are borrowed and integrated with interval models for a systematic graphical representation of system with interval valued uncertainties. The latter also leads to a systematic derivation of Interval valued Analytical Redundancy Relationships (I-ARRs) from the uncertain BG. A novel methodology for robust fault detection is developed by utilizing the rules of interval arithmetic for the generation of robust adaptive interval valued thresholds over the nominal residuals. This way, the benefits of bounding approach and BG are integrated for better diagnosis of uncertain systems. The developed methodology is implemented on an uncertain steam generator system in real time. Moreover, a comparative study is done between BG LFT enabled thresholds and I-ARR enabled thresholds via experimental results.

The prognostic issues are addressed in Chapter 3, wherein a novel hybrid prognostic approach is developed using BG enabled Analytical Redundancy Relationships (ARRs) and Particle Filtering (PF) algorithms. The latter addresses the prognostic issues of a system parameter known *a priori*, which forms the prognostic candidate. The novel methodology of hybrid prognostics is developed by casting the problem as a joint state-parameter estimation problem, a hybrid prognostic approach, wherein the fault model is constructed by considering the statistical degradation model of the system parameter. The system parameter is known *a priori* to be undergoing degradation. Measurements are obtained from BG- derived nominal residual given by Interval valued ARR (I-ARR) developed in Chapter 2. Using Particle Filters algorithms, estimation of state of the system parameter under degradation (prognostic candidate) along with the associated unknown and possibly time varying degradation progression parameters(s) (DPPs) is achieved and tracked, to obtain the state of damage in probabilistic terms, which is used for prediction of RUL of the system with respect to that

parameter. Estimations of the current state of health of the prognostic candidate and the parameters that influence the degradation progression are achieved in probabilistic terms. Prediction of the Remaining Useful Life (RUL) is also achieved in probabilistic terms. Moreover, a novel methodology is developed for obtaining the observations from the nominal part of the I-ARR for the estimation and prediction processes. The associated uncertainties arising out of noisy measurements, parametric degradation process, environmental conditions etc. are effectively managed to produce a reliable prediction of RUL with suitable confidence bounds. The methodology is studied via simulations as well as real time experiments.

In Chapter 4, the developed methodology of hybrid prognostics is suitably exploited for an efficient health monitoring of a component/subsystem. For this purpose, a BG model suited for diagnostics and prognostics of Proton Exchange Membrane Fuel Cell (PEMFC) is utilized. Here, the electrical and electrochemical (EE) part of PEMFC is considered uncertain. A BG-LFT model of the latter is developed. The developed hybrid prognostic methodology is applied on the EE part of an industrial PEMFC involving the degradation data sets that are obtained in real time. Moreover, a novel methodology is developed for obtaining the observations from the nominal part of the uncertain ARR (derived from BG-LFT model) for the estimation and prediction processes. The obtained results are a clear indicative of the high efficiency, accuracy and reliability of the proposed approach and assure the reliability of developed methodology for prognostics of the uncertain dynamic systems.

The work developed in this thesis proposes not only a logical continuation of the work that has been done before, **but also develops a novel thematic within the MOCIS group**. It is the first PhD Thesis devoted to the development of prognostic approaches in the BG framework.

Contributions of the Thesis

The results obtained during the development of this work have been the subject of following publications:

Journal Rank A

- M. Jha, G. Dauphin-Tanguy, B. Ould Bouamama, *Robust Fault Detection of Uncertain Systems with Interval Valued Uncertainties in Bond Graph Framework*, **in review process**, Journal of Process Control, Elsevier.

- Jha, M.S., Dauphin-Tanguy,G., Ould-Bouamama,B., *Particle Filter Based Hybrid Prognostics for Health Monitoring of Uncertain Systems in Bond Graph Framework*, **in review process**, Mechanical systems and Signal Processing, Elsevier.
- Mayank Shekhar Jha, Mathieu Bressel, Belkacem Ould-Bouamama, Genevieve Dauphin-Tanguy, Mickael Hilairret and Daniel Hissel, *Particle Filter Based Hybrid Prognostics of Proton Exchange Membrane Fuel Cell in Bond Graph Framework*, **Submitted** to Applied Energy, Elsevier.

International Conferences:

- M. Jha, G. Dauphin-Tanguy, B. Ould Bouamama, *Robust FDI Based On LFT BG And Relative Activity At Junction*, in: Control Conference (ECC), 2014 European, IEEE, 2014, pp. 938-943.
- M. Jha, G. Dauphin-Tanguy, B. Ould Bouamama, *Integrated Diagnosis and Prognosis of Uncertain Systems: A Bond Graph Approach* in: Second European Conference of the PHM Society 2014 European Conference of the PHM Society 2014 Proceedings, Nantes, France, 2014, pp. 391-400.
- M. Jha, G. Dauphin-Tanguy, B. Ould Bouamama, *New Concept of Junction Activity in a Bond Graph Model: Application for Fault Identification*, Conference: 11th International Conference on Bond Graph Modeling and Simulation., Monterey, California ,USA.
- Mayank Shekhar Jha, Mathieu Bressel, Belkacem Ould-Bouamama, Genevieve Dauphin-Tanguy, Mickael Hilairret and Daniel Hissel, *Particle Filter Based Prognostics of PEM Fuel Cell in Bond Graph Framework*, **Selected for Presentation and Publication in 3^{ème} Conférence Internationale des Energies**

1. Background, Tools and Techniques

This chapter introduces the concept of condition based maintenance, diagnostics and prognostics. Emphasis is laid upon the suitability and relation of prognostics with diagnostics techniques. Diagnostic approaches are reviewed and special emphasis is laid upon BG based diagnostic techniques, for which extensive literature review is provided. BG-LFT enabled robust diagnosis is discussed in a detailed manner and the associated limitations are also highlighted. Additionally, the bounding approaches and interval based approaches are reviewed. This way, the motivations for integration of the benefits of BG LFT method and interval based approaches is highlighted. Thereafter, the concept of prognostics is discussed and an extensive review is provided for prognostics related works. In particular, model based prognostic approaches and hybrid prognostics are reviewed in detail. Prognostics based upon Bayesian techniques is discussed. Moreover, the existing approaches of prognostics in BG framework are provided and significant limitations are discussed. As such, the motivations for development of efficient prognostics in BG framework are highlighted and justified.

1.1 Condition Based Maintenance

Traditionally, two kinds of maintenance philosophies have been employed over critical equipment or component of a system; preventive or corrective. Preventive measures refer to approaches that use time based intervals to schedule the maintenance activities. On the contrary, corrective measures translate to such actions that are applied to restore the health of the critical component after it has failed, or functions outside the prescribed functionality limits. As such, the use of preventive approaches often lead to conservative estimates regarding the likelihood of equipment failure and result in their replacement long before they may fail in reality. The common characteristic of both the approaches remains in non-consideration of the “actual” condition of the component, for planning the maintenance actions. Due to the associated limitations, both the approaches are costly for the industries as the systems become more and more complex and expensive, as shown in Fig. 1.1. As such, the need to reduce maintenance costs, minimize the risk of catastrophic failures, and maximize system availability has led to a new maintenance philosophy.

Condition-based maintenance (CBM), or predictive maintenance, represents a new maintenance philosophy, where maintenance activities are only performed when there is objective evidence of an impending fault or failure condition, whilst also ensuring safety, reliability, and reducing overall total life costs (Bengtsson, 2004).

The goal of a CBM approach remains in optimization of the overall maintenance and logistic costs by performing the maintenance actions only in case of abnormal behavior of the component or system. As such, there is a huge shift in the maintenance approach towards CBM which provides reduced number of scheduled preventative actions, minimized requirement and cost of inventory maintenance of spare parts, whilst also avoiding, potentially catastrophic, in-service equipment failures (Vachtsevanos, George et al., 2007).

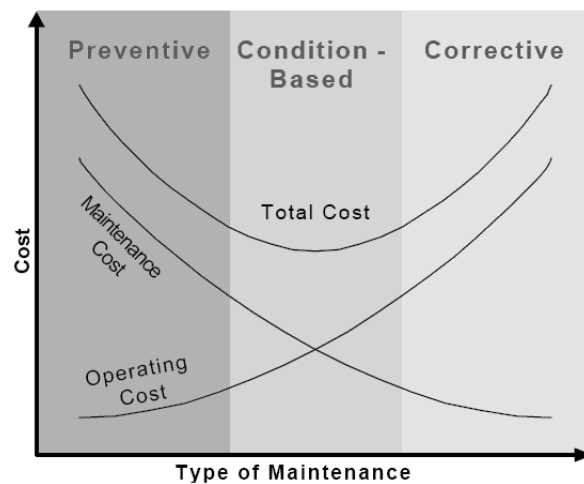


Fig. 1.1 Cost associated with different maintenance approaches (Lebold et al., 2003)

CBM is a maintenance strategy whereby equipment is maintained according to its condition, rather than on an elapsed time or running hour's basis and thus, involves monitoring of system data to provide an accurate assessment of the health, or state, of a component/system. It is followed by maintenance activities based on its observed health. It involves using real-time system monitoring and data processing. A CBM program consists of three key steps (Jardine et al., 2006), as shown in :

1. Data acquisition step (collection of information), to obtain data relevant to the system health.
2. Data processing step to handle and analyze the data or signals collected in Step 1 for better understanding of the data.

3. Maintenance decision-making step to recommend efficient maintenance policies.

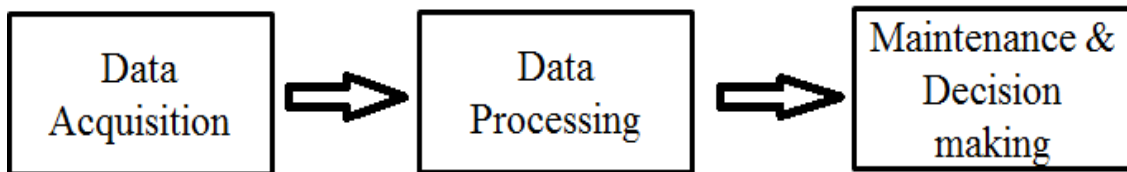


Fig. 1.2. Three basic steps of BBM program (Jardine et al., 2006).

The two main pillars of condition based maintenance strategy are *diagnostics* and *prognostics*. *Diagnostics* involves identifying the root cause of a problem whereby the problem has already occurred and *Prognostics* involves predicting the future health of the equipment either before or after a problem occurred (Jardine et al., 2006). Moreover, as stated in Sikorska et al. (Sikorska et al., 2011), diagnostics involves identifying and quantifying the damage that has occurred (and is thus retrospective in nature), while prognostics is concerned with prediction of the damage that is yet to occur.

Irrespective of the objectives of any CBM program, the three key steps of CBM given in Fig. 1.2 are always followed to accomplish the goals of *Diagnostics* and *Prognostics*. The three basic steps are discussed in very brief here. They can be found detailed in Jardine et al. (Jardine et al., 2006) and the references therein.

- *Data acquisition* is a process of collecting and storing useful data (information) and forms an essential step in implementation.
- A CBM program for machinery fault (or failure, which is usually caused by one or more machinery faults) diagnostics and prognostics. Data collected can be categorized into two main types: the event data and condition monitoring data. The former includes the information on what happened (e.g., installation, breakdown, overhaul, etc., and what the causes were) and/or what was done (e.g., minor repair, preventive maintenance, oil change, etc.) to the component/system. Such data is useful in assessing the performance of current health indicators and can even be used either as feedback to the system designer for consideration of system redesign or improvement of condition indicators. Condition monitoring data are the measurements related to the health condition/state of the component/system (Jardine

et al., 2006), which include but not limited to vibration data, acoustic data, oil analysis data, temperature, pressure, moisture, humidity, weather or environment data, etc.

- *Data processing* comprises of cleaning, processing and potentially outlier data reduction in the data collected in raw format, before any informed decision can be made based on this data. Cleaning includes removing wrongly assigned failure modes to certain events data, removing NaNs (Not a Number Values), outliers etc. Sophisticated statistical and signal processing techniques can also be utilized to extract useful information from the data that are otherwise hidden within.
- *Decision Making* step is about issuing a recommendation over the over-all health of the component/system. It generally involves an intrusive or nonintrusive actions (Vachtsevanos, George et al., 2007). For instance, a data set reflecting that the system is operating outside the recommended limits of functionalities would call for change of its operating routines, whereas at the later stage of fault development it would result in its replacement.

1.1.1 Diagnostics

The foundation of a CBM approach is based upon robust and reliable fault diagnostic capabilities. Fault diagnostic algorithms are designed to detect system performance, monitor degradation levels, and identify faults (failures) based on physical property changes, through detectable phenomena (Vachtsevanos, George et al., 2007).

The term fault diagnostics is typically used to describe a broad range of capabilities that include, generally, the following three kinds of basic tasks (Vachtsevanos, George et al., 2007):

- **Fault detection:** This step involves identifying the occurrence of a fault, or failure, in a monitored system, or the identification of abnormal behavior which may indicate a fault condition.
- **Fault isolation:** This step involves identifying which component/subsystem/system has a fault condition, or has attained the failure state.
- **Fault identification:** It involves determining the nature and extent of the fault.

In the context of CBM, following questions should be answered by the diagnostic process involved (Sikorska et al., 2011):

1. Whether the component/system is in degraded state?
2. Which failure mode has initiated the degradation?
3. How severe is the degradation?

Compared to prognostic methods, there is a vast amount of available literature that throws light upon various kinds of diagnostic methods, including theory and practical applications. The different approaches of diagnostics are described in Section 1.4, laying major main emphasis on *model based approaches*, which form the center of this work's contribution.

1.1.2 Prognostics

Prognostics is derived from the Greek word *Prognostikos* and means foreknowing or fore-seeing. ISO13381-1 defines prognostics as: “*the estimation of time to failure and risk for one or more existing and future failure modes*”.

As detailed in Vachtsevanos et al. (Vachtsevanos, George et al., 2007), prognostics promises to produce major improvements over the traditional maintenance approaches, including both reduced operational and support (O&S) costs and complete life-cycle total ownership costs (TOC). “With the provision of a sufficient lead-time between the detection of an incipient fault condition and the occurrence of equipment failure, maintenance actions can become proactive instead of reactive, allowing necessary remedial maintenance work to be planned in advance” (Vachtsevanos, George et al., 2007). This is on contrary to more traditional maintenance approaches, in which equipment failure typically occurs without prior notice, leading to delays in organizing the necessary personnel, spares, and tools, necessary to return the equipment to good health.

In last one decade, with on-growing rapid research in the area of prognostics, a lot of definitions have been proposed as tabulated in Table 1-I. They essentially imply that (Sikorska et al., 2011):

1. Prognostics involves predicting the time progression of a specific failure mode from its incipience to the time of component failure (Sikorska et al., 2011).
2. Prognostics is related to, but not same as, diagnostics.
3. Prognostics requires the consideration of :
 - i. existing failure modes and deterioration rates.
 - ii. initiation criteria for future failure modes.
 - iii. Inter-relationship between failure modes and their deterioration rates.

- iv. the effect of maintenance on failure degradations
- v. the conditions and assumptions underlying the prognostic approach

To realize the benefits of prognostic capabilities, a reliable estimate of how long a system can continue to be operated safely, i.e. the remaining useful life (RUL) of the system, until a detected fault condition progresses to a failure condition, is sought. Since prognostics is associated with predicting the future, it inherently involves a large degree of uncertainty (Vachtsevanos, George et al., 2007). Indeed, the task of prognostics is considered to be significantly more difficult task than diagnostics, since the evolution of equipment fault conditions is subject to stochastic processes which have not yet happened (Engel et al., 2000).

In essence, the degradation process undergone by the component from a healthy state to the failure state must be studied to predict at any time the RUL. Consider Fig. 1.3 that shows degradation curves for three different failure modes that may correspond to different component degradation in system (e.g. bearing wear, frictional wear, electrical resistance drift etc.) or same component degradation but of dissimilar kind (e.g. inner race spall, outer race spall, cage crack in a rolling element bearing). Each degradation pattern may vary depending upon the factors that trigger the damage process and may follow a variable degradation pattern (even under the same environmental conditions and operational routines). Anomalous events may modify the deterioration rate and thus, can accelerate or slow down the degradation process.

In face of all such conditions, the prognostic procedures must be able to answer the one important question: How much time remains before the component achieves the state of failure. In other words, determining accurate and reliable RUL estimate forms the core objective of any prognostic procedure.

In essence, prognostic approaches should answer the followings (Sikorska et al., 2011):

1. How quickly is degradation expected to progress from its current state to functional failure?
2. What novel events will change (e.g. accelerate, retard) this expected degradation behavior?
3. How should the other factors (e.g. the type of model, measurement noise) affect the given estimate of RUL?

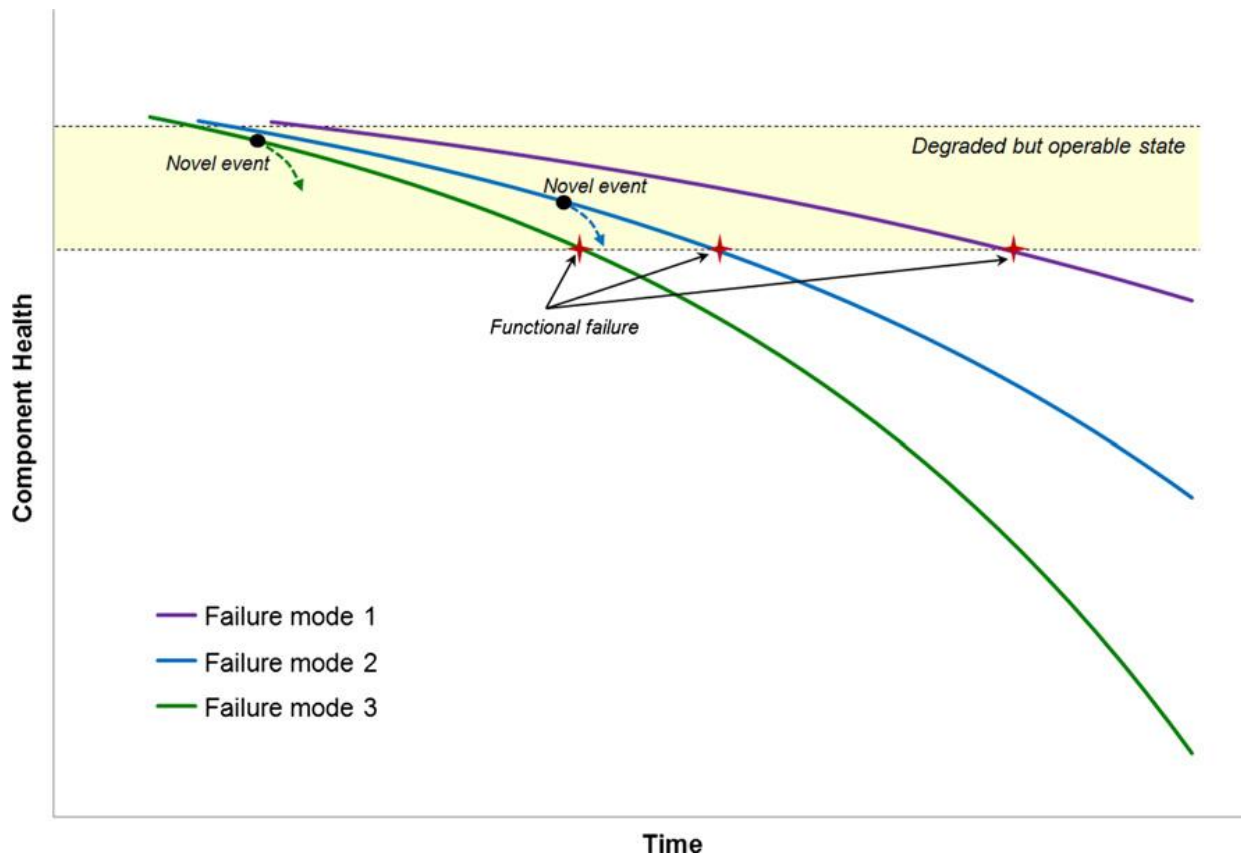


Fig. 1.3 Component health degradation curve (Sikorska et al., 2011)

1.1.2.1 The Remaining Useful Life Probability Density Function and Confidence Limits

Due to presence of various kinds of uncertainties brought by the process noise, variable environmental conditions, measurement noise, anomalous events etc. the prediction of RUL is generally done in probabilistic terms as probability density function (PDF) as depicted in Fig. 1.4. The component under prognostication should be removed from service before a high probability of failure is attained for which, *just-in-time-point* is defined that corresponds to 95% probability that component has not yet failed (Vachtsevanos, George et al., 2007).

In real sense, the RUL PDF is a conditional PDF that changes with increasing time. Thus, the RUL PDF must be recomputed at each time t based on new information that the component has not yet failed at that time. As the time passes, with more information obtained about the damage, more reliability upon the RUL estimation is gained. This leads to reduction in the variance of the RUL PDF as time advances and the PDF becomes narrower. The desirable time evolution profile of RUL PDF is shown in Fig. 1.5.

Table 1-I Various definitions of Prognostics (Sikorska et al., 2011).

First Author & Reference	Prognostics is... (direct quote)
Engel (Engel et al., 2000)	The capability to provide early detecting of the precursor and/or incipient fault condition of a component, and to have the technology and means to manage and predict the progression of this fault condition to component failure.
Hess (Hess et al., 2006)	Predictive diagnostics, which includes determining the remaining life or time span of proper operation of a component.
Wu (Wu et al., 2007)	The prediction of future health states and failure modes based on current health assessment, historical trends and projected usage loads on the equipment and/or process.
Katipamul (Katipamula et al., 2005)	Address(ing) the use of automated methods to detect and diagnose degradation of physical system performance, anticipate future failures, and project the remaining life of physical systems in acceptable operating state before faults or unacceptable degradations of performance occur.
Smith (Smith et al., 2003)	The capability to provide early detection and isolation of precursor and/or incipient fault condition to a component or sub-element failure condition, and to have the technology and means to manage and predict the progression of this fault condition to component failure.
Baruah (Baruah et al., 2005)	Prognostics builds upon the diagnostic assessment and are defined as the capability to predict the progression of this fault condition to component failure and estimate the remaining useful life (RUL).
Heng et al. (Heng et al., 2009)	The forecast of an asset's remaining operational life, future condition, or risk to completion.

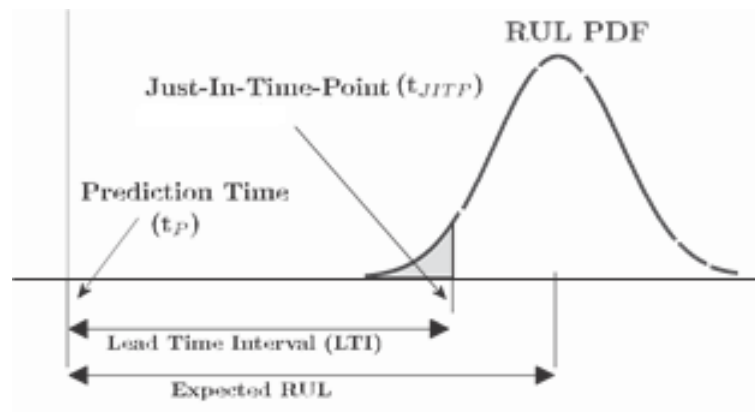


Fig. 1.4 RUL PDF and just-in-time removal-from-service point (Vachtsevanos, George et al., 2007)

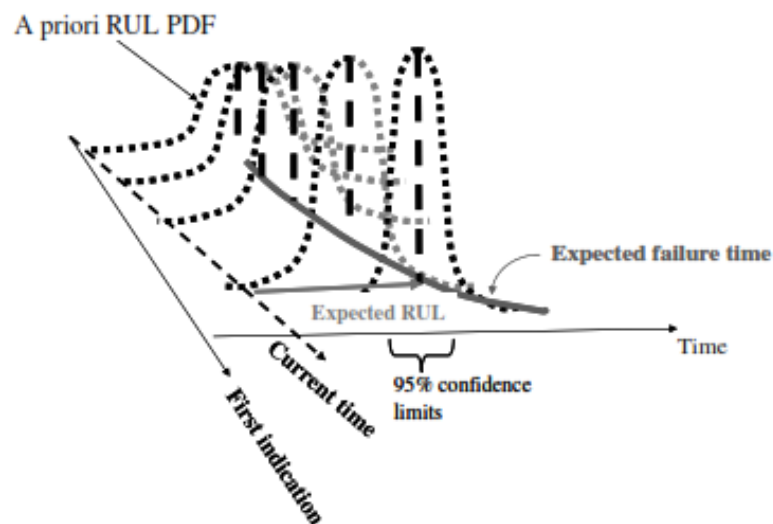


Fig. 1.5 Time evolution of RUL PDF (Vachtsevanos, George et al., 2007)

Because of the inherent uncertainty associated with the degradation process, future operational conditions/routines and various sorts of errors associated with the prognostic methodology employed, confidence limits on the RUL prediction is essential and plays a vital role in assessment of the reliability of the prediction. As stated in Sikorska et al. (Sikorska et al., 2011): “*Confidence limits are even more important in prognostic modeling than for diagnostic prediction. While the latter can (in theory) be deterministic and externally verifiable at the time of prediction (e.g. actual crack size), prognostic model outputs can only be verified retrospectively. Business decisions based on prognostic information should therefore be based on the bounds of the RUL confidence interval rather than a specific value of expected life*”.

As corroborated by other significant works too, prediction of RUL without any associated confidence bounds renders the whole prognostic process virtually useless for industrial certification and critical applications (Saxena et al., 2010; Uckun et al., 2008).

1.2 Prognostics and Health Management

The term prognostics and health management (PHM) has emerged very recently, which describes systems that are developed to implement a CBM philosophy. The term PHM originated from the military applications and was the name given to the capability being developed for the new F-35 Joint-Strike Fighter (JSF) to enable the vision of autonomic logistics and to meet the overall affordability and supportability goals of the latest military fighter aircraft (Hess et al., 2006). In the development of a PHM system, the term prognostics has a much wider definition than fault prediction and is used to describe a wide variety of activities including fault/failure detection, fault/failure isolation, enhanced diagnostics, material condition assessment, performance monitoring, and prognostics (Hess et al., 2006). Fig. 1.6 illustrates the typical stages within a CBM/PHM system, from signal pre-processing and feature extraction, fault detection and classification, to the prediction (prognostics) of RUL and finally, appropriate maintenance scheduling.

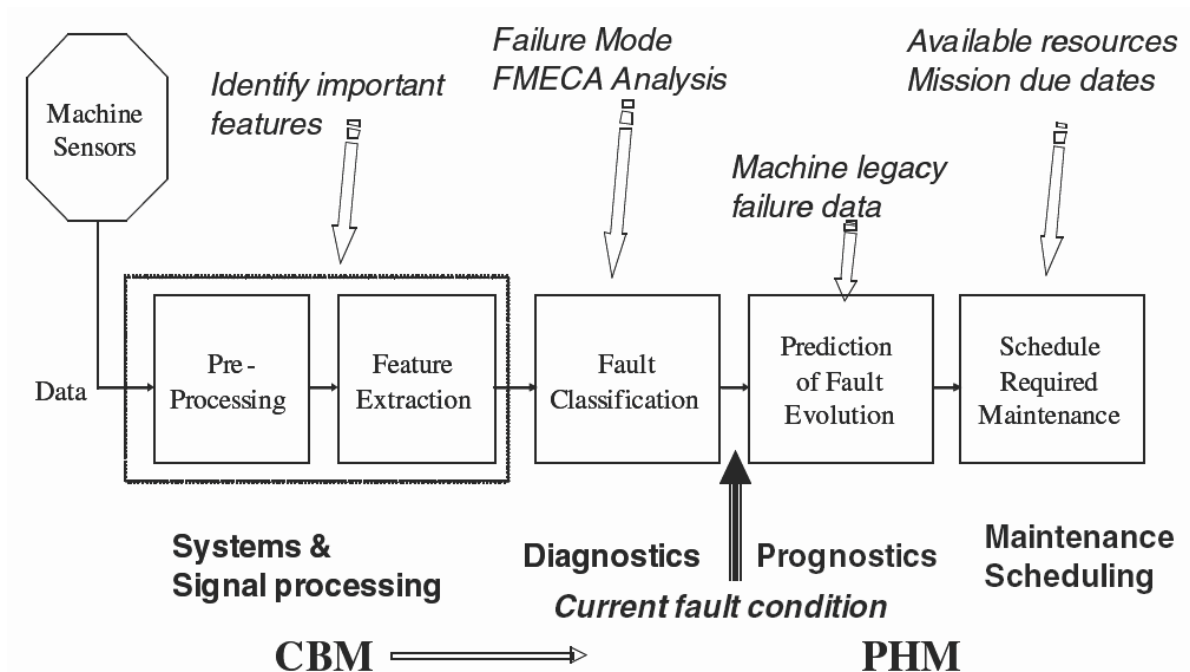


Fig. 1.6. Stages within a typical PHM system (Hess et al., 2006)

Apart from the maintenance benefits brought by implementation of a comprehensive PHM, a lot of additional benefits are produced such as (Vachtsevanos, George et al., 2007), (Hess et al., 2006):

1. The provision of a lead-time between detection of an incipient fault condition and actual system failure, presents an opportunity for improvements in management of associated logistic systems.
2. Integration of PHM into logistics systems can lead to automatic ordering of spare parts for those in which incipient failures are detected, thus, resulting in maintenance of only a small inventory of replacement parts. This can lead to a successful implementation of just-in-time (JIT) manufacturing philosophy for mission critical equipment with optimized on-site inventory costs.
3. PHM systems with prognostics capabilities have the potential to dramatically reduce the costs of providing maintenance contracts to equipment operators, whilst also improving the original equipment manufacturer (OEMs) profit margins. The sale of developed prognostic technologies could also provide a new and growing source of after-sales revenue.

1.3 The Diagnostics-Prognostics Process

As seen above, diagnostic and prognostic process form the basic and most important building blocks of CBM enabled PHM architecture. In this section, the relationship between diagnostic and prognostics is highlighted.

As seen previously, diagnostic processes are mainly involved in assessing the identification and quantification of damage that has been triggered (or commencement of degradation process). Thus, diagnostic processes are retrospective in nature (Sikorska et al., 2011). However, prognostic processes are involved with prediction of the damage that is yet to occur. Thus, prognostic approaches rely heavily upon the diagnostic outputs (type of component under degradation, a result rendered by fault detection and fault isolation unit). Therefore, prognostic procedures should not be done in isolation. Fig. 1.7 summarizes the various stages of diagnostics and prognostic processes and their mutual dependence.

1.4 Diagnostics Approaches

Diagnostics mainly consist of procedures that detect any kind of malfunction in the system/subsystem/component which may lead to an unacceptable anomaly in the overall system (Frank, 1990). Such a kind of malfunction may manifest form of :

- Abrupt faults: the fault occurs in a stepwise fashion and then stays present (e.g. sudden connection cut-off of a wire in an electrical rival circuit).
- Incipient faults: The fault increases gradually in a drift like fashion (e.g. gradual increase of resistivity in electrical circuit).

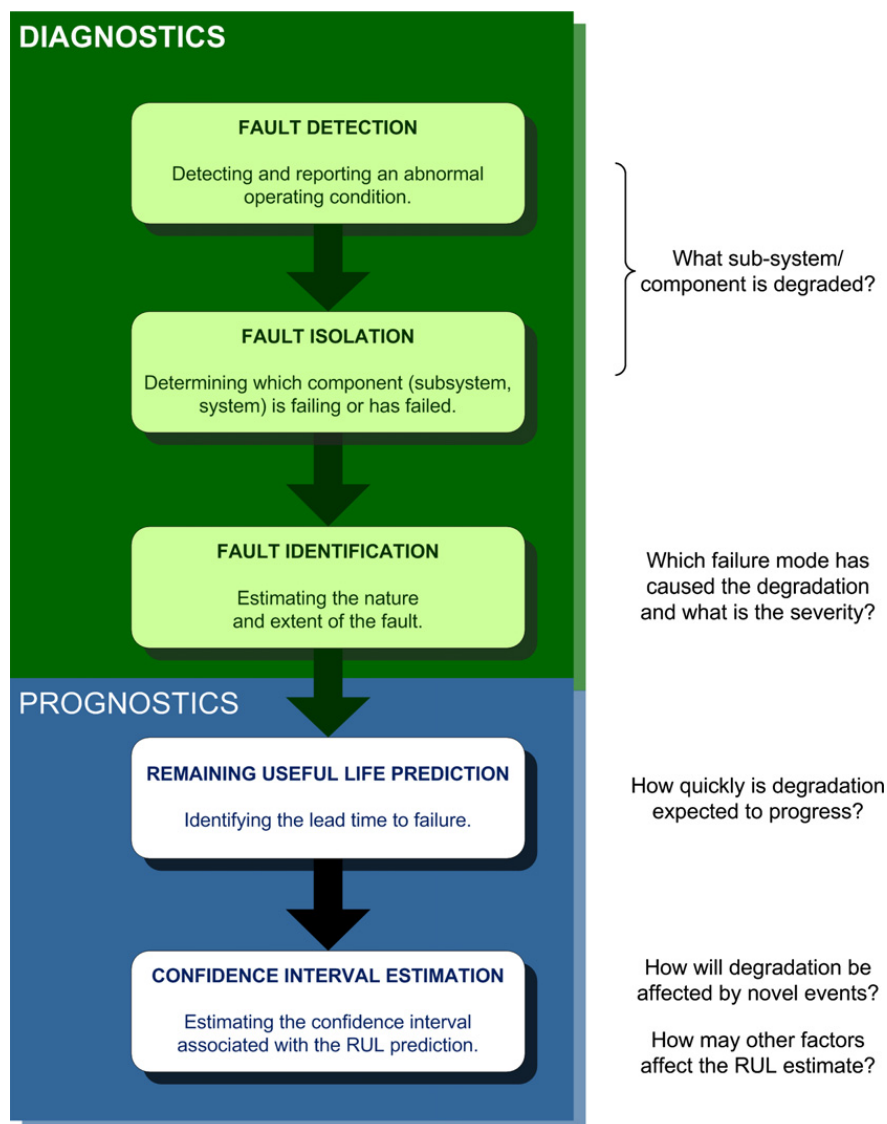


Fig. 1.7 Steps of Diagnostics and Prognostics and their relation (Sikorska et al., 2011)

- Intermittent faults: The kind of faults that occur and disappear quickly (e.g. faulty relays in an electrical circuit).

For a plant, the manifested faults can be divided into three classes as (Chen, Jie et al., 2012a):

- Actuator faults: malfunction in the actuation of the system (e.g. blockage in source of flow, voltage etc.)
- Sensor faults: consists of considerable measurement variations, sensor–drift, bias in sensor off-set etc.
- Parametric (Process) faults: faults that change/alter the basic process of the systems. They usually manifest in constituting parameters of the system (e.g. leakage of tank, discharging of the capacitor etc.)

Diagnostic approaches can be broadly divided into three categories, described in Jardine et al. (Jardine et al., 2006) as : Data-driven approaches and Model-based approaches. Data-driven techniques are in turn classified into two major techniques: Statistical approaches, Artificial Intelligence approaches. These approaches are discussed very briefly here. However, special emphasis is laid upon model based techniques as they form the center of the diagnostic methodology developed in this work.

1.4.1 Data-Driven Approaches

The general principle of data-driven approaches to fault diagnostics is to utilize pattern recognition techniques to map data in the measurement, or feature, space, to equipment faults within the fault space (Jardine et al., 2006). These approaches are broadly divided into two main categories as discussed below in very brief. For a detailed discussion and description of various techniques, references Qin et al. (Qin, 2012) and Jardine et al. (Jardine et al., 2006) are suggested.

Statistical approaches: Statistical process control (SPC) is a widely implemented technique, wherein deviations are measured in signal behavior about a predefined range or distribution. If a signal deviates outside the defined control limits this may be indicative of a fault condition. An example of using SPC for damage detection is discussed in Fugate et al. (Fugate et al., 2001). Hypothesis testing is another widely used method where fault detection is cast as a hypothesis test problem with null hypothesis H_0 : Fault A is present,

against another hypothesis H_1 : fault A is not present. Null hypothesis is rejected or accepted based upon test statistics which are constructed to summarize the condition monitoring information. See Sohn et al. (Sohn et al., 2002) for an example implementing hypothesis testing for fault detection. Another mostly used employed statistical approach is principal component analysis (PCA) and partial least squares (PLS). PCA is generally applied to high-dimensional datasets to transform a number of related variables to a smaller set of uncorrelated variables, i.e. dimensionality reduction. The basic principle of PCA for fault diagnostics is to derive a PCA model using a dataset of normal fault-free behavior. Future observations are compared with this model using statistical measures such as the T^2 and Q statistics (Venkatasubramanian et al., 2003b). If the measured statistics exceed a defined limit, a potential fault condition is flagged. PLS is a multivariate regression algorithm based upon PCA. A comprehensive overview of PCA/ PLS applied to fault diagnostic problems can be found in (Yoon et al., 2001) and a more recent reference is Qin et al. (Qin, 2012). Cluster analysis, a multivariate statistical analysis method, is a statistical classification approach that groups signals into different fault categories on the basis of the similarity of the characteristics or features they possess. It seeks to minimize within-group variance and maximize between-group variance (Jardine et al., 2006). Application of cluster analysis in machinery fault diagnosis is discussed in Artes et al. (Artes et al., 2003).

AI approaches: These approaches require efficient procedures to obtain training data (experimental data) and specific knowledge required for training the models. The application of relies upon the availability of a fault pattern library, or database, of historical failure examples, which relate extracted features from monitored systems to specific fault conditions (Jardine et al., 2006). The objective in applying classification based techniques is to model the relationships between fault features, or fault indicator measurements, and fault classes. In the literature, two popular AI techniques for diagnosis are artificial neural networks (ANNs) (Sorsa et al., 1993) and Expert Systems (Liao, S.-H., 2005). Other AI techniques used include fuzzy logic systems; fuzzy–neural networks (FNNs), neural–fuzzy systems and evolutionary algorithms (EAs), Bayesian networks, discriminant analysis, support vector classification etc. A review of recent developments in applications of AI techniques for fault diagnostics is given by Korbicz et al. (Korbicz et al., 2012).

Although, in general, such data-driven methods are useful where model of the system/plant is not known or, the physics of the failure cannot be understood/modelled correctly, such methods require availability of large experimental data sets under different

faulty scenario. Moreover, physical explanations of trained models are generally not available, rendering no capability for the model to be adapted for unseen (un-trained) faulty situations.

1.4.2 Model Based Approaches

Model based diagnosis (MBD) methods utilize the physics based mathematical models of the monitored system. There has been an extensive amount of work in past three decades in this field. Mainly, two kinds of communities are involved on model based techniques: the FDI (Fault Detection and Isolation) community and the DX (Principles of Diagnosis) community (de Kleer et al., 1992),(De Kleer et al., 1987). While the former community has researchers with background of control engineering, the latter involves members with background in computer science and intelligent systems. There have been attempts to exploit the benefits of the two by forming the Bridge task group (de Kleer et al., 2004),(Cordier et al., 2000). In this work, the methodology developed involves techniques mainly from FDI community, due to which they are discussed in detail.

The main works of FDI community in MBD can be referred in the literature such as (Blanke et al., 2010),(Chen, Jie & Patton, 2012a), (Isermann, 2005) etc. As discussed in Section 1.1.1, the MBD approaches mainly consist of three basic tasks: fault detection, fault isolation and fault identification. Most of MBD approaches operate by comparing the observed behavior of the process against a reference behavior provided by a nominal model of the system. In situations when the observed behavior is different from the nominal behavior, the diagnosis method uses this difference, to express a non-zero residual vector. This residual vector forms the basis of detection and isolation. The residual generation phase differs from method to method employed for FDI and forms the most important step. Theoretically, the value of residual is zero in absence of any fault or anomaly in the system. However, presence of measurement noises, variable environmental conditions, variation in operational routines/conditions, model uncertainties etc. lead to a possible non-null residual vector, false alarms, missed alarms, incorrect diagnosis etc. In fact, FDI community generally regards MBD approaches as two stage process (Chow et al., 1984), :

Residual generation: As described in Chen et al.(Chen, Jie & Patton, 2012a), the purpose of this phase is to generate a fault indicating signal (residual), using available input and output information from the monitored system. The resulting difference generated from the comparison of available system measurements with *a priori* information represented by the

system's mathematical model is called the residual or symptom signal. The residual should be normally zero or close to zero when no fault is present, whilst distinguishably different from zero when a fault occurs. The algorithm used to generate residuals is called a residual generator.

Decision Maker: This block examines residuals for the likelihood of faults and a decision rule is then applied to determine if any faults have occurred. The decision procedure may perform a simple threshold test on the instantaneous values or moving averages of the residuals. Moreover, it may consist of statistical methods, e.g., generalized likelihood ratio testing or sequential probability ratio testing (Chen, Jie & Patton, 2012a). The generic MBD approach is shown in Fig. 1.8.

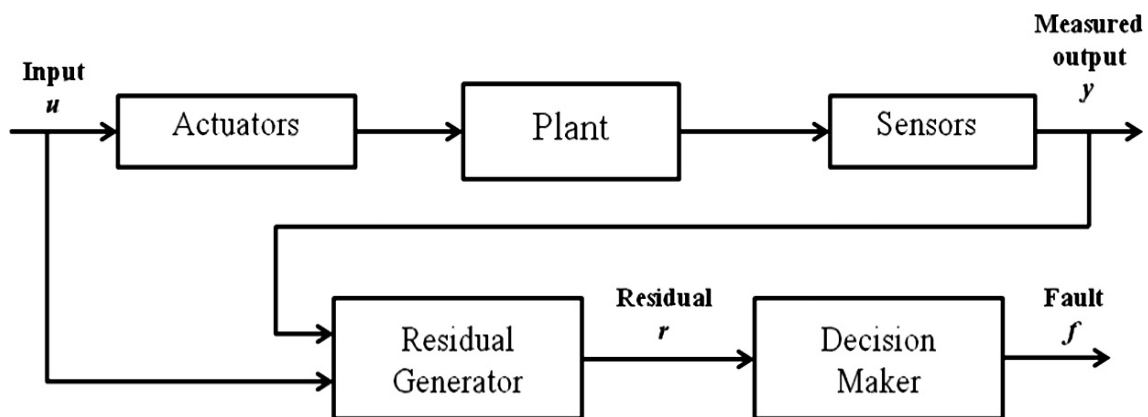


Fig. 1.8. Architecture of generic fault diagnosis scheme (Bouamama et al., 2014)

The model-based a priori knowledge can be broadly classified as qualitative or quantitative as shown in Fig. 1.9 (Venkatasubramanian et al., 2003a),(Samantaray, Arun Kumar et al., 2008):

- Quantitative models: The process is expressed in terms of mathematical functional relationships between the inputs and outputs of the system.
- Qualitative models: System variable relationships are expressed in terms of qualitative functions centered around different units in a process.

Quantitative approaches usually employ different strategies to compare the behavior of the system with that of a nominal model of the system. The mathematical models are used in conjunction with the respective methods to generate residual. Quantitative methods are

discussed in detail in Venkatasubramanian et al. (Venkatasubramanian et al., 2003b). Some of the usually employed methods are discussed here with special emphasis on Bond Graph (BG) based methods, since in this work, dynamic systems are modelled in BG modelling paradigm.

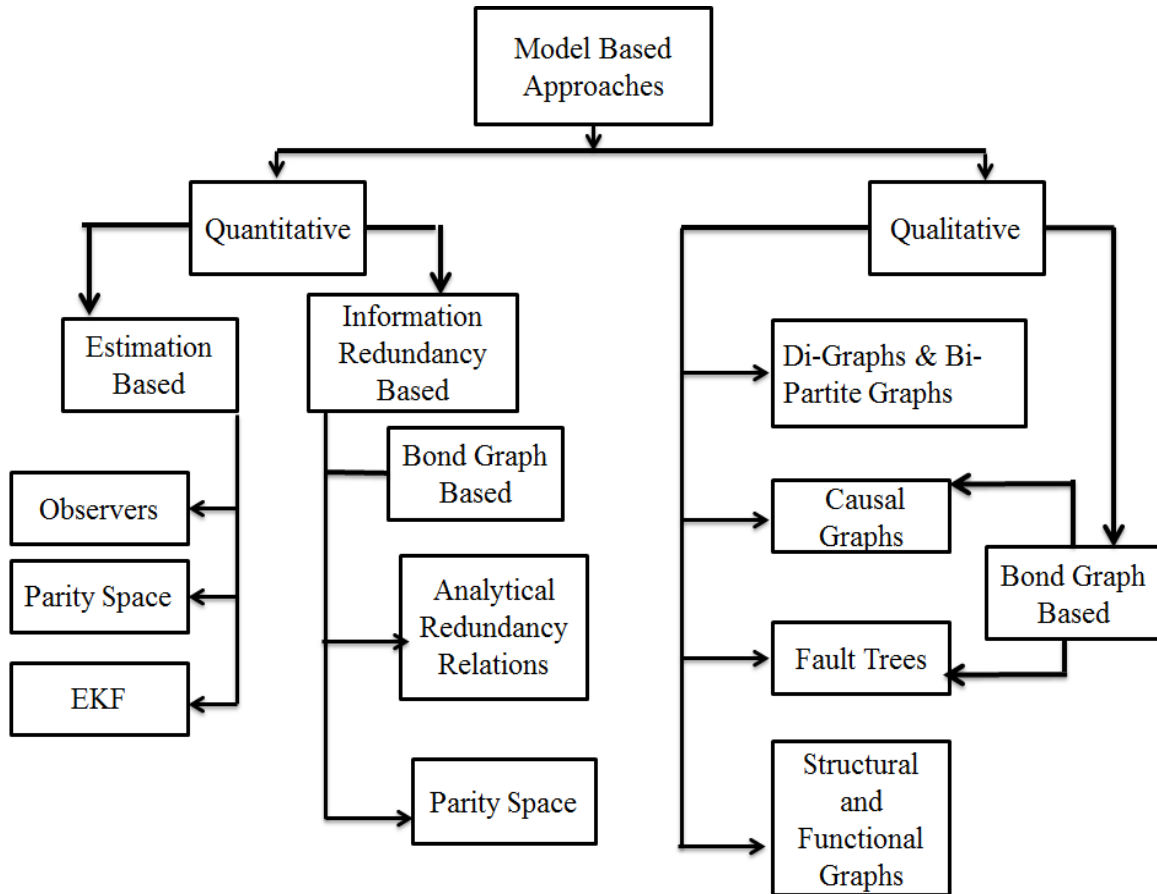


Fig. 1.9. Model based Diagnostic Methods

- Observers and Filter based approaches:** Observers are dynamic systems that are aimed at reconstructing the states of a state-space model of the system on the basis of the measured inputs and outputs (Pouliezios et al., 2013). Basically, the state of the system is estimated fully or partially, from the system measurements (or subset of measurements) by using either various observers (Luenberger, Unknown Input Observers etc.) in a deterministic setting or Kalman filters (or Extended Kalman Filters (EKF) and its variants) in stochastic setting. The weighted output estimation error (or innovations in stochastic setting), is used as residual to compare the measured and estimated states and hence, generate the fault indicator. Observer/filter

based approaches can be found reviewed in great detail in (Isermann, 2005),(Chen, Jie & Patton, 2012a), (Blanke et al., 2010) etc.

- **Parity Space approaches:** This approach systematically exploits the mathematical redundancy provided by the mathematical model of the system (Chow & Willsky, 1984). Systems equations are manipulated to eliminate unknown variables and generate a set of analytical redundancy relations from which, relations between fault hypothesis and measurement residuals is established (Frank, 1990),(Chen, Jie & Patton, 2012a). Detailed discussions on ARR methods and their construction can be found in Blanke et al (Blanke et al., 2001), Staroswiecki et al. etc.

Qualitative approaches exploit the underlying system model structure, causal relationships, rule based relationships etc. to draw diagnostic inferences and propagate the fault related information to diagnostic candidate. These approaches consist of various techniques most of which can be accomplished through graphical approaches for modelling. For example, Digraphs establishes cause –effect relationships with arcs between nodes that model the cause to effect flow. Signed Di-graphs have directed arcs with positive or negative sign attached to them(Nam et al., 1996). A comprehensive review of various qualitative approaches can be found in (Venkatasubramanian et al., 2003a). A more contemporary review that throws light upon the Bipartite graphs, fault trees, casual graphs, signed directed graphs, possible conflicts, temporal causal graphs, probabilistic causal graphs such as Bayesian networks and Dynamic Bayesian networks can be found in the recent extensive survey by Ould-Bouamama et al. (Bouamama et al., 2014) and the references therein. Qualitative diagnosis has also been achieved successfully from BG modelling perspective and are detailed in Samantaray et al. (Samantaray, Arun Kumar & Ould-Bouamama, 2008) . Major disadvantage of such approaches lie in their qualitative reasoning that may lead to inability of fault discrimination and implicit analysis for robustness. These methods are not detailed any further here as they have not been exploited in this work.

1.4.3 Bond Graph Based Quantitative Diagnosis

Bond graph modelling technique was invented by Paynter in 1959 (Paynter, 1961). It is a topological modelling language based on the power exchange between the components of a dynamic system, captured in a graphical form. The key aspect of BG modelling is the representation of power transfer as causality between the different dynamic components, making it a universal, multi-disciplinary modelling language. BG owing to its well defined

structural properties and causal properties is capable of dealing with multiple domains of engineering in a holistic way. The power exchange link is called a *bond*, and associated with every bond are two generic power variables named *effort* e and *flow* f , such that $e \times f = \text{power}$. The set of components, bonds, and junction structure define the global structure of the dynamic system. Cause and effect relationship between various variables of BG are modelled by the notion of causality. Causality in BG models is depicted by a perpendicular stroke on a bond. It determines whether the flow for a bond is computed from the effort, or vice versa. If all of the energy storage elements in a model are in integral form, the system is in integral causality. BGs are normally used in *integral causality* for simulation studies and analysis and control related purposes. Due to vastness of the available literature, detailed discussions on BG methodology has been skipped here. However, the basic concepts have been provided in Appendix A, along with the definition of BG related variables, notion of causality, etc. For a detailed introduction from *ab initio* and various related aspects, the readers are referred to following works (Karnopp et al., 2012), (Borutzky, Wolfgang, 2009a), (Mukherjee et al., 2006) and (Thoma et al., 2000).

Owing to the behavioral, structural and causal properties that provide a very systematic method for modeling the multi-energetic systems in a unified framework, BGs in integral causality have traditionally been thoroughly exploited for simulation and analysis for various systems/coupled multi-energetic systems.

Since the introduction of a technique of ARR generation from a BG model by covering causal paths in Tagina et al. (Tagina et al., 1995), BG has been extensively exploited in last one decade which includes supervision of highly non-linear and complex thermo-chemical systems (Medjaher, K. et al., 2006), non-linear mechatronic systems (Merzouki et al., 2007), intelligent and autonomous systems, industrial chemical reactors (El Harabi et al., 2010), hybrid systems (Arogeti et al., 2013; Borutzky, W, 2014; Chang Boon et al., 2010; Ming et al., 2011; Triki et al., 2014) etc. Quantitative BG based approaches utilize BG models to derive ARRs which in turn generate system residuals, thus assessing the system fault status. Its ability to represent complex systems mathematically and graphically makes various aspects of FDI feasible such as monitorability, isolability (ability to monitor fault candidates and their isolation)(Samantaray, Arun K et al., 2006b), and design of supervision system (Medjaher, Kamal, 2011; Ould-Bouamama et al., 2012) gives an excellent updated comprehensive review of various works on supervision based on BG with application to the

non-linear and complex continuous stirred-tank reactor (CSTR) system and (Ould-Bouamama et al., 2014) reviews the usage of various graphical methods including BG for FDI.

To illustrate the ARR generation procedure, which forms a basic building block for diagnosis, a pedagogical example is presented in the next section.

1.4.3.1 Direct –Current Motor: A Pedagogical Example

To illustrate various features of BG modelling based diagnosis, a pedagogical example of Direct-Current (DC) motor is chosen, schematic of is shown in Fig. 1.10. The variables describing the dynamics are listed in Table 1-II.

The BG model in preferred integral causality is given in Fig. 1.11. The various constraints in form of behavioral equations C_B , measurement equations C_M and structural equations C_S that are related to BG model are given in Table 1-III.

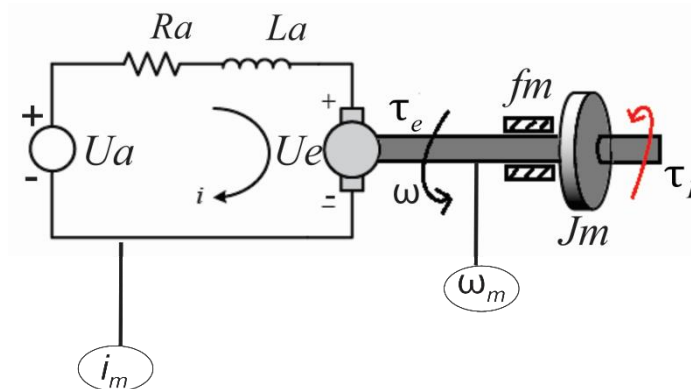


Fig. 1.10 Schematic of the pedagogical DC Motor

1.4.3.2 Fault Detection: Generation of deterministic ARR from BG model

The fault detection comprises of ARR generation as its main step. The ARR is obtained from the constraint relations at the junctions of the BG model subsystems. The subsystem must be observable and over-constrained (Samantaray, Arun K et al., 2006a). The constraint relation is expressed in terms of known variables of the system. The evaluated value of the ARR gives a residual.

Table 1-II Variables of the pedagogical DC motor

Symb	Designation	Symbo	Designation
Ra	Stator resistance(Ω)	fm	viscous friction (N)
La	Stator Inductance(H)	Jm	Inertia (rotor, load)($kg\cdot m^2$)
ke	Motor torque constant (N- m/Amp)	τ_L	Mechanical Torque (Load) (Nm)
i_m	Measured current (A)	$\omega(t)$	Angular velocity(rad/sec)
$Ua(t)$	Input voltage(Volts)	$\omega_m(t)$	Measured angular velocity
i	Motor Current (A)	U_R	Voltage in Resistance (V)
τ_f	Frictional Torque (N-m)	U_e	Back emf (V)
τ_J	Inertial Torque (Nm)	U_L	Induced Voltage (V)
τ_e	Motor Torque (Nm)		

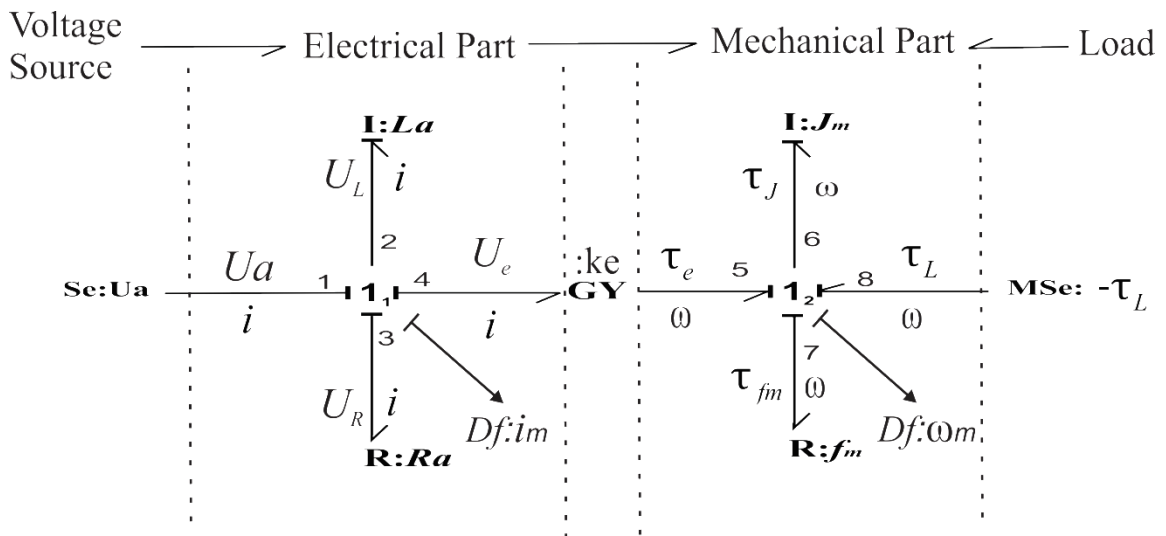


Fig. 1.11. BG model of the pedagogical DC motor in preferred integral causality

Table 1-III. Equations governing the BG model of Fig. 1.11

Behavioral Equations	Measurement Equations	Structural Constraints
$C_B : \begin{cases} C_{Ra} : U_R(t) = Ra.i(t) \\ C_{La} : i(t) = \frac{1}{La} \int U_L(t) dt \\ C_{fm} : \tau_{fm} = fm.\omega(t); \\ C_{Jm} : \omega(t) = \frac{1}{Jm} \int \tau_J(t) dt \end{cases} \quad (1.1)$	$C_M : \begin{cases} C_{i_m} : i_m(t) = i(t) \\ C_{\omega_m} : \omega_m(t) = \omega(t) \end{cases} \quad (1.2)$	$C_S : \begin{cases} C_{1_1} : U_L(t) = Ua(t) - U_R(t) - U_e(t) \\ C_{1_2} : \tau_J(t) = -\tau_L(t) - \tau_{fm}(t) + \tau_e(t) \\ C_{GY} : \begin{cases} U_e = ke.\omega(t) \\ \tau_e = ke.i(t) \end{cases} \end{cases} \quad (1.3)$

Detector Dualization: BG models in integral causality have measurement sensors being represented by *effort* detector or *flow* detectors. The detectors are modeled by *De* or *Df* elements representing the effort detector and flow detector respectively. The effort detector is always connected to 0-junction and measures the common effort between all the bonds connected to it whereas, flow detector is always connected to 1-junction measuring the common flow between all the bonds connected. For diagnosis, the detectors are dualized which means that the effort detector *De* becomes a signal source of effort *SSe*, and imposes the effort at the 0-junction connected to the detector. Similarly, flow detector *Df*, becomes *SSf* and imposes flow at the 1-junction connected to the detector. This transformation of detectors as signal sources is defined as detector dualization. The procedure is illustrated in Fig. 1.12.

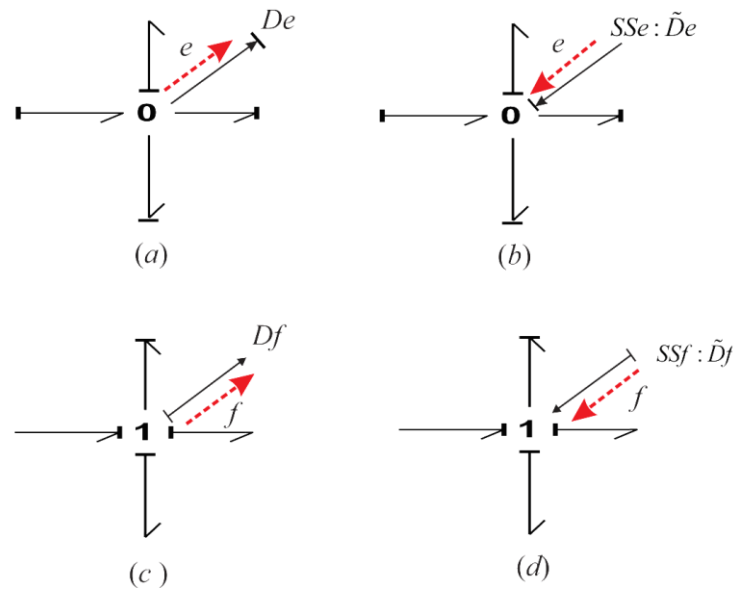


Fig. 1.12 (a). Effort detector De (b). Source of effort SSe
(c). Flow Detector Df (d). Source of flow SSf

Causality Inversion approach for deterministic ARR generation: The ARR is derived systematically through inversion of causality as described in Ould Bouamama et al. (Bouamama et al., 2003).

In the context of BG modelling, an $ARR: f(SSe, SSf, Se, Sf, MSe, MSf, \theta)$ where θ is vector of system parameters. Causality inversion approach is summarized as:

Step 1: Diagnostic BG is obtained by assigning preferred derivative causality to the BG model and causality of detectors is inverted wherever possible.

Step 2: Structural constraints at junctions associated to dualized detectors are written.

Step 3: For each of the 0 (or 1) junctions with at least an associated detector:

- Causal path is covered to eliminate unknown variables such that in the constraint relationship is sensitive to only known and measured variables. Causal paths are covered from unknown to known (measured) variables.
- In case of redundant sensors : If there are direct causal paths from one or more detectors in inverted causality SSf (SSe) to the non-inverted one Df (De), without passing through any passive or two-port element, the ARRs are equal to the difference between the measures of the redundant sensors.

For illustration purpose, the procedure described is applied on the pedagogical DC motor model presented in Section 1.4.3.1, as follows:

Step 1: As shown in Fig. 1.13, Diagnostic BG is obtained by inverting the causality of BG model in Fig. 1.11 to a preferred derivative causality. Detectors are dualized to form respective signal sources.

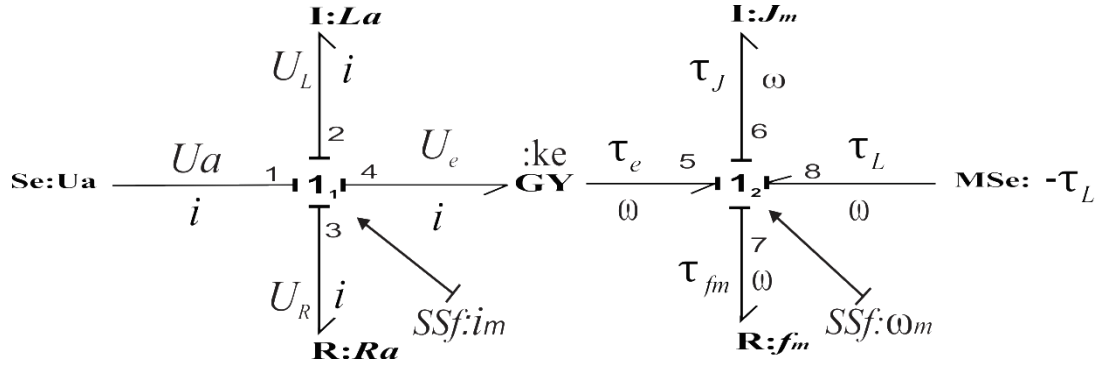


Fig. 1.13 Diagnostic BG model in preferred derivative causality

Step 2: From (1.3), Structural equations at junction 1_1 and 1_2 respectively are:

$$\begin{aligned} C_{1_1} : U_L(t) - U_a(t) - U_R(t) - U_e(t) &= 0 \\ C_{1_2} : -\tau_J(t) - \tau_L(t) - \tau_{fm}(t) + \tau_e(t) &= 0 \end{aligned} \quad (1.4)$$

Step 3: The causal paths covered independently at both the junctions along with derived ARR are tabulated in Table 1-IV.

Table 1-IV Causal paths covered and obtained ARR expressions

Causal path covered	ARR obtained:
$U_R \rightarrow C_{Ra} \rightarrow i \rightarrow C_{i_m} \rightarrow SSf : i_m$ $U_L \rightarrow C_{La} \rightarrow i \rightarrow C_{i_m} \rightarrow SSf : i_m$ $U_e \rightarrow C_{GY} \rightarrow \omega \rightarrow C_{\omega_m} \rightarrow SSf : \omega_m$ $U_a \rightarrow Se : U_a$	$ARR_1 : U_a(t) - Ra.i_m(t) - La \frac{di_m(t)}{dt} - ke.\omega_m(t) \quad (1.5)$
$\tau_{fm} \rightarrow C_{fm} \rightarrow \omega \rightarrow C_{\omega_m} \rightarrow SSf : \omega_m$ $\tau_{Jm} \rightarrow C_{Jm} \rightarrow \omega \rightarrow C_{\omega_m} \rightarrow SSf : \omega_m$ $\tau_e \rightarrow C_{GY} \rightarrow i \rightarrow C_{i_m} \rightarrow SSf : i_m$ $\tau_L \rightarrow MSe : \tau_L$	$ARR_2 : -\tau_L(t) - fm.\omega_m(t) - Jm \frac{d\omega_m(t)}{dt} + ke.i_m(t) \quad (1.6)$

Residual r , is the evaluated value of ARR, $r = Eval(ARR)$. For fault detection, theoretically, if $r=0$, fault is not detected. Otherwise, with $r \neq 0$, fault is detected.

1.4.3.3 Fault Isolation

A Boolean fault signature is formed by the residual structures and represents the structural sensitivity of faults on the residuals. Fault Signature Matrix (FSM), $FSM \in \mathbb{R}^{m \times (n+2)}$ is a Boolean table, containing fault signature vectors, fault monitorability vector and fault isolability vector (Medjaher, K. et al., 2006; Touati et al., 2012b) with $m =$ number of components considered and $n = Card(ARRs)$.

Each entry of the FSM (s_{ji}) constitutes of Boolean values. The fault signature vector (V_{E_j}) of the j^{th} component $E_j (j=1, \dots, m)$ is determined by row vector $V_{E_j} = [s_{j1}, s_{j2}, \dots, s_{jn}]$. s_{ji} is assigned value as,

$$s_{ji} = \begin{cases} 1, & \text{if } r_i \text{ is sensitive to a fault in the component } E_j \\ 0, & \text{otherwise} \end{cases} \quad (1.7)$$

where $i = 1, \dots, n$.

Thus, it is implied that if $s_{ji} = 1$, a fault in the component E_j influences the residual r_i or r_i is triggered. On the contrary, if $s_{ji} = 0$ then, a fault in component E_j cannot trigger the residual r_i . Moreover, ability to monitor a specific fault in a specific residual is assessed by fault monitorability vector $M_b = [m_{b1}, m_{b2}, \dots, m_{bm}]^T$. A component fault E_j is monitorable if at least one s_{ji} , of its signature vectors V_{E_j} , is different from zero i.e. $\exists i | (i = 1, \dots, n), s_{ji} \in V_{E_j} \neq 0$.

Isolability vector $I_b = [i_{b1}, i_{b2}, \dots, i_{bm}]^T$ assesses whether a fault candidate is isolable or not. A component fault E_j is isolable if its signature vector V_{E_j} is different from all other signature vectors. The elements of isolability vector I_b take Boolean values as,

$$i_{bj} = \begin{cases} 1, & \text{if } \forall l | (l = 1, \dots, m), l \neq j : V_{E_j} \neq V_{E_l} \\ 0, & \text{otherwise} \end{cases} \quad (1.8)$$

Table 1-V Fault Signature Matrix (FSM)

$j \setminus i$	r_1	r_2	\dots	r_n	M_b	I_b
E_1	s_{11}	s_{12}	\dots	s_{1n}	m_{b1}	i_{b1}
E_2	s_{21}	s_{22}	\dots	s_{2n}	m_{b2}	i_{b2}
\cdot	\cdot	\cdot	\cdot	\cdot	\cdot	\cdot
\cdot	\cdot	\cdot	\cdot	\cdot	\cdot	\cdot
\cdot	\cdot	\cdot	\cdot	\cdot	\cdot	\cdot
E_m	s_{m1}	s_{m2}	\dots	s_{mn}	m_{bm}	i_{bm}

Considering the DC motor example, FSM is created as shown in Table 1-VI by taking into account the residual given by ARR₁ in (1.5) and (1.6). It can be seen that all the fault candidates are monitorable. However, none is isolable.

Table 1-VI Fault Signature Matrix of pedagogical DC motor model

Fault Candidates	$ARR_1 : r_1$	$ARR_2 : r_2$	M_b	I_b
$Df : i_m$	1	1	1	0
$Df : \omega_m$	1	1	1	0
$Se : Ua$	1	0	1	0
$R : R_1$	1	0	1	0
$I : La$	1	0	1	0
$R : fm$	0	1	1	0
$I : Jm$	0	1	1	0
$GY : ke$	1	1	1	0

1.4.4 Robustness in Model Based Diagnosis

Minimization of effects of uncertainty lies as the main focus in several domains of engineering. As defined in Chen et al. (Chen, J et al., 1999), the robustness problem is defined as the maximization of the detectability and isolability of faults together with the minimization of the effect of the uncertainty and disturbance on the FDI procedure.

The uncertainties are brought in by many sources such as uncertain system parameters, variable environmental conditions, variable operational routines, measurement noise, etc. These factors can be seen arising mainly due to the difference between the intrinsic properties

of the systems/components and their explicit available knowledge and associated noises. Some examples are:

- Complete information for an accurate mathematical model is rarely available. This percolates in form of non-precise information on system structure, system parameters etc.
- System parameters usually vary with time in an unpredictable manner and with varying environmental/operational conditions.
- Noises in the measurement acquisition process, bias, drift, non-linearity, inaccuracy due to calibration process etc.

Such factors and many more, constitute the discrepancies that cause mismatch between the actual process and the system model even under no fault conditions. The latter gives rise to missed alarms and false alarms (Chen, J & Patton, 1999).

From MBD context, many approaches have been developed to make the diagnostic process sensitive to faults only. Mainly two kinds of approaches can be distinguished as:

- **Active approaches** refer to methods that tend to make residuals insensitive to uncertainty but sensitive to faults. This is usually achieved by decoupling the residuals from uncertainties. Some of the methods developed are representation of model uncertainties as unknown inputs (Chen, Jie et al., 2012b; Hamelin et al., 2000), structured uncertainties (Kam et al., 2005), higher order terms (of linearized model around a set-point) as unstructured uncertainties (Kinnaert, 1999), using set of models representing different parameter settings and using frequency domain models (transfer functions) with parameters in intervals (Hamelin & Sauter, 2000) etc. Most of these approaches are applicable to select class of non-linear models. For general class of non-linearity and unclassified disturbances, specific methods need to be developed. A brief discussion in this context can be found in Samantaray et al. .
- **Passive approaches** refer to methods where the effect of uncertainty is not perfectly decoupled, instead is propagated in the residual. They correspond to decision making strategy by propagating the model uncertainties to the residuals, where the uncertainty is bound by an interval. In other words, thresholds are used to check its containment. As long as the residual remains under the prescribed limits set by thresholds, the change in residual does not imply a faulty condition, as the latter may

be caused due to a genuine fault or uncertainties. Thereafter, decision rules may be formulated based upon simple threshold tests on instantaneous residual values or their moving average using adaptive thresholds (Emami-Naeini et al., 1988),(Rambeaux et al., 2000; Shi et al., 2005), interval models (discussed in Section 1.4.4.2 and 2.2), cumulative sums (Basseville et al., 1993) or statistical methods such as generalized likelihood ratio test or sequential probability ratio test (Niu et al., 2015; Tartakovsky et al., 2014).

The obvious advantages are that non-linearity of the system does not pose any constraint on threshold generation. Moreover, system representation does not need to be altered. However, the associated disadvantage is that weak faults may lead to non-detection. Additionally, the threshold width determines the chances of missed detection. As such, it becomes imperative to develop the adaptive bounding thresholds in the most efficient way.

In BG framework, Bond graphs in Linear fractional Transformations (BG-LFT)(Dauphin-Tanguy et al., 1999) have been widely utilized for robust fault detection. In this work, bounding approaches employing interval models, in particular, interval arithmetic (Moore, 1979), are used to develop efficient thresholds in conjunction with BG-LFTs. Thus, these two approaches are briefly reviewed. However, the discussion on threshold generation methodology using BG-LFT is provided in Appendix B.

Modelling of the parametric uncertainty and robustness in FDI has also been achieved through *Incremental* BG (Borutzky, Wolfgang et al., 2001, 2002), which are constructed systematically from the original BG by replacing the BG elements by their respective incremental models. The theory of incremental BG modelling is well developed (Borutzky, Wolfgang et al., 2004) and recently, robustness in FDI has also been approached for uncertain systems (Borutzky, Wolfgang, 2009b, 2011). As shown in (Borutzky, Wolfgang & Dauphin-Tanguy, 2004), the incremental bond graph approach is equivalent to the BG-LFT approach and a comparative study of both of the approaches can also be found therein.

1.4.4.1 Robust Fault detection using Bond Graphs in Linear Fractional Transformation (BG-LFT)

LFT was introduced by Redheffer as a mathematical model (Redheffer, 1960). On BG models, it was introduced by G. Dauphin-Tanguy in 1999 (Dauphin-Tanguy & Kam, 1999) to model the structured parametric uncertainties. As detailed in Kam et al. (Sié Kam et al.,

2005), BG-LFT is the methodology of describing parametric uncertainties on BG elements. The latter also details the characterization of parametric uncertainties in LFT form. Various details about BG-LFT modelling and its representation, is provided in Appendix B. Also, the fault detection method along with threshold generation strategy is described therein. Readers unfamiliar to BG-LFT technique are strongly suggested to go through it before proceeding ahead.

In this methodology, the additive and multiplicative parametric uncertainties are propagated into the ARR such that, the residual consists of two perfectly separable parts: a nominal part r , that describes the system operation/behavior and an uncertain part a , which is used to generate an adaptive envelope around the residual. As such, the residual is sensitive to faults and remains robust to considered parametric uncertainty. Summation of the absolute values of uncertain effort/flow $\sum |w_i|$, brought in by parametric uncertainties at the respective BG junction and sensitive to the respective ARR, determines the values of the lower and upper limits/thresholds of the envelope as $-\sum |w_i|$ and $\sum |w_i|$ respectively, thus bounding the nominal residual as $-\sum |w_i| \leq r \leq \sum |w_i|$.

Past one decade has seen an extensive use of BG-LFT based methodology for FDI of uncertain systems which was introduced in Djeziri et al. (Djeziri, Mohand Arab et al., 2007) for detection of backlash phenomenon in mechatronic systems. The BG-LFT model of uncertain system is considered in derivative causality to facilitate the derivation of ARRs, not containing any unknown variables (system initial conditions). The effects of parametric uncertainties are compensated for, by the use of adaptive thresholds. The envelope thus generated, serves the purpose of efficient *passive* diagnosis. BG-LFT methodology has been widely exploited for robust FDI and employed on various kinds of uncertain systems. For example, in (Djeziri, Mohand Arab et al., 2009b), BG-LFT model of uncertain steam generator is used for robust FDI, (Djeziri, M. A. et al., 2009a) describes the robust monitoring of an electric vehicle, (Niu et al., 2014) employs BG-LFT based modelling and fault detection and auto-regressive kernel regression based threshold monitoring, (Loureiro et al., 2014) uses BG-LFT generated thresholds for robust FDI of autonomous vehicles. Recently, Touati et al. (Touati et al., 2012b) extended the methodology by including measurement uncertainties on BG-LFT model so that both parametric and measurement

uncertainties may be propagated to thresholds for robust FDI. A case of under-constrained system with causality conflict can be referred in (Djeziri, M. A. et al., 2009a).

Advantages of BG-LFT for robust fault detection are many, such as:

- Structured graphical representation of parametric uncertainties on the nominal BG.
- Systematic procedure of decoupling ARR into nominal residual and uncertain part.
- The method is not bound by any limitation arising due to non-linearity of the system.
- Can be applied to real systems without any numerical complexity.
- Can be applied to complex multi-energetic systems.

Even though there has been a wide and successful implementation of the BG-LFT method for FDI in various domains of engineering, little efforts have been put in studying and developing the method of threshold generation itself. Width of thresholds determines their sensitivity to fault. An over-estimation in threshold calculation (complete but not sound) may result in missed alarms (non-detection of fault) whereas; false alarms are caused when width is too sharp (sound but not complete)(Armengol et al., 2001).

Limitations of this method arise mainly due to the fashion by which thresholds over the nominal residual are generated. Existing methodology generates threshold by the summation of the absolute values of uncertain effort/flow as $-\sum |w_i| \leq r \leq \sum |w_i|$. Such an approach is pretty naïve in accounting the cumulative effect of uncertain effort /flow brought in at the junction as:

- The parametric uncertainty bounds considered for threshold generations are necessarily symmetrical owing to their modelling discussed above. With threshold limits being simply the summation of their absolute values, this leads to over/under estimation of threshold limits and them being necessarily symmetrical in nature. Such an over-estimation can be high and non-negligible when parameters that deviate only uni-directionally (like friction) are involved.
- The methodology of bounding the nominal residual is pretty naïve in accounting the cumulative effect of uncertain effort /flow brought in at the junction as, the residual may be sensitive, positively or negatively, with respect to the parametric fault. It is referred to as *sensitivity* s_{ij} (Calderón-Espinoza et al., 2007; Chang et al., 1994), of the model associated with j^{th} ARR, r_j , with respect to i^{th} fault, f_i ,

mathematically expressed as in (1.9), is function of process measurements and system parameters.

$$s_{ij} = \frac{\partial r_j}{\partial f_i} \quad (1.9)$$

1.4.4.2 Bounding approaches

Bounding approaches typically use interval models to model the uncertain system variables, parameters etc. Interval models allow variation of the interval variable within pre-defined numeric intervals (Moore, 1979). These approaches have been extended and developed in various forms, each having their own merits and de-merits and broadly, fall under bounding approaches which present an alternative to the statistical ones that assume probabilistic description of uncertainty. From robust fault detection's perspective, interval techniques have been developed in various ways each having their own distinguishing philosophy as discussed below:

- Classical interval analysis : This approach uses interval arithmetic(Moore et al., 2009), to infer the results involving interval models. Consisting of well-developed techniques, it has been used widely for various purposes such as reliable computing (Lin et al., 2007), global optimization(Hansen et al., 2003) etc. For FDI purposes, some works are (Karim et al., 2008; Rinner et al., 2004). Interval analysis has not been exploited widely for FDI, mainly owing to the fact that in presence of multi-incident interval variables it provides over-bounded results(not complete and sound) (Armengol Llobet, 2000). However, in absence of multi-incident interval instances, exact results can be achieved.
- Modal intervals: is completion of interval analysis in arithmetic sense and lattice sense. It involves the notion of “dual” intervals that reduce and nullify the over-boundedness of the results obtained in presence of multi-incident intervals (Armengol et al., 2001; Armengol Llobet, 2000; Herrero et al., 2012),(Sainz et al., 2014).
- Set membership approaches: These methods explicitly calculate the outer bounds of the set of parameters of the interval model that are consistent with the real system measurement (Jaulin et al., 1993; Milanese et al., 2013). The feasible set of parameters is parameterized in form of: ellipsoids (Milanese et al., 1996),

parallelotopes (Chisci et al., 1996), polytopes (Janati-Idrissi et al., 2002), zonotopes .

1.5 Approaches of Prognostics

RUL prediction forms the core of any prognostic procedure. In this section, various approaches used for RUL prediction and associated issues are discussed with special emphasis on model based approaches and Bayesian techniques. In particular, non-linear Bayesian estimation using Particle filtering method is discussed, as the work presented in this thesis depends mainly on the same.

Due to versatility of the techniques used in recent one decade, the prognostic approaches have been classified in various ways (ISO13381-1, 2004; Jardine et al., 2006; Lee et al., 2006; Liao, S.-H., 2005; Vachtsevanos, George et al., 2007) etc. Also, there is little consensus among the reviewers upon the uniformity of the diverse classifications. The recent literature review in Sikorska et al. (Sikorska et al., 2011) describes this aspect in detail by listing the various classification groups along with the references that propose the same. Therein, a classification approach is proposed specifically designed for RUL prediction. For informational purposes, the latter is shown in Fig. 1.15.

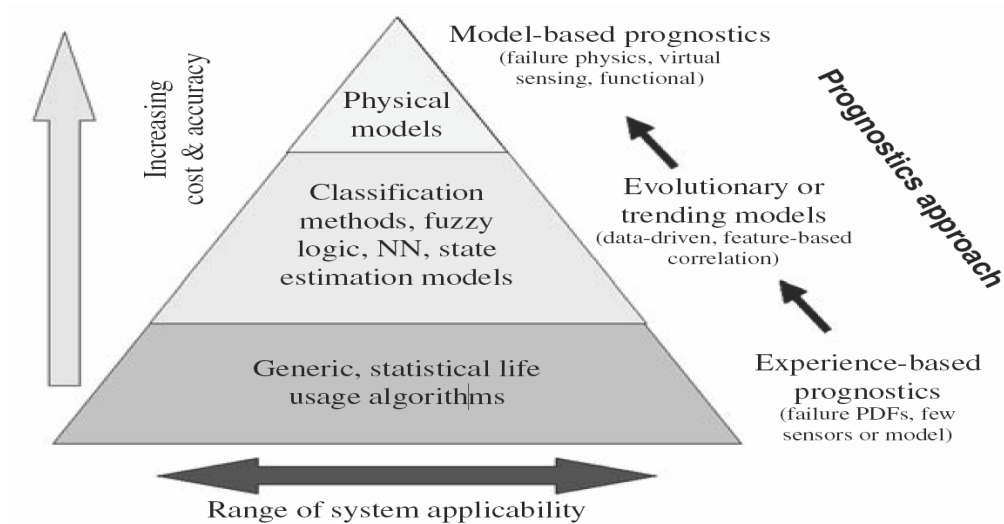


Fig. 1.14 Prognostic approaches classified in Vachtsevanos et al. (Vachtsevanos, George et al., 2007)

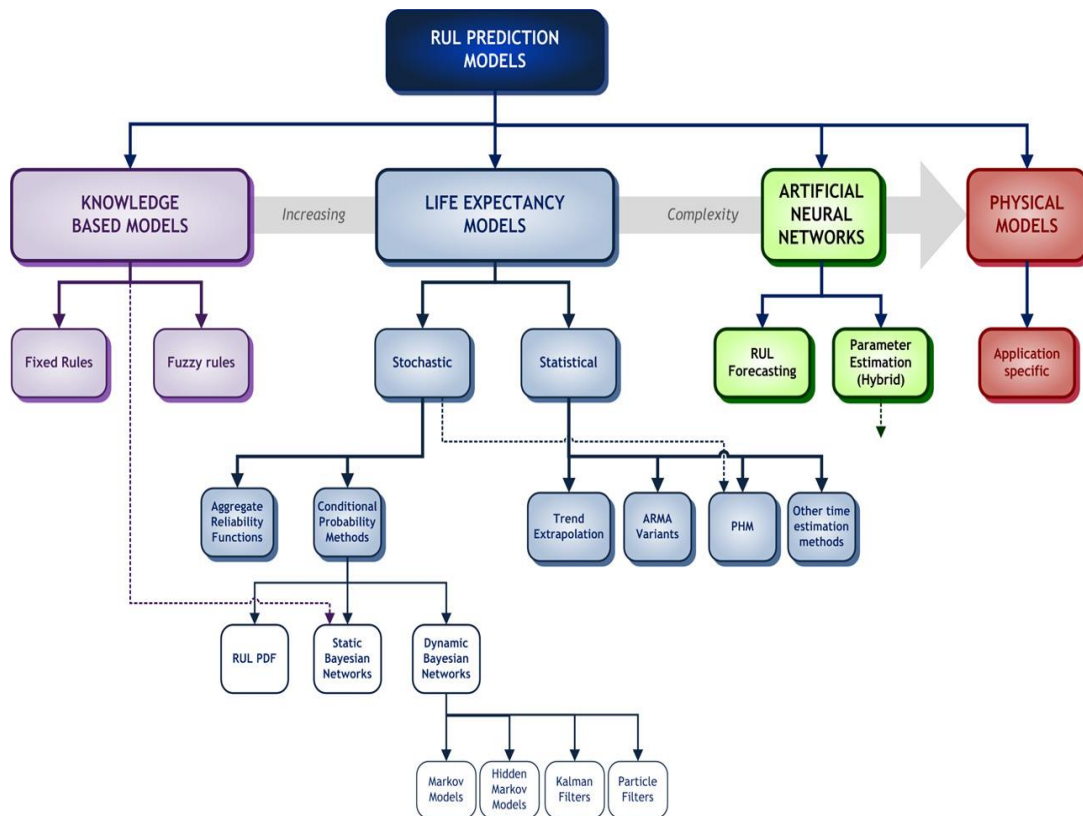


Fig. 1.15 A recent prognostic models classification described in Sikorska et al. (Sikorska et al., 2011)

1.5.1 Experience based Approaches

These approaches depend upon the statistical information collected that assess the historical failure rate of the components. Such data is used to develop life-usage models in terms of distributions of failure rates over time. Mean time between failures (MTBF) is indicated primarily by such models and plays the crucial role of scheduling the preventive/maintenance actions. In essence, the life expectancy of the component is derived from the observed actual condition and the database of previous failure events. Some of methods in this category include:

Expert Systems: Generally based on heuristic facts obtained by experts over a period of time and accumulated experience, these systems consist of a huge knowledge data that apply a particular rule (mostly if-then type statements) to particular problems encountered. Of course, here the precision and accuracy in building the knowledge base is the key aspect (Biagetti et al., 2004). Major disadvantages include the problem of combinatorial explosion encountered in presence of numerous inputs and desired outputs (Garga et al., 2001). Also, the efficiency is limited to efficiency of the experts form the data base.

Life expectancy models: These models usually employ probability based models to assess the RUL. This approach is motivated by the fact that often the historical failure data take statistical form. As such, obtaining the information needed for prognosis becomes a fairly an easy task mainly because most of the required information reside in probability density functions (e.g. confidence limits). There is a plethora of literature on application of statistical distributions to model failure data (Blischke et al., 2011; Helton, 1993; Rausand et al., 2004). Such models assume that the times to failure of identical components can be considered statistically identical and independent random variables and thus be described by a PDF (Sikorska et al., 2011; Vachtsevanos, George et al., 2007). Typically, the applied distributions to model failure data are Exponential, Normal, Lognormal, Gaussian and Weibull functions. Most commonly applied distribution in reliability engineering is the Weibull function mainly due to its ability to describe many different failure types. The classical bathtub curve (Klutke et al., 2003) as shown in Fig. 1.16, is most commonly described as a piecewise function composed of three regions (hazard functions,): $\beta < 1$ signifies hazard rate increasing (wear-in or infant mortality failures), $\beta = 1$ signifies hazard rate constant (random failures) and finally, $\beta > 1$ again signifies increase of hazard rates (wear-out failures). Failure data are fitted to the Weibull distribution(s) using various techniques such as parameter estimation methods, least squares, moments and maximum likelihood etc. Major limitations of this approach are:

- Accurate curve fitting demands a considerably large sample set of failures incurred during extensive testing or operations.
- In situations when the component degradation process is variable or failure distribution is exponential, reliability analysis on its own proves insufficient for accurate RUL prediction.
- As the failure trend is generalized over large sets of population, obtaining an accurate RUL prediction on individual component unit to unit basis is generally unreliable.

1.5.2 Data-Driven Techniques

Data-driven prognostic approaches usually apply one of two strategies: The first strategy consists of a two-stage process. Firstly, appropriate dimensionality reduction (e.g. Principle component Analysis etc.), feature extraction, or pattern matching techniques are used to map system signals or features onto a single dimension damage, degradation, or health index.

Upon identification of the actual/current state of damage, the signals are extrapolated in future until a pre-fixed threshold is exceeded or reached. Various approaches fall under such a strategy such as trend extrapolation, time-series prediction etc. The second strategy comprises of using directly modelling the relationship between monitored signals or features, and the remaining life of the system. This in turn calls for machine learning techniques where degradation pattern, damage progression is learnt to train mathematical models. With the help of accurately trained models, the RUL is predicted. Employment of artificial neural networks (ANNs) and their numerous variants fall under this category. A comprehensive review about data-driven techniques can be found in .

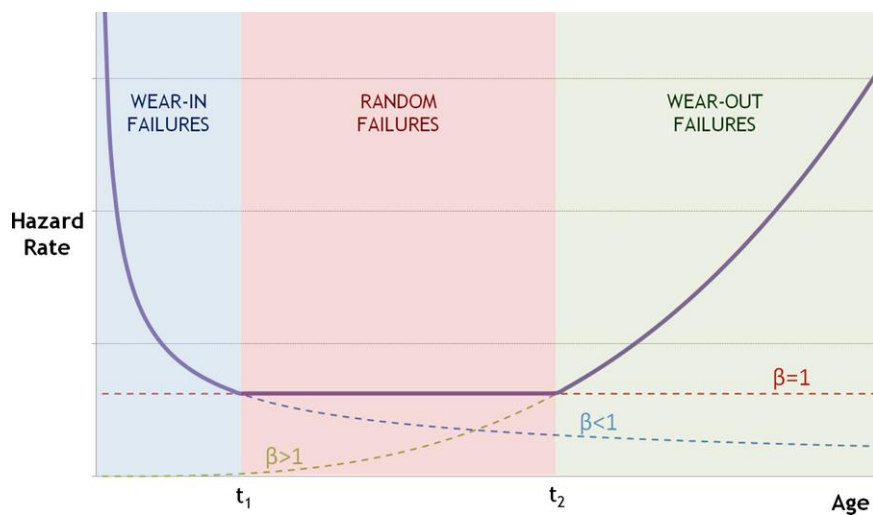


Fig. 1.16 Classical bathtub curve (Sikorska et al., 2011)

Trend evaluation: Forming the simplest form of data-driven techniques, the RUL is predicted based upon the trend analysis of single monotonic parameter. The chosen parameter is plotted as function of time and is extrapolated or interpolated using standard regression techniques, till a pre-defined threshold is reached. As such, they are not efficient with damage progressions that are noisy, non-monotonic, highly non-linear, with variable deterioration rates or multiple failure modes (Engel et al., 2000).

Time series forecasting: The issue of RUL prediction posed as time-series forecasting problem is addressed by variety of autoregressive models (Wu et al., 2007) and exponential smoothing techniques (Byington et al., 2002). Autoregressive moving average (ARMA), Autoregressive integrated moving average (ARIMA) and ARMAX models have been widely

exploited for prognostic problems as the latter shares the common objective of prediction or forecasting (Box et al., 2011). In all cases, the future value is assumed a linear function of past observations and random errors. Each of these three types of autoregressive models vary slightly in the linear equation used to relate inputs, outputs and noise. ARMA and ARMAX models can remove temporal trends, and hence, they are used only for stationary data. On the other hand, ARIMA models enforce integration and thus are able to handle systems with low frequency disturbances or trends (Sikorska et al., 2011). The ARMA models and associated variants are generally useful for short-term predictions. They prove less reliable for long-term predictions owing to the dynamic noise, poor uncertainty management for prediction, issues arising out of initial conditions and accumulation of errors in the predictor (Wu et al., 2007).

Artificial Neural Networks (ANNs): ANNs are perhaps the most used and exploited data-driven models for prognostics. ANNs model the relationships between input and output variables with a model structure inspired by the neural network structure present in the brain. The network weights and biases, which define the inter-connections between the neurons, are adapted during a training process to maximize the fit between the input and output data on which the models are trained. ANNs are widely employed in conjunction with time series modelling to predict the future state of component health based upon current state given by the ANNs. Then, RUL is predicted based upon the pre-fixed threshold. Usually employed feed-forward ANNs, estimate the current degradation index (state) by using system features (extracted signals, feature pattern etc.) as inputs. They generate the one step ahead prediction by using the previous values of state of degradation (degradation index). The next iteration then uses this prediction to produce long term predictions. Examples of such applications on ANNs for prognostics can be found in (Herzog et al., 2009; Vachtsevanos, G et al., 2001). The application of dynamic wavelet neural network (DWNN) for prediction of RUL can be referred in (Wang, P. et al., 2001). The DWNN is an example of recurrent neural network (RNN) that incorporate feedback within network structure to predict the time series evolution. The applications of the latter for prognostics can be found in literature (Heimes, 2008; Tian, 2012). Also, attempts in modelling and establishing a direct relationship between system features and RUL have been successfully made .

Although this approach promises reliable results given the ANN models are accurately trained, it has major drawbacks as:

- ANN models must be trained and they learn by examples. As such, enough and sufficient number of failure instance examples are required for an accurate training.
- A poorly trained ANN generally gives bad prediction performance. Moreover, well trained models too remain vulnerable to bad/non-acceptable performances when faced with damage progression behavior or failure instances, for which they were not trained.
- Additionally, ANNs generalize the system behavior (degradation progression trend) to the whole component population. Varying failure modes, varying failure rate etc. lead to large individual unit to unit variations. In such cases, ANNs performance remains unsatisfactory.

A plethora of other techniques can be found such as Gaussian process regression (Goebel et al., 2008), Gaussian-hidden Markov models (Tobon-Mejia et al., 2012), ensemble techniques (Hu, C. et al., 2012), techniques depending upon scope of information available (Baraldi et al., 2013a), relevance vector machine techniques (Caesarendra et al., 2010; Widodo et al., 2011; Zio et al., 2012), logistic regression techniques (Caesarendra et al., 2010), neuro-fuzzy logic based methods etc.

A comprehensive and latest review of various data-driven techniques are found in (An et al., 2015; Tsui et al., 2015).

1.5.3 Model Based Prognostic Approaches

The model based approaches constitute the highest hierarchical level in the pyramidal structure of prognostic approaches (see Fig. 1.14) signifying their capability of attaining maximum accuracy and versatility (scope of adaptation to problem variables) as well as incurred cost.

Typically, physics-of-failure models of the prognostic candidate component derived from first principles of physics, have been used extensively under this category. There exists an extensive literature employing fatigue models for modelling the initiation and propagation of cracks in structural components (Cadini et al., 2009; Swanson et al., 2000; Zio et al., 2011), model for electrolytic overstress related ageing (Celaya et al., 2011), usage of Arrhenius equation for prediction of resistance drift in thin film resistors (Kuehl, 2010), usage of physics inspired power model (Maricau et al., 2009) or log-linear model (Lu et al., 1997) for

degradation of current drain in CMOS (complementary metal-oxide semi-conductor) and usage of physics-inspired exponential degradation model for aluminum electrolytic capacitors in (Kulkarni et al., 2012). Vachtsevanos et al. (Vachtsevanos, George et al., 2007) have included time-series models such as ARMA, ARIMA, ARMAX etc as model based approaches. However, as such models do not enhance the understanding of the physics of underlying degradation and instead are data-based; they have been discussed in Section 1.4.1.

With the model of degradation available, this approach popularly employs various recursive Bayesian estimation techniques to estimate the current state of health (parameter estimation method) and to predictions of RUL. Such a framework involving recursive Bayesian techniques, efficiently addresses the issues related to state of component health under variable degradation progression, uncertainty management for RUL prediction with respect to noisy environment, variable operational loads etc. by efficiently fusing the information from model, obtained observations, uncertain future loading conditions etc. In Bayesian framework, the state of health is modelled as random variable such that the posterior estimate obtained in probabilistic terms, leads to efficient estimation of hidden damage progression, uncertainty quantification, confidence limits on RUL prediction etc. (Daigle, M. et al., 2010; Daigle, M. J. et al., 2011a, 2013; Roychoudhury et al., 2011). Various Bayesian estimators have been applied with successful outcomes. Fig. 1.17 comprehensively details the various estimators that have been employed depending upon the system at hand. Below, only a select few are reviewed concisely from prognostics purpose. Details about the same and others can be found in , and the numerous references therein.

Filter for estimation and prediction process is chosen depending upon the assumptions that may be made about the system and the desired performance (Daigle, M. et al., 2012). Well-known Kalman filter, an optimal estimator for linear systems has been used for prognostics in (Celaya et al., 2011). Extended Kalman filter (EKF) or unscented Kalman filter may also be used for joint state-parameter estimation as presented in (Plett, 2004) and (Daigle, M. J. et al., 2014) respectively. However, they remain restricted to additive Gaussian noise. Also, EKF being sub-optimal diverges quickly if the initial estimate of state is different from the reality by big measure or the model considered for estimation is not correct (Saha et al., 2009b).

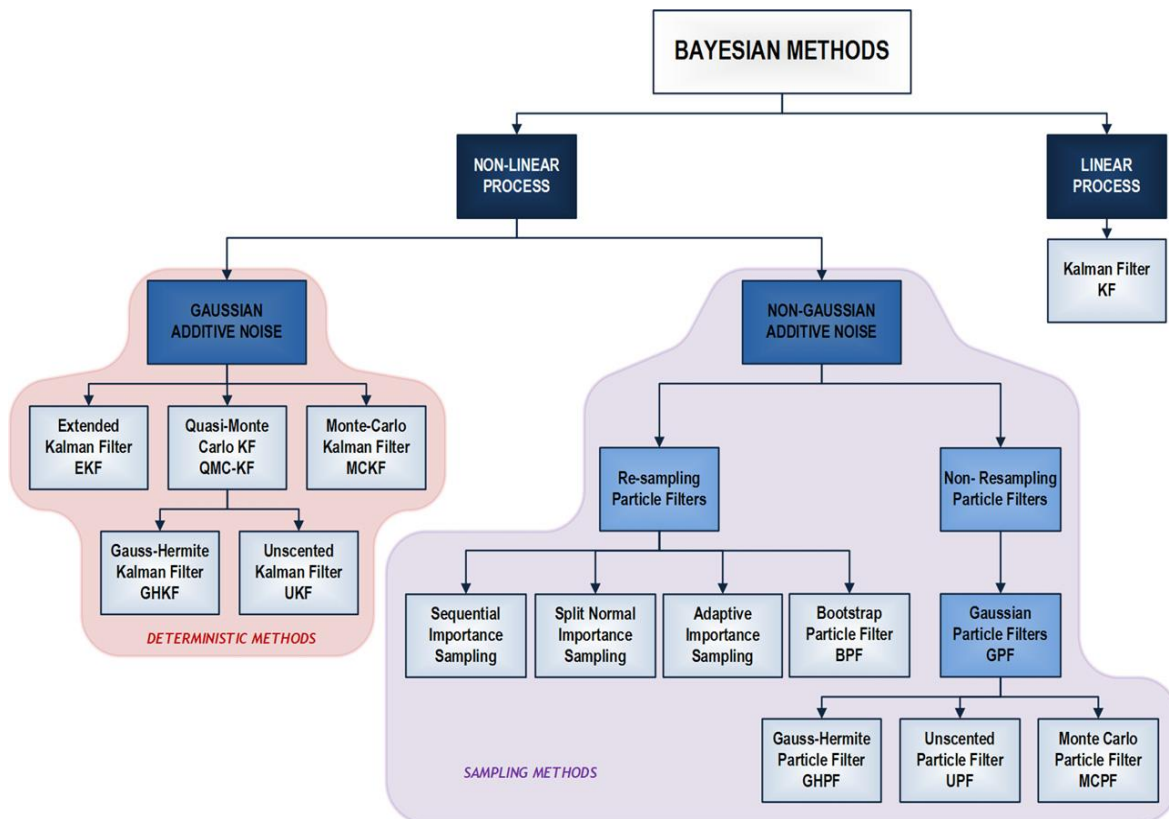


Fig. 1.17 Various estimation techniques to obtain the posterior distribution (Sikorska et al., 2011)

Set in Monte-Carlo framework, particle-filters (PF) or Sequential Monte Carlo methods (Arulampalam et al., 2002; Doucet et al., 2001), form a suitable filter choice in this context, as it can be applied to non-linear systems corrupted with non-Gaussian noises for which, optimal solutions may be unavailable or intractable. Comprehensive comparison of filters for prognostic purposes are found in (An et al., 2015), (Daigle, M. et al., 2012; Saha et al., 2009b).

Recently, particle filters have been exploited voraciously for prognostic methods (Orchard, M. E., 2007). Significant works include prediction of end of discharge and end of life (EOL) in lithium-ion batteries (Saha et al., 2009a), battery health monitoring (Saha et al., 2009c), prediction of battery grid corrosion (Abbas et al., 2007), estimation and prediction of crack growth (Bechhoefer, 2008; Cadini et al., 2009; Zio, 2012; Zio & Pelsoni, 2011), fuel cell prognostics (Jouin et al., 2014), application to damage prognostics in pneumatic valve from the Space Shuttle cryogenic refueling system (Daigle, M. & Goebel, 2010; Daigle, M. J. et al., 2011b), estimation-prediction of wear as concurrent damage problem in centrifugal pumps with a variance control algorithm (Daigle, M. J. & Goebel, 2013), employment in

distributed prognosis (Roychoudhury & Daigle, 2011), exploring uncertainty management options for prognostics (Baraldi et al., 2013b). Particle filters attract considerable attention (An et al., 2013), owing to the ever growing efforts being made for betterment in performances and computational efficiency, such as the use of correction loops (Orchard, M. et al., 2008), fixed-lag filters (Daigle, M. et al., 2009) and the recently proposed adaption of the degradation model with a kernel smoothing method (Hu, Y. et al., 2015).

The major advantage of model based approaches is that there is a clear understanding of the underlying degradation process. They have the ability to incorporate physical understanding of the process and the ability to make predictions under different loading and operational conditions. The major issue which must however be addressed is the accurate and reliable modelling of the degradation progression. Often, such accurate degradation models are not available.

1.5.4 Hybrid Prognostics

To overcome the problem of non-availability of highly accurate degradation models, there has been an attempt recently, to fuse the model based techniques and data-driven techniques in order to ameliorate the overall prognostic approach. Hybrid prognostic approaches have been introduced only recently, and benefit from the fusion of the advantages of the former two (Dragomir et al., 2007; Jouin et al., 2014; Kumar et al., 2008; Liao, L. et al., 2014; Neerukatti et al., 2014; Zhang et al., 2009).

Here, the first step usually involves identification of the failure mode, critical component or the subsystem that is undergoing degradation or is supposed to be monitored. Such system components/sub-systems can be identified as the potential degradation candidates through Failure Modes, Mechanisms and Effect Analysis (FMMEA) or otherwise (Kapur et al., 2014). Then, the degradation models (DM) that capture the underlying damage progression can then be obtained in various ways. Physics –of –failure models provide a certain kind of degradation models which are used in model based prognostics.

When the physics of failure is not well known and hence, the DMs at hand are not accurate or reliable, data-driven approaches and statistical based approaches can be employed to obtain the DMs. The DM can be obtained statistically by finding a mathematical model that best fits a given set of degradation data. In this context, commonly employed DM to fit the data are :

- Linear model: $D(t) = at + b$
- Logarithmic model: $D(t) = a \ln(t) + b$
- Power model: $D(t) = bt^a$
- Exponential model: $D(t) = b \times e^{at}$

where $D(t)$ can be any index representing the degradation (change, percentage change etc.) and a and b are the model parameters. For example, in (Celaya et al., 2011) percentage capacitance loss data from an observed accelerated test is used as the DM with the associated model parameters being determined through non-linear least square regression and noise variance given by associated regression residuals. In (Saha et al., 2009b), relevance vector machine regression is performed over parametric data collected during ageing tests of batteries to find the representative ageing curves and exponential growth models are fit over them to find suitable decay parameters which in turn, are estimated online for prognostication. In (Jouin et al., 2014) voltage drop is used as indicator of the ageing Proton exchange membrane fuel cell and degradation model is approximated by a linear part and logarithmic/exponential part.

Once the DM has been obtained with acceptable accuracy, recursive Bayesian techniques as discussed in Section 1.5.3 can be employed to estimate the current state of health. This way, benefits of Bayesian estimation are fused with data-driven or statistical approaches to let the obtained DMs adapt as the current information arrives sequentially.

1.5.5 Prognostics in BG Framework

Almost all of the previous attempts in BG framework to develop prognostics have been residual based (Djeziri, M. et al., 2013a; Djeziri, M. et al., 2013b; Medjaher, Kamal et al., 2009, 2013; Yu et al., 2011). These are very few in number and consider the progression of damage deterministic in nature.

In fact, all the previous attempts have been unsuccessful in adapting to the current progression of damage. Moreover, the RUL is obtained without confidence limits which makes such predictions highly unreliable for industrial certification and critical applications (Saxena et al., 2010; Uckun et al., 2008). Additionally, the uncertainties associated with measurements, operating conditions, process noise etc. have not been taken into account. In

summary, the previous attempts in BG framework have not been successful in providing efficient RUL predictions.

1.6 Conclusions

A comprehensive summary of previous works related to diagnostics and prognostics is provided in this chapter. Special emphasis is laid upon BG-LFT based diagnostics which has been widely used for robust diagnosis of uncertain systems. Limitations of BG-LFT based diagnosis have been highlighted. Interval based methods have also been discussed concisely to provide a suitable background for the next chapter in which the benefits of BG-LFT method are integrated with properties of Interval arithmetics to develop a novel method for diagnostics of uncertain systems.

Also, a comprehensive summary of various prognostics approaches has been provided. Special stress has been laid upon model based prognostics and hybrid prognostics and the related works are extensively reviewed. Existing approaches in BG framework have been highlighted and their significant limitations have been discussed. This is done primarily to justify the second major objective of this thesis, which is the development of efficient prognostics in BG framework.

2. Robust Fault Detection with Interval Valued Uncertainties

A mathematical model of any real system is in reality, just an approximation of the true, physical reality of the system dynamics. There is always the scope of discrepancy between the model of the system and the actual dynamics of the system in reality. The discrepancy between the physical system and the mathematical model is due to two main reasons: the lack of information on the behavior of the physical system; and the need for a simplistic model so that available analytical tools may be applicable. Typical sources of the discrepancy include unmodelled (usually high-frequency) dynamics, neglected non-linearities in the modeling, effects of deliberate reduced-order models, system-parameter variations due to environmental changes etc. Dynamic perturbations/disturbances in many industrial control systems may also be caused by inaccurate description/modeling of component characteristics, torn-and-worn effects on plant components, or shifting of operating points, etc. Such perturbations may be represented by variations of certain system parameters over some possible value ranges (complex or real). They affect the low-frequency range performance and are called “parametric uncertainties”. Similarly, the variation in the sensor measurement errors over time is a known phenomenon, often modeled as sensor drift; error in sensor outputs, zero-offset errors etc. are commonly considered as measurement uncertainty. These modelling errors may adversely affect the stability and performance of a control system.

Such systems which are vulnerable to modeling defects, sensitive to unmodelled parametric variations, measurement uncertainties etc. are usually considered under the category of uncertain systems. In the BG framework, modeling of uncertain systems and their robust FDI has been approached via BG-LFT technique (described in Appendix B).

In this chapter, system parameters and measurements are considered as interval models in Bond Graph framework. The properties of Interval arithmetic are exploited for modeling uncertain system parameters and uncertain measurements, as interval models. The various structural and causal properties of BG-LFT technique are borrowed and integrated with interval models for a systematic graphical representation of system with interval valued uncertainties. Such a representation leads to a systematic derivation of Analytical Redundancy Relationships (ARR) relations sensitive to interval valued system parameters

and system measurements. Such ARR relations are termed as Interval valued Analytical Redundancy Relationships (I-ARRs). Then, Interval Arithmetic properties are exploited to obtain a nominal part and an interval valued part from the I-ARR expression. A novel methodology for robust fault detection is developed by utilizing the rules of interval arithmetic for the generation of robust adaptive interval valued thresholds over the nominal residuals. This way, the benefits of bounding approach and BG are integrated for better diagnosis of uncertain systems. The developed methodology is implemented on an uncertain steam generator system in real time. The uncertain BG of the system is described and I-ARRs are derived. Moreover, a comparative study is done between BG LFT enabled thresholds and I-ARR enabled thresholds via experimental results.

2.1 Assumptions

In this chapter, following assumptions are made:

- System parameters/components are uncertain.
- Sensor measurements (outputs) are uncertain
- Actuator/control inputs are not uncertain

Moreover, it is assumed that the BG-LFT model of the uncertain system under consideration can be constructed. This in turn, implies that the mathematical model is proper and observable (Sié Kam & Dauphin-Tanguy, 2005). The BG methodology allows by causal manipulations, the verification of these properties directly on the BG model (Sueur et al., 1989).

2.2 Interval Arithmetic: A Brief Discussion

Interval Arithmetic (IA) deals with computations involving intervals defined as set of real numbers $\{x \mid \underline{X} \leq x \leq \bar{X}\}$ denoted here as $X = [\underline{X}, \bar{X}]$ in which \bar{X} is the supremum and \underline{X} is the infimum. The set of closed intervals is $I(\mathfrak{R}) = \{[a, b] \mid a, b \in \mathfrak{R}, a \leq b\}$. Being extension to real numbers; a real number x can be treated as the degenerate interval $[\underline{X}, \bar{X}]$ where, $\underline{X} = \bar{X} = x$. *Computing with interval is computing with sets.* Important properties of intervals and rules of interval arithmetic can be referred in (Moore et al., 2009). Here, only those properties and definitions are given that are relevant to the work described.

Definition 2.1 For the interval X , midpoint of X is given by

$$\text{mid}(X) = \frac{1}{2}(\bar{X} + \underline{X})$$

□

Definition 2.2 For any interval X , the width of the interval is defined and denoted by

$$\text{width}(X) = \bar{X} - \underline{X}$$

□

Property 2.1 Any interval X can be expressed as,

$$\begin{aligned} X &= \text{mid}(X) + \left[-\frac{1}{2} \text{width}(X), \frac{1}{2} \text{width}(X) \right] \\ &= \text{mid}(X) + \frac{1}{2} \text{width}(X) [-1, 1] \end{aligned}$$

□

Property 2.2 Interval Arithmetic Operations: For two intervals X and Y such that, $\{x | \underline{X} \leq x \leq \bar{X}\}$ and $\{y | \underline{Y} \leq y \leq \bar{Y}\}$

- $X + Y = [\underline{X} + \underline{Y}, \bar{X} + \bar{Y}]$
- $X - Y = X + (-Y)$
 $= X + [-\bar{Y}, -\underline{Y}] = [\underline{X} - \bar{Y}, \bar{X} - \underline{Y}]$
- $X \cdot Y = [\min S, \max S]$ where $S = \{\underline{X}\underline{Y}, \underline{X}\bar{Y}, \bar{X}\underline{Y}, \bar{X}\bar{Y}\}$
- $X / Y = X \cdot (1/Y)$

$$\text{where } 1/Y = \{y : 1/y \in Y\} = [1/\bar{Y}, 1/\underline{Y}]; 0 \notin Y.$$

□

Property 2.3 Inclusion Isotonicity of Interval Arithmetic: Let \odot stand for addition, subtraction, multiplication, or division. Then, if A, B, C and D are intervals such that, $A \subseteq C$ and $B \subseteq D$, then

$$A \odot B \subseteq C \odot D$$

□

Given a real function f of real variables $x = [x_1, x_2, \dots, x_n]^T$ belonging to intervals $X = [X_1, X_2, \dots, X_n]^T$ (Moore et al., 2009):

Definition 2.3: The *interval extension function* (IEF), $F(X)$, is any interval valued function that satisfies $F(x_1, x_2, \dots, x_n) = f(x_1, x_2, \dots, x_n)$. For degenerate interval arguments, the result must be the degenerate interval $[f(x_1, x_2, \dots, x_n), f(x_1, x_2, \dots, x_n)]$. \square

Definition 2.4: : *Natural interval extension* (NIE) F , of f is obtained, by replacing the real arguments with interval arguments and real operators (arithmetic etc.) by their equivalent interval operators, in the syntactic expression of the real function f . \square

Definition 2.5: We say that is $F = F(X_1, X_2, \dots, X_n)$ *inclusion isotonic* if

$$Y_i \subseteq X_i \quad \forall i = 1, 2, \dots, n \Rightarrow F(Y_1, Y_2, \dots, Y_n) \subseteq F(X_1, X_2, \dots, X_n) \quad \square$$

As such, for inclusion isotonic interval extension $F(X)$ such that $X = X_1 \cup X_2$, $R_f(X) \subseteq F(X_1) \cup F(X_2) \subseteq F(X)$ stands true. Thus, an IEF which is *inclusion isotonic* guarantees the exact range containment.

Definition 2.6: A *rational interval function* (RIF) is an interval-valued function whose values are defined by a specific finite sequence of interval arithmetic operations. \square

For example, for $x_1 \in X_1, x_2 \in X_2, x_3 \in X_3$, a function p defined as $p(X_1, X_2, X_3) = X_1 e^{X_1 - X_2^3 + X_3^2} + X_2^3$ can be computed through the finite sequences of interval arithmetic (in order) as $p(X_1, X_2, X_3): T_1 = X_2^3, T_2 = X_1 - T_1, T_3 = T_2 + X_3^2, T_4 = e^{T_3}, T_5 = X_1 \cdot T_4, T_5 + T_1$. Hence, p is a rational interval function.

Lemma 2.1: All rational interval functions are inclusion isotonic. Involving only interval arithmetic operators, which are inclusion isotonic, from the transitivity of partially ordered relation \subseteq , it follows that they are always inclusion isotonic. \square

Theorem 2.1 (Fundamental Theorem of Interval Analysis): If F is an inclusion isotonic interval extension of f , then $f(X_1, X_2, \dots, X_n) \subseteq F(X_1, X_2, \dots, X_n)$. \square

The corresponding *rational interval function* (RIF) can be found from NIE by expressing it as finite sequence of interval arithmetic operations as code list. As such, a RIF is inclusion isotonic and following result is obtained.

Corollary 2.1: If F is a rational interval function (RIF) and an interval extension function (IEF) of f , then $f(X_1, X_2 \dots X_n) \subseteq F(X_1, X_2 \dots X_n)$. \square

2.3 Modelling Uncertainties as Intervals

In this section, the novel modeling of parametric and measurement uncertainties in the interval form is described. Nominal model of any deterministic physical system may be modelled in BG form, in preferred integral causality, with nominal system parameters composed of basic elements with $\theta \in \mathbb{R}^{N_\theta}$ such that C, I, R, TY and GY are respectively the capacitance element vector, *inertial* element vector, *dissipation* element vector, *transformer* element vector and *gyrator* element vector. Sub-script n denotes the nominal value of the parameters. The sensor vector is formed by $\mathbf{Y}(t) \in [D\mathbf{e}(t), D\mathbf{f}(t)]^T$ with $D\mathbf{e}(t) \in \mathbb{R}^{N_{de}}$ being *effort sensor* vector and $D\mathbf{f}(t) \in \mathbb{R}^{N_{df}}$ being the *flow sensor* vector. The control/input vector is formed by $\mathbf{U}(t) \in [S\mathbf{e}(t), S\mathbf{f}(t)]^T$ with $S\mathbf{e}(t) \in \mathbb{R}^{N_{se}}$ and $S\mathbf{f}(t) \in \mathbb{R}^{N_{sf}}$ being respectively, the *source of effort* and *source of flow* vectors. In this section, uncertainty over nominal system parameters and measurements are modelled in interval form and represented on BG.

2.3.1 System Parameter Uncertainty

An uncertain system parameter θ , can be represented in interval form as,

$$[\underline{\theta}, \bar{\theta}] = [\theta_n - \Delta\theta_l, \theta_n + \Delta\theta_u] \quad (2.1)$$

$$\underline{\theta} = \sup \{a \in \mathbb{R} \cup \{-\infty, \infty\} \mid \forall \theta \in [\underline{\theta}, \bar{\theta}], a \leq \theta\} \quad (2.2)$$

$$\bar{\theta} = \inf \{b \in \mathbb{R} \cup \{-\infty, \infty\} \mid \forall \theta \in [\underline{\theta}, \bar{\theta}], \theta \leq b\} \quad (2.3)$$

The *lower bound* $\underline{\theta}$ is defined as in (2.2) and the *upper bound* $\bar{\theta}$ is defined as in (2.3), with *inf* and *sup* as the *infimum* and *supremum* operators respectively. $\Delta\theta_l$ and $\Delta\theta_u$ are the additive uncertainty/deviation on the left and right sides respectively, over its nominal value θ_n such that $\Delta\theta_l \geq 0$ and $\Delta\theta_u \geq 0$. Any parameter θ_n may be treated as a *degenerate interval* $[\theta_n, \theta_n]$,

with equal upper and lower bounds. This way, an uncertain parameter may be modelled as combination of its nominal interval value and uncertain additive interval as,

$$\left[\underline{\theta}, \bar{\theta} \right] = [\theta_n, \theta_n] + [-\Delta\theta_l, \Delta\theta_u] \quad (2.4)$$

The multiplicative form of representation of uncertainty is particularly useful for accounting relative uncertainty/errors. The *multiplicative interval uncertainty* denoted $\left[\underline{\delta}_\theta, \bar{\delta}_\theta \right]$, may be obtained as in (2.5), where $\Delta\theta_l \geq 0, \Delta\theta_u \geq 0$.

$$\left[\underline{\delta}_\theta, \bar{\delta}_\theta \right] = \left[-\Delta\theta_l/\theta_n, \Delta\theta_u/\theta_n \right] \quad (2.5)$$

Then, (2.4) may equivalently be written as,

$$\left[\underline{\theta}, \bar{\theta} \right] = \theta_n \cdot \left(1 + \left[\underline{\delta}_\theta, \bar{\delta}_\theta \right] \right) \quad (2.6)$$

In case the constitutive law is written in terms of $\frac{1}{\theta}$, it may be expressed as,

$$\left[\frac{1}{\underline{\theta}}, \frac{1}{\bar{\theta}} \right] = \frac{1}{[\theta_n - \Delta\theta_l, \theta_n + \Delta\theta_u]} = \frac{1}{\theta_n} \cdot \left(1 + \left[\underline{\delta}_{1/\theta}, \bar{\delta}_{1/\theta} \right] \right) \quad (2.7)$$

with $\theta_n \neq 0$; $0 \notin \left[\frac{1}{\underline{\theta}}, \frac{1}{\bar{\theta}} \right]$.

Value of $\left[\underline{\delta}_{1/\theta}, \bar{\delta}_{1/\theta} \right]$ is obtained from (2.7) by applying rules of Interval arithmetic as,

$$\begin{aligned} \left[\underline{\delta}_{1/\theta}, \bar{\delta}_{1/\theta} \right] &= \frac{\theta_n}{[\theta_n - \Delta\theta_l, \theta_n + \Delta\theta_u]} - 1 \\ \left[\underline{\delta}_{1/\theta}, \bar{\delta}_{1/\theta} \right] &= \left[\frac{\theta_n}{\theta_n + \Delta\theta_u}, \frac{\theta_n}{\theta_n - \Delta\theta_l} \right] - 1 \\ \left[\underline{\delta}_{1/\theta}, \bar{\delta}_{1/\theta} \right] &= \left[\frac{-\Delta\theta_u}{\theta_n + \Delta\theta_u}, \frac{\Delta\theta_l}{\theta_n - \Delta\theta_l} \right] \end{aligned} \quad (2.8)$$

2.3.1.1 Representation on Bond Graph

For any BG element $\theta \in \{R, I, C, TF, GY\}$, the nominal degenerate interval $\theta_n \in \{R_n, I_n, C_n, TF_n, GY_n\}$ is decoupled from its uncertain interval part $[\delta_\theta]\theta_n \in \{[\delta_R]R_n, [\delta_I]I_n, [\delta_C]C_n, [\delta_{TF}]TF_n, [\delta_{GY}]GY_n\}$ where, for notational simplicity, $\left[\underline{\delta}_\theta, \bar{\delta}_\theta \right] \cong [\delta_\theta]$. The latter closely resembles to LFT representation on BG, where the

parametric uncertainty is bounded such that upper and lower bounds remain equal. Representation of the uncertain flow (f_i) and effort (e_i) brought in at the junction by interval uncertainty, is done by fictive effort or flow input $MSe:[w_i]$ and $MSf:[w_i]$ respectively, modulated by $[\delta_{\theta_i}] * (\theta_{i,n} \cdot e_i)$ and $[\delta_{\theta_i}] * (\theta_{i,n} \cdot f_i)$ respectively.

For pedagogical illustration, an example of resistor element R , in *resistance* (imposed flow) causality is considered.

- Nominal case (see Fig. 2.1) : The characteristic equation with parameter in nominal state (without any uncertainty) is expressed as,

$$e_R = R \cdot f_R \quad (2.9)$$

- Uncertain case (see Fig. 2.2): With multiplicative interval uncertainty $[\underline{\delta}_R, \overline{\delta}_R]$ the characteristic law is expressed as,

$$[\underline{e}_R, \overline{e}_R] = [\underline{R}, \overline{R}] \cdot f_R = R_n \left(1 + [\underline{\delta}_R, \overline{\delta}_R] \right) \cdot f_R \quad (2.10)$$

$$[\underline{e}_R, \overline{e}_R] = \underbrace{[\underline{R}_n, \overline{R}_n] \cdot f_R}_{e_{R_n}} + \underbrace{([\underline{\delta}_R, \overline{\delta}_R] \cdot R_n) \cdot f_R}_{e_{R_{unc}}}$$

$$[\underline{e}_R, \overline{e}_R] = \underbrace{[\underline{R}_n, \overline{R}_n] \cdot f_R}_{e_{R_n}} - \underbrace{[w_R]}_{-e_{R_{unc}}} \quad (2.11)$$

where $[w_R] = -[\underline{\delta}_R, \overline{\delta}_R] \cdot Z_R = -[\underline{\delta}_R, \overline{\delta}_R] \cdot R_n \cdot f_R$.

Interval valued uncertain effort $e_{R_{unc}}$ is brought at the 1-junction by $[w_R]$.

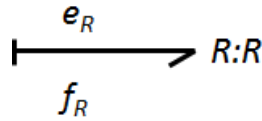


Fig. 2.1 Nominal R element (resistance causality)

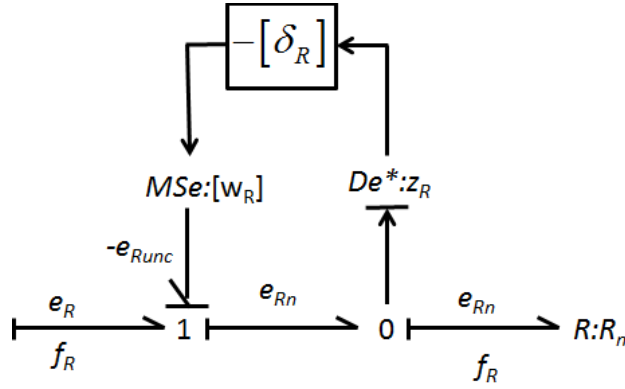


Fig. 2.2 Uncertain R element (resistance causality) in Interval form

Similarly, in conductance (imposed effort) causality (see 2.2), uncertain interval form

$\left[\frac{1}{\underline{R}}, \frac{1}{\overline{R}} \right]$ can be expressed with multiplicative uncertainty interval $\left[\underline{\delta}_{1/R}, \overline{\delta}_{1/R} \right]$ (c.f. (2.7), (2.8))

as, $\left[\underline{\delta}_{1/R}, \overline{\delta}_{1/R} \right] = \left[\frac{-\Delta R_u}{R_n + \Delta R_u}, \frac{\Delta R_l}{R_n - \Delta R_l} \right]$. The characteristic law $f_R = \frac{e_R}{R}$ can be expressed using

uncertain interval form as,

$$\left[\underline{f_R}, \overline{f_R} \right] = \left[\frac{1}{\underline{R}}, \frac{1}{\overline{R}} \right] \cdot e_R = \frac{1}{R_n} \cdot \left(1 + \left[\underline{\delta}_{1/R}, \overline{\delta}_{1/R} \right] \right) \cdot e_R \quad (2.12)$$

$$\left[\underline{f_R}, \overline{f_R} \right] = \underbrace{\frac{e_R}{R_n}}_{f_{Rn}} + \underbrace{\left(\left[\underline{\delta}_{1/R}, \overline{\delta}_{1/R} \right] \cdot (1/R_n) \cdot e_R \right)}_{f_{Runc}} \quad (2.13)$$

$$\left[\underline{f_R}, \overline{f_R} \right] = \frac{e_R}{R_n} - \underbrace{\left[w_{1/R} \right]}_{-f_{Runc}}$$

where the interval valued fictive input $\left[w_{1/R} \right] = - \left[\underline{\delta}_{1/R}, \overline{\delta}_{1/R} \right] \cdot z_{1/R} = - \left[\underline{\delta}_{1/R}, \overline{\delta}_{1/R} \right] \cdot (1/R_n) \cdot e_R$.

Fig. 2.3 shows the uncertain R element representation on BG.

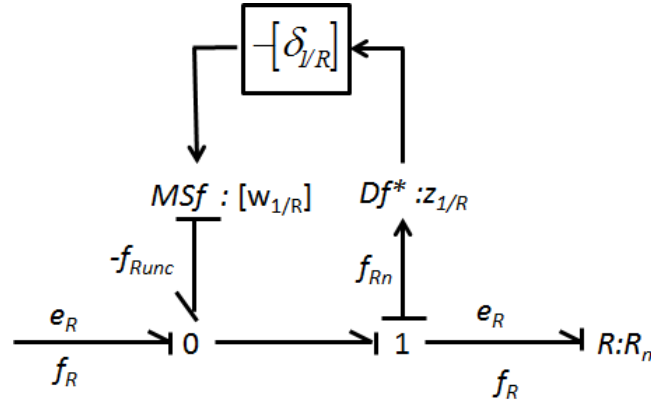


Fig. 2.3 Uncertain R element (conductance causality) in Interval form

It should be noted that in Fig. 2.2 and Fig. 2.3, the negative sign added to the uncertain interval block and effort/flow bonds, comes from the energy balance convention used at the 1-*junction* and 0-*junction* respectively, representing a source with half-oriented arrow towards the corresponding junction. De^* and Df^* represent the virtual sensors used to distinguish the real measurements from fictive ones.

Interval uncertainty can be modelled and represented, similarly, on other uncertain BG elements I , C , GY , TF , RS etc., using the established LFT form (see Appendix B). The difference lies in the treatment of fictive effort (or flow) in interval form being modulated by multiplicative interval uncertainty of the corresponding element.

2.3.2 Measurement Uncertainty

Measurement uncertainties can be explicitly represented on BG model in preferred derivative causality used for diagnosis. In BG model, the detectors are modeled by De or Df elements representing the effort detector and flow detector respectively. The effort detector is always connected to 0-*junction* and measures the common effort between all the bonds connected to it whereas flow detector is always connected to 1-*junction* measuring the common flow between all the bonds connected.

For diagnosis based on ARR generation, the detectors are dualized (Samantaray, Arun K et al., 2006b) which means that the effort detector De becomes a *source of effort signal* SSe and imposes the effort signal at the 0-*junction* connected to the detector. Flow detector Df becomes a *source of flow signal* SSf and imposes flow at the 1-*junction* connected to the detector.

The observed uncertain measurement Sn_m can be treated in interval form $\left[\underline{Sn_m}, \overline{Sn_m} \right]$ such that,

$$\begin{aligned} \left[\underline{Sn_m}, \overline{Sn_m} \right] &= [Sn_t - \Delta Sn_l, Sn_t + \Delta Sn_u] \\ \left[\underline{Sn_m}, \overline{Sn_m} \right] &= [Sn_t, Sn_t] + [-\Delta Sn_l, \Delta Sn_u] \end{aligned} \quad (2.14)$$

where Sn_t is the true measurement which is un-observed and $\Delta Sn_l, \Delta Sn_u$ are respectively, the lower and upper bounds that model the permissible limits on sensor drifts, measurement bias, tolerance errors etc.

2.3.2.1 Representation on Bond Graph

Uncertain effort detector can be considered as,

$$\left[\underline{SSe}, \overline{SSe} \right]_{measure} = \left[\underline{SSe_t}, \overline{SSe_t} \right]_{true} + [-\Delta SSe_l, \Delta SSe_u] \quad (2.15)$$

The uncertainty interval is modelled by virtual source of effort $MSe^* : [-\Delta SSe_l, \Delta SSe_u]$, representing the exchange of effort information which is propagated from the detectors to rest of the model through causal paths (bonds) to eliminate the unknown variables. For notational simplicity, $MSe^* : [-\Delta SSe_l, \Delta SSe_u]$ is denoted as $MSe^* : [\zeta_{sse}]$ as illustrated in Fig. 2.4. From the latter, following equations can be deduced.

$$\begin{aligned} \left[\underline{e_1}, \overline{e_1} \right]_{true} &= \left[e_4, e_4 \right]_{measured} - [-\Delta SSe_l, \Delta SSe_u] = SSe + MSe^* : \left(-[-\Delta SSe_l, \Delta SSe_u] \right) \\ \left[\underline{e_2}, \overline{e_2} \right]_{true} &= \left[e_5, e_5 \right]_{measured} - [-\Delta SSe_l, \Delta SSe_u] = SSe + MSe^* : \left(-[-\Delta SSe_l, \Delta SSe_u] \right) \\ \left[\underline{e_3}, \overline{e_3} \right]_{true} &= \left[e_6, e_6 \right]_{measured} - [-\Delta SSe_l, \Delta SSe_u] = SSe - MSe^* : \left([-\Delta SSe_l, \Delta SSe_u] \right) \end{aligned} \quad (2.16)$$

Similarly, uncertain flow detector is modelled as,

$$\left[\underline{SSf}, \overline{SSf} \right]_{measure} = \left[\underline{SSf_t}, \overline{SSf_t} \right]_{true} + [-\Delta SSf_l, \Delta SSf_u] \quad (2.17)$$

The uncertainty interval is modelled by virtual source of flow $MSf^* : [-\Delta SSf_l, \Delta SSf_u]$ (denoted as $MSf^* : [\zeta_{ssf}]$), representing the flow information. It is illustrated in Fig. 2.5 and following equations are derived.

$$\begin{aligned}
 \left[\underline{f}_1, \overline{f}_1 \right]_{true} &= \left[f_4, f_4 \right]_{measured} - \left[-\Delta SSf_l, \Delta SSf_u \right] = SSf + MSf^* : \left(- \left[-\Delta SSf_l, \Delta SSf_u \right] \right) \\
 \left[\underline{f}_2, \overline{f}_2 \right]_{true} &= \left[f_5, f_5 \right]_{measured} - \left[-\Delta SSf_l, \Delta SSf_u \right] = SSf + MSf^* : \left(- \left[-\Delta SSf_l, \Delta SSf_u \right] \right) \\
 \left[\underline{f}_3, \overline{f}_3 \right]_{true} &= \left[f_6, f_6 \right]_{measured} - \left[-\Delta SSf_l, \Delta SSf_u \right] = SSf - MSf^* : \left(\left[-\Delta SSf_l, \Delta SSf_u \right] \right)
 \end{aligned} \tag{2.18}$$

This way, on an uncertain BG, $[\zeta_{sse}]$ (or $[\zeta_{ssf}]$) can be connected to the junction which is connected to the dualized detector SSe (or SSf) when the bond is connected to: passive linear or non-linear elements (R, C or D), active elements (Se, Sf), junction elements ($0, 1$ GY, TF).

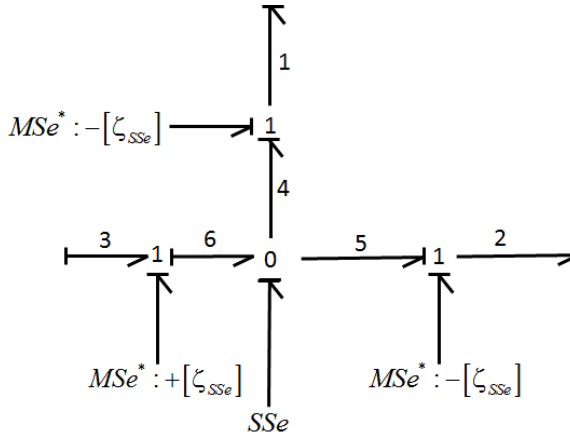


Fig. 2.4. Effort measurement uncertainty in interval form.

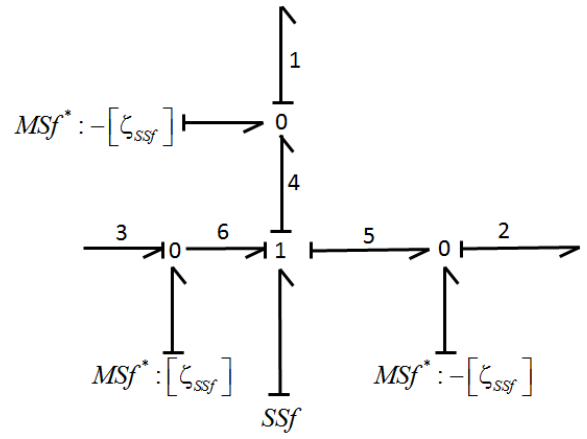


Fig. 2.5. Flow measurement uncertainty in interval form.

For illustration, Fig. 2.7 shows a BG consisting of nominal R and C elements, such that R is in conductance causality (imposed effort) and C is in normal integral causality. The characteristic equations are:

$$\begin{aligned}
 f_1 &= (1/R)e_1 \\
 e_2 &= \frac{1}{C} \int f_2 dt
 \end{aligned} \tag{2.19}$$

In Fig. 2.7, uncertain elements R and C are considered in interval form and represented on uncertain BG, connected to 0 -junction in preferred derivative causality. The uncertain effort sensor is dualized and connected. The uncertainty is modelled by virtual source of effort $MSe^* : [\zeta_{sse}]$. f_4, f_5 are the unknown variables at the junction, which can be obtained by covering the causal paths represented by the dashed lines in Fig. 2.7. Then, f_4 can be obtained as shown in (2.20) and (2.21).

$$[e_3, \bar{e}_3] = e_4 + MSE^* = SSe - [\zeta_{SSe}] \quad (2.20)$$

$$\begin{aligned} [f_4, \bar{f}_4] &= f_3 = f_7 - [w_{1/R}] \\ &= e_1 \frac{1}{R_n} + [\delta_{1/R}, \bar{\delta}_{1/R}] \frac{1}{R_n} e_1 \\ &= [e_3, \bar{e}_3] \frac{1}{R_n} + [\delta_{1/R}, \bar{\delta}_{1/R}] \frac{1}{R_n} [e_3, \bar{e}_3] \\ &= (SSe - [\zeta_{SSe}]) \frac{1}{R_n} + (SSe - [\zeta_{SSe}]) [\delta_{1/R}, \bar{\delta}_{1/R}] \frac{1}{R_n}; \\ &= SSe \frac{1}{R_n} + [\delta_{1/R}, \bar{\delta}_{1/R}] \frac{1}{R_n} SSe + (-[\zeta_{SSe}]) \cdot \left(\frac{1}{R_n} + \frac{1}{R_n} \cdot ([\delta_{1/R}, \bar{\delta}_{1/R}]) \right) \\ &= SSe \cdot \frac{1}{R_n} + [w_{1/R}] + \underbrace{(-[-\Delta SSe_l, \Delta SSe_u])}_{-[\zeta_{SSe}]} ([1/R, \bar{1/R}]) \end{aligned} \quad (2.21)$$

From (2.21), the flow brought in by parametric uncertainty on R and measurement uncertainty may be identified. Following the similar approach for C , flow f_5 , can be found as,

$$[f_5, \bar{f}_5] = C_n \cdot \frac{d(SSe)}{dt} + \underbrace{[\delta_C, \bar{\delta}_C]}_{[w_C, \bar{w}_C]} \cdot (C_n) \cdot \frac{d(SSe)}{dt} + [C, \bar{C}] \cdot \frac{d([\zeta_{SSe}])}{dt} \quad (2.22)$$

where, $[w_C, \bar{w}_C]$ is flow due to parametric uncertainty and $[C, \bar{C}] \frac{d([\zeta_{SSe}])}{dt}$ is the flow due to measurement uncertainty. The derivative of the interval error can be evaluated as,

$$[C, \bar{C}] \frac{d([\zeta_{SSe}])}{dt} = [C, \bar{C}] \cdot \frac{([- \Delta SSe_l, \Delta SSe_u]_{t_i} - [- \Delta SSe_l, \Delta SSe_u]_{t_{i-1}})}{t_i - t_{i-1}} \quad (2.23)$$

with,

$$[- \Delta SSe_l, \Delta SSe_u]_{t_i} - [- \Delta SSe_l, \Delta SSe_u]_{t_{i-1}} = [- \Delta SSe_{l,t_i} - \Delta SSe_{u,t_{i-1}}, \Delta SSe_{u,t_i} + \Delta SSe_{l,t_{i-1}}] \quad (2.24)$$

Note that (2.24) is a direct result from IA and is a better approximation compared to the one made in (Touati et al., 2012b) where, the worst case *max* operator is employed for the same.

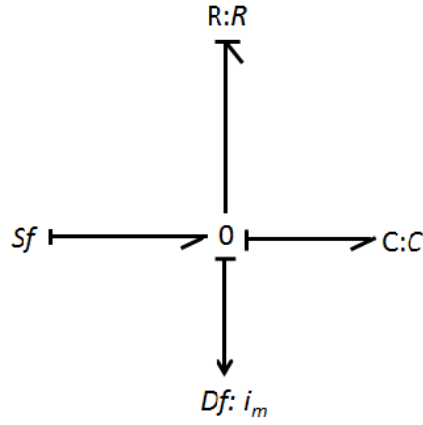


Fig. 2.6 Nominal BG of R-C elements

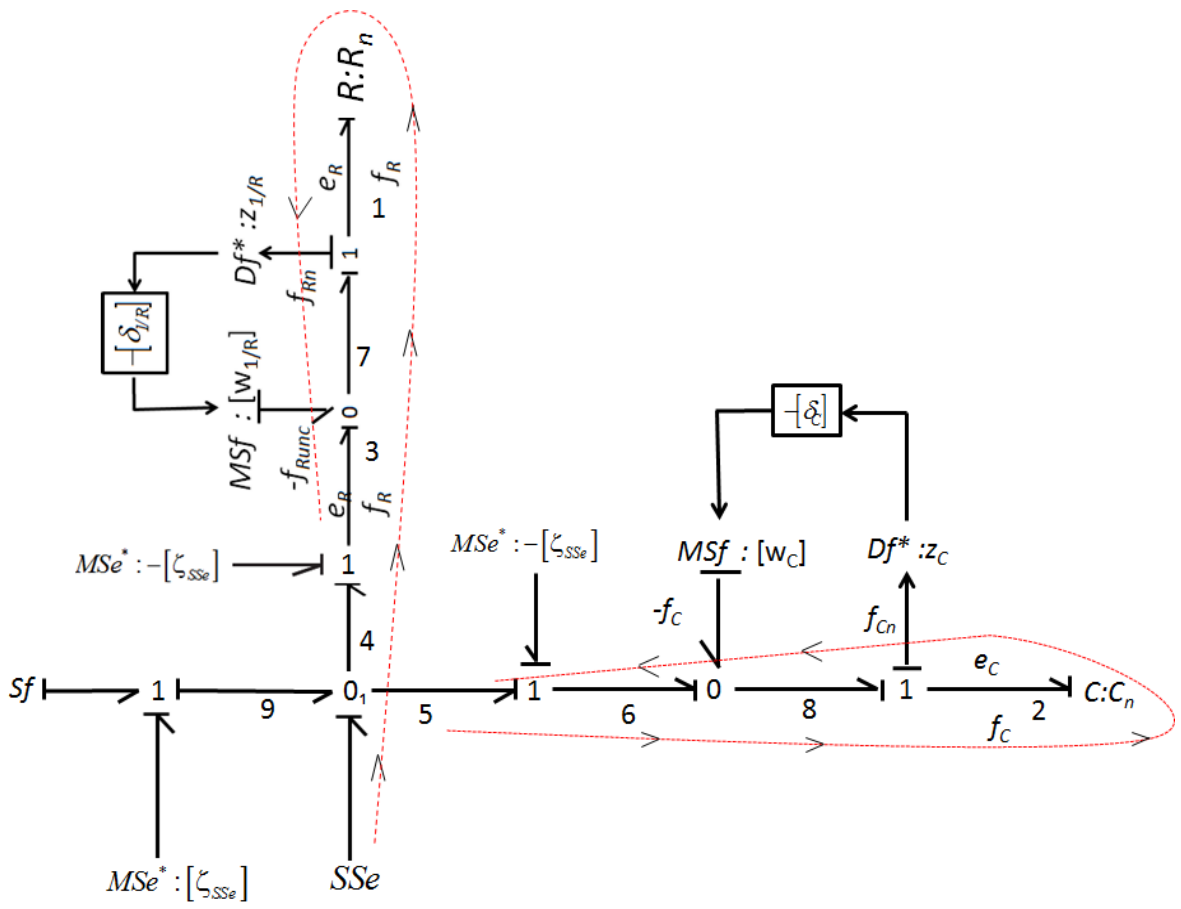


Fig. 2.7. Uncertain BG of R and C elements with uncertain effort measurement

2.4 Interval Valued Analytical Redundancy Relations

For achieving robust FDI, the methodology of ARR generation as presented in Section 1.4.3.2 and Appendix B, is adapted to obtain interval valued ARRs (I-ARRs) in presence of parametric uncertainties and measurement uncertainties as intervals on a BG model. The I-ARRs are produced by energetic assessment at the junctions (0 and 1) of BG which are detectable i.e. connected to at least one detector (effort or flow). As shown in Section 1.4.3.2, dualization of sensors means conversion of De and Df respectively, to SSe (source of effort signal) and Df (source of flow).

With the considered uncertain parameter vector as $[\underline{\theta}, \bar{\theta}] \in \mathbb{R}^{N_m}$ where $N_m \leq N_\theta$, uncertain dualized effort detector vector as $[\underline{SSe}, \overline{SSe}] \in \mathbb{R}^{N_{Sse}}$ ($N_{Sse} \leq N_{De}$) and uncertain dualized flow detector vector as $[\underline{SSf}, \overline{SSf}] \in \mathbb{R}^{N_{SSf}}$ ($N_{SSf} \leq N_{Df}$), following steps are taken to generate I-ARRs:

Step 1: Preferred derivative causality is assigned to the nominal model and detectors De (Df) are dualized to SSe (SSf), wherever possible.

Step 2: Parametric uncertainties and measurement uncertainties are modelled in interval form and represented on the nominal BG, as explained in Section 2.3.1.1 and Section 2.3.2.1 respectively, to obtain the uncertain BG.

Step 3: The candidate ARRs are generated from “1” or “0” junction, where power conservation equation dictates that sum of efforts or flows, respectively, is equal to zero, as:

- for 0-junction:

$$\sum s. [\underline{f}, \bar{f}] + \sum Sf + \sum_{i=0}^{i \leq N_m} s_i \cdot MSf : [w_i] = 0 \quad (2.25)$$

- for 1-junction:

$$\sum s. [\underline{e}, \bar{e}] + \sum Se + \sum_{i=0}^{i \leq N_m} s_i \cdot MSe : [w_i] = 0 \quad (2.26)$$

with s being the sign rendered to the *bond* due to energy convention.

Step 4: The unknown effort or flow variables are then eliminated using covering causal paths from unknown variables to known (measured) variables (dualized detectors), to obtain the I-ARRs, $\left[\underline{R}, \overline{R}\right]$ containing only known variables as shown in (2.27). The nominal part is characterized by point valued function Ψ_1 , with point valued nominal parameters as coefficients of point valued measured variables as shown in (2.29). It is separated from interval valued part identified as interval function Ψ_2 sensitive to interval valued uncertainties as shown in (2.30).

$$\left[\underline{R}(t), \overline{R}(t)\right] : \Psi \left(\theta_n, \left[\underline{\theta}, \overline{\theta}\right], [w_i], [\zeta_{sse}], [\zeta_{ssf}], \right. \\ \left. \sum Se, \sum Sf, \mathbf{SSe}(t), \mathbf{SSf}(t) \right) \quad (2.27)$$

$$\left[\underline{R}(t), \overline{R}(t)\right] : r_n(t) + \left[\underline{B}(t), \overline{B}(t)\right] \quad (2.28)$$

$$r_n(t) = \Psi_1 \left(\theta_n, \mathbf{SSe}(t), \mathbf{SSf}(t), \sum Se, \sum Sf \right) \quad (2.29)$$

$$\left[\underline{B}(t), \overline{B}(t)\right] = \Psi_2 \left(\left[\underline{\theta}, \overline{\theta}\right], \left[\underline{\delta}_0, \overline{\delta}_0\right], [\zeta_{sse}], [\zeta_{ssf}], \mathbf{SSe}(t), \mathbf{SSf}(t) \right) \quad (2.30)$$

Here, $\left[\zeta_{sse_i}\right]$ and $\left[\zeta_{ssf_i}\right]$ are respectively, the simplified notation as introduced in (2.15) and (2.17), for every $\left[\underline{SSe}, \overline{SSe}\right] \in \left[\underline{\mathbf{SSe}}, \overline{\mathbf{SSe}}\right]$ and $\left[\underline{SSf}, \overline{SSf}\right] \in \left[\underline{\mathbf{SSf}}, \overline{\mathbf{SSf}}\right]$.

Hereafter, $r_n(t)$ being the numerical evaluation of the nominal part Ψ_1 will be referred to as *nominal residual* and Ψ_2 will be termed as *uncertain residual interval function* (URIF).

Note: There can be cases when the characteristic equation of the BG elements is such that the point valued nominal parameters sensitive to interval valued measurement variables cannot be perfectly decoupled. In such situations, the concept of midpoint of an interval (see **Definition 2.1**) and width (see **Definition 2.2**) of an interval is employed to split the interval into two parts consisting of point valued data (mid-point) and interval valued data (see **Property 2.1**).

Example 2.1 Consider Fig. 2.7. that represents the uncertain R and C elements in derivative causality and dualized SSf . Following the **Step 3** and **Step 4** described above, and taking help of the flows obtained in (2.21) and (2.22), the I-ARR can be derived through energetic assessment at 0_1 ,

$$\left[\underline{R(t)}, \overline{R(t)} \right] = Sf - \left(\begin{array}{l} SSe.(1/R_n) + [w_{1/R}] + \underbrace{(-[-\Delta SSe_l, \Delta SSe_u])}_{-[\zeta_{sse}]} \left(\left[\underline{1/R}, \overline{1/R} \right] \right) \\ + C_n \cdot \frac{d(SSe)}{dt} + \underbrace{[\underline{\delta_C}, \overline{\delta_C}]}_{[w_C, \overline{w_C}]} \cdot (C_n) \cdot \frac{d(SSe)}{dt} + [\underline{C}, \overline{C}] \cdot \frac{d([\zeta_{sse}])}{dt} \end{array} \right) \quad (2.31)$$

The nominal part and interval valued part can be de-coupled as,

$$\left[\underline{R(t)}, \overline{R(t)} \right] : r_n(t) + \left[\underline{B(t)}, \overline{B(t)} \right]$$

$$r_n(t) = Sf - SSe.(1/R_n) - C_n \cdot \frac{d(SSe)}{dt} \quad (2.32)$$

$$\left[\underline{B(t)}, \overline{B(t)} \right] = - \left(\left[w_{1/R} \right] + (-[\zeta_{sse}]) \left(\left[\underline{1/R}, \overline{1/R} \right] \right) + [\underline{\delta_C}, \overline{\delta_C}] \cdot (C_n) \cdot \frac{d(SSe)}{dt} + [\underline{C}, \overline{C}] \cdot \frac{d([\zeta_{sse}])}{dt} \right)$$

□

Example 2.2 Consider Fig. 2.6 and Fig. 2.7. However, the characteristic equation of R element is considered as a non-linear relation given in (2.33). It models a situation of turbulent flow across a hydraulic valve; a situation that frequently arises in hydraulic systems.

$$f_1 = (1/R) \sqrt{e_1}; \quad e_1 \geq 0 \quad (2.33)$$

Then, unlike (2.21), $\left[\underline{f_4}, \overline{f_4} \right]$ is obtained as shown in (2.34) where $\left[\underline{e_3}, \overline{e_3} \right] = SSe - [\zeta_{sse}]$. The latter remains unchanged as obtained in (2.20).

$$\begin{aligned} \left[\underline{f_4}, \overline{f_4} \right] &= f_3 = f_7 - [w_{1/R}] \\ &= (1/R_n) \sqrt{e_1} + [\underline{\delta_{1/R}}, \overline{\delta_{1/R}}] \cdot (1/R_n) \sqrt{e_1} \\ &= \sqrt{[\underline{e_3}, \overline{e_3}]} \cdot (1/R_n) + [\underline{\delta_{1/R}}, \overline{\delta_{1/R}}] \cdot (1/R_n) \cdot \sqrt{[\underline{e_3}, \overline{e_3}]} \\ &= \left[\sqrt{\underline{e_3}}, \sqrt{\overline{e_3}} \right] (1/R_n) + [\underline{\delta_{1/R}}, \overline{\delta_{1/R}}] \cdot (1/R_n) \cdot \left[\sqrt{\underline{e_3}}, \sqrt{\overline{e_3}} \right] \end{aligned} \quad (2.34)$$

Clearly, nominal part $(1/R_n)$ that remains sensitive to the interval valued part $\left[\sqrt{\underline{e_3}}, \sqrt{\overline{e_3}} \right]$, cannot be linearly separated. It should be noted that for any interval X , such that $\underline{X} \geq 0$, arithmetic rules provide the result: $\sqrt{X} = \left[\sqrt{\underline{X}}, \sqrt{\overline{X}} \right]$.

To obtain point valued nominal part using **Property 2.1**, $[\underline{f}_4, \overline{f}_4]$ found in (2.34) can be expressed as,

$$\begin{aligned} [\underline{f}_4, \overline{f}_4] = & \text{mid} \left(\left[\sqrt{e_3}, \sqrt{e_3} \right] (1/R_n) \right) + \frac{1}{2} \text{width} \left(\left[\sqrt{e_3}, \sqrt{e_3} \right] (1/R_n) \right) [-1, 1] \\ & + [\underline{\delta}_{1/R}, \overline{\delta}_{1/R}] \cdot (1/R_n) \cdot \left[\sqrt{e_3}, \sqrt{e_3} \right] \end{aligned} \quad (2.35)$$

Moreover, the associated I-ARR (see(2.31)) is derived as,

$$\begin{aligned} [\underline{R}(t), \overline{R}(t)] : & Sf - \text{mid} \left(\left[\sqrt{e_3}, \sqrt{e_3} \right] (1/R_n) \right) - C_n \cdot \frac{d(SSe)}{dt} \\ & - \frac{1}{2} \text{width} \left(\left[\sqrt{e_3}, \sqrt{e_3} \right] (1/R_n) \right) [-1, 1] \\ & - [\underline{\delta}_{1/R}, \overline{\delta}_{1/R}] \cdot (1/R_n) \cdot \left[\sqrt{e_3}, \sqrt{e_3} \right] \\ & - [\underline{\delta}_C, \overline{\delta}_C] \cdot (C_n) \cdot \frac{d(SSe)}{dt} + [\underline{C}, \overline{C}] \cdot \frac{d([\zeta_{sse}])}{dt} \end{aligned} \quad (2.36)$$

Then, nominal part and interval valued part can be de-coupled as,

$$\begin{aligned} [\underline{R}(t), \overline{R}(t)] : & r_n(t) + [\underline{B}(t), \overline{B}(t)] \\ r_n(t) = & Sf - \text{mid} \left(\left[\sqrt{e_3}, \sqrt{e_3} \right] (1/R_n) \right) - C_n \cdot \frac{d(SSe)}{dt} \\ [\underline{B}(t), \overline{B}(t)] = & -\frac{1}{2} \text{width} \left(\left[\sqrt{e_3}, \sqrt{e_3} \right] (1/R_n) \right) [-1, 1] \\ & - [\underline{\delta}_{1/R}, \overline{\delta}_{1/R}] \cdot (1/R_n) \cdot \left[\sqrt{e_3}, \sqrt{e_3} \right] \\ & - [\underline{\delta}_C, \overline{\delta}_C] \cdot (C_n) \cdot \frac{d(SSe)}{dt} + [\underline{C}, \overline{C}] \cdot \frac{d([\zeta_{sse}])}{dt} \end{aligned} \quad (2.37)$$

2.5 Interval Valued Robust Thresholds

Proposition 2.1: For point valued variable vectors $\theta, \delta_\theta, \theta_n, SSe(t), SSf(t), \Delta SSe, \Delta SSf$, bounded by interval limit $\Delta SSe \in [-\Delta SSe_l, \Delta SSe_u]$, $\Delta SSf \in [-\Delta SSf_l, \Delta SSf_u]$, $\theta \in [\underline{\theta}, \overline{\theta}]$, $\delta_\theta \in [\underline{\delta}_\theta, \overline{\delta}_\theta]$, given that the Uncertain Residual Interval Function (URIF) is expressed as finite sequence of

interval arithmetic operations, the range of URIF guarantees the containment of negative value of point valued nominal residual.

Proof: Consider the function

$$\Psi_2(\boldsymbol{\theta}, \boldsymbol{\delta}_0, \boldsymbol{\theta}_n, \text{SSe}(t), \text{SSf}(t), \Delta \text{SSe}, \Delta \text{SSe}) \quad (2.38)$$

such that the URIF $\Psi_2\left(\left[\underline{\boldsymbol{\theta}}, \overline{\boldsymbol{\theta}}\right], \left[\underline{\boldsymbol{\delta}}_0, \overline{\boldsymbol{\delta}}_0\right], \boldsymbol{\theta}_n, [\zeta_{\text{SSe}}], [\zeta_{\text{SSf}}], \text{SSe}(t), \text{SSf}(t)\right)$ is obtained by replacing the point valued arguments and arithmetic operators by the corresponding interval arguments and interval arithmetic operators respectively, in the syntactic expression of Ψ_2 . From **Definition 2.4**, the URIF Ψ_2 can be considered as Natural Interval Extension Function of Ψ_2 .

Now, from **Definition 2.6**, if Ψ_2 is expressed as finite sequence of interval arithmetic operations (evaluated as class code during implementation (Moore et al., 2009)) then, it can be considered as *Rational Interval Function* (RIF) of Ψ_2 .

From **Property 2.3**, and **Lemma 2.1**, Ψ_2 is an inclusion-isotonic function.

Then, from **Theorem 2.1**, following can be guaranteed,

$$\Psi_2\left(\boldsymbol{\theta}, \boldsymbol{\delta}_0, \boldsymbol{\theta}_n, \Delta \text{SSe}, \Delta \text{SSe}, \text{SSe}(t), \text{SSf}(t)\right) \subseteq \Psi_2\left(\left[\underline{\boldsymbol{\theta}}, \overline{\boldsymbol{\theta}}\right], \left[\underline{\boldsymbol{\delta}}_0, \overline{\boldsymbol{\delta}}_0\right], \boldsymbol{\theta}_n, [\zeta_{\text{SSe}}], [\zeta_{\text{SSf}}], \text{SSe}(t), \text{SSf}(t)\right) \quad (2.39)$$

At any time t , let $b(t)$ be the resultant of additive deviations $\boldsymbol{\delta}_0, \Delta \text{SSe}, \Delta \text{SSe}$ on nominal residual, such that, $\Delta \text{SSe} \in [-\Delta \text{SSe}_1, \Delta \text{SSe}_u]$, $\Delta \text{SSf} \in [-\Delta \text{SSf}_1, \Delta \text{SSf}_u]$, $\boldsymbol{\theta} \in \left[\underline{\boldsymbol{\theta}}, \overline{\boldsymbol{\theta}}\right]$, $\boldsymbol{\delta}_0 \in \left[\underline{\boldsymbol{\delta}}_0, \overline{\boldsymbol{\delta}}_0\right]$.

Then,

$$\Psi_2(\boldsymbol{\theta}, \boldsymbol{\delta}_0, \boldsymbol{\theta}_n, \text{SSe}(t), \text{SSf}(t), \Delta \text{SSe}, \Delta \text{SSe}) = b(t) \quad (2.40)$$

From (2.40) and (2.30), following can be guaranteed,

$$b(t) \subseteq \left[\underline{B}(t), \overline{B}(t)\right] \quad (2.41)$$

Now, at all times, due to energy conservation at the BG junction where the I-ARR is derived,

$$\begin{aligned} r_n(t) + b(t) &= 0 \\ \Rightarrow b(t) &= -r_n(t) \end{aligned} \quad (2.42)$$

From (2.42) and (2.41),

$$-r_n(t) \subseteq \left[\underline{B(t)}, \overline{B(t)} \right] \quad (2.43)$$

Hence, the evaluated interval range of Ψ_2 guarantees the containment of $-r_n(t)$, given that additive deviation of uncertain candidates remain within their prescribed interval bounds.

□

Lemma 2.2: *Alternatively, $r_n(t) \subseteq -\left[\underline{B(t)}, \overline{B(t)} \right]$.*

Proof: This directly follows from Property 2.3 such that,

$$\begin{aligned} -r_n(t) &\subseteq \left[\underline{B(t)}, \overline{B(t)} \right] \\ \Rightarrow (-1)(-r_n(t)) &\subseteq [-1, -1] \left[\underline{B(t)}, \overline{B(t)} \right] \\ \Rightarrow r_n(t) &\subseteq -\left[\underline{B(t)}, \overline{B(t)} \right] \end{aligned}$$

□

Proposition 3.2: *Given that a fault is considered when any of the uncertain candidates sensitive to the considered I-ARR, deviate out of their permissible interval limits,*

- *under nominal conditions $-r_n(t) \subseteq \left[\underline{B(t)}, \overline{B(t)} \right]$ is verified.*
- *fault is detected if $-r_n(t) \not\subseteq \left[\underline{B(t)}, \overline{B(t)} \right]$.*

Proof: Proof follows directly from **Proposition 2.1**, where $-r_n(t) \subseteq \left[\underline{B(t)}, \overline{B(t)} \right]$ is verified if, for point valued variable vectors $\theta, \delta_\theta, \theta_n, \text{SSe}(t), \text{SSf}(t), \Delta\text{SSe}, \Delta\text{SSe}$, following stands true:

$$\Delta\text{SSe} \in [-\Delta\text{SSe}_1, \Delta\text{SSe}_u], \Delta\text{SSf} \in [-\Delta\text{SSf}_1, \Delta\text{SSf}_u], \theta \in [\underline{\theta}, \overline{\theta}], \delta_\theta \in [\underline{\delta}_\theta, \overline{\delta}_\theta] \quad \square$$

Lemma 3.2: *As it follows from **Proposition 2.1** and **Lemma 2.1**:*

- *under nominal conditions: $r_n(t) \subseteq -[\underline{B(t)}, \overline{B(t)}]$ is verified.*
- *fault is detected if $r_n(t) \not\subseteq -[\underline{B(t)}, \overline{B(t)}]$*

□

Thus, in this section, a fault detection methodology is established where URIF $[\underline{B(t)}, \overline{B(t)}]$ of an I-ARR $[\underline{R(t)}, \overline{R(t)}]$, serves as threshold over nominal residual $r_n(t)$ robust to considered system parametric uncertainties and measurement uncertainties.

2.6 Application: Robust Fault Detection of Steam Generator System

The methodology is validated on an uncertain model of a steam generator system installed in CRISAL laboratory (Ould Bouamama et al., 2006), (Medjaher, K. et al., 2006). The detailed BG-LFT modeling of the uncertain steam generator system with parametric uncertainties and its subsequent robust passive diagnosis is described in (Djeziri, Mohand Arab et al., 2009b).

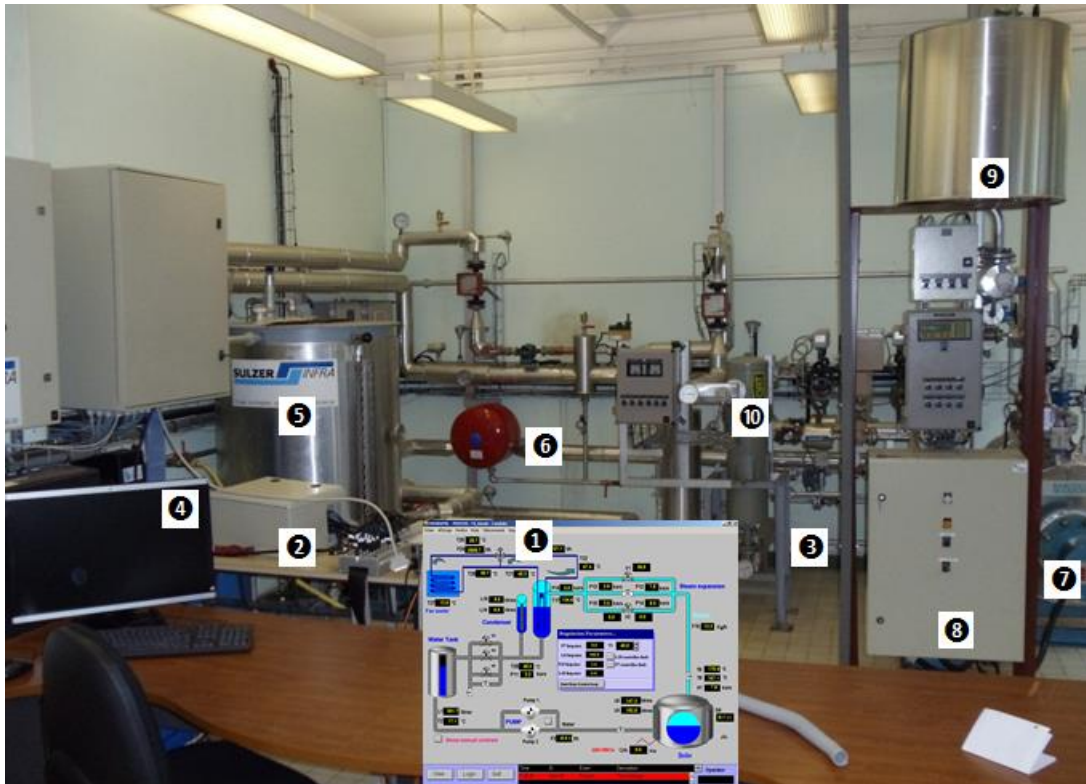


Fig. 2.8 Steam Generator Setup and Supervision Interface 1:Supervision Interface 2: DSPACE data Acquisition 3: Main power switch 4: Screen for monitoring 5: Water Tank 6: Pump Circuit 7: Boiler 8: Safety Switch 9: Vapour output 10: Condenser and Heat Exchanger

2.6.1 Uncertain Steam Generator System

The piping and instrument diagram of the steam generator system is given in Fig. 2.9, comprising of a feed water supply system, a tank, a pump, a pipe and a boiler of 55kW and total volume of 0.170 m^3 . The considered faults are: water leak in tank, valve blockage at pump outlet flow, water leak in boiler and fault on thermal resistor system. Word bond graph of the system is shown in Fig. 2.10.

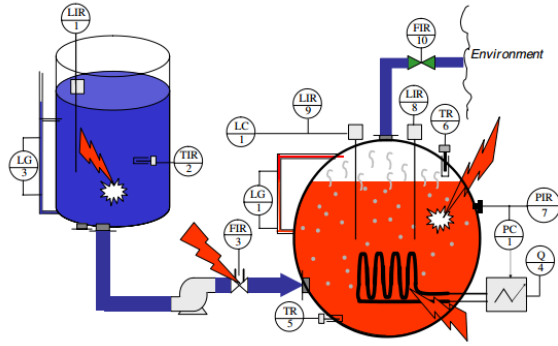


Fig. 2.9 Schematic of Steam Generator System with Faults

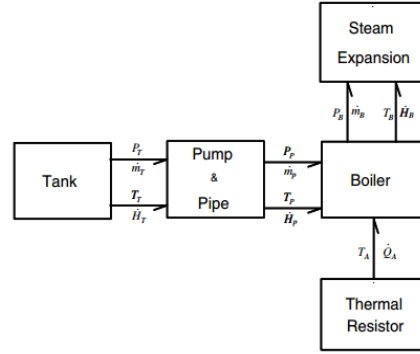


Fig. 2.10 Word Bond Graph of the system

It represents the coupling of thermal- hydraulic energies present in the system with the help of power variables based on pseudo BG modeling analysis. The hydraulic power is characterized by the pair Pressure –mass flow (P, \dot{m}) . Thermal power is characterized by the pair Temperature-Enthalpy flow (T, \dot{H}) for convection and the pair Temperature–Thermal flow (T, \dot{Q}) for conduction. The deterministic (nominal) diagnostic BG in preferred derivative causality is given in Fig. 2.11. The four sub-systems tank, pump and pipe, boiler and thermal resistor carry uncertainties on their respective parameters and the measurements of pressure in tank and boiler.

2.6.1.1 Tank

As shown in Fig. 2.11, the two port $C:C_T$ element consisting of hydraulic port: C_h , and thermal port: C_t , respectively, models the coupling between the hydraulic and thermal capacity of the tank. $De:P_T$ and $De:T_2$ represent the pressure sensor and temperature sensor present in the tank. Initially, the tank is filled in at ambient temperature. As such, the initial input mass flow \dot{m}_m is assumed zero.

Due to cylindrical shape of the tank, hydraulic capacity C_h is given as,

$$C_h = A_T \cdot (\rho_T \cdot g)^{-1} \quad (2.44)$$

where, A_T is the area of the tank, ρ_T is the water density and g is the gravity constant.

The uncertainty on C_h is considered in interval form as,

$$[\underline{C}_h, \overline{C}_h] = C_{h,n} + C_{h,n} \cdot [\underline{\delta}_{C_h}, \overline{\delta}_{C_h}] \quad (2.45)$$

$$[\underline{C}_h, \overline{C}_h] = \frac{A_{T,n}}{\rho_T g} + \frac{A_{T,n}}{\rho_T g} \cdot [\underline{\delta}_{A_T}, \overline{\delta}_{A_T}] \quad (2.46)$$

where, $\overline{\delta}_{A_T}$ is given by measurement of corrosion layer or scale deposit on the tank wall and $\underline{\delta}_{A_T}$ is the negative tolerance value provided by the manufacturer. It should be noted that $[\underline{\delta}_{A_T}, \overline{\delta}_{A_T}]$ is not symmetric. The uncertain effort brought in by to $[\underline{\delta}_{A_T}, \overline{\delta}_{A_T}]$ is identified in (2.47). It is modeled as $MSf : [w_{Ch}]$ on the uncertain BG shown in Fig. 2.12.

$$MSf : [w_{Ch}] = -[\underline{\delta}_{A_T}, \overline{\delta}_{A_T}] \cdot \frac{A_{T,n}}{\rho_T g} \cdot \frac{de_3}{dt} \quad (2.47)$$

Valve V_T present at the bottom of the tank is controlled manually to introduce water leakage in the tank. It represents a parametric fault. The mass flow rate, \dot{m}_{v_T} , through the valve is given by the non-linear Bernoulli relation,

$$\begin{aligned} \dot{m}_{v_T} &= Cd_T(x) \cdot sign(\Delta P) \cdot \sqrt{|\Delta P|} \\ \Delta P &= P_T - P_{atm} \end{aligned} \quad (2.48)$$

where ΔP is the pressure difference across the valve with atmospheric pressure P_{atm} being the reference. x is the valve stem position between 0 and 1, where 0 means fully closed state and 1 implies fully open state. Cd_T is a function representing the coefficient of discharge depending on the valve characteristics and $sign$ is used to adjust the direction of flow. The installed characteristics vary such that the relationship between volumetric flow rate through the valve and valve stem position is not perfectly linear. It is experimentally determined for four positions of the valve as shown in Table 2-I. Value of the Coefficient of discharge Cd_T is obtained for each of the valve positions.

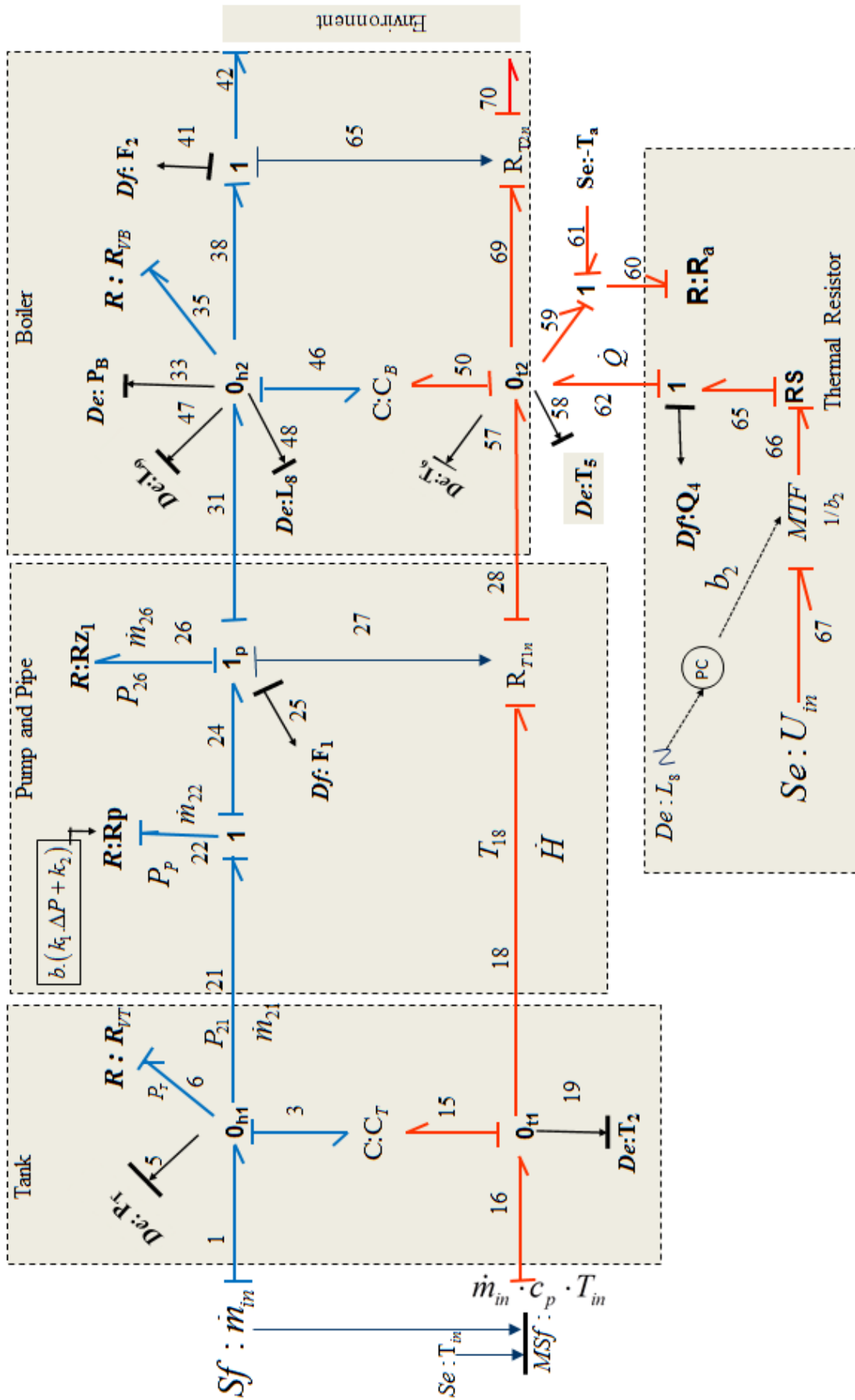


Fig. 2.11 Deterministic Bond Graph Model of Steam Generator

Table 2-I Stem Position of Valve present in Tank and Discharge Coefficient

Valve Stem Position	$V_{T,1}$	$V_{T,2}$	$V_{T,3}$	$V_{T,4}$
Discharge Coefficient	$Cd_{T,1}$	$Cd_{T,2}$	$Cd_{T,3}$	$Cd_{T,4}$
	6.32×10^{-3}	6.678×10^{-3}	6.987×10^{-3}	7.14×10^{-3}

During normal functioning of the system, the stem position of valve V_T present at the bottom of the water tank, is at $V_{T,1}$ (with discharge coefficient $Cd_{T,1}$). The limit on the modulation of valve stem is fixed at stem-position $V_{T,2}$ (with discharge coefficient $Cd_{T,2}$). Thus, nominal value of discharge flow coefficient is $Cd_{T,1}$. The uncertainty in valve outflow is brought by uncertain position of the valve stem (between $V_{T,1}$ and $V_{T,2}$). The latter is accounted by limiting the variation of the discharge coefficient Cd_T until $Cd_{T,2}$. This implies $Cd_T \in [Cd_{T,1}, Cd_{T,2}]$ or $Cd_T = Cd_{T,1} + [0, \Delta Cd_T]$, where $\Delta Cd_T = Cd_{T,2} - Cd_{T,1}$. Thus, nominal value of Cd_T is $Cd_{T,1}$ and the uncertain interval limit is given by ΔCd_T .

The valve dynamics is modeled by non-linear resistor $R:R_{vT}$ as shown in Fig. 2.11. The associated characteristic equation is

$$f_6 = Cd_T \cdot \text{sign}(P_T) \cdot \sqrt{|P_T|} \quad (2.49)$$

The uncertain flow $MSf: [w_{R_{vT}}]$ is determined in (2.50). It is brought-in at junction $\mathbf{0}_{h1}$ by f_{12} as shown in Fig. 2.12.

$$MSf: [w_{vT}] = -[0, \Delta Cd_T] \text{sign}(e_6) \cdot \sqrt{|e_6|} \quad (2.50)$$

Uncertainty on measurement of pressure sensor P_T is considered as,

$$\left[\underline{P_{T,m}}, \overline{P_{T,m}} \right] = P_{T,r} + \left[-\Delta P_{T,l}, \Delta P_{T,u} \right] \quad (2.51)$$

where $P_{T,m}$ is the measured signal (observed), $P_{T,r}$ is the true value of pressure (unobserved) and $\Delta P_{T,l}$ and $\Delta P_{T,u}$ are obtained from the the *measurement error interval* provided by the

manufacturer ($\pm 1.5\%$ of measured value). Measurement error is modeled in interval form as $[-\Delta P_{T,l}, \Delta P_{T,u}] \equiv [\zeta_{P_T}]$ and represented as a modulated effort source $MSe^* : -[\zeta_{P_T}]$.

Energetic assessment at junction $\mathbf{0}_{11}$ in the deterministic model of Fig. 2.11 gives

$$\dot{H}_{15} = \dot{m}_{21} \cdot c_p \cdot T_2 \quad (2.52)$$

where \dot{H}_{15} is the enthalpy flow at C_T element, c_p is the specific heat at constant pressure and T_2 is the fluid temperature measurement inside the tank. The uncertainty is due to variation of c_p , which is evaluated by polynomial interpolation algorithm. As shown in Fig. 2.12, uncertainty on C_T element is modeled by $MSf: [w_{C_T}]$. It is determined as,

$$MSf: [w_{C_T}] = - \left[\underline{\delta_{c_p}}, \overline{\delta_{c_p}} \right] \dot{m}_{21} \cdot c_{p,n} \cdot T_2 \quad (2.53)$$

2.6.1.2 Pump and Pipe System

As shown in Fig. 2.11, the pump and the pipe are modeled separately by two resistance elements $R:R_p$ and $R:R_{z,l}$ respectively.

$R:R_p$ is modulated by characteristic equation of the pump considered as,

$$\dot{m}_{22} = f(P_p, b_1) = b_1 (k_1 (P_{24} - P_{21}) + k_2) \quad (2.54)$$

$$\text{or, } P_p = \frac{1}{k_1} \left(\frac{\dot{m}_{22}}{b_1} - k_2 \right) \quad (2.55)$$

where, P_{21} and P_{24} are respectively, the input and output pressures of the pump, k_1 and k_2 are uncertain pump characteristic parameters. b_1 is a Boolean parameter that switches its state depending upon the level of water in the boiler as,

$$b_1 = \begin{cases} 0 & \text{if } L_8 < L_{8,ref} + L_8 \\ 1 & \text{if } L_8 > L_{8,ref} - L_8 \end{cases}$$

The parameters k_1 and k_2 are known with uncertainty of $\pm 5\%$; they are modelled as $[\underline{\delta}_{k_1}, \overline{\delta}_{k_1}]$ and $[\underline{\delta}_{k_2}, \overline{\delta}_{k_2}]$. The corresponding uncertain pressure e_{23} is modelled by $MSe: [w_{Rp}]$. It is expressed as,

$$MSe: [w_{Rp}] = -\frac{1}{k_{1,n}} \cdot [\underline{\delta}_{1/k_1}, \overline{\delta}_{1/k_1}] \left(\frac{\dot{m}_{22}}{b_1} - k_{2,n} \right) + \frac{k_{2,n}}{k_{1,n}} \cdot [\underline{\delta}_{k_2}, \overline{\delta}_{k_2}] \left(1 + [\underline{\delta}_{1/k_1}, \overline{\delta}_{1/k_1}] \right) \quad (2.56)$$

Pipe is modelled by a resistor element $R:R_{z1}$ which depends upon tube characteristics and supply valve. Assumption of *Poiseuille* flow in the tube leads to,

$$R_{z1} = (8 \cdot \rho_l \cdot L_p) / \pi \cdot r_{1p} \quad (2.57)$$

where $r_{1p} = r_p^4$, L_p is the pipe length and r_p is the pipe radius.

Considering L_p and r_p as uncertain parameters, the interval valued uncertainty on R_{z1} is a function of interval uncertainty of several parameters. It can be determined as,

$$\left(1 + [\underline{\delta}_{R_{z1}}, \overline{\delta}_{R_{z1}}] \right) \cdot R_{z1,n} = 8 \cdot (\rho_l / \pi) \cdot L_{p,n} \cdot (1 / r_{1p,n}) \cdot \left(1 + [\underline{\delta}_{L_p}, \overline{\delta}_{L_p}] \right) \cdot \left(1 + [\underline{\delta}_{1/r_{1p}}, \overline{\delta}_{1/r_{1p}}] \right) \quad (2.58)$$

As $R_{z1,n} = 8 \cdot (\rho_l / \pi) \cdot L_{p,n} \cdot (1 / r_{1p,n})$,

$$[\underline{\delta}_{R_{z1}}, \overline{\delta}_{R_{z1}}] = \underbrace{[\underline{\delta}_{L_p}, \overline{\delta}_{L_p}] + [\underline{\delta}_{1/r_{1p}}, \overline{\delta}_{1/r_{1p}}]}_{G([\underline{\delta}_{L_p}, \overline{\delta}_{L_p}], [\underline{\delta}_{1/r_{1p}}, \overline{\delta}_{1/r_{1p}}])} + [\underline{\delta}_{L_p}, \overline{\delta}_{L_p}] \cdot [\underline{\delta}_{1/r_{1p}}, \overline{\delta}_{1/r_{1p}}] \quad (2.59)$$

Value on the left of (2.59) is the range of an interval function $G([\underline{\delta}_{L_p}, \overline{\delta}_{L_p}], [\underline{\delta}_{1/r_{1p}}, \overline{\delta}_{1/r_{1p}}])$.

Function G can be considered as *Natural Interval Extension* of

$g(\delta_{L_p}, \delta_{1/r_{1p}}) = \delta_{L_p} + \delta_{1/r_{1p}} + \delta_{L_p} \cdot \delta_{1/r_{1p}}$. By definition, $0 \in [\underline{\delta}_{L_p}, \overline{\delta}_{L_p}]$ and $0 \in [\underline{\delta}_{1/r_{1p}}, \overline{\delta}_{1/r_{1p}}]$. Thus, a

direct interval arithmetic computation on (2.59) gives an over bounded result due to presence of multi-incident intervals. It can be avoided by splitting the domain-parameter space as shown in (2.60), where G_1 and G_2 are monotonic over their respective interval domains. A sharp range value is calculated by taking the join (union) over ranges of G_1 and G_2 .

$$\begin{aligned} [\underline{\delta}_{R_{z1}}, \overline{\delta}_{R_{z1}}] &= \text{range} \left(G \left(\left[\underline{\delta}_{L_p}, \overline{\delta}_{L_p} \right], \left[\underline{\delta}_{1/r_{1p}}, \overline{\delta}_{1/r_{1p}} \right] \right) \right) \\ &= \text{range} \left(G_1 \left(\left[\underline{\delta}_{L_p}, 0 \right], \left[\underline{\delta}_{1/r_{1p}}, 0 \right] \right) \right) \cup \text{range} \left(G_2 \left(\left[0, \overline{\delta}_{L_p} \right], \left[0, \overline{\delta}_{1/r_{1p}} \right] \right) \right) \end{aligned} \quad (2.60)$$

Numerical value of $[\underline{\delta}_{r_p}, \overline{\delta}_{r_p}]$ can be obtained from interval uncertainty $[\underline{\delta}_{r_p}, \overline{\delta}_{r_p}]$ by the usage of the relation $r_{1p} = r_p^4$ and logarithmic differentiation, so that

$$\frac{[-\Delta_{r_p}, \Delta_{r_p}]}{r_{p,n}} = 4 \frac{[-\Delta_{r_p}, \Delta_{r_p}]}{r_{p,n}} \text{ or, } [\underline{\delta}_{r_p}, \overline{\delta}_{r_p}] = 4 \cdot [\underline{\delta}_{r_p}, \overline{\delta}_{r_p}].$$

The dynamics of the flow through pipe \dot{m}_{26} , is determined by Bernoulli's law in turbulent regime as,

$$\dot{m}_{26} = (1/R_{z1}) \cdot \sqrt{P_{26}} = (1/R_{z1}) \cdot \sqrt{P_{24} - P_{29}} \quad (2.61)$$

As shown in Fig. 2.11, it is modelled by non-linear resistor element R: R_{z1} , in resistance causality; the pressure effort is determined as,

$$P_{26} = R_{z1}^2 \cdot \dot{m}_{26}^2 = R_{z1} \cdot F_1^2 \quad (2.62)$$

where F_1 is the flow measurement of \dot{m}_{26} . As represented in Fig. 2.12, the uncertain pressure effort brought by uncertain R_{z1} is modeled as $MSf : [w_{R_{z1}}]$ where,

$$MSf : [w_{R_{z1}}] = -2 \cdot [\underline{\delta}_{R_{z1}}, \overline{\delta}_{R_{z1}}] \cdot R_{z1,n} \cdot F_1^2 \quad (2.63)$$

The enthalpy flow through the pipe is expressed by measured variables F_1 and T_2 as,

$$\dot{H}_{18} = \dot{H}_{28} = T_2 \cdot c_p \cdot F_1 \quad (2.64)$$

The associated hydraulic-thermal coupling is modelled by resistor element R: R_{T1} . The uncertain thermal energy issued due to variation of specific heat c_p is modeled as $MSf : [w_{RT1}]$. It is determined as,

$$MSf : [w_{RT1}] = [\underline{\delta}_{c_p}, \overline{\delta}_{c_p}] \cdot c_{p,n} \cdot T_2 \cdot F_1 \quad (2.65)$$

2.6.1.3 Boiler

As shown in Fig. 2.11, the hydraulic and thermal energies inside the boiler are modelled by a two port C element $C:C_B$ and the heat transfer from the boiler to the environment is characterized by $R:R_a$ element. It is instrumented with two redundant sensors of temperature $De: T_5$ and $De: T_6$, two redundant water level sensors $De: L_8$ and $De: L_9$, an uncertain pressure sensor $De: P_B$, a volumetric flow sensor at the output of the boiler $Df: F_2$, and a power sensor $Df: Q$. Heat flow \dot{Q} is modelled as,

$$\dot{Q} = \frac{1}{R_{an}} (\Delta T) = \lambda \cdot \frac{A_B}{e_B} (T_{50} - T_{62}) \quad (2.66)$$

where λ is the thermal conductivity, e_B is the wall thickness and $(T_{50} - T_{62})$ is the temperature difference between the sides of the section A_B of the boiler wall. The thermal resistance for heat transfer carries interval uncertainty $[\underline{\delta}_{1/R_a}, \overline{\delta}_{1/R_a}]$ as function of $[\underline{\delta}_{1/A_B}, \overline{\delta}_{1/A_B}]$ and $[\underline{\delta}_{e_B}, \overline{\delta}_{e_B}]$. It can be determined as shown in (2.67), where sharp range values are obtained by splitting the interval parameter space as done in (2.60).

$$\begin{aligned} [\underline{\delta}_{1/R_a}, \overline{\delta}_{1/R_a}] &= [\underline{\delta}_{1/A_B}, \overline{\delta}_{1/A_B}] + [\underline{\delta}_{e_B}, \overline{\delta}_{e_B}] \\ &+ [\underline{\delta}_{1/A_B}, \overline{\delta}_{1/A_B}] \cdot [\underline{\delta}_{e_B}, \overline{\delta}_{e_B}] \end{aligned} \quad (2.67)$$

In this work, the experimentally identified value of δ_{R_a} used in (Djeziri, Mohand Arab et al., 2009b) is employed to obtain the uncertainty on R_a in the interval form. From (2.66), the associated uncertain flow is obtained as,

$$MSf : [w_{R_a}] = -[\underline{\delta}_{1/R_a}, \overline{\delta}_{1/R_a}] (1/R_{an}) \cdot (T_5 - T_a) \quad (2.68)$$

As shown in Fig. 2.11, volumetric flow is a function of variation of steam–liquid mass; it is given as,

$$\dot{m}_{46} = d(\rho_l(P_B).V_l + \rho_v(P_B).V_v) / dt = \dot{m}_{31} - \dot{m}_{38} \quad (2.69)$$

$$\begin{aligned} \dot{H}_{50} &= d(\rho_l(P_B).V_l.h_l(P_B) + \rho_v(P_B).V_v.h_v(P_B)) / dt \\ &= \dot{H}_{28} - \dot{H}_{70} - \dot{Q}_{59} + \dot{Q}_{62} \end{aligned} \quad (2.70)$$

where ρ_l, h_l and ρ_v, h_v are, respectively, the density and specific enthalpy of the water and steam inside the boiler; each of them being a function of the boiler pressure P_B . They are calculated using a polynomial interpolation algorithm. V_l is the volume of water, measured by level sensor $De:L_8$. V_v is the volume of steam determined as $V_v = V_B - V_l$, where V_B is the volume of the boiler. P_B is the measured pressure inside the boiler ($SSe: P_B$).

The uncertainties $\delta_{\rho_l}, \delta_{h_l}$ and $\delta_{\rho_v}, \delta_{h_v}$ on ρ_l, h_l and ρ_v, h_v respectively, arise due to error in their identification using polynomial interpolation algorithm. As such, an approximate error interval of $\pm 5\%$ is assumed on their calculated nominal value.

Due to the presence of the multi-incident intervals, the hydraulic uncertainty (δ_{1,C_B}) and thermal uncertainty (δ_{2,C_B}) can be determined, respectively, as shown in (2.71) and (2.72) where for notational simplicity $\delta_i = [\underline{\delta}_i, \overline{\delta}_i]$. They are evaluated by splitting the parameter space and taking the join of the ranges of the found monotonic interval functions.

$$\left[\underline{\delta}_{1,C_B}, \overline{\delta}_{1,C_B} \right] = \delta_{\rho_l} + \delta_{V_l} + \delta_{\rho_l} \delta_{V_l} + \delta_{\rho_v} + \delta_{V_v} + \delta_{\rho_v} \delta_{V_v} \quad (2.71)$$

$$\begin{aligned} \left[\underline{\delta}_{2,C_B}, \overline{\delta}_{2,C_B} \right] &= \delta_{1,C_B} + \delta_{h_l} + \delta_{V_l} \delta_{h_l} + \delta_{\rho_l} \delta_{h_l} \\ &+ \delta_{\rho_l} \delta_{V_l} \delta_{h_l} + \delta_{h_v} + \delta_{V_v} \delta_{h_v} + \delta_{\rho_v} \delta_{h_v} + \delta_{\rho_v} \delta_{V_v} \delta_{h_v} \end{aligned} \quad (2.72)$$

From (2.69), (2.71) and (2.72), interval uncertainty on mass flow $MSf : [w_{1,C_B}]$ and heat flow $MSf : [w_{2,C_B}]$ can be respectively, expressed as ,

$$MSf : [w_{1,C_B}] = - \left[\underline{\delta}_{1,C_B}, \overline{\delta}_{1,C_B} \right] \cdot \frac{d(\rho_{l,n}(P_B).V_{l,n} + \rho_{v,n}(P_B).V_{v,n})}{dt} \quad (2.73)$$

$$MSf : [w_{2,C_B}] = - \left[\underline{\delta}_{2,C_B}, \overline{\delta}_{2,C_B} \right] \cdot \frac{d(\rho_{l,n}(P_B).V_{l,n}.h_{l,n}(P_B) + \rho_{v,n}(P_B).V_{v,n}.h_{v,n}(P_B))}{dt} \quad (2.74)$$

Valve V_B present at the bottom of the tank is manually controlled and introduces water leakage (parametric fault) in the tank, representing a fault modeled at junction $\mathbf{0}_{h2}$ in Fig. 2.11. The valve is modeled by non-linear resistor element $R : R_{V_B}$ as,

$$f_{35} = \dot{m}_{vB} = Cd_B(x).sign(\Delta P).\sqrt{|\Delta P|} \quad (2.75)$$

$$\Delta P = e_{35} \quad (2.76)$$

where Cd_B is the coefficient of discharge proportional to the flow rate. The installed valve characteristics are determined experimentally for four valve positions as shown in Table 2-II.

Table 2-II Stem Position of Valve present in boiler and Discharge Coefficient

Valve Stem Position	$V_{B,1}$	$V_{B,2}$	$V_{B,3}$	$V_{B,4}$
Discharge Coefficient	$Cd_{B,1}$	$Cd_{B,2}$	$Cd_{B,3}$	$Cd_{B,4}$
	5.4678×10^{-3}	5.78×10^{-3}	6.278×10^{-3}	6.478×10^{-3}

During normal functioning of the system, stem position of the valve V_B , present at the bottom of the water tank is at $V_{B,1}$ (with discharge coefficient $Cd_{B,1}$) and the position $V_{B,2}$ (with discharge coefficient $Cd_{B,2}$). The limit on the modulation of valve stem is fixed to $V_{B,2}$ (stem position with discharge coefficient $Cd_{B,2}$). Thus, nominal value of discharge flow coefficient is $Cd_{B,1}$. The uncertainty in valve outflow is brought by uncertain position of the valve stem (between $V_{B,1}$ and $V_{B,2}$). The latter is accounted by limiting the variation of the discharge coefficient Cd_B , as $Cd_B \in [Cd_{B,1}, Cd_{B,2}]$ or $Cd_B = Cd_{B,1} + [0, \Delta Cd_B]$, where $\Delta Cd_B = Cd_{B,2} - Cd_{B,1}$. Thus, while $Cd_B \in [Cd_{B,1}, Cd_{B,2}]$, system is nominal with “no fault” in leakage. The corresponding uncertain flow $MSf : [w_{vB}]$ represented in Fig. 2.12 by f_{32} is determined as,

$$MSf : [w_{vB}] = -[0, \Delta Cd_B] sign(e_{35}).\sqrt{|e_{35}|} \quad (2.77)$$

Measurement from pressure sensor SSe : P_B suffers the sensor bias (offset) and thus, is considered uncertain as,

$$[P_{B,m}, \overline{P_{B,m}}] = P_{B,r} + [-\Delta P_{B,l}, \Delta P_{B,u}] \quad (2.78)$$

where, $P_{B,m}$ is the measured reading and $P_{B,r}$ is the actual reading. $[-\Delta P_{B,l}, \Delta P_{B,u}]$ models the uncertainty in the pressure measurement readings. Measurement error tolerance interval is

provided in the manufacturer's data-sheet based upon which uncertain interval bounds are fixed. Measurement Interval uncertainty is represented as modulated effort sources $MSe^* : -[\zeta_{P_B}]$, as shown in Fig. 2.12.

2.6.1.4 Thermal Resistor

The RS element models the electrical resistance (considered as an active resistor that generates thermal power) of the heating element. The nominal value of the resistor RS_n is calculated using the electrical power given by sensor $Df: \dot{Q}_4$ as,

$$f_{62} = \dot{Q}_A = b_2 \cdot \frac{U_{in}^2}{RS_n} \quad (2.79)$$

$$b_2 = \begin{cases} 0 & \text{if } P_B < P_{B,ref} + P_B \\ 1 & \text{if } P_B > P_{B,ref} - P_B \end{cases}$$

where, U_{in} is the input voltage modulated by Boolean parameter b_2 sensitive to the pressure in the boiler. There is a gradual positive shift in the nominal behavior of resistor at higher operating temperature range of 110°C-150°C. The upper interval limit $\overline{\delta_{1/RS}}$, is set by observing the deviation on nominal value without any faults introduced. The corresponding lower limit $\underline{\delta_{1/RS}}$, signifies the error in the identification of nominal value (lower limit of tolerance) provided by the manufacturer. Represented in Fig. 2.12, the interval valued uncertain heat flow denoted $MSf : [w_{1/RS}]$, is given as,

$$MSf : [w_{RS}] = -[\underline{\delta_{1/RS}}, \overline{\delta_{1/RS}}] \dot{Q}_4 \quad (2.80)$$

$$= b_2 \cdot [\underline{\delta_{1/RS}}, \overline{\delta_{1/RS}}] \frac{U_{in}^2}{RS_n}$$

From Fig.8, the enthalpy outflow from the boiler to the expansion system can be expressed as follows,

$$\dot{H}_{70} = T_{50} \cdot c_v \cdot \dot{m}_{38} \quad (2.81)$$

where, c_v is the uncertain steam heat capacity at constant volume. T_{50} and \dot{m}_{38} are given respectively, by $SSE:T_5$ and volumetric mass flow sensor $Df:F_2$. The corresponding uncertain

heat flow is due to error in estimation of the value of c_v . The latter is represented as $MSf : [w_{RT_2}]$ in Fig. 2.12; it can be expressed as,

$$MSf : [w_{RT_2}] = - \left[\underline{\delta_{c_v}}, \overline{\delta_{c_v}} \right] \cdot c_{v_n} \cdot T_6 \cdot F_2 \quad (2.82)$$

2.6.2 Interval Valued ARR generation

The approach presented in Section 2.4 and Section 2.5 is followed to generate interval valued ARRs from the uncertain BG of the system in Fig. 2.12.

For detection of leakage fault in the tank, energetic assessment at junction 0_{h1} gives,

$$[\underline{R}_1, \overline{R}_1] = f_2 + f_5 - [\underline{f_4}, \overline{f_4}] - [\underline{f_7}, \overline{f_7}] - f_{20}$$

where

$$\begin{aligned} f_2 = 0, f_{20} = f_{24} = F_1, f_5 = 0, \\ [\underline{f_7}, \overline{f_7}] &= Cd_{T,n} \cdot \text{sign}(P_T) \cdot \left[\sqrt{|P_T - \Delta_{P_{T,u}}|}, \sqrt{|P_T + \Delta_{P_{T,l}}|} \right] \\ &+ [0, Cd_{T,2}] \cdot \text{sign}(P_T) \cdot \left[\sqrt{|P_T - \Delta_{P_{T,u}}|}, \sqrt{|P_T + \Delta_{P_{T,l}}|} \right] \\ [\underline{f_4}, \overline{f_4}] &= \frac{A_{T,n}}{\rho_T g} \cdot \frac{dP_T}{dt} + [\underline{\delta_{A_T}}, \overline{\delta_{A_T}}] \cdot \frac{A_{T,n}}{\rho_T g} \cdot \frac{dP_T}{dt} \\ &+ [\underline{A_T}, \overline{A_T}] \cdot (1 / \rho_T g) \cdot \frac{d[\zeta_{P_T}]}{dt} \end{aligned} \quad (2.83)$$

where, $[\zeta_{P_T}] = [-\Delta P_{T,l}, \Delta P_{T,u}] \cdot \Delta P_{T,l}$ and $\Delta P_{T,u}$ are obtained from the the *measurement error interval* provided by the manufacturer ($\pm 1.5\%$ of the measured value). The nominal residual $r_{1,n}$ and *URIF* $[\underline{B}_1, \overline{B}_1]$ are determined as,

$$r_{1,n} = -\text{mid}\left(Cd_{T,n} \cdot \text{sign}(P_T) \cdot \left[\sqrt{|P_T - \Delta_{P_{T,u}}|}, \sqrt{|P_T + \Delta_{P_{T,l}}|}\right]\right) - \frac{A_{T,n}}{\rho_T g} \cdot \frac{dP_T}{dt} - F_1 \quad (2.84)$$

$$\begin{aligned} [\underline{B}_1, \overline{B}_1] = & -\left[0, Cd_{T,2}\right] \text{sign}(P_T) \cdot \left[\sqrt{|P_T - \Delta_{P_{T,u}}|}, \sqrt{|P_T + \Delta_{P_{T,l}}|}\right] + -\left[\underline{\delta}_{A_T}, \overline{\delta}_{A_T}\right] \cdot \frac{A_{T,n}}{\rho_T g} \cdot \frac{dP_T}{dt} \\ & -\left[\underline{A}_T, \overline{A}_T\right] \cdot (1/\rho_T g) \cdot \frac{d\left([\underline{-\Delta P_{T,l}}, \overline{\Delta P_{T,u}}]\right)}{dt} \\ & -\frac{1}{2} \text{width}\left(Cd_{T,n} \cdot \text{sign}(P_T) \cdot \left[\sqrt{|P_T - \Delta_{P_{T,u}}|}, \sqrt{|P_T + \Delta_{P_{T,l}}|}\right]\right) [-1, 1] \end{aligned} \quad (2.85)$$

The second ARR is generated from the junction $\mathbf{1}_p$ connected to *SSf*: F_l . It is sensitive to fault due to valve blockage (or pipe plugging) at the pump output. Energetic assessment at $\mathbf{1}_p$ junction gives,

$$[\underline{R}_2, \overline{R}_2] = [\underline{e}_{24}, \overline{e}_{24}] + [\underline{e}_{25}, \overline{e}_{25}] - e_{26} - [\underline{e}_{29}, \overline{e}_{29}] + [\underline{e}_{27}, \overline{e}_{27}]$$

with

$$e_{26} = R_{z1}^2 \cdot F_1^2, [\underline{e}_{29}, \overline{e}_{29}] = P_B - [\underline{\zeta}_{P_B}], [\underline{e}_{27}, \overline{e}_{27}] = [w_{Rz1}],$$

$$\begin{aligned} [\underline{e}_{24}, \overline{e}_{24}] = & [\underline{e}_{21}, \overline{e}_{21}] - [\underline{e}_{22}, \overline{e}_{22}] + [\underline{e}_{23}, \overline{e}_{23}] = (P_T - [\underline{\zeta}_{P_T}]) \\ & - \left((1/k_{1,n}) \cdot ((\dot{m}_{22}/b) - k_{2,n})\right) + [w_{Rp}] \end{aligned}$$

The nominal $r_{2,n}$ and *URIF* $[\underline{B}_2, \overline{B}_2]$ are determined as,

$$r_{2,n} = P_T - (1/k_{1,n}) \cdot ((\dot{m}_{22}/b) - k_{2,n}) - R_{z1}^2 \cdot F_1^2 - P_B \quad (2.86)$$

$$\begin{aligned} [\underline{B}_2, \overline{B}_2] = & MSe : [w_{Rz1}] + MSe : [w_{Rp}] - [\underline{-\Delta_{P_{T,l}}}, \overline{-\Delta_{P_{T,u}}}] + [\underline{-\Delta_{P_{B,l}}}, \overline{-\Delta_{P_{B,u}}}] \\ = & -2 \cdot [\underline{\delta}_{R_{z1}}, \overline{\delta}_{R_{z1}}] \cdot R_{z1,n} \cdot F_1^2 - \frac{1}{k_{1,n}} \cdot [\underline{\delta}_{1/k_1}, \overline{\delta}_{1/k_1}] \left(\frac{\dot{m}_{22}}{b_1} - k_{2,n} \right) + \frac{k_{2,n}}{k_{1,n}} \cdot [\underline{\delta}_{k_2}, \overline{\delta}_{k_2}] \left(1 + [\underline{\delta}_{1/k_1}, \overline{\delta}_{1/k_1}] \right) \\ & - [\underline{-\Delta_{P_{T,l}}}, \overline{-\Delta_{P_{T,u}}}] + [\underline{-\Delta_{P_{B,l}}}, \overline{-\Delta_{P_{B,u}}}] \end{aligned} \quad (2.87)$$

Third ARR is generated from the junction $\mathbf{0}_{h2}$ connected to the dualized detector *SSe*: P_B sensitive to the leakage fault in the boiler.

$$[\underline{R}_3, \overline{R}_3] = f_{31} - f_{37} - [\underline{f_{40}}, \overline{f_{40}}] - [\underline{f_{34}}, \overline{f_{34}}]$$

with

$$[\underline{f_{31}}, \overline{f_{31}}] = \dot{m}_{31} = F_1, [\underline{f_{37}}, \overline{f_{37}}] = [\underline{f_{38}}, \overline{f_{38}}] = F_2,$$

$$\begin{aligned} \left[\underline{f_{40}}, \overline{f_{40}} \right] &= d(\rho_l(P_B) \cdot L_8 + \rho_v(P_B) \cdot (V_B - L_8)) / dt + \left[\underline{\delta_{1,C_B}}, \overline{\delta_{1,C_B}} \right] \cdot \frac{d(\rho_{l,n}(P_B) \cdot V_{l,n} + \rho_{v,n}(P_B) \cdot V_{v,n})}{dt} \\ \left[\underline{f_{34}}, \overline{f_{34}} \right] &= Cd_{B,n} \cdot \text{sign}(P_B) \cdot \left[\sqrt{|P_B - \Delta_{P_{B,u}}|}, \sqrt{|P_B + \Delta_{P_{B,l}}|} \right] \\ &+ \left[0, Cd_{B,2} \right] \text{sign}(P_B) \cdot \left[\sqrt{|P_B - \Delta_{P_{B,u}}|}, \sqrt{|P_B + \Delta_{P_{B,l}}|} \right] \end{aligned}$$

The nominal residual $r_{3,n}$ and URIF $[\underline{B_3}, \overline{B_3}]$ are determined as,

$$\begin{aligned} r_{3,n} &= -d(\rho_l(P_B) \cdot L_8 + \rho_v(P_B) \cdot (V_B - L_8)) / dt + F_1 - F_2 \\ &- \text{mid} \left[Cd_{B,n} \cdot \text{sign}(P_B) \cdot \left[\sqrt{|P_B - \Delta_{P_{B,u}}|}, \sqrt{|P_B + \Delta_{P_{B,l}}|} \right] \right] \end{aligned} \quad (2.88)$$

$$\begin{aligned} \left[\underline{B_3}, \overline{B_3} \right] &= - \left[0, Cd_{B,2} \right] \text{sign}(P_B) \cdot \left[\sqrt{|P_B - \Delta_{P_{B,u}}|}, \sqrt{|P_B + \Delta_{P_{B,l}}|} \right] \\ &- \left[\underline{\delta_{1,C_B}}, \overline{\delta_{1,C_B}} \right] \cdot \frac{d(\rho_{l,n}(P_B) \cdot V_{l,n} + \rho_{v,n}(P_B) \cdot V_{v,n})}{dt} \\ &- \frac{\text{width}}{2} \left[Cd_{B,n} \cdot \text{sign}(P_B) \cdot \left[\sqrt{|P_B - \Delta_{P_{B,u}}|}, \sqrt{|P_B + \Delta_{P_{B,l}}|} \right] \right] \left[-1, 1 \right] \end{aligned} \quad (2.89)$$

In Fig. 2.12, the fourth ARR is generated from the thermal 0_{t2} junction connected to the dualized $SSe:T_5$ as,

$$\begin{aligned} \left[\underline{R_4}, \overline{R_4} \right] &= f_{28} + \left[\underline{f_{62}}, \overline{f_{62}} \right] - f_{59} - f_{69} - \left[\underline{f_{50}}, \overline{f_{50}} \right] \\ &+ \left[\underline{f_{51}}, \overline{f_{51}} \right] + \left[\underline{f_{52}}, \overline{f_{52}} \right] + \left[\underline{f_{53}}, \overline{f_{53}} \right] + \left[\underline{f_{54}}, \overline{f_{54}} \right] \end{aligned}$$

with,

$$f_{28} = \dot{H}_{28} = F_1 \cdot c_{p,n} \cdot T_2,$$

$$\left[\underline{f_{62}}, \overline{f_{62}} \right] = \dot{Q}_4 = (1 / RS_n) U_{in}^2 + MSf : [w_{RS}]$$

$$f_{59} = (1 / R_{an})(T_5 - Ta),$$

$$f_{69} = \dot{H}_{70} = T_5 \cdot c_{v,n} \cdot F_2$$

$$\left[\underline{f_{50}}, \overline{f_{50}} \right] = \frac{d(\rho_{l,n}(P_B) \cdot V_{l,n} \cdot h_{l,n}(P_B))}{dt} + \frac{d(\rho_{v,n}(P_B) \cdot V_{v,n} \cdot h_{v,n}(P_B))}{dt}$$

$$\left[\underline{f_{51}}, \overline{f_{51}} \right] = MSf : [w_{R_a}], \left[\underline{f_{52}}, \overline{f_{52}} \right] = MSf : [w_{2C_B}], \left[\underline{f_{53}}, \overline{f_{53}} \right] = MSf : [w_{RT2}], \left[\underline{f_{54}}, \overline{f_{54}} \right] = MSf : [w_{RT1}]$$

The nominal residual $r_{4,n}$ and URIF $[\underline{B}_4, \overline{B}_4]$ are determined as,

$$r_{4,n} = F_1 \cdot c_{p,n} \cdot T_2 + (1 / RS_n) U_{in}^2 - (1 / R_{an}) (T_5 - T_a) \quad (2.90)$$

$$- T_6 \cdot c_{v,n} \cdot F_2 - \frac{d(\rho_{l,n}(P_B) \cdot V_{l,n} \cdot h_{l,n}(P_B))}{dt} - \frac{d(\rho_{v,n}(P_B) \cdot V_{v,n} \cdot h_{v,n}(P_B))}{dt}$$

$$[\underline{B}_4, \overline{B}_4] = [w_{RT1}] + [w_{RS}] + [w_{2C_B}] + [w_{RT2}] + [w_{R_a}] \quad (2.91)$$

$$= \left[\underline{\delta}_{c_p}, \overline{\delta}_{c_p} \right] c_{p,n} T_2 \cdot F_1 + b_2 \cdot \left[\underline{\delta}_{1/RS}, \overline{\delta}_{1/RS} \right] \frac{U_{in}^2}{RS_n}$$

$$- \left[\underline{\delta}_{2,C_B}, \overline{\delta}_{2,C_B} \right] \frac{d(\rho_{l,n}(P_B) \cdot V_{l,n} \cdot h_{l,n}(P_B) + \rho_{v,n}(P_B) \cdot V_{v,n} \cdot h_{v,n}(P_B))}{dt}$$

$$- \left[\underline{\delta}_{c_v}, \overline{\delta}_{c_v} \right] \cdot c_{v,n} \cdot T_6 \cdot F - \left[\underline{\delta}_{1/R_a}, \overline{\delta}_{1/R_a} \right] (1 / R_{an}) \cdot (T_5 - T_a)$$

2.6.3 Experimental Results

The nominal and uncertainty values of the various system parameters and measurement errors are tabulated in Table 2-III. The interval computations are achieved using INTLAB (Rump, 1999) library, which is a toolbox for MATLAB supporting real and complex interval computations. The real time computation are done using dSPACE® real time interface implemented via SIMULINK.

Nominal Conditions: Fig. 2.13 shows the four residuals found in the previous section under no fault conditions, with all the parameters remaining inside their pre-defined interval bounds. The latter translate to the following facts:

- Stem position of the valve V_T , present at the bottom of the water tank is between $V_{T,1}$ (discharge coefficient $Cd_{T,1}$) and the position $V_{T,2}$ (discharge coefficient $Cd_{T,2}$)
- Stem position of the valve V_B , present at the bottom of the boiler is between $V_{B,1}$ (discharge coefficient $Cd_{B,1}$) and the position $V_{B,2}$ (discharge coefficient $Cd_{B,2}$)
- None of the system parameters are modulated manually.

Table 2-III Nominal Values and Uncertainty Values

	Physical Name	Nominal Value	Interval Uncertainty	Uncertainty value		Physical Name	Nominal Value	Interval Uncertainty	Uncertainty value
A_T	Tank Section	0.436 m ²	$[\underline{\delta_{A_T}}, \overline{\delta_{A_T}}]$	[-0.004, 0.009]	e_B	Thickness of the Boiler Metal	0.008 m	$[\underline{\delta_{e_B}}, \overline{\delta_{e_B}}]$	[-0.085, 0.085]
Cd_T	Discharge coefficient in Tank Valve	0.00632	$[0, \Delta Cd_T]$	[0, 0.358×10 ⁻³]	A_B	Boiler Section	1.887 m ²	$[\underline{\delta_{1/A_B}}, \overline{\delta_{1/A_B}}]$	[-0.0067, 0.0067]
$P_{T,m}$	Pressure in Tank	Measured	$[\underline{P_{T,m}}, \overline{P_{T,m}}]$	Measured	R_a	Heat transfer Parameter	2858 W/K	$[\underline{\delta_{1/R_a}}, \overline{\delta_{1/R_a}}]$	[-0.0027, 0.0027]
ΔP_T	Pressure Sensor Bias in Tank	Measured	$[\Delta P_T, \overline{\Delta P_T}]$	[-4.3, 4.9] Pa	V_B	Boiler Volume	0.175 m ³	0	0
c_p	Fluid specific Heat at constant Pressure	Variable	$[\underline{\delta_{c_p}}, \overline{\delta_{c_p}}]$	[-0.015, 0.015]	ρ_v	Steam Density	Variable	$[\underline{\delta_{\rho_v}}, \overline{\delta_{\rho_v}}]$	[-0.02, 0.02]
k_1	Pump Characteristic	-8.33×10 ⁷ ms	$[\underline{\delta_{k_1}}, \overline{\delta_{k_1}}]$	[-0.05, 0.05]	h_v	Specific enthalpy of steam	Variable	$[\underline{\delta_{h_v}}, \overline{\delta_{h_v}}]$	[-0.023, 0.023]
k_2	Pump Characteristic	0.97 kg/s	$[\underline{\delta_{k_2}}, \overline{\delta_{k_2}}]$	[-0.05, 0.05]	h_l	Fluid specific enthalpy	Variable	$[\underline{\delta_{h_l}}, \overline{\delta_{h_l}}]$	[-0.023, 0.023]
R_{z1}	Pipe Hydraulic Resistance	2550Pa s/kg	$[\underline{\delta_{R_{z1}}}, \overline{\delta_{R_{z1}}}]$	[-0.01, 0.01]	Cd_B	Discharge coefficient in Boiler Valve	0.00546	$[0, \Delta Cd_B]$	[0, 0.284×10 ⁻³]
λ	Thermal Conductivity of the boiler Wall	0.174 W/m K	$[\underline{\delta_{\lambda}}, \overline{\delta_{\lambda}}]$	0	$P_{T,m}$	Pressure in Boiler	Measured	$[\underline{P_{T,m}}, \overline{P_{T,m}}]$	[-1.2%, 1.2%]
RS	Thermal Electrical Resistance	2.406 Ω	$[\underline{\Delta RS}, \overline{\Delta RS}]$	[0,0.5]	ΔP_T	Pressure Sensor Bias in Tank	Measured	$[\Delta P_T, \overline{\Delta P_T}]$	[-1.9, 1.9] Pa

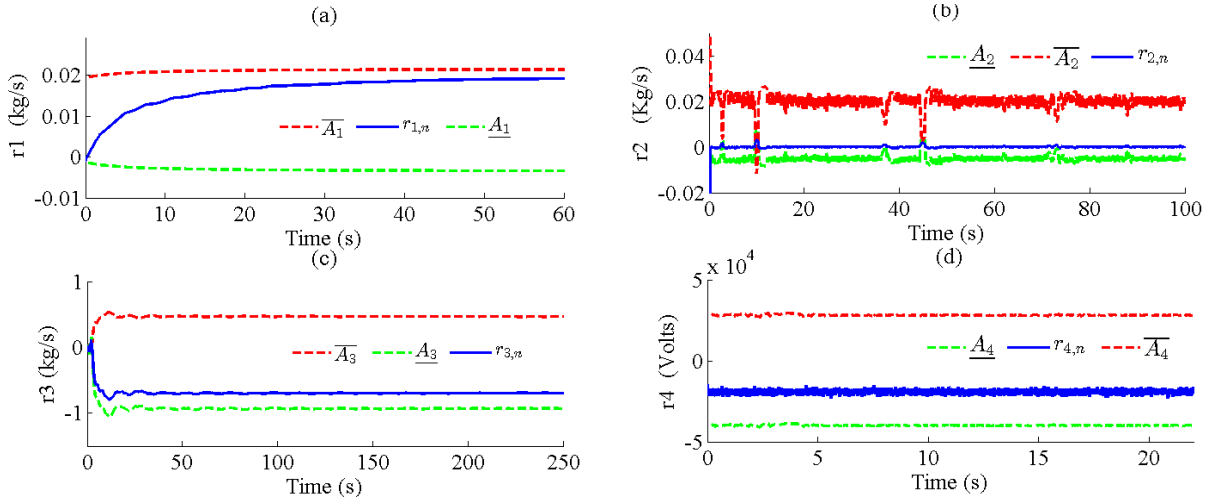


Fig. 2.13 Nominal Conditions (a) Nominal Residual $r_{1,n}$ and Thresholds as range of $[\underline{A}_1, \overline{A}_1] = -[\underline{B}_1, \overline{B}_1]$; (b) Nominal Residual $r_{2,n}$ and Thresholds as range of $[\underline{A}_2, \overline{A}_2] = -[\underline{B}_2, \overline{B}_2]$, (c) Nominal Residual $r_{3,n}$ and Thresholds as range of $[\underline{A}_3, \overline{A}_3] = -[\underline{B}_3, \overline{B}_3]$, (d) Nominal Residual $r_{4,n}$ and Thresholds as range of $[\underline{A}_4, \overline{A}_4] = -[\underline{B}_4, \overline{B}_4]$.

There are four types of faults introduced in the system.

Fault in Tank: Fig. 2.14 (a) shows the variation in outflow of valve V_T , present at the bottom of the water tank. At $t=6s$, the valve stem position is manually changed from its nominal state (between $V_{T,1}$ and $V_{T,2}$) to $V_{T,3}$ (see Table 2-I). This leads to increase in the flow output as shown in Fig. 2.14 (a). The latter translates to the fact that associated discharge coefficient Cd_T is outside of the allowed interval limits i.e. $Cd_T \notin [Cd_{T,1}, Cd_{T,2}]$. The fault is detected when the corresponding nominal residual $r_{1,n}$ deviates outside the bounds of associated URIF, as shown in Fig. 2.14 (b).

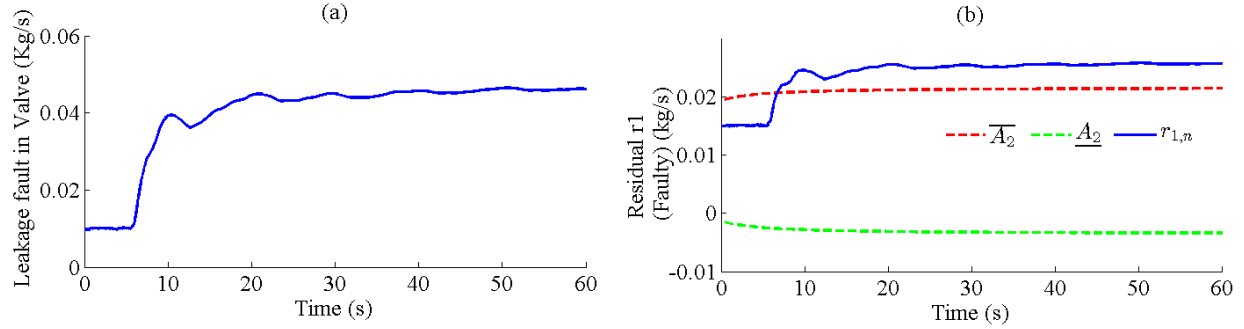


Fig. 2.14 Fault in Water Tank (a) Leakage of water (b) Fault Detection with Nominal Residual $r_{1,n}$ and Thresholds as range of $[\underline{A}_1, \overline{A}_1] = -[\underline{B}_1, \overline{B}_1]$.

Fault in Pipe: As shown in Fig. 2.15 (a), the resistance of the pipe is increased by modulating the stopper at the output of the pump. The volumetric flow is measured by $Df:F_I$ (kg/s). It is modulated abruptly to the closed state; the supply of output flow is cut. As shown in Fig. 2.15 (b), the parametric deviation (fault) results in deviation of $r_{2,n}$ outside the associated URIF bounds.

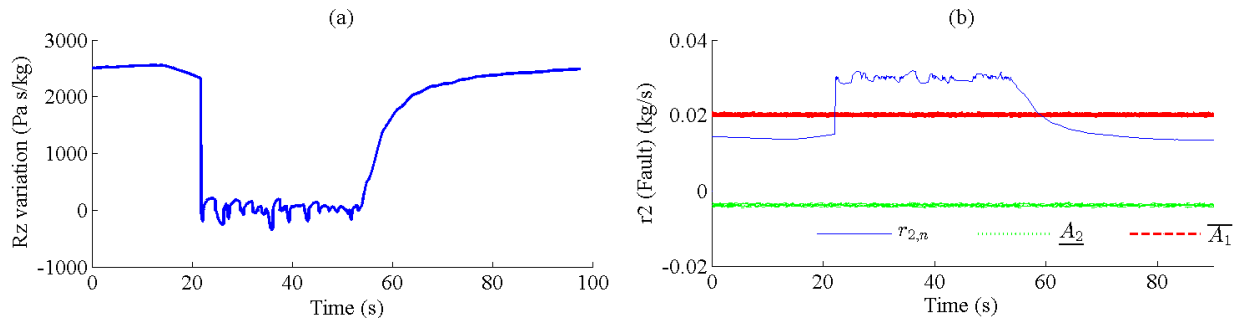


Fig. 2.15 Fault in Pipe (a) Variation of resistance R_z (b) Fault Detection with Nominal Residual $r_{2,n}$ and Thresholds as range of $[\underline{A}_2, \overline{A}_2] = -[\underline{B}_2, \overline{B}_2]$.

Fault in Boiler: Fig. 2.16 (a) shows the variation in outflow of valve V_B , present at the bottom of the boiler. The valve stem position is manually changed between $t=30s$ and $t=110s$; the nominal state (between $V_{B,1}$ and $V_{B,2}$) is modulated to $V_{B,3}$ (see Table 2-II). This leads to increase in the flow output as shown in Fig. 2.16 (a). The latter translates to the fact that associated discharge coefficient Cd_B is outside of the allowed interval limits i.e.

$Cd_B \notin [Cd_{B,1}, Cd_{B,2}]$. The fault is detected when the corresponding nominal residual $r_{3,n}$ deviates outside the bounds of associated URIF, as shown in Fig. 2.16 (a).

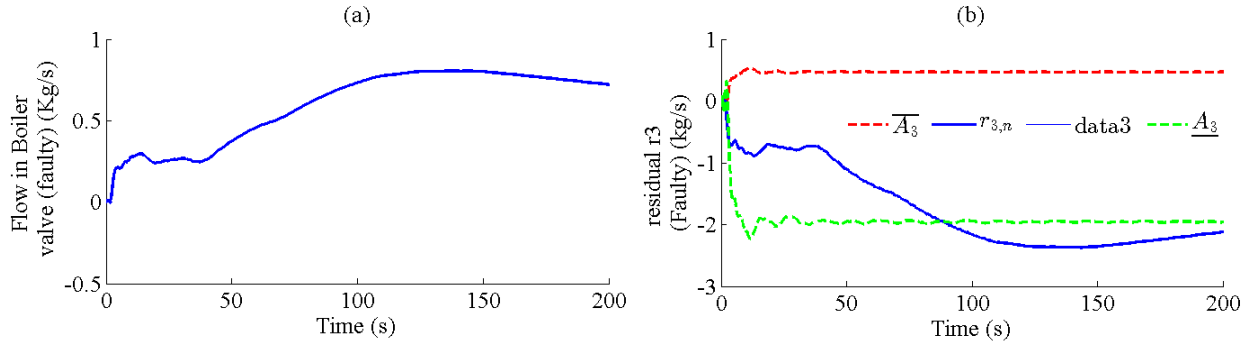


Fig. 2.16 Fault in Boiler Valve V_B (a) Water leakage (b) Fault Detection with Nominal Residual $r_{3,n}$ and Thresholds as range of $[A_3, \bar{A}_3] = -[B_3, \bar{B}_3]$.

Fault in the Thermal Resistor: In Fig. 2.17 (a), between $t=13s$ and $t=22s$, value of the thermal resistor (electrical resistance) is modulated linearly. It crosses the corresponding upper limit of $+0.5ohm$ at around $t=16s$. As shown in Fig. 2.17 (b), $r_{3,n}$ deviates outside the upper threshold limit and thus, fault is detected. The residual is corrupted with unavoidable sensor noise (visible as sharp peaks).

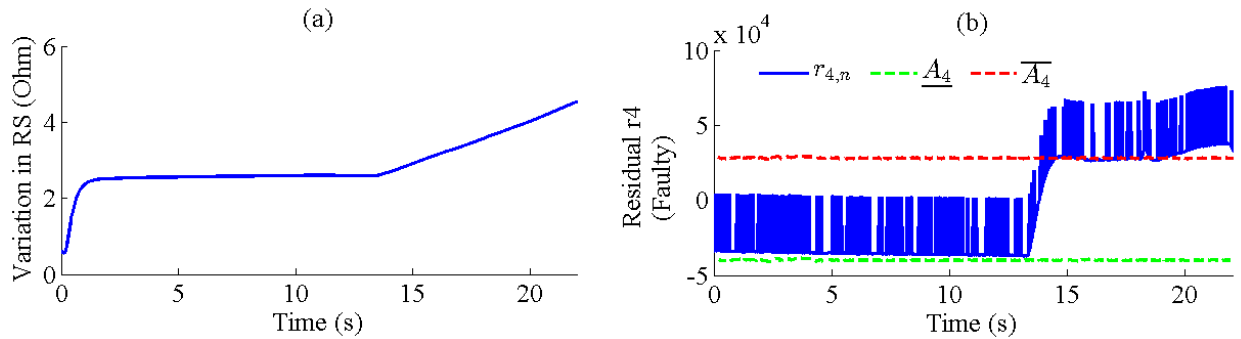


Fig. 2.17 Fault in electrical resistor (a) Increase in the Resistance RS (b) Fault Detection with Nominal Residual $r_{4,n}$ and Thresholds as range of $[A_4, \bar{A}_4] = -[B_4, \bar{B}_4]$.

2.6.4 Comparison with BG-LFT Robust FDI

Uncertain parameters existing in industrial multi-energetic systems may be broadly classified into two categories:

- **Uncertain physical components:** Comprising of manufactured industrial equipments or components like electrical resistances, capacitors, area-radius of a hydraulic tank etc.
- **Uncertain physical phenomenon:** Comprising of physical processes that deviate or exhibit natural variation based upon different operational conditions, operational environment etc. For example, physical phenomena such as friction, loading, inertia, rigidity, progressively varying electrical resistances etc.

Parameters of the former type carry uncertainty in terms of manufacturing errors or tolerance of manufacturing (percentage error) on the either side of its fabricated value. Usually, the uncertainties on such components are quantified statistically and lead to an equal magnitude of uncertainty on either side of the nominal value. For example, an electrical resistor of 4 Ohm with 1% uncertainty i.e. $\pm 0.04\text{Ohms}$. On the other hand, a physical phenomenon may vary on either side of the nominal value, or uni-directionally (friction, corrosion layer etc.) under different operational or environmental conditions. Hence, the upper and lower bounds on the allowed deviation may not be necessarily equal.

In BG-LFT method (see Appendix B), the parametric uncertainties are quantified in a statistical manner so that the magnitude of the uncertainty on either sides of the nominal value is equal, or uncertain limits over the nominal value remains the same. In other words, in BG –LFT method the uncertainty over all of the considered parameters are quantified in a similar manner, irrespective of whether the considered system parameter is a varying physical component or physical process. As BG is unified language of modelling multi-energetic systems, such an approach promises to limit the scope of uncertainty quantification in presence of various types of physical phenomena that vary uni-directionally or unequally, on either sides of their nominal value.

To illustrate the aforementioned aspect, consider a parameter vector θ , two uncertain parameters $\{\theta_1, \theta_2\}$ and a parameter set consisting of only certain parameters, $\theta' = \theta - \{\theta_1, \theta_2\}$. Without the loss of generality, in the discussion that follows, it is assumed that the energetic assessment is done at a 1-*junction*, to obtain the constraint relations: BG-LFT derived ARR: R and I-ARR: $[\underline{R}, \overline{R}]$. Moreover, it is assumed that there are only two uncertain system parameters sensitive to R and $[\underline{R}, \overline{R}]$.

BG-LFT Method: In BG-LFT context, an uncertain parameter θ_i , ($i=1,2$) is modelled as:

$$\theta_i = \theta_{i,n} \pm \Delta\theta_i; \quad \Delta\theta_i \geq 0 \quad (2.92)$$

$$\text{or, } \theta_i = \theta_{i,n} (1 \pm \delta_{\theta_i}); \quad \delta_{\theta_i} = \frac{\Delta\theta_i}{\theta_{i,n}} \quad (2.93)$$

where $\Delta\theta_i$ is the additive uncertainty, quantified statistically and δ_{θ_i} is the corresponding multiplicative uncertainty. Thus, the lower and upper limits on the parametric deviation remain equal. Let the ARR R be sensitive to θ and system measurements, system inputs and their derivatives etc. Then, R can be considered consisting of nominal part r and uncertain part b (see Appendix B) as $R_{BG-LFT} = r_{BG-LFT,n} + b$. The nominal part is sensitive to certain parameters, nominal value of uncertain parameters, system inputs and output measurements, whereas the uncertain part b is sensitive to parametric uncertainties and uncertain effort (R is assumed to be derived at 1-*junction*) brought by the respective parametric uncertainties. Here,

$$b = w_{\theta_1} + w_{\theta_2} \quad (2.94)$$

with the uncertain efforts, $w_{\theta_1} = \Delta_{\theta_1} e_{\theta_1}$ and $w_{\theta_2} = \Delta_{\theta_2} e_{\theta_2}$; where e_{θ_i} is the effort brought by the additive uncertainty Δ_{θ_i} on θ_i , at the BG junction. The lower threshold a_{lower} , and upper threshold a_{upper} , are formed as:

$$\begin{aligned} a_{upper} &= w_{\theta_1} / + / w_{\theta_2} / \\ &= \Delta\theta_1 \cdot e_{\theta_1} / + / \Delta\theta_2 \cdot e_{\theta_2} / \\ &= \Delta\theta_1 / e_{\theta_1} / + \Delta\theta_2 / e_{\theta_2} / \end{aligned} \quad (2.95)$$

$$\begin{aligned} a_{lower} &= -a_{upper} \\ &= -\Delta\theta_1 / e_{\theta_1} / -\Delta\theta_2 / e_{\theta_2} \end{aligned} \quad (2.96)$$

Clearly, as the thresholds are sensitive to absolute values of the uncertain efforts, the sign of the latter is not accounted in the development of thresholds.

I-ARR Context: On the other hand, as described in Section 2.3- 2.5, uncertain parameters as interval models require the knowledge of parametric variation within an interval bound. As such, knowledge of statistical properties (distribution) of uncertainty is not mandatory. The uncertainty bounds can be chosen based upon the nature of the parametric variation. As such, the interval bounds of uncertainty are not necessarily symmetric or non-zero, with respect to the nominal parametric value. This leads to an efficient modelling of uncertainty for physical components and physical phenomenon. While for the former, the uncertainty interval bounds are usually given by the statistical distribution around the nominal value, intervals bounds for the latter are usually non-symmetric and depend upon the underlying nature of parametric deviation during system operation. Thus, the uncertain parameter θ_i , ($i=1,2$) can be modelled as (see Section 2.3- 2.5):

$$\left[\underline{\theta}_i, \overline{\theta}_i \right] = \theta_{i,n} + \left[-\Delta\theta_{i,l}, \Delta\theta_{i,u} \right]; \quad \Delta\theta_{i,l} \neq \Delta\theta_{i,u}, \Delta\theta_{i,l} \geq 0, \Delta\theta_{i,u} \geq 0 \quad (2.97)$$

In the I-ARR context, the energetic assessment at 1-*junction* leads to interval valued URIF $\left[\underline{B}, \overline{B} \right]$, given as:

$$\left[\underline{B}, \overline{B} \right] = \left[-\Delta\theta_{1,l}, \Delta\theta_{1,u} \right] e_{\theta_1} + \left[-\Delta\theta_{2,l}, \Delta\theta_{2,u} \right] e_{\theta_2} \quad (2.98)$$

Clearly, the signs of efforts e_{θ_i} , ($i=1,2$) are taken into account for determination of threshold limits. Moreover, interval arithmetic is involved in the determination of the range of URIF (interval limits). The upper and lower thresholds generated from the interval bounds of the range of URIFs, for different sign configurations of uncertain efforts, are shown in Table 2-IV. Therein, it is observed that when the bounds of the interval uncertainty are symmetric (lower limit equals upper limit), the upper and lower thresholds obtained from URIF range bounds are equal to the BG-LFT derived ones. In other words, if the interval limits of the uncertainty are symmetric with respect to zero (i.e. magnitude of additive uncertainty on either sides of the

nominal value is equal), BG-LFT enabled thresholds can be obtained from the interval limits of URIFs.

Table 2-IV URIF Bounds and BG-LFT Thresholds with Symmetric and Non-Symmetric Interval Uncertainty

		URIF	
		Range Interval	
URIF	Range Interval Limits	Limits	BG-LFT Thresholds
		with Symmetric	(Symmetric Uncertainty
		Interval Uncertainty	Limits)
		$\Delta\theta_1 = \Delta\theta_{1,l} = \Delta\theta_{1,u}$	$\pm\Delta\theta_1, \pm\Delta\theta_2$
		$\Delta\theta_2 = \Delta\theta_{2,l} = \Delta\theta_{2,u}$	
$e_{\theta_1} \geq 0, e_{\theta_2} \geq 0$	$\underline{B} = -\Delta\theta_{1,l} \cdot e_{\theta_1} - \Delta\theta_{2,l} e_{\theta_2}$ $\bar{B} = \Delta\theta_{1,u} \cdot e_{\theta_1} + \Delta\theta_{2,u} e_{\theta_2}$	$\underline{B} = -\Delta\theta_1 \cdot e_{\theta_1} - \Delta\theta_2 e_{\theta_2}$ $\bar{B} = \Delta\theta_1 \cdot e_{\theta_1} + \Delta\theta_2 e_{\theta_2}$	$a_{lower} = -\Delta\theta_1 / e_{\theta_1} / -\Delta\theta_1 / e_{\theta_2} /$ $a_{upper} = \Delta\theta_1 / e_{\theta_1} / +\Delta\theta_1 / e_{\theta_2} /$
$e_{\theta_1} \geq 0, e_{\theta_2} \leq 0$	$\underline{B} = -\Delta\theta_{1,l} e_{\theta_1} - \Delta\theta_{2,u} e_{\theta_2} $ $\bar{B} = \Delta\theta_{1,u} e_{\theta_1} + \Delta\theta_{2,l} e_{\theta_2} $	$\underline{B} = -\Delta\theta_1 e_{\theta_1} - \Delta\theta_2 e_{\theta_2} $ $\bar{B} = \Delta\theta_1 e_{\theta_1} + \Delta\theta_2 e_{\theta_2} $	$a_{lower} = -\Delta\theta_1 / e_{\theta_1} / -\Delta\theta_1 / e_{\theta_2} /$ $a_{upper} = \Delta\theta_1 / e_{\theta_1} / +\Delta\theta_1 / e_{\theta_2} /$
$e_{\theta_1} \leq 0, e_{\theta_2} \geq 0$	$\underline{B} = -\Delta\theta_{1,u} e_{\theta_1} - \Delta\theta_{2,l} e_{\theta_2} $ $\bar{B} = \Delta\theta_{1,l} e_{\theta_1} + \Delta\theta_{2,u} e_{\theta_2} $	$\underline{B} = -\Delta\theta_1 e_{\theta_1} - \Delta\theta_2 e_{\theta_2} $ $\bar{B} = \Delta\theta_1 e_{\theta_1} + \Delta\theta_2 e_{\theta_2} $	$a_{lower} = -\Delta\theta_1 / e_{\theta_1} / -\Delta\theta_1 / e_{\theta_2} /$ $a_{upper} = \Delta\theta_1 / e_{\theta_1} / +\Delta\theta_1 / e_{\theta_2} /$
$e_{\theta_1} \leq 0, e_{\theta_2} \leq 0$	$\underline{B} = -\Delta\theta_{1,u} e_{\theta_1} - \Delta\theta_{2,u} e_{\theta_2} $ $\bar{B} = \Delta\theta_{1,l} e_{\theta_1} + \Delta\theta_{2,l} e_{\theta_2} $	$\underline{B} = -\Delta\theta_1 e_{\theta_1} - \Delta\theta_2 e_{\theta_2} $ $\bar{B} = \Delta\theta_1 e_{\theta_1} + \Delta\theta_2 e_{\theta_2} $	$a_{lower} = -\Delta\theta_1 / e_{\theta_1} / -\Delta\theta_1 / e_{\theta_2} /$ $a_{upper} = \Delta\theta_1 / e_{\theta_1} / +\Delta\theta_1 / e_{\theta_2} /$

The same analysis can be exercised at 0-junction with two or more uncertain parameters.

Thus, following significant observations can be made:

- BG-LFT method models uncertainty with symmetric bounds. As such, various physical phenomena cannot be modelled accurately.
- BG-LFT thresholds are necessarily symmetric with respect to zero.

- BG-LFT method of modelling uncertainty is a special case of interval valued uncertainty approach in BG, where the uncertainty interval has symmetric bounds.
- BG-LFT enabled thresholds can be obtained from URIF range bounds when the uncertainty intervals have symmetric bounds.

2.6.5 BG-LFT Enabled Threshold Generation for Steam Generator System

The BG-LFT enabled thresholds are assessed for the four residuals, derived from steam generator system in Section 2.6.2. Each of the uncertain parameters is considered with symmetric uncertainty limits as shown in (2.93). Physical processes that deviate uni-directionally are considered in such a way that uncertainty limits are symmetric with respect to their respective nominal values.

Table 2-V Uncertainty Values for BG-LFT Type Threshold Generation

	Physical Name	Nominal Value	Interval Uncertainty	BG-LFT Uncertainty
A_T	Tank Section	0.436m ²	$[\underline{\delta}_{A_T}, \overline{\delta}_{A_T}] = [-0.004, 0.009]$	$\pm\delta_{A_T} = 0.009$
Cd_T	Discharge coefficient in Tank Valve	0.623	$[0, \Delta Cd_T] = [0, 0.358 \times 10^{-3}]$	$\pm\Delta Cd_T = \pm 0.358 \times 10^{-3}$
RS	Thermal Electrical Resistance	2.406 Ω	$[\underline{\Delta RS}, \overline{\Delta RS}] = [0, 0.5]$	$\pm\Delta RS = \pm 0.5$
Cd_B	Discharge coefficient in Boiler Valve	0.61	$[0, \Delta Cd_B] = [0, 0.284 \times 10^{-3}]$	$\pm\Delta Cd_B = \pm 0.284 \times 10^{-3}$

Parametric values that have been modified for BG-LFT threshold generation are listed in Table 2-V. Rests of the parametric uncertainties remain same as listed previously in Table 2-III. In Table 2-VI, for each of the four residuals, the corresponding BG-LFT thresholds are listed. In Fig. 2.18 and Fig. 2.19 , the four residuals are shown with URIFs and BG-LFT enabled thresholds for a comparative study.

Table 2-VI Threshold generation using BG-LFT method

Residual	Uncertain part	BG-LFT Thresholds
$r_{1,n}$	$a_1 = \left Cd_{T,2} \cdot \text{sign}(P_T - \Delta_{P_T}) \cdot \sqrt{ P_T - \Delta_{P_T} } \right +$ $\left \delta_{A_T} \cdot \frac{A_{T,n}}{\rho_T g} \cdot \frac{dP_T}{dt} \right + \left (A_{T,n} + \delta_{A_T} A_{T,n}) (1/\rho_T g) \cdot 2 \cdot \frac{\Delta_{P_T}}{\Delta t} \right $	$-a_1 \leq r_{1,n} \leq a_1$
$r_{2,n}$	$a_2 = w_{Rz1} + w_{Rp} + \max \Delta_{P_T} + \max \Delta_{P_B} $	$-a_2 \leq r_{2,n} \leq a_2$
$r_{3,n}$	$a_3 = \left Cd_{B,1} \cdot \text{sign}(P_B - \Delta_{P_B}) \cdot \sqrt{ P_B - \Delta_{P_B} } \right $ $+ \left \delta_{1,C_B} \cdot \frac{d(\rho_{l,n}(P_B) \cdot V_{l,n} + \rho_{v,n}(P_B) \cdot V_{v,n})}{dt} \right $	$-a_3 \leq r_{3,n} \leq a_3$
$r_{4,n}$	$a_4 = w_{RT1} + w_{RS} + w_{RT2} + w_{R_s} + w_{2C_B} $	$-a_4 \leq r_{4,n} \leq a_4$

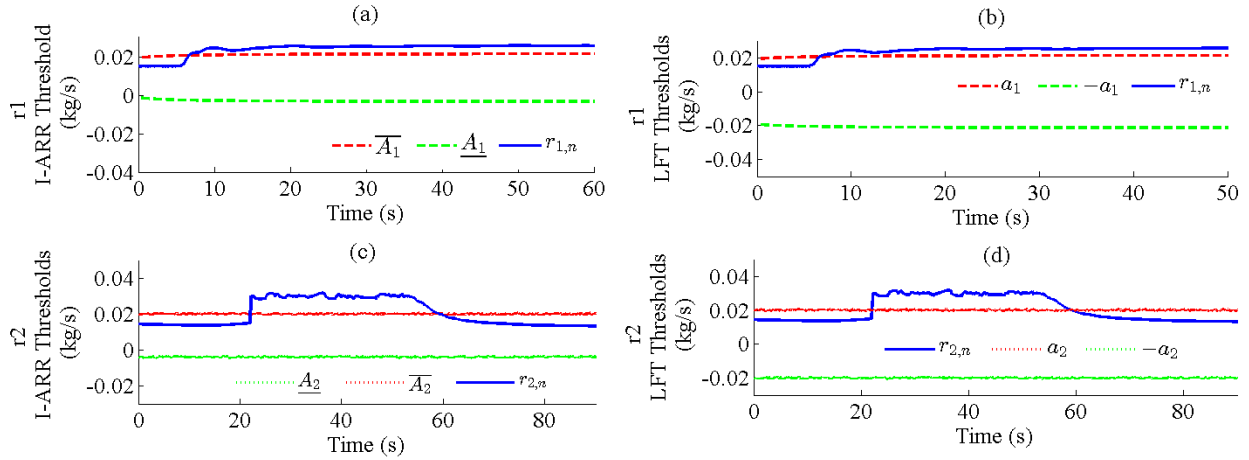


Fig. 2.18 (a) Fault Detection with Nominal Residual $r_{1,n}$ and Thresholds as range of $[A_1, \bar{A}_1] = -[B_1, \bar{B}_1]$ (b) Fault Detection with Nominal Residual $r_{1,n}$ and $-a_1, a_1$ as BG-LFT Thresholds (c) Fault Detection with Nominal Residual $r_{2,n}$ and Thresholds as range of $[A_2, \bar{A}_2] = -[B_2, \bar{B}_2]$ (d) Fault Detection with Nominal Residual $r_{2,n}$ and $-a_2, a_2$ as BG-LFT Thresholds.

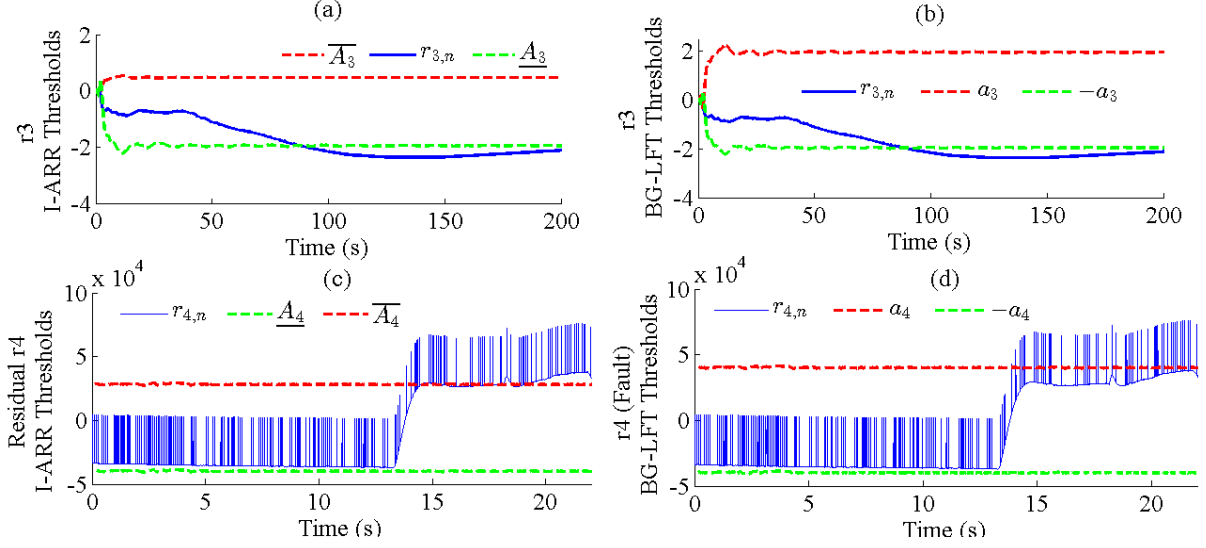


Fig. 2.19 (a) Fault Detection with Nominal Residual $r_{3,n}$ and Thresholds as range of $[\underline{A}_3, \overline{A}_3] = -[B_3, \overline{B}_3]$ (b) Fault Detection with Nominal Residual $r_{2,n}$ and $-a_3, a_3$ as BG-LFT Thresholds (c) Fault Detection with Nominal Residual $r_{4,n}$ and Thresholds as range of $[\underline{A}_4, \overline{A}_4] = -[B_4, \overline{B}_4]$ (d) Non Detection of Fault with Nominal Residual $r_{4,n}$ and $-a_4, a_4$ as BG-LFT Thresholds.

Following observations can be made from Fig. 2.18 and Fig. 2.19:

- BG-LFT thresholds: The limits of uncertainty interval are symmetric. For example, consider $r_{1,n}$ which is sensitive to uncertain discharge coefficient Cd_T . The lower limit of the corresponding threshold is determined by considering the negative value of its additive uncertainty so that $Cd_{T,n} \in [-\Delta Cd_T, \Delta Cd_T]$, whereas in reality, the allowed deviation limits are such that $Cd_T \in [0, \Delta Cd_T]$. Similar arguments hold for uncertain discharge coefficient Cd_B , RS and A_T .
- Due to the aforementioned aspect, the BG-LFT thresholds are symmetric in nature and result in over-estimated threshold width. As observed in Fig. 2.18 (b), Fig. 2.18 (d), Fig. 2.19 (b), and Fig. 2.19 (d), the BG-LFT generated thresholds are symmetric in nature. Moreover, the width of the thresholds is greater in value than their interval valued ones.

- Consider $r_{1,n}$, $r_{2,n}$ and $r_{3,n}$, like I-ARR enabled URIFs, the BG-LFT thresholds are successful in fault detection. This can be attributed to the fact that, with respect to $r_{1,n}$, $r_{2,n}$ and $r_{3,n}$, the parametric uncertainties involved in their corresponding URIFs are not mutually compensating in nature (see (2.85), (2.87), (2.89)). In other words, the uncertainties affect their URIF threshold development, in a similar fashion. As such, in URIF, the upper uncertainty interval limit of an uncertain candidate does not interact (add or subtract) with lower uncertainty interval limit of other uncertain candidate.
 - However, the aforementioned aspect is always true for BG-LFT thresholds irrespective of whether uncertain candidates are mutually compensating or non-compensating. For example, $r_{4,n}$ is sensitive to uncertain candidates that are mutually compensating in nature (positively and negatively sensitive to nominal residual, see (2.91)). The I-ARR enabled URIFs lead to efficient threshold bounds as shown in Fig. 2.19 (c). The latter is due to system dynamic dependent, interaction of upper interval limits of a set of uncertain candidates with lower interval limits of another set of uncertain candidates.
- However, on the other hand, the naïve summation of the absolute values of each uncertain flow/effort results in over-estimated thresholds. It leads to non-detection of the fault as shown in Fig. 2.19 (d).

2.7 Conclusions and Contribution

The methodology of modeling parametric and measurement uncertainties in interval form on Bond Graph (BG) models is a novel contribution of this work, and forms the initial step towards integrating interval analysis based capabilities in BG framework for fault detection and health monitoring of uncertain systems. The methodology to generate Interval valued Analytical Redundancy Relations (I-ARRs) and corresponding robust thresholds over the *nominal residual* is presented. I-ARRs are derived directly from the BG junctions with the help of structural and causal properties of the uncertain BG. The interval valued *uncertain residual interval function* (URIF) can be directly obtained from the uncertain BG. The method of modeling uncertainties in interval form alleviates the limitation of quantifying the uncertainties with symmetric bounds (equal limits on the left and right side of nominal value) associated with BG-LFT method. In fact, this leads to the generation of adaptive thresholds which are not necessarily symmetric with respect to the nominal residual. Moreover, it is shown that BG-LFT enabled robust FDI is only a special case when interval valued uncertainties have symmetric interval bounds/limits. The proposed methodology is applied and validated over uncertain steam generator system. The usefulness of the proposed methodology over the previously used BG-LFT generated thresholds in fault detection is shown via real experimental results. As the methodology presented here is a novel contribution of the thesis, it has led to following works:

- M. Jha, G. Dauphin-Tanguy, B. Ould Bouamama, *Robust FDI Based On LFT BG And Relative Activity At Junction*, in: Control Conference (ECC), 2014 European, IEEE, 2014, pp. 938-943.
- M. Jha, G. Dauphin-Tanguy, B. Ould Bouamama, *Integrated Diagnosis and Prognosis of Uncertain Systems: A Bond Graph Approach* in: Second European Conference of the PHM Society 2014 European Conference of the PHM Society 2014 Proceedings, - Nantes France, 2014, pp. 391-400.
- M. Jha, G. Dauphin-Tanguy, B. Ould Bouamama, *Robust Fault Detection of Uncertain Systems with Interval Valued Uncertainties in Bond Graph Framework*, **in review process**, Journal of Process Control, Elsevier.

3.A Methodology of Hybrid Prognostics

Benefits of system level prognostics are many and cannot be over-emphasized (Sun et al., 2012). For almost all practical purposes, any plant (the dynamic system of interest) is a feedback closed loop system such that the system outputs follow a desired reference. As such, the system level prognostics present unique challenges in that incipient parametric degradation may progress unnoticed in presence of controller compensated system outputs, resulting in non-estimation of the same till the saturation limit of controller is reached. BG derived ARR's being sensitive to system parameters and control inputs can be exploited for the same at local component level while being in closed loop regime. Such a kind of BG enabled health monitoring, can be achieved in a unified framework at global system level. The main objective of work presented in this chapter is to address the problem of prognostics in BG modelling paradigm, by exploiting its structural and causal properties while the system is considered uncertain globally and functions in feedback closed control loop. The parametric uncertainty is modeled in interval form. Prognostic issues are approached by posing the problem as a joint state-parameter estimation problem, a hybrid prognostic approach, wherein the fault model is constructed by considering the statistical degradation model of the system parameter. The system parameter is known *a priori* to be undergoing degradation. Measurements are obtained from BG-derived nominal residual given by Interval valued ARR's (I-ARR's) developed in Chapter 2. Using Particle Filters algorithms, estimation of the system parameter state under degradation (prognostic candidate) along with the associated unknown and possibly time varying degradation progression parameters(s) (DPP's) is achieved and tracked to obtain the state of damage in probabilistic terms. These terms are used for prediction of RUL of the system with respect to that parameter. The novel method of hybrid prognostics is applied over a torsion bar mechatronic system. A detailed study is presented via simulations and experiments in real time.

3.1 Assumptions and Objectives

Nominal model of any deterministic physical system may be modelled in BG form, in preferred integral causality, with nominal system parameters composed of basic elements with $\theta \in \mathbb{R}^{N_\theta}$ such that C , I , R , TY and GY are respectively the capacitance element vector, *inertial*

element vector, *dissipation* element vector, *transformer* element vector and *gyrator* element vector. Sub-script n denotes the nominal value of the parameters. The sensor vector is formed by $\mathbf{Y}(t) \in [\mathbf{De}(t), \mathbf{Df}(t)]^T$ with $\mathbf{De}(t) \in \mathbb{R}^{N_{De}}$ being *effort sensor* vector and $\mathbf{Df}(t) \in \mathbb{R}^{N_{Df}}$ being the *flow sensor* vector. The control/input vector is formed by $\mathbf{U}(t) \in [\mathbf{Se}(t), \mathbf{Sf}(t)]^T$ with $\mathbf{Se}(t) \in \mathbb{R}^{N_{Se}}$ and $\mathbf{Sf}(t) \in \mathbb{R}^{N_{Sf}}$ being respectively the *source of effort* and *source of flow* vectors.

In this chapter, following assumptions are made:

- Only system parameters are considered uncertain. Sensors are considered non-faulty;
- Single system parameter (prognostics candidate) is assumed to be under progressive degradation. In fact, single mode of degradation is assumed to affect only the system parameter which is the prognostics candidate.
- The system parameter (prognostics candidate) that undergoes degradation is assumed to be known *a priori*. The issue of isolation or isolability of the prognostic (faulty) candidate is assumed resolved. Let $\theta^d(t) \in \boldsymbol{\theta}$ be such prognostic candidate.
- Degradation model (DM) of $\theta^d(t) \in \boldsymbol{\theta}$ is assumed to be known *a priori*.
- For an I-ARR derived, only one system parameter sensitive to it (known *a priori*) varies with time.
- Noise associated with measurements (residuals) is assumed normally distributed Gaussian in nature.

Objectives are:

- Reliable estimation of health of prognostic candidate and hidden degradation parameters that accelerate or vary the degradation progression.
- Reliable prediction of the RUL of the prognostic candidate, accounting various associated uncertainties.

3.2 Degradation Model

As discussed in Section 1.5.4, a hybrid prognostic procedure requires availability of degradation model of the prognostics candidate. This degradation model can be based upon the

physics of failure/degradation as sought in model based prognostics approaches or obtained through various data-driven methods (Guo et al., 2015).

In this work, it is assumed that DM of the prognostic candidate θ^d is known and available *a priori*. Moreover, the DM is assumed to be statistically obtained as,

$$\theta^d(t) = g^d(\boldsymbol{\gamma}^d(t), \mathbf{v}^{\theta^d}(t)); \quad \theta^d(t=0) = \theta_n^d \quad (3.1)$$

where $g^d(\cdot)$ denotes the linear/non-linear *degradation progression function* (DPF) obtained from the corresponding DM. It models the way the degradation progresses in $\theta^d(t)$. $\boldsymbol{\gamma}^d(t) \in \mathbb{R}^{N_{\gamma^d}}$ represents the vector of *degradation progression parameters* (DPP), $\mathbf{v}^{\theta^d}(t) \in \mathbb{R}^{N_{v^{\theta^d}}}$ is the respective associated process noise vector and θ_n^d denotes the nominal value of θ^d .

3.2.1 Obtaining Degradation model in BG Framework

In BG framework, the DM of a system parameter under degradation $\theta^d \in \boldsymbol{\theta}$, $\boldsymbol{\theta} \in \mathbb{R}^{N_\theta}$ can be obtained from the time evolution profile of the respective ARR to which it is sensitive, assuming that the rest of the system parameters sensitive to the same do not undergo any kind of progressive fault or degradation (Medjaher, Kamal & Zerhouni, 2013), (Borutzky, Wolfgang, 2015). Here, consider the point valued part of the d^{th} I-ARR, $r^d(t)$ such that with $\boldsymbol{\theta}' = \boldsymbol{\theta} \setminus \theta^d(t)$, $t > 0, r_n^d(t) \neq 0$,

$$r^d(t) = \Psi_1^d \left(\theta^d(t), \boldsymbol{\theta}'_n, \mathbf{SSe}(t), \mathbf{SSf}(t), \mathbf{Se}(t), \mathbf{Sf}(t) \right) \quad (3.2)$$

where, sub-script n denotes nominal value. The computed values of $r^d(t)$ at time sample points gives an implicit relation of the degradation profile of $\theta^d(t)$ in time. Assuming that *implicit function theorem* is satisfied (Krantz et al., 2012), (3.2) gives a real valued function ψ_d such that,

$$\theta^d(t) = \psi_d \left(r^d(t), \boldsymbol{\theta}'_n, \mathbf{SSe}(t), \mathbf{SSf}(t), \mathbf{Se}(t), \mathbf{Sf}(t) \right) \quad (3.3)$$

Parameter identification techniques or non-linear least square regression can be applied to obtain degradation progression function (DPF) $g^d(\cdot)$ as an algebraic equation or in parameterized Ordinary Differential Equation form, and the associated process noise vector is obtained from ψ_d . The latter as a function of system measurements inputs (known variables) and their derivatives etc., is always corrupted with noise.

Note that residual based DM should be obtained prior to prognostics. This routine can be performed offline i.e. prior to the phase when system's health monitoring is of interest.

3.3 Methodology for Hybrid Prognostics in BG Framework

In this section, the methodology for prognostics is described. The method consists of robust detection of beginning of the parametric degradation, construction of a *fault model* (with respect to the candidate of prognostics), construction of observation equation from I-ARR which is sensitive to the prognostics candidate, estimation of the state of health of the parameter, estimation of hidden parameters that influence the degradation rate and RUL predictions.

3.3.1 Robust Detection of Degradation Beginning

The problem of detecting the degradation beginning is treated as robust fault detection problem. As the primary interests lie in the latter, and not in fault detection *per se*, the uncertainty on sensors is not considered. Moreover, the proposed estimation procedure takes into account measurement noise for an optimal estimation and RUL prediction. The robust fault detection methodology using interval valued thresholds developed in Chapter 2 is applied to detect the commencement of considered prognostic candidate's degradation. However, only parametric uncertainties are considered. The procedure is given in brief.

Step 1: Preferred derivative causality is assigned to the nominal model. Step 2: Parametric uncertainties are modelled in interval form and represented on the nominal BG, as explained in Chapter 3, Section 2.3, to obtain uncertain BG.

Step 3: I-ARRs are derived as explained in Chapter 2, Section 2.4, to obtain I-ARRs accounting for only parametric uncertainties in interval form. The nominal residual $r_n(t)$ can be perfectly decoupled from URIF $\left[\underline{B}(t), \overline{B}(t) \right]$ in absence of interval valued measurement uncertainties.

$$\left[\underline{R}, \overline{R} \right] : \Psi \left(\theta_n, \left[\underline{\theta}, \overline{\theta} \right], [w_i], \sum Se, \sum Sf, SSe(t), SSf(t) \right) \quad (3.4)$$

$$\left[\underline{R}(t), \overline{R}(t) \right] : r_n(t) + \left[\underline{B}(t), \overline{B}(t) \right] \quad (3.5)$$

$$r_n(t) = \Psi_1 \left(\theta_n, SSe(t), SSf(t), \sum Se, \sum Sf \right) \quad (3.6)$$

$$\left[\underline{B}(t), \overline{B}(t) \right] = \Psi_2 \left(\left[\underline{\theta}, \overline{\theta} \right], \left[\underline{\delta}_0, \overline{\delta}_0 \right], SSe(t), SSf(t) \right) \quad (3.7)$$

Step 4: From **Proposition 2.1** (see Chapter 2, Section 2.5), under nominal conditions,

$$-r_n(t) \subseteq \left[\underline{B}, \overline{B} \right](t) \quad (3.8)$$

Degradation (start of parametric deviation) is detected if,

$$-r_n(t) \not\subseteq \left[\underline{B}, \overline{B} \right](t) \quad (3.9)$$

Pseudo algorithm is given in Table 3-I.

Table 3-I Fault detection with d^{th} I-ARR

Algorithm 1: Fault detection with d^{th} I-ARR

Input: $\left\{ \begin{array}{l} \Psi_1^i (Se, Sf, \theta_n, SSe(k), SSf(k)) \\ \text{FC_}\Psi_2^i \left(\left[\underline{\theta}, \overline{\theta} \right], \left[\underline{\delta}_0, \overline{\delta}_0 \right], SSe(k), SSf(k) \right) \end{array} \right\}$

Output: fault detection

$$r_n^i(k) = \Psi_1^i (Se, Sf, \theta_n, SSe(k), SSf(k))$$

$$\left[\underline{B}(k), \overline{B}(k) \right] = \text{FC_}\Psi_2^i \left(\left[\underline{\theta}, \overline{\theta} \right], \left[\underline{\delta}_0, \overline{\delta}_0 \right], SSe(k), SSf(k) \right)$$

if $-r^i(k) \geq \underline{B}(k)$ **and** $-r^i(k) \leq \overline{B}(k)$

fault detection \leftarrow **false**

else

fault detection \leftarrow **true**

end if

3.3.2 Fault Model Construction

A fault model is constructed in state space to achieve the estimation of $\theta^d(t)$ based upon information (measurement) provided by the values of nominal residual sensitive to $\theta^d(t)$, $r_n^d(t)$. This section describes the construction of the fault model. A methodology of obtaining observation equation from $r_n^d(t)$ is also detailed.

3.3.2.1 State Equation

The parameter under degradation $\theta^d(t)$ is included as a tuple $(\theta^d, \gamma^d, g^d)$ to model the damage progression in state space form. The *fault model* for $(\theta^d, \gamma^d, g^d)$ is constructed in state –space form by considering the parameter $\theta^d(t)$ as the state variable augmented with the DPP vector as,

$$\dot{\mathbf{x}}^d(t) = \mathbf{f}^d(\mathbf{x}^d(t), \mathbf{v}^{x_d}(t)) \quad (3.10)$$

where, $\mathbf{x}^d(t) = [\theta^d(t), \gamma^d(t)]^T$ is the augmented state vector and \mathbf{f}^d is state transition function following the Markovian assumption.

3.3.2.2 Residual Based Observation Equation

Previously for fault estimation purposes, the residual based information about the fault value has been obtained by exploiting bicausality notion (Touati et al., 2012a) (Benmoussa et al., 2014). It forms a systematic way of obtaining the *sensibility function* that relates fault value to residuals. However, several necessary modifications are incurred (bicausality related) on the BG model already in-use. In order to avoid the associated complexities, the authors have refrained from employing the former approach. Moreover, the objective is to exploit the nominal residual for the estimation of state variables. This way, the nominal residual used for detection of degradation beginning can further be used for estimation of state of health of the prognostic candidate and associated DPPs. This is possible if the ARR expression is altered to obtain the observation equation in an appropriate way, such that the nominal residual provides the measurements of state variables. To this end, a simple algebraic approach is proposed.

Proposition 3.1: *Under the single degradation hypothesis, assuming the nominal part $r_n^d(t)$ of an I-ARR can be expressed as a linear combination of non-linear functions of $\theta^d(t)$, the measurement of the state $\theta^d(t)$ can be obtained from the negative value of $r_n^d(t)$.*

Proof: Let $\theta^d(t)$ be the prognostic candidate and $\theta' = \theta \setminus \theta^d(t)$. Assuming $r_n^d(t)$ can be expressed as:

$$r_n^d(t) = \Xi \left(\theta'_n, \text{SSe}(t), \text{SSf}(t), \text{Se}(t), \text{Sf}(t) \right) + A^T \boldsymbol{\varphi}(\theta_n^d) \quad (3.11)$$

where $\forall i | i = 1, 2 \dots m$, $A^{m \times 1} = [a_1 \ a_2 \dots a_m]^T$ is a vector of known (measured system variables) with $a_i = \phi_i(\theta'_n, \text{SSe}(t), \text{SSf}(t), \text{Se}(t), \text{Sf}(t))$ and $\boldsymbol{\varphi}^{m \times 1}(\theta^d(t)) = [\varphi_1(\theta^d(t)), \varphi_2(\theta^d(t)), \dots, \varphi_m(\theta^d(t))]^T$ is the vector of non-linear functions of $\theta^d(t)$. Then, $\forall t \geq 0$ power conservation at the BG junction where the corresponding I-ARR is derived, gives,

$$r^d(t) = \Xi \left(\theta'_n, \text{SSe}(t), \text{SSf}(t), \text{Se}(t), \text{Sf}(t) \right) + A^T \boldsymbol{\varphi}(\theta^d(t)) = 0 \quad (3.12)$$

or:

$$\begin{aligned} r^d(t) &= \Xi \left(\theta'_n, \text{SSe}(t), \text{SSf}(t), \sum \text{Se}, \sum \text{Sf} \right) + A^T \boldsymbol{\varphi}(\theta_n^d) + \left(A^T \boldsymbol{\varphi}(\theta^d(t)) - A^T \boldsymbol{\varphi}(\theta_n^d) \right) = 0 \\ r^d(t) &= r_n^d(t) + A^T \left(\boldsymbol{\varphi}(\theta^d(t)) - \boldsymbol{\varphi}(\theta_n^d) \right) = 0 \\ A^T \left(\boldsymbol{\varphi}(\theta^d(t)) - \boldsymbol{\varphi}(\theta_n^d) \right) &= -r_n^d(t) \end{aligned} \quad (3.13)$$

Thus, degradation state $\theta^d(t)$ can be linked implicitly to the measurements of $-r_n^d(t)$. Observation equation can be formed as,

$$y^d(t) = -r_n^d(t) = A^T \left(\boldsymbol{\varphi}(\theta^d(t)) - \boldsymbol{\varphi}(\theta_n^d) \right) \quad (3.14)$$

Corollary: *When $\boldsymbol{\varphi}(\theta_n^d) = \boldsymbol{\varphi}(\theta_n^d) = \theta_n^d$, the vector $A = a_1$, $a_1 = \phi_1(\theta'_n, \text{SSe}(t), \text{SSf}(t), \sum \text{Se}, \sum \text{Sf})$, can be understood as the coefficient function linking the fault value to the residual. It can be found as,*

$$a_1 = \frac{\partial(r_n^d(t))}{\partial(\theta^d(t))} \quad (3.15)$$

The same result can be obtained through bi-causality notion (not analyzed in this work) where, a_1 is understood as the *sensibility function* which links the respective nominal residual to fault value as,

$$\frac{-r_n^d(t)}{\frac{\partial(r_n^d(t))}{\partial(\theta^d(t))}} = \theta^d(t) \quad (3.16)$$

The observation equation argument in (3.14) includes known variables (sensor measurements, system parameters, inputs etc.) and their derivatives. It is heavily corrupted with noise, especially due to presence of terms such as derivative(s) of measured variables. In this work, the noise is considered additive, *independent and identically distributed* (i.i.d.) drawn from a zero mean Gaussian distribution and is assumed uncorrelated to $\mathbf{x}^d(t)$. Thus from (3.14), observation equation is formed as,

$$y^d(t) = h^d(\mathbf{x}^d(t)) + w^d(t) \quad (3.17)$$

where $h^d(\cdot)$ is a *nonlinear measurement function* obtained from (3.14) and $w^d(t) \sim \mathcal{N}(0, \sigma_{w^d}^2)$.

The standard deviation σ_{w^d} , is approximated from residual measurements.

3.3.3 Estimation of the State of Degradation

In discrete time step $k \in \mathbb{N}$, the fault model $(\theta^d, \gamma^d, g^d)$ can be described in stochastic framework as,

$$\mathbf{x}_k^d = \mathbf{f}_k^d(\mathbf{x}_{k-1}^d, \mathbf{v}_{k-1}^{x_d}) \quad (3.18)$$

$$y_k^d = h^d(\mathbf{x}_k^d) + w_k^d \quad (3.19)$$

where $\mathbf{x}_k^d = [\theta_k^d, \boldsymbol{\gamma}_k^d]^T$, \mathbf{f}_k^d is state transition function (possibly non-linear) and is described by first order Markov model. Measurements y_k^d are assumed conditionally independent, given the state process \mathbf{x}_k^d . The likelihood function becomes as,

$$p(y_k^d | \theta_k^d, \boldsymbol{\gamma}_k^d) = \frac{1}{\sigma_{w_k^d} \sqrt{2\pi}} \exp\left(-\left(y_k^d - h^d(x_k^d)\right)^2 / 2\sigma_{w_k^d}^2\right) \quad (3.20)$$

After detection of degradation by the FDI module as a fault at time step k_d , the prediction of EOL/RUL at prediction time k , requires the estimate of $\theta_k^d, \boldsymbol{\gamma}_k^d$. This problem is cast as joint state-parameter estimation problem in particle filter (PF) framework, where the estimation at time k is obtained as *probability density function* (pdf) $p(\theta_k^d, \boldsymbol{\gamma}_k^d | y_{k_d:k}^d)$, based upon history of measurements from the time of beginning of degradation k_d up to k , $y_{k_d:k}^d$.

In the following section, the method applied for degradation estimation and consequent prognostics is explained assuming that degradation begins at the start. In reality information about k_d will be given by fault detection module as described in Section 3.3.1.

The state distribution is approximated by set of discrete weighted samples or particles, $\{(\theta_k^{d,i}, \boldsymbol{\gamma}_k^{d,i}), w_k^i\}_{i=1}^N$, where N is the total number of particles and for i^{th} particle at time k , $\theta_k^{d,i}$ is the estimate of the state (*system faulty* parameter here) and $\boldsymbol{\gamma}_k^{d,i}$ is the estimate of *fault progression parameters*. The weight associated with each particle is denoted by w_k^i . The posterior density at any time step k is approximated as:

$$p(\theta_k^d, \boldsymbol{\gamma}_k^d | y_{0:k}^d) \approx \sum_{i=1}^N w_k^i \cdot \delta_{(\theta_k^d, \boldsymbol{\gamma}_k^d)}(d\theta_k^d d\boldsymbol{\gamma}_k^d) \quad (3.21)$$

where $\delta_{(\theta_k^d, \boldsymbol{\gamma}_k^d)}(d\theta_k^d d\boldsymbol{\gamma}_k^d)$ denotes the Dirac delta function located at $(\theta_k^d, \boldsymbol{\gamma}_k^d)$ and sum of the weights $\sum_{i=1}^N w_k^i = 1$. Here, *sampling importance resampling* (SIR) PF is employed for estimation

of $p(\theta_k^d, \Upsilon_k^d | y_{0:k}^d)$, assuming particles $\{(\theta_{k-1}^{d,i}, \Upsilon_{k-1}^{d,i}), w_{k-1}^i\}_{i=1}^N$ are available as realizations of posterior probability $p(\theta_{k-1}^d, \Upsilon_{k-1}^d | y_{0:k-1}^d)$ at time $k-1$, with the following main steps:

- Realizations of *prediction* $p(\theta_k^d, \Upsilon_k^d | y_{0:k-1}^d)$, is obtained in form of new set of particles $\{(\theta_k^{d,i}, \Upsilon_k^{d,i}), w_k^i\}_{i=1}^N$, with weights being chosen using the principle of *importance sampling*. The proposal *importance density* is chosen as the transitional prior $p(\mathbf{x}_k^{d,i} | \mathbf{x}_{k-1}^{d,i})$ such that particles are generated by sampling from probability distribution of system noise $\mathbf{v}_{k-1}^{x_d}$ and simulation of the system dynamics of (3.18).
- Each sampled particle $(\theta_k^{d,i}, \Upsilon_k^{d,i})$ is then *updated*. The weight w_k^i is associated to each of the particles based on the likelihood of observation y_k^d made at time k as,

$$w_k^i = p(y_k^d | \theta_k^{d,i}, \Upsilon_k^{d,i}) / \sum_{j=1}^N p(y_k^d | \theta_k^{d,j}, \Upsilon_k^{d,j}) \quad (3.22)$$

Note that with the choice of *importance density* as the prior, the weights were obtained as,

$$w_k^i \propto w_{k-1}^i p(y_k^d | \theta_k^{d,i}, \Upsilon_k^{d,i}) \quad (3.23)$$

- To avoid the *degeneracy problem*, a new set of particles is *resampled* (with replacement) from the approximation of posterior distribution $p(\theta_k^d, \Upsilon_k^d | y_{0:k}^d)$ constructed on weighted samples previously drawn, such that weights are reset equally to $w_k^i = 1/N$. The objective behind *resampling* is the elimination of particles with small weights and focus on particles with large weights for estimation. In this work, *systematic resampling* scheme is preferred as it is easy to implement and takes $O(N)$ time and the algorithm can be referred in (Arulampalam et al., 2002).
- The *prediction*, *update* and *resample* procedures form a single iteration step and are applied at each time step k . The algorithm for SIR filter is given in Table 3-II. Details about other variants of *sequential importance sampling* PFs can be referred in (Arulampalam et al., 2002).

Table 3-II Estimation using SIR filter

Algorithm 2: Estimation using SIR filter

Inputs: $\{(\theta_{k-1}^{d,i}, \boldsymbol{\gamma}_{k-1}^{d,i}), \mathbf{w}_{k-1}^i\}_{i=1}^N, \mathbf{y}_k^d$

Output: $\{(\theta_k^{d,i}, \boldsymbol{\gamma}_k^{d,i}), \mathbf{w}_k^i\}_{i=1}^N$

for $i=1$ **to** N **do**

$\boldsymbol{\gamma}_k^{d,i} \sim P(\boldsymbol{\gamma}_k^{d,i} | \boldsymbol{\gamma}_{k-1}^{d,i})$

$\theta_k^{d,i} \sim P(\theta_k^{d,i} | \theta_{k-1}^{d,i}, \boldsymbol{\gamma}_{k-1}^{d,i})$

$\mathbf{w}_k^i \sim P(\mathbf{y}_k^d | \theta_k^{d,i}, \boldsymbol{\gamma}_k^{d,i})$

end for

$W \leftarrow \sum_{i=1}^N \mathbf{w}_k^i$

for $i=1$ **to** N **do**

$\mathbf{w}_k^i \leftarrow \mathbf{w}_k^i / W$

end for

$\{(\theta_k^{d,i}, \boldsymbol{\gamma}_k^{d,i}), \mathbf{w}_k^i\}_{i=1}^N \leftarrow \text{RESAMPLE} \{(\theta_k^{d,i}, \boldsymbol{\gamma}_k^{d,i}), \mathbf{w}_k^i\}_{i=1}^N$

3.3.3.1 Random Walk Noise Variance Control

Consider the DPP vector $\boldsymbol{\gamma}^d \in \mathbb{R}^{N_{\boldsymbol{\gamma}^d}}$ such that $\forall j \in \{1, \dots, N_{\boldsymbol{\gamma}^d}\}, \boldsymbol{\gamma}^{d,j} \in \boldsymbol{\gamma}^d, \hat{\boldsymbol{\gamma}}^{d,j}$ is the estimated value, and $\boldsymbol{\gamma}^{d,j*} \in \boldsymbol{\gamma}^{d*}, \boldsymbol{\gamma}^{d*} \in \mathbb{R}^{N_{\boldsymbol{\gamma}^d}}$ is the respective true value vector. Also consider the interval vector $[\boldsymbol{\gamma}_l^{d*}, \boldsymbol{\gamma}_u^{d*}] \in \mathbb{R}^{N_{\boldsymbol{\gamma}^d}}$, consisting of intervals $[\boldsymbol{\gamma}_l^{d,j*}, \boldsymbol{\gamma}_u^{d,j*}] \in [\boldsymbol{\gamma}_l^{d*}, \boldsymbol{\gamma}_u^{d*}]$, that contain the true value $\boldsymbol{\gamma}^{d,j*} \in [\boldsymbol{\gamma}_l^{d,j*}, \boldsymbol{\gamma}_u^{d,j*}]$. Moreover, for every $\boldsymbol{\gamma}^{d,j} \in \boldsymbol{\gamma}^d$, consider an associated constant (proportional gain) $P^{d,j}$ such that $P^{d,j} \in \mathbf{P}^d, \mathbf{P}^d \in \mathbb{R}^{N_{\boldsymbol{\gamma}^d}}$.

$\boldsymbol{\gamma}^{d,j}$ is modeled as a *random walk process* $\boldsymbol{\gamma}_k^{d,j} = \boldsymbol{\gamma}_{k-1}^{d,j} + \boldsymbol{\xi}_{k-1}^{d,j}$ where, $\boldsymbol{\xi}_{k-1}^{d,j}$ is sampled from an artificial random zero-mean Gaussian distribution i.e. $\boldsymbol{\xi}_{k-1}^{d,j} \sim \mathcal{N}(0, \sigma_{\boldsymbol{\xi}_{k-1}^{d,j}}^2)$. Here, $\sigma_{\boldsymbol{\xi}_{k-1}^{d,j}}^2$ denotes the associated variance $\mathbf{v}_{k-1}^{\boldsymbol{\xi}_{k-1}^{d,j}}$ at time $k-1$ i.e. $\sigma_{\boldsymbol{\xi}_{k-1}^{d,j}}^2 \equiv \mathbf{v}_{k-1}^{\boldsymbol{\xi}_{k-1}^{d,j}}$ for notational simplicity where, $\forall j \in \{1, \dots, N_{\boldsymbol{\gamma}^d}\}, \mathbf{v}_{k-1}^{\boldsymbol{\xi}_{k-1}^{d,j}} \in \mathbf{v}^{\boldsymbol{\xi}^d}$ and $\mathbf{v}^{\boldsymbol{\xi}^d} \in \mathbb{R}^{N_{\boldsymbol{\gamma}^d}}$. Moreover, associated with every $\mathbf{v}_{k-1}^{\boldsymbol{\xi}_{k-1}^{d,j}}$, consider a

reference variance (spread) $v^{\xi^{d,j*}}, v^{\xi^{d,j*}} \in \mathbf{v}^{\xi^{d,*}}$. The artificial random walk noise permits the estimation of $\theta^d(t)$ to converge to its true value during the estimation process. Selection of the variance of the random walk noise is essentially a tradeoff between values that are big enough to allow the convergence in reasonable amount of time, yet small enough to let the parameter values be tracked smoothly once convergence is reached. One of the efficient ways of ensuring good estimation of $\theta^d(t)$ is to reduce the random walk noise variance $v_{k-1}^{\xi^{d,j}}$, once a suitable convergence is reached. In this regard, performance enhancement has been achieved by the usage of proportional control law type variance adaptation method; it is proposed, demonstrated and implemented in (Daigle, M. J. & Goebel, 2013). Therein,

- Variance (spread) is quantified by the statistically robust metric *Relative Median Absolute Deviation* (RMAD) obtained as,

$$RMAD(X) = \frac{\text{Median}_i(|X_i - \text{Median}_j(X_j)|)}{\text{Median}_j(X_j)} \quad (3.24)$$

where, X_i is an element for a data set X .

- The variance is adapted in a proportional control law way where the normalized error between the current RMAD $v_k^{\xi^{d,j}}$ (e.g. 80%) and a reference $v^{\xi^{d,j*}}$ (e.g. 10%) is multiplied by a proportional gain constant $P^{d,j}$. Current RMAD $v_k^{\xi^{d,j}}$ is then increased or decreased by that amount. Thereafter, current random walk noise $\xi_k^{d,j}$ is sampled from a zero mean Gaussian distribution with the modified variance $v_k^{\xi^{d,j}}$.

However, there-in, the adaptation that progresses in arbitrarily decided multiple stages, requires a proper tuning of reference value $v^{\xi^{d,j*}}$ and proportional gain constant $P^{d,j}$, for each stage. Such a procedure can be a tedious task especially in presence of multiple DPP. Although the objective that rests in achieving proper convergence and subsequent smooth tracking is clearly achievable, availability of no guidelines for a proper selection of number of stages and $v^{\xi^{d,j*}}$, makes the task complicated. In this paper, random walk variance is controlled in similar

fashion as in (Daigle, M. J. & Goebel, 2013), however, with the distinguishing feature that variance adaptation is triggered by $\bar{\gamma}_k^{d,j}$:

$$\bar{\gamma}_k^{d,j} = \begin{cases} \frac{1}{L+1} \sum_{l=0}^{l=L} \text{mean}(\hat{\gamma}_{k-l}^{d,j}) & \text{if } k \geq L \\ \text{mean}(\hat{\gamma}_k^{d,j}) & \text{if } k < L \end{cases} \quad (3.25)$$

with θ^d at time k , being the average of the estimation mean $\hat{\gamma}^{d,j}$ in a running window of previous L estimates. Fig. 3.1 shows the schematic of the proposed algorithm.

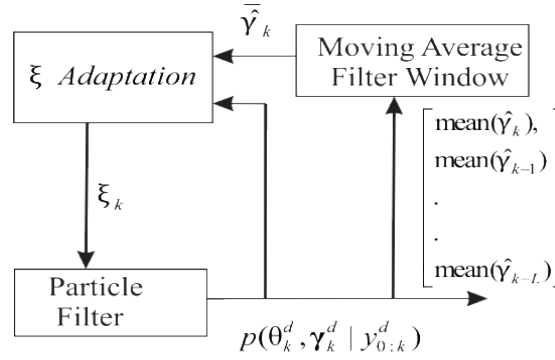


Fig. 3.1 Schematic of variance control scheme

The fact that degradation model of $\theta^d(t)$ is known, leads to an approximate knowledge of the true value of $\gamma^{d,j*}$. The adaptation of $\xi^{d,j}$ is triggered when $\bar{\gamma}_k^{d,j} \in [\gamma_l^{d,j*}, \gamma_u^{d,j*}]$. The interval $[\gamma_l^{d,j*}, \gamma_u^{d,j*}]$ can be decided based upon the approximate knowledge of $\gamma^{d,j*}$, obtained from the DM. The main objective rests in letting the variance be regulated in an automatic way. The corresponding pseudo-algorithm is given in Table 3-III.

Table 3-III Variance Adaptation Scheme

Algorithm 3: ξ Adaptation

Inputs: $\{(\theta_k^{d,i}, \gamma_k^{d,i}), w_k^i\}_{i=1}^N, \mathbf{v}_k^\xi, [\gamma_l^{d*}, \gamma_u^{d*}], \mathbf{v}_{k=0}^\xi, \mathbf{v}^{\xi*}, \mathbf{P}^d$

Outputs: ξ_k

for all $j \in \{1, \dots, N_{\gamma^d}\}$ **do**

if $k \geq L$

$\bar{\gamma}_k^{d,j} \leftarrow \frac{1}{L+1} \sum_{l=0}^{l=L} \text{mean}(\hat{\gamma}_{k-l}^{d,j})$

else

$\bar{\gamma}_k^{d,j} \leftarrow \text{mean}(\hat{\gamma}_k^{d,j})$

end if

if $\bar{\gamma}_k^{d,j} \in [\gamma_l^{d,j*}, \gamma_u^{d,j*}]$ **then**

$\mathbf{v}_k^{\xi^{d,j}} = \text{RMAD}\{\gamma_k^{d,j,i}\}_{i=1}^N$

$\mathbf{v}_k^{\xi^{d,j}} = \mathbf{v}_k^{\xi^{d,j}} \left(1 + \mathbf{P}^{d,j} \frac{\mathbf{V}_k^{\xi^{d,j}} - \mathbf{V}^{\xi^{d,j*}}}{\mathbf{V}^{\xi^{d,j*}}}\right)$

else

$\mathbf{v}_k^{\xi^{d,j}} = \mathbf{v}_{k=0}^{\xi^{d,j}}$

end if

$\xi_k^{d,j} \leftarrow \text{Sample}\mathcal{N}(0, \mathbf{v}_k^{\xi^{d,j}})$

end for

3.3.4 Remaining Useful Life Prediction

Prognostics involves assessment of the time which the system has before the latter fails (or requires maintenance procedures), due to the degradation of considered system parameters.

In this work, it is achieved by prediction of the RUL of the parameter under degradation. The critical/failure value θ_{fail}^d of $\theta^d(t)$ is specified beforehand.

Like previous attempts (Daigle, M. & Goebel, 2010; Daigle, M. J. & Goebel, 2011a, 2013; Jouin et al., 2014), the corresponding RUL prediction at time k , $RUL_k^{\theta^d}$, is framed as generation of l^d – step ahead long term prediction $p(\theta_{k+l^d}^d, \gamma_{k+l^d}^d | y_{0:k}^d)$ based upon the current joint state-

parameter estimate $p(\theta_k^d, \gamma_k^d | y_{0:k}^d)$ obtained, with $l^d = 1, \dots, T^d - k$, where T^d is the time horizon of interest i.e. time until $\theta_{k+l^d}^d \geq \theta_{fail}^d$. The l^d -step ahead state distribution is computed by propagating each of the particles $\{(\theta_k^{d,i}, \gamma_k^{d,i}), w_k^i\}_{i=1}^N$ constituting the joint estimation $p(\theta_{k+l^d}^d, \gamma_{k+l^d}^d | y_{0:k}^d)$, $l^{d,i}$ steps ahead until $\theta_{k+l^{d,i}}^{d,i} \geq \theta_{fail}^d$ as,

$$p(\theta_{k+l^d}^d, \gamma_{k+l^d}^d | y_{0:k}^d) \approx \sum_{i=1}^N w_k^i \cdot \delta_{(\theta_{k+l^{d,i}}^{d,i}, \gamma_{k+l^{d,i}}^{d,i})} (d\theta_{k+l^d}^d d\gamma_{k+l^d}^d) \quad (3.26)$$

where, for the i^{th} particle, the corresponding weight during the $l^{d,i}$ -step propagation is kept equal to weight w_k^i at time of prediction k . Then, for i^{th} particle, $RUL_k^{\theta^{d,i}} = k + l^{d,i} - k = l^{d,i}$ and the corresponding $RUL_k^{\theta^d}$ is obtained as:

$$p(RUL_k^{\theta^d} | y_{0:k}^d) \approx \sum_{i=1}^N w_k^i \delta_{(RUL_k^{\theta^{d,i}})} (dRUL_k^{\theta^d}) \quad (3.27)$$

The prediction of $RUL_k^{\theta^d}$ is done in the absence of future observations $y_{k+1:k+l^d}^d$, as they are not available. Pseudo-algorithm for RUL prediction is given in Table 3-IV.

Table 3-IV Prediction of RUL

Algorithm 4: RUL Prediction
Inputs: $\{(\theta_k^{d,i}, \gamma_k^{d,i}), w_k^i\}_{i=1}^N$
Variable: l
Outputs: $\{RUL_k^{\theta^{d,i}}, w_k^i\}_{i=1}^N$
for $i=1$ to N do
$l=0$
while $\theta_{k+l}^{d,i} \leq \theta_{fail}^d$ do
$\gamma_{k+1}^{d,i} \sim p(\gamma_{k+1}^{d,i} \gamma_k^{d,i})$
$\theta_{k+1}^{d,i} \sim p(\theta_{k+1}^{d,i} \theta_k^{d,i}, \gamma_k^{d,i})$
$l \leftarrow l + 1$
end while
$RUL_k^{\theta^{d,i}} \leftarrow l$
end for

3.4 Health monitoring of Prognostic Candidate

The beginning of degradation is detected by the fault detection module described in Section 3.3.1. Subsequently, estimation and prediction of RUL is triggered. The initial value of state is set as:

$$\theta_{t=t_d}^d \sim U(\theta_n^d - \Delta\theta_l, \theta_n^d + \Delta\theta_u); t = t_d \quad (3.28)$$

where, t_d is the time when beginning of degradation is detected and the associated uncertainty interval limits $[-\Delta\theta_l, \Delta\theta_u]$ decide the bounds of the uniform distribution. This is due to the fact that thresholds used for detection are sensitive to other uncertain parameters and as such, $\theta_{t=t_d}^d = \theta_n^d$ can not be assured. Such an approximation does not affect the estimation process as it guarantees to include the true initial state of $\theta^d(t)$. The complete algorithm is shown in Table 3-V. Fig. 3.2 shows the schematic description of the methodology presented in this chapter.

Table 3-V Health monitoring of θ_0^d with respect to r_n^d

Algorithm 5: Health monitoring of θ_0^d with respect to r_n^d

while *system is running* **do**

Detect the beginning of degradation using

Algorithm 1

if *fault detection* =true **then**

//set initial conditions

$$\theta_0^d \sim U(\theta_n^d - \Delta\theta_l, \theta_n^d + \Delta\theta_u)$$

$$\gamma_0^d = 0$$

$$y_0^d = -r_n^d(k)$$

do Estimation using **Algorithm 2**

do ξ Adaptation using **Algorithm3**

do RUL prediction using **Algorithm4**

end if

end while

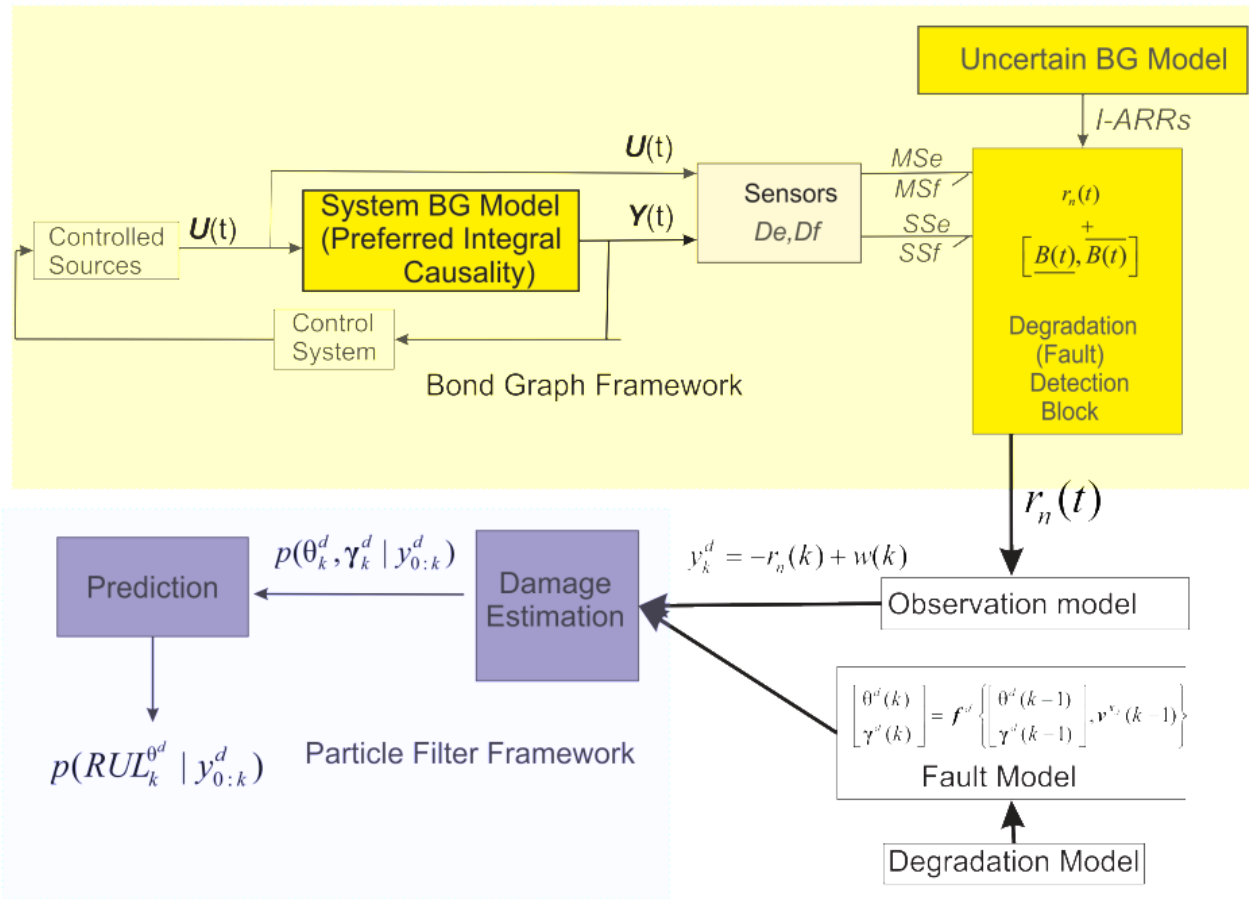


Fig. 3.2 Schematic description of the Health Monitoring Methodology

3.5 Evaluation Metrics

In this section, various metrics employed to evaluate the performance of estimation, prediction etc. are briefly discussed. Readers are advised to refer Saxena et al. (Saxena et al., 2010) for details and works of Daigle et al. (Daigle, M. J. & Goebel, 2013), for the case study involving the same.

3.5.1 Estimation performance

The estimation performance is evaluated using two metrics that quantify the accuracy and spread.

Root mean square error (RMSE): This metric expresses the relative estimation accuracy as:

$$\text{RMSE}_X = \sqrt{\text{Mean}_k \left[\left(\frac{X - X^*}{X^*} \right)^2 \right]} \quad (3.29)$$

where, for species X , X^* denotes the corresponding true values. Mean_k denotes the mean over all values of k .

Relative median absolute deviation (RMAD): As detailed in Section 3.3.3.1, RMAD expresses the spread of estimation relative to median as a percentage. It is averaged over multiple values of k to obtain average RMAD for γ^d as:

$$\overline{\text{RMAD}}_{\gamma^d} = \text{Mean}_k (\text{RMAD}_{\gamma^d, k}) \quad (3.30)$$

where $\text{RMAD}_{\gamma^d, k}$ is the RMAD of γ^d at time k .

3.5.2 Prediction performance

For a particular prediction time point k_p , the prediction accuracy for θ^d is evaluated by *Relative Accuracy* (RA) metric as:

$$\text{RA}_{\theta^d, k_p} = \left(1 - \frac{\left| \text{RUL}_{\theta^d, k_p}^* - \text{Mean}(\text{RUL}_{\theta^d, k_p}) \right|}{\text{RUL}_{\theta^d, k_p}^*} \right) \quad (3.31)$$

where $\text{RUL}_{\theta^d, k_p}^*$ denotes the true *RUL* at time k_p for θ^d . The overall accuracy is determined by averaging $\text{RA}_{\theta^d, k_p}$ over all the prediction points. The latter being denoted as $\overline{\text{RA}}_{\theta^d}$ is determined in (3.32). The associated spread at k_p and overall spread is determined by finding the corresponding RMADs. They are denoted respectively as $\text{RMAD}_{\text{RUL}_{\theta^d}}$ and $\overline{\text{RMAD}}_{\text{RUL}_{\theta^d}}$

$$\overline{\text{RA}}_{\theta^d} = \text{Mean}_{k_p} (\text{RA}_{\theta^d, k_p}) \quad (3.32)$$

3.5.3 Prognostics performance

$\alpha - \lambda$ metric (Saxena et al., 2010) is employed to summarize the prognostic performance where $\alpha \in [0, 1]$ defines the bounds of true *RUL* as $(1 \pm \alpha)\text{RUL}_{\theta^d, k_p}^*$ and $\lambda \in [0, 1]$ denotes the

fraction of time between the initial prediction time point and the true end of life (EOL). The third parameter $\beta \in [0,1]$ signifies the desired (pre-fixed) fraction of the RUL prediction probability mass percentage, that must fall between the cones of accuracy determined by α , for the respective RUL prediction to be acceptable. In this work, for all λ (all k), $\beta = 0.5$ which translates to the requirement of 50% of probability mass distribution of RUL_{θ^d, k_p} falling within $[(1-\alpha)RUL_{\theta^d, k_p}^*, (1+\alpha)RUL_{\theta^d, k_p}^*]$ for the prediction at k_p , to be acceptable.

3.6 Case Study on Mechatronic System through Simulations

The method presented in this paper is applied on a mechatronic Torsion Bar 1.0 system shown in Fig. 3.3 (Kleijn, C., 2011; Tarasov et al., 2014) which is integrated with 20 SIM, a BG dedicated software (Broenink, 1997). Real time implementation is achieved through 20 SIM 4C 2.1, a prototyping environment that enables C-code implementation in real time on ARM-9 processor based torsion bar system (Kleijn, C., Differ H.G., 2013). The interval computations, estimation, variance control and prediction algorithms are written in *Matlab Function Block* in Simulink. The embedded code is generated through Simulink Coder in Matlab2013a[®]. INTLAB is used to implement interval calculations during simulation. For real time C-code generation, relevant/required functionalities are borrowed from INTLAB.

3.6.1 Nominal System

The functional schematic model of the mechatronic system, detailed in (Kleijn, C., 2011), is shown in Fig. 3.4. It consists of the Maxon[®] servo motor that provides the controlled actuation (rotation) to the disks and is equipped with voltage amplifier A_m , inductance La , resistance Ra , rotor inertia J_m , associated motor friction coefficient f_m and torque constant k_m . The high stiffness transmission belt provides the torque transmission with the transmission ratio k_{belt} to the motor disk with rotational inertia J_{Md} . The motor disk is connected to load disk with rotational inertia J_{Ld} , through a flexible shaft that constitutes the drive train. The shaft is modelled as spring-damper element having damping coefficient b_s and spring constant as k_s . The friction in the bearings of the motor disk and load disk is modelled as viscous friction with respective damping parameters as b_{Md} and b_{Ld} . Friction arising due to belt is lumped with

viscous friction coefficient at motor disk in b_{Md} . The setup is equipped with motor encoder and load encoder that measure, respectively, the angular position of motor shaft and load disk (2000 pulses per revolution). Angular position motor disk is obtained by dividing the motor encoder counts by belt ratio. The BG model of the nominal system in integral causality is given in Fig. 3.5. The control input from PI controller (controlled variable: motor speed ω_m) modulates the input voltage $MSe: U_{PI}$. The measured angular velocities (obtained from angular positional measurements) of motor shaft and load disk are represented as $Df: \omega_M$ and $Df: \omega_{Ld}$ respectively. Belt is considered of high stiffness and the rigidity is not considered in the model. Also, the frictional loss due to the action of belt is lumped with frictional loss at motor bearing and it is modelled as resistor element $R: b_{Md}$. GY element models the conversion of electrical current to electrical torque in the DC motor with corresponding coefficient being $m_{GY} = k_m$. TF element models the transmission of velocity through the belt from motor shaft to the motor disk.

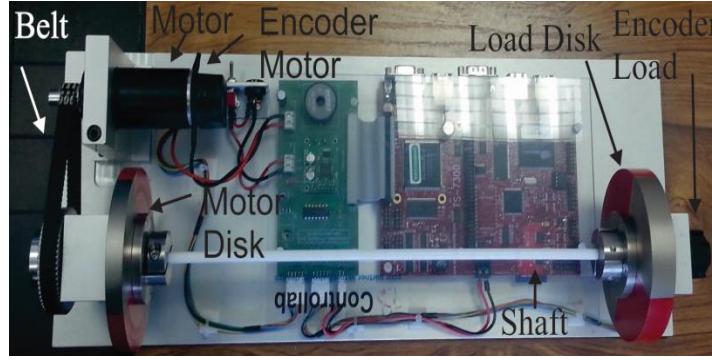


Fig. 3.3 Mechatronic Torsion Bar 1.0 system

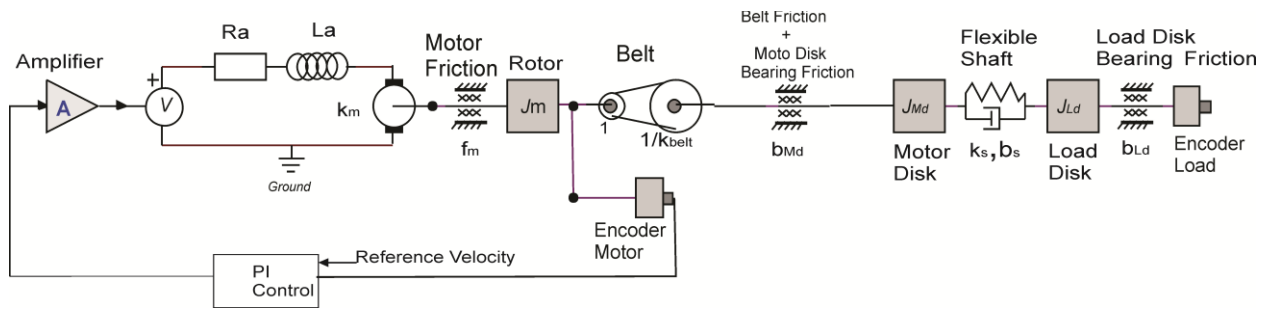


Fig. 3.4 Schematic Model Of The Mechatronic System

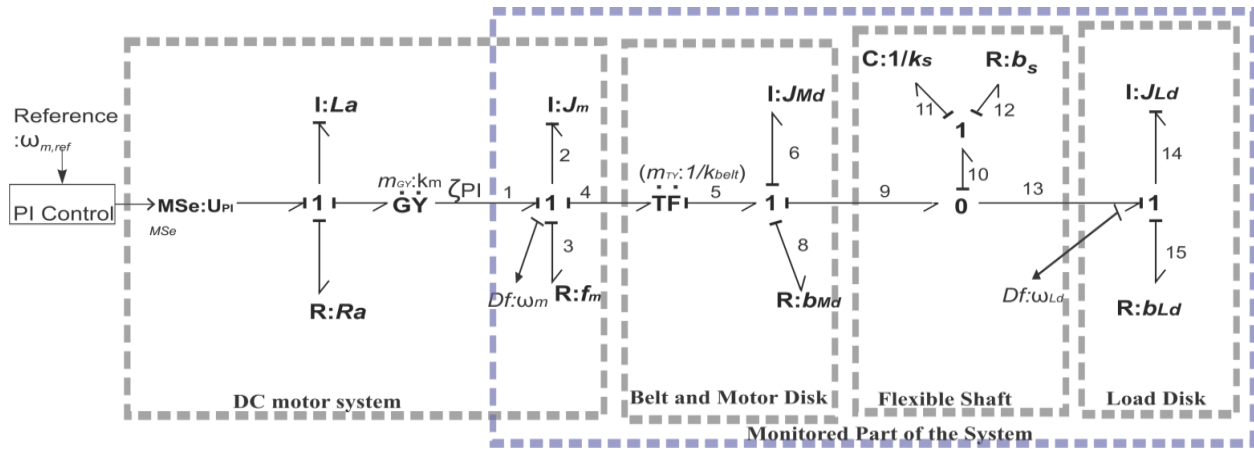


Fig. 3.5 Bond Graph Model (Preferred Integral Causality) Of The Nominal System

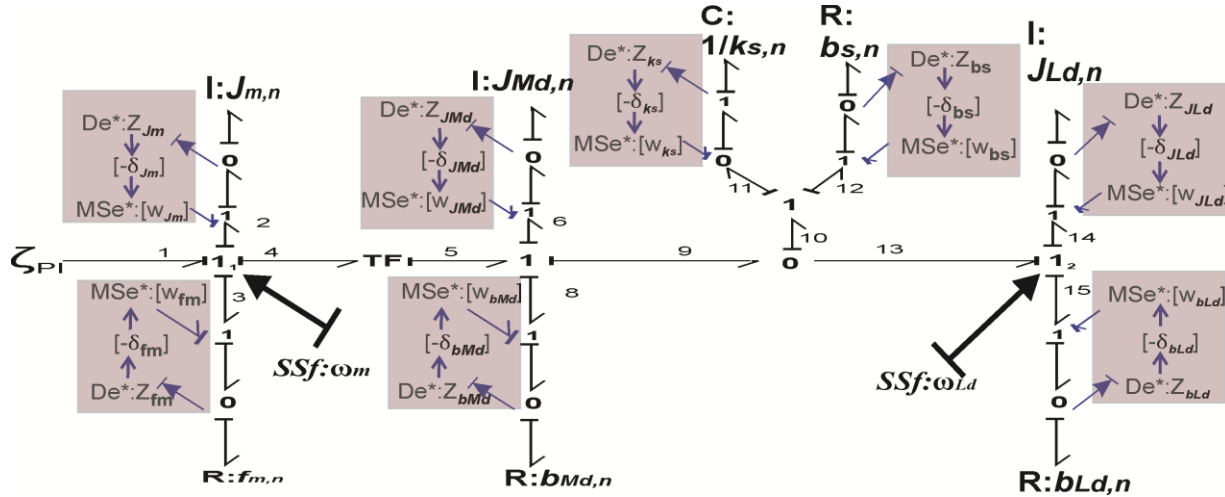


Fig. 3.6 Bond Graph Model Of Monitorable Part In Preferred Derivative Causality With Parametric Uncertainties As Intervals

The corresponding coefficient of transformation $m_{TY} = 1/k_{belt}$ where k_{belt} is the ratio between number of teeth on motor disk to motor shaft (Kleijn, C., 2011). The electrical part of the DC motor is not monitorable as there is no sensor installed in it.

Only the monitorable part (marked in Fig. 3.6) is used for analysis. It must be noted that the system is considered **operating in feedback closed loop (Proportional-Integral (PI) control)** regime. Analysis or development of the control strategy is not described, as the main interest of the work does not lie in the same.

3.6.2 Inter valued ARRs and Robust Thresholds

The uncertain BG of the monitorable part in preferred derivative causality is shown in Fig. 3.6, with parametric uncertainty modelled and represented in interval form. The global system is considered uncertain with uncertain parameter vector $[\underline{\theta}, \bar{\theta}]$:

$$[\underline{\theta}, \bar{\theta}] = \left[[J_m, \bar{J}_m], [f_m, \bar{f}_m], [J_{Md}, \bar{J}_{Md}], [b_{Md}, \bar{b}_{Md}], [J_{Ld}, \bar{J}_{Ld}], [b_{Ld}, \bar{b}_{Ld}], [k_s, \bar{k}_s], [b_s, \bar{b}_s] \right]^T \quad (3.33)$$

The latter has input in form of controlled electrical torque input generated by the DC motor. Both the sensors are dualized and impose corresponding flows as $Y(t) = [SSf_1 : \omega_m, SSf_2 : \omega_{Ld}]^T$. C element remains in integral causality with the initial condition given by the flow at respective 0-junction, provided by encoder readings as $f_{10} = f_9 - f_{13} = (\omega_m / k_{belt}) - \omega_{Ld}$

Following the steps described in Section 3.3.1, I-ARR can be generated from the detectable junction $\mathbf{1}_1$ of Fig. 3.6:

$$\begin{aligned} \left[\underline{R}, \overline{R} \right]_1 &= \tau_{PI} - \left(J_{m,n} \dot{\omega}_m + \left[\underline{\delta}_{J_m}, \overline{\delta}_{J_m} \right] J_{m,n} \dot{\omega}_m \right) - \left(f_{m,n} \omega_m + \left[\underline{\delta}_{f_m}, \overline{\delta}_{f_m} \right] f_{m,n} \omega_m \right) \\ &- \left(1/k_{belt} \right) \left(\left(J_{Md,n} (\dot{\omega}_m / k_{belt}) + \left[\underline{\delta}_{J_{Md}}, \overline{\delta}_{J_{Md}} \right] J_{Md,n} (\dot{\omega}_m / k_{belt}) \right) + \left(b_{Md,n} (\omega_m / k_{belt}) + \left[\underline{\delta}_{b_{Md}}, \overline{\delta}_{b_{Md}} \right] b_{Md,n} (\omega_m / k_{belt}) \right) \right) \\ &\left(+ \left(k_{s,n} \int (\frac{\omega_m}{k_{belt}} - \omega_{Ld}) dt + \left[\underline{\delta}_{k_s}, \overline{\delta}_{k_s} \right] k_{s,n} \int (\frac{\omega_m}{k_{belt}} - \omega'_{Ld}) dt + b_{s,n} (\frac{\omega_m}{k_{belt}} - \omega_{Ld}) + \left[\underline{\delta}_{b_s}, \overline{\delta}_{b_s} \right] b_{s,n} (\frac{\omega_m}{k_{belt}} - \omega_{Ld}) \right) \right) \end{aligned} \quad (3.34)$$

Electrical torque MSe : τ_{PI} is the PI controlled input to the monitorable part of the system and is given as:

$$MSe : \tau_{PI} = k_m \cdot i_m = k_m \cdot \frac{(U_{PI} - k_m \cdot \omega_m)}{Ra} (1 - e^{-(Ra/La) \times t}) \quad (3.35)$$

where, U_{PI} is the PI controlled voltage input and i_m is the motor stator current. The nominal part $r_{1,n}(t)$ is formed by collecting point valued nominal parameters as coefficients of known (measured) variables. The interval valued ARR is expressed as:

$$\left[\underline{R}, \overline{R} \right]_1 = r_{1,n}(t) + \left[\underline{B(t)}, \overline{B(t)} \right]_1 \quad (3.36)$$

$$\begin{aligned} r_{1,n}(t) &= \tau_{in} - J_{m,n} \dot{\omega}_m - f_{m,n} \omega_m \\ &- \frac{1}{k_{belt}} \left(J_{Md,n} \frac{\dot{\omega}_m}{k_{belt}} + b_{Md,n} \frac{\omega_m}{k_{belt}} + k_{s,n} \int (\frac{\omega_m}{k_{belt}} - \omega_{Ld}) dt + b_{s,n} (\frac{\omega_m}{k_{belt}} - \omega_{Ld}) \right) \end{aligned} \quad (3.37)$$

$$\begin{aligned} \left[\underline{B(t)}, \overline{B(t)} \right]_1 &= - \left(\left[\underline{\delta}_{J_m}, \overline{\delta}_{J_m} \right] J_{m,n} \dot{\omega}_m \right) - \left(\left[\underline{\delta}_{f_m}, \overline{\delta}_{f_m} \right] f_{m,n} \omega_m \right) \\ &- \frac{1}{k_{belt}} \left(\left(\left[\underline{\delta}_{J_{Md}}, \overline{\delta}_{J_{Md}} \right] J_{Md,n} \frac{\dot{\omega}_m}{k_{belt}} + \left[\underline{\delta}_{b_{Md}}, \overline{\delta}_{b_{Md}} \right] b_{Md,n} \frac{\omega_m}{k_{belt}} \right) \right. \\ &\left. + \left(\left[\underline{\delta}_{k_s}, \overline{\delta}_{k_s} \right] k_{s,n} \int (\frac{\omega_m}{k_{belt}} - \omega_{Ld}) dt + \left[\underline{\delta}_{b_s}, \overline{\delta}_{b_s} \right] b_{s,n} (\frac{\omega_m}{k_{belt}} - \omega_{Ld}) \right) \right) \end{aligned} \quad (3.38)$$

Only one I-ARR has been derived here at $\mathbf{1}_1$, which serves the purpose of approach demonstration. Following similar steps, another independent I-ARR can be derived from $\mathbf{1}_2$ junction.

3.6.3 Nominal Conditions

The nominal parameter values and respective *multiplicative interval uncertainty* is tabulated in Table 3-VI. Fig.3.8 shows the nominal outputs with measured motor velocity ω_m being PI controlled with reference $\omega_{m,ref} = 112.5 \text{ rad/s}$ such that motor disk velocity ω_{Md} is regulated to $\omega_{Md,ref} = \omega_{m,ref} / k_{belt} = 30 \text{ rad/s}$. Noise is added to sensor outputs. It corrupts the residual and is approximated as $w^d(t) \sim \mathcal{N}(0, \sigma_{w^d}^2)$; $\sigma_{w^d} = 0.01 \text{ V}$. Negative value of residual $-r_{1,n}^d(t)$ is contained within the interval threshold bounds, determined in (3.38).

Table 3-VI Nominal and uncertainty values of System Parameters

Parameter	Nominal Value	Multiplicative Uncertainty	Parameter	Nominal Value	Multiplicative Uncertainty
θ	θ_n	$[\underline{\delta}_\theta, \overline{\delta}_\theta]$	θ	θ_n	$[\underline{\delta}_\theta, \overline{\delta}_\theta]$
k_s	1.786 N.m/rad	[-0.1,0.1]	J_m	$6.76 \times 10^{-6} \text{ kg.m}^2 / \text{rad}$	[-0.02,0.02]
R_s	5.11×10^{-4} N.m/rad	[-0.1,0.1]	f_m	$2 \times 10^{-6} \text{ N.m.s/rad}$	[0,0.3]
k_m	3.89×10^{-4} Nm/A	-	J_{Md}	$9.07 \times 10^{-4} \text{ kg.m}^2 / \text{rad}$	[-0.1,0.1]
k_{belt}	3.75	-	b_{Md}	5.025×10^{-3} N.m.s/rad	[0,0.2]
La	1.34×10^{-3} H	-	J_{Ld}	$1.37 \times 10^{-3} \text{ kg.m}^2 / \text{rad}$	[-0.1,0.1]
Ra	1.23 Ω	-	b_{Ld}	$2.5 \times 10^{-5} \text{ N.m.s/rad}$	[0,0.2]
			μ	0.27	[-0.1,0.1]

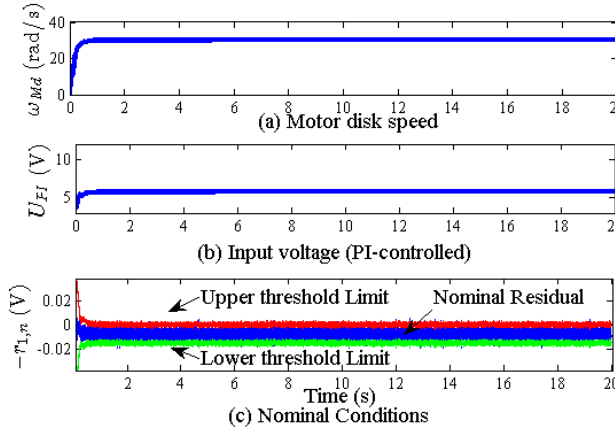


Fig. 3.7 Nominal Conditions (a) Motor disk speed (b) Input voltage (c) nominal residual and interval valued thresholds

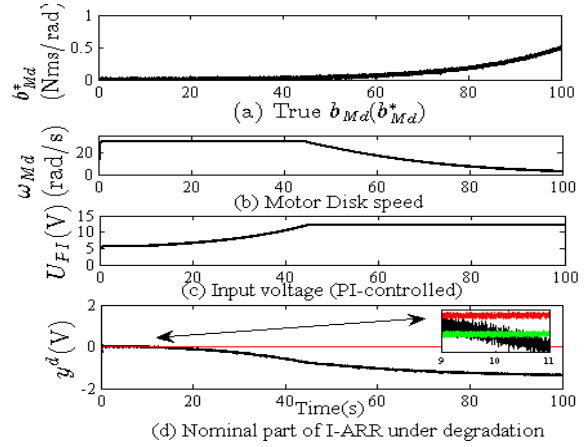


Fig. 3.8 Simulation of degradation (a) injected degradation (b) motor disk speed (c) input voltage to the system (d) nominal residual $r_{1,n}(t)$

3.6.4 Generation of Parametric degradation

Degradation of motor disk bearing friction parameter b_{Md} , is simulated by considering the degradation model exponential in nature as:

$$b_{Md}(t) = \begin{cases} g_1(b_{Md}, \gamma_1) + v_{b_{Md}} \\ b_{Md,n} e^{\gamma_1(t)} + v_{b_{Md}} \end{cases} \quad (3.39)$$

where g_1 is the DM, $\theta^d(t) = b_{Md}$ is the state variable and DPP vector $\gamma^d = \{\gamma^d\} = \gamma_1$ and $v_{b_{Md}} \sim \mathcal{N}(0, \sigma_{b_{Md}}^2)$ is the process noise. Fig. 3.8 shows corresponding outputs. The fault is detected at $t_d = 10$ s when residual crosses the interval thresholds. Note that ω_{Md} is controlled at 30 rad/s until $t = 44.2$ s while the PI controller is effective. Thereafter, as the saturation limit value of actuator (motor) input voltage (12V) is reached, the speed ω_{Md} starts to decrease and reaches $\omega_{Md,stop} = 3$ rad/s at $t = 100$ s. The latter is the time point at which system is considered to have obtained the failure state. The residual being sensitive to the input torque and hence the input voltage, captures the degradation evolution throughout the system's lifetime.

3.6.5 Fault Model

Residual based state measurement is obtained from observation equation formed by using the Nominal Part of I-ARR $[\underline{R}, \overline{R}]_1$, $r_{1,n}(t)$ (cf. (3.16), (3.13) and (3.15)) as:

$$0 = r_{1,n}(t) + (b_{Md}(t) - b_{Md,n}) \cdot \frac{\partial(r_{1,n}(t))}{\partial(b_{Md})} \quad (3.40)$$

$$y^d = -r_{1,n}(t) + w^d(t) = (b_{Md}(t) - b_{Md,n}) \frac{-\omega_m(t)}{k_{belt}^2} + w^d(t)$$

where $w^d(t) \sim \mathcal{N}(0, \sigma_{w^d}^2)$ approximates the noise corrupting $-r_{1,n}(t)$. For estimation, the fault model denoted as tuple $(g_1, b_{Md}(t), \gamma_1)$, is formulated as:

$$\begin{aligned} b_{Md,k} &= b_{Md,k-1} \cdot e^{\gamma_{1,k-1} \Delta t} + v_{b_{Md},k-1} \\ \gamma_{1,k} &= \gamma_{1,k-1} + \xi_{1,k-1} \\ y_k^d &= (b_{Md,k} - b_{Md,n}) \frac{-\omega_{m,k}}{k_{belt}^2} + w_k^d \end{aligned} \quad (3.41)$$

where, $\xi_1(t) \sim \mathcal{N}(0, \sigma_{\xi_1}^2)$ is the additive random walk noise. The estimation of state of parameter $b_{Md}(t)$ is triggered at $t_d = 10s$. Initial estimate $b_{Md,t_d=10s} \sim U(0.045, 0.055)$ N.m.s/rad, contains $b_{Md,n} = 0.005$ N.m.s/rad. The true value of DPP γ_1 is kept such that $\omega_{Md,stop}$ is reached at 100s. $\gamma_1^* = 0.05$ Nm/rad. Sample time for simulation $\Delta t = 0.1s$ and number of particles $N=500$. Simulation is run until $t_f = 100s$ when \hat{b}_{Md} reaches the failure value $b_{Md,fail} = 0.45$ N.m.s/rad.

3.6.6 Degradation Estimation

Estimated \hat{b}_{Md} is shown in Fig. 3.9. The true state b_{Md}^* is estimated accurately with $RMSE_{b_{Md}} = 4.21\%$. In fact, estimation spread decreases as the estimation progresses, indicating the desirable performance. Estimation of b_{Md} largely depends upon quality of estimation achieved with γ_1 . Fig. 3.10 shows the estimation of γ_1 achieved with $[\gamma_{1,l}^*, \gamma_{1,u}^*] = [0.03, 0.07]$ N.m./rad, $P=0.001$, $v^{\xi_1^*} = 10\%$, initial artificial noise variance $\sigma_{\xi_1, k=0}^2 = 0.02^2$. The particle filter assumes measurement noise variance equal to 4 times that of residual noise variance $\sigma_{w_1}^2 = 0.01^2$. The convergence is achieved very quickly but with large initial estimation spread. This is due to the high artificial noise variance set for the desirable quick convergence. The estimation spread shown in Fig. 3.10 (b), is reduced (effective from $t = 20$ s) until $v^{\xi_1^*} = 10\%$ is achieved around

$t=50$ s and thereafter, γ_1^* is tracked smoothly with controlled spread; $RMSE = 3.02\%$. For only comparison purpose Fig. 3.10 (c) shows performance with no variance control where the estimation continues with large spread even after the convergence is achieved

3.6.7 RUL Prediction

Using $\alpha = 0.1, \beta = 0.5$ and for all λ_k , RUL prediction is shown in Fig. 3.11. The RUL distributions obtained until $t = 52$ s, are not good predictions and suffer with large variance spread due to the large corresponding spread in $\hat{\gamma}_1$ (see Fig. 3.10 (a)) making them virtually useless. However, after $t = 52$ s, the RUL distributions are well within accuracy cone such that, more than 50% of RUL probability mass lies within accuracy cone. Ignoring the initial period of convergence, the overall prediction performance is very good with $\overline{RMAD}_{RUL} = 9.8$ and $\overline{RA} = 97.15\%$.

3.6.8 A Qualitative Analysis

As seen in the previous section, accuracy and spread of RUL prediction is directly influenced by the estimation quality of DPP, which in turn depends on initial setting and tuning of the several parameters involved. They are discussed here qualitatively. Note that estimation obtained in Fig. 3.10 (a) forms the most desirable performance. In subsequent discussion, only the specified PF parameters are played with, keeping rest of them same as for Fig. 3.10 (a).

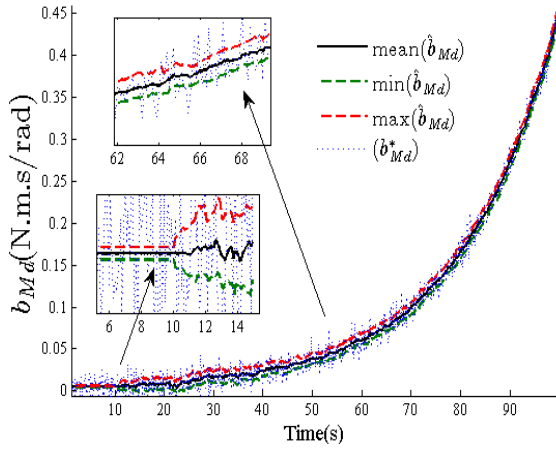


Fig. 3.9 State estimation of the prognostic candidate system parameter b_{Md}

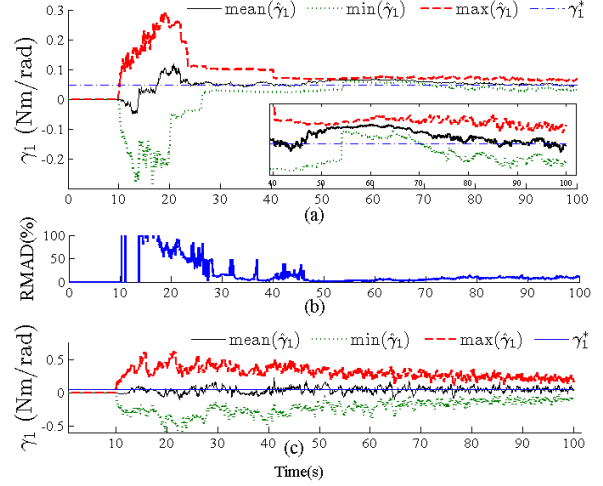


Fig. 3.10 Estimation performance (a) Estimation of DPP with variance adaptation (b) Estimation spread associated (c) Estimation performance without variance adaptation only for comparison purpose

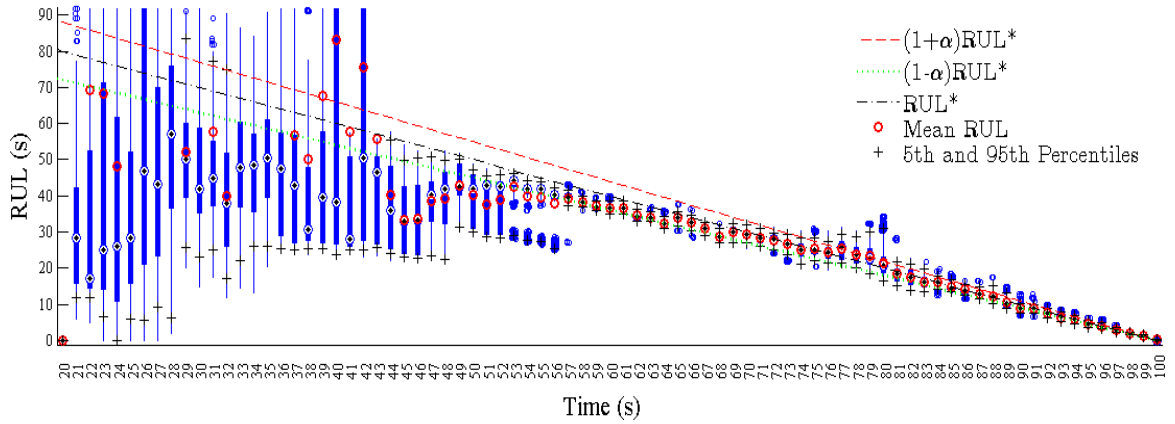


Fig. 3.11 RUL Prediction performance with respect to estimation in Fig. 3.9 and Fig. 3.10 (a).

Initial artificial random walk noise $\sigma_{\xi_1, k=0}^2$ (or $v_{k=0}^{\xi_1}$): The initial variance of random walk noise is set according to the magnitude order of DPP γ^{d,j^*} . It is kept high enough so that $\bar{\gamma}_{1,k}$ is captured quickly as $\bar{\gamma}_{1,k} \in [\gamma_{1,l}^*, \gamma_{1,u}^*]$. It is the most important factor that determines good tuning of parameters in succession. A very high value of the latter, leads to worse estimation performance. Fig. 3.12 (a) shows estimation with $\sigma_{\xi_1, k=0}^2 = 0.04^2$ (read high) wherein, although, quick convergence of mean $\hat{\gamma}_1$ is seen, the estimation continues further with a very wide spread for a

long time before it is gradually reduced, owing to variance adaptation scheme. On the contrary, a very low variance will result in very late convergence, if at all. Fig. 3.12 (b) has $\sigma_{\xi_1, k=0}^2 = 0.001^2$ leading to a very late convergence. For tuning of other related parameters in this paper, an initial high value of variance $\sigma_{\xi_1, k=0}^2$ is chosen.

Proportional Gain P : Proportional gain determines how fast the estimation spread is reduced to the reference v^{ξ^*} . As observed in Fig. 3.10 (a), an appropriate choice of latter was found as $P_I = 0.001$. It resulted in smooth tracking after convergence was achieved. A high gain value results in quick reduction of estimation spread; however, it is accompanied with continuous shrink and expansion as shown in Fig. 3.12 (c) with $P_I=0.005$. Although, a very high gain value may bring down variance spread quickly; however, it may be followed by poor convergence results as shown in Fig. 3.13 (c) and (d), with $P_I=0.01$. On the contrary, a very low P_I renders a non-effective variance adaptation as shown in Fig. 3.12 (d) with $P_I = 0.0001$, adding no significant benefits in RUL prediction.

Desired RMAD (v^{ξ^*}): The pre-fixed v^{ξ^*} for ξ_1 , determines how much freedom is given to γ_1 after the estimation spread is brought under control. An appropriate choice of v^{ξ^*} gives enough freedom for convergence even after actual variance is well under v^{ξ^*} , as shown in Fig. 3.10 (a) between $t=50s$ and $t=80s$ with $v^{\xi^*}=10\%$. In extreme cases, where P_I is chosen of high value (rate of RMAD reduction depends on P_I) and v^{ξ^*} is set very low, the estimation may remain stagnant near, but not equal to γ_1^* . This is shown in Fig. 3.13 (c) with $P_I=0.01$ (read high) and desired RMAD $v^{\xi^*}=6\%$ (read very low).

True DPP interval $[\gamma_l^{d,j^*}, \gamma_u^{d,j^*}]$: The main objective of the latter remains in triggering the variance adaptation. As such, if width of $[\gamma_{1,l}^*, \gamma_{1,u}^*]$ is kept too tight around γ_1^* , $\bar{\gamma}_{1,k}$ may never be captured inside the $[\gamma_{1,l}^*, \gamma_{1,u}^*]$ band. This may lead to a very insignificant effect of variance adaptation on the estimation performance. Fig. 3.13a shows the estimation with $[\gamma_{1,l}^*, \gamma_{1,u}^*] = [0.04, 0.06]$ Nm/rad, which can considered “too tight” around $\gamma_1^* = 0.05$ Nm/rad. Here, the variance adaption is not effective enough. On the contrary, if the interval width is

appropriately set (assuming that initial estimate is outside of it), $\bar{\gamma}_{1,k}$ is captured quickly and variance control is triggered early, as shown in Fig. 3.13(b) with $[\gamma_{1,l}^*, \gamma_{1,u}^*] = [0.01, 0.09]$ Nm/rad. This leads to early reduction in variance. However, a bad choice of P_1 (read high) and early variance adaptation, may lead to a rapid reduction in spread, followed by stagnation of estimation around $\gamma^{d,j*}$, before converging slowly to the same, as shown in Fig. 3.13 (d) with $P_l = 0.005$ and $[\gamma_{1,l}^*, \gamma_{1,u}^*] = [0.01, 0.09]$ Nm/rad.

Residual noise variance (measurement noise) assumed by PF: Noise corrupting the residual measurements that can be non-Gaussian due to presence of derivative terms and integral terms, can be dealt by PF, without any restrictions. In this work, the explicit distribution of the residual noise present is not found. Instead, it is approximated as normally distributed Gaussian in nature. The related standard deviation and variance is found out from residual measurements. Moreover, generally, the variance of measurement noise (residual noise here) assumed by PF, is greater than approximated actual measurement noise. This is done to counter the sample impoverishment problem which happens when very few particles have significant weight while most other particles with non-significant weight are abandoned during the resampling process (Li et al., 2014). Higher residual noise variance assumed by PF allows higher particles being sampled for estimation, thus reducing the problem of sample degeneracy and consequent impoverishment. As followed in other works, in this work too, the residual noise assumed by PF is greater than actual residual noise and is tuned to improve performance.

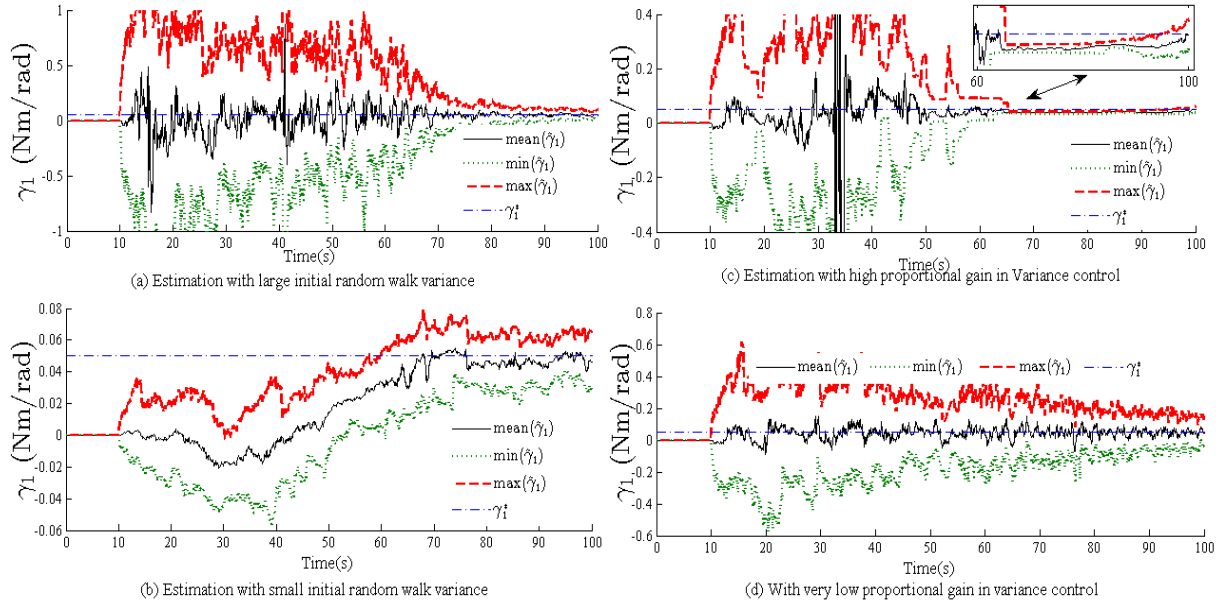


Fig. 3.12 Estimation of DPP γ_1 for qualitative analysis (a) Large initial random walk variance $\sigma_{\xi_1, k=0}^2 = 0.04^2$ (b) Small initial random walk variance $\sigma_{\xi_1, k=0}^2 = 0.001^2$ (c) High proportional gain in variance control $P_I=0.005$ (d) Very low proportional gain in variance adaptation $P_I=0.0001$

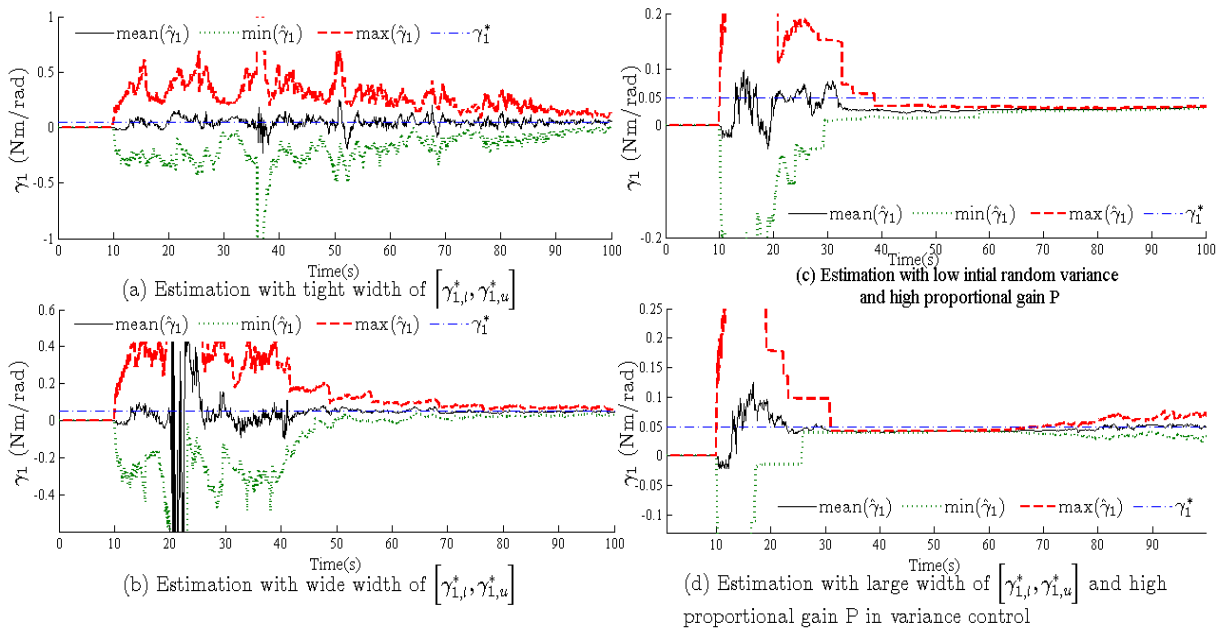


Fig. 3.13 Estimation of DPP γ_1 for qualitative analysis (a) Tight width $[\gamma_{1,l}^*, \gamma_{1,u}^*] = [0.04, 0.06]$ Nm/rad (b) Wide width with $[\gamma_{1,l}^*, \gamma_{1,u}^*] = [0.01, 0.09]$ Nm/rad (c) High gain value, $P_I=0.01$ and very low desired RMAD $v^{\xi^*} = 6\%$ (d) High gain $P_I=0.005$ and large width $[\gamma_{1,l}^*, \gamma_{1,u}^*] = [0.01, 0.09]$ Nm/rad

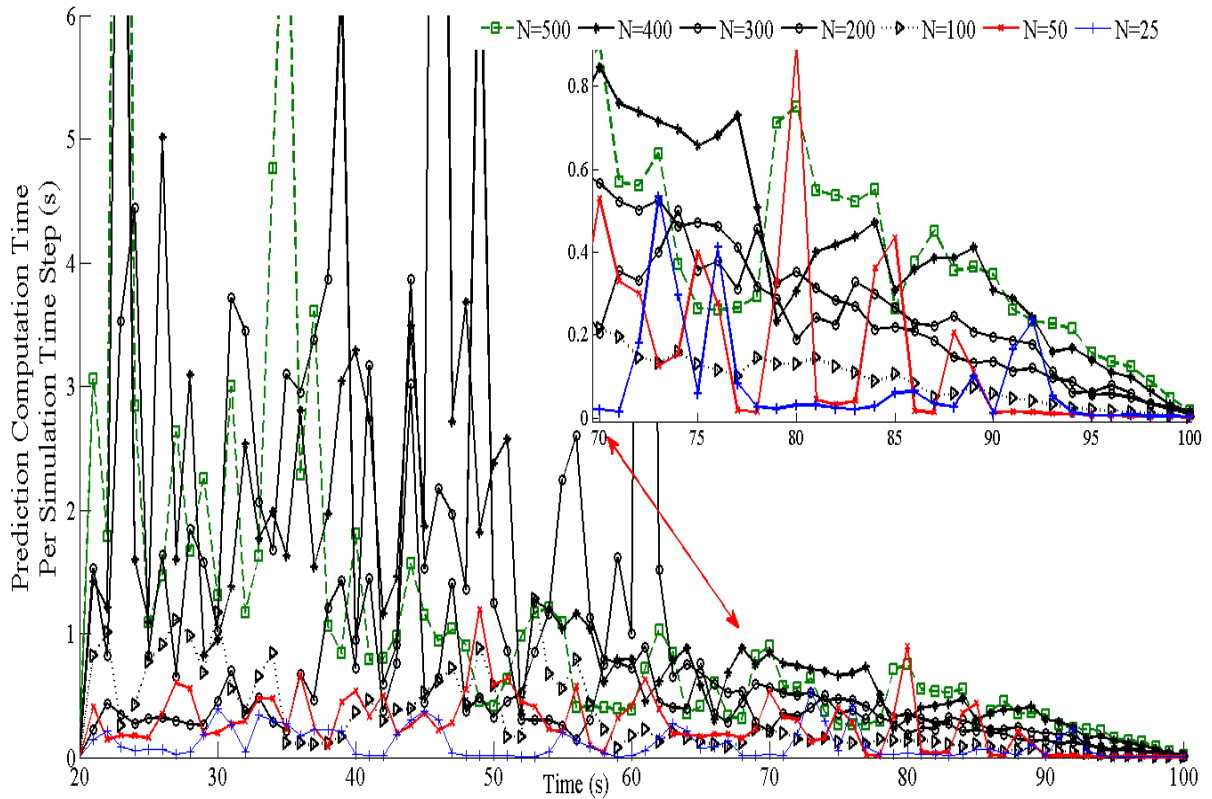


Fig. 3.14 Prediction computational time for per step for different number of particles

3.6.9 Computational Complexity

The time taken per step for estimation and RUL prediction depends on the number of particles used. With $N=500$, on an average, 0.03s was consumed per step. Fig. 3.14 shows the RUL prediction computation time per step for the RUL prediction performance of Fig. 3.11. In addition to the number of particles N , computational time for RUL prediction varies:

- Inversely with the time at which prediction is made: The farther is the time from EOL at which RUL prediction is made, the longer it takes to simulate to EOL. This makes the computational time large.
- Inversely with estimated DPP $\hat{\gamma}$: At a certain time of prediction, higher is the rate of damage progression, smaller is time taken to simulate to EOL. As seen in Fig. 3.10 (a), before $t=50s$, the estimation value of $\hat{\gamma}_1$ is lower than true value accompanied with large variance. Therefore, for a specific N , the computation time per step before

$t=50s$ is higher and with large variations. After $t=50s$, with a nearly uniform $\hat{\gamma}_1$ estimation and lesser spread (see Fig. 3.10(a)), the computation time follows an almost uniform monotonic decreasing trend (see Fig. 3.14).

Simulations were run on a 2.49-GHz dual core processor with 8GB RAM. With $N=500$, and sample time of 0.1s (which translates to 10 computational steps per second); it took on an average 32 minutes to simulate system dynamics, estimation and RUL prediction till 100s. With $N=50$, the same took 110 seconds. This indicates that through employment of lesser number of particles, the RUL predictions could be achieved in real time, for experimental purposes. Moreover, for real experiments run on compiled C, the run time reduces drastically by an order of magnitude.

3.7 Application: Health Monitoring of Mechanical Torsion Bar System

The methodology developed here is applied in real time over the mechatronic system (torsion bar system) presented in Section 3.6, to assess the health monitoring capability of the method proposed therein.

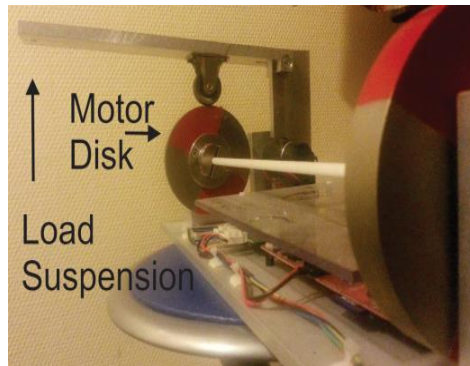


Fig. 3.15 Fabricated Mechanical Lever type arrangement for Load (Mass) Suspension

For experiments, a mechanical lever type arrangement is fabricated as shown in Fig. 3.15, which introduces frictional torque τ_{Mech} over the motor disk by suspension of load in form of sand. The associated frictional torque is due to Coulomb friction existing between the surfaces (μ being friction coefficient) and is modulated by the suspended load M as,

$$\begin{aligned}\tau_{Mech} &= f_{mech} \cdot r_{Md} \\ f_{mech} &= \mu Mg (\omega_{Md} / |\omega_{Md}|)\end{aligned}\quad (3.42)$$

with r_{Md} as the radius of the motor disk. In the BG model presented in Section 3.6.1, it is incorporated as non-linear resistance element at motor disk as shown in(3.43), and corresponding characteristic equation becomes as given in (3.44).

$$R = b_{Md} + \mu.M(t).r_{Md}g / |\omega| \quad (3.43)$$

$$e_8 = R(f_8) = b_{Md}\omega_{Md} + \mu.M(t).r_{Md}g \times (\omega_{Md} / |\omega_{Md}|) \quad (3.44)$$

Involving only non-destructive experiments, μ is assumed undergoing no wear. The nominal value of μ , μ_n is found out by suspension of known load value and calculation of the nominal friction value. The corresponding I-ARR $[\underline{R}, \overline{R}]_1$ found in (3.34) changes to $[\underline{R}, \overline{R}]_2$ as,

$$[\underline{R}, \overline{R}]_2 = r_{2,n}(t) + [\underline{B}(t), \overline{B}(t)]_2$$

$$r_{2,n}(t) = \tau_{in} - J_{m,n}\dot{\omega}_m - f_{m,n}\omega_m - \frac{1}{k_{belt}} \left(\begin{aligned} &J_{Md,n} \frac{\dot{\omega}_m}{k_{belt}} + b_{Md,n} \frac{\omega_m}{k_{belt}} + \mu_n M_n g r_{Md} \operatorname{sgn}(\omega_m / k_{belt}) \\ &+ k_{s,n} \int (\frac{\omega_m}{k_{belt}} - \omega_{Ld}) dt + b_{s,n} (\frac{\omega_m}{k_{belt}} - \omega_{Ld}) \end{aligned} \right) \quad (3.45)$$

$$\begin{aligned} [\underline{B}(t), \overline{B}(t)]_2 &= - \left([\underline{\delta}_{J_m}, \overline{\delta}_{J_m}] J_{m,n} \dot{\omega}_m \right) - \left([\underline{\delta}_{f_m}, \overline{\delta}_{f_m}] f_{m,n} \omega_m \right) \\ &- \frac{1}{k_{belt}} \left(\begin{aligned} &[\underline{\delta}_{J_{Md}}, \overline{\delta}_{J_{Md}}] J_{Md,n} \frac{\dot{\omega}_m}{k_{belt}} + [\underline{\delta}_{b_{Md}}, \overline{\delta}_{b_{Md}}] b_{Md,n} \frac{\omega_m}{k_{belt}} + [\underline{\delta}_{\mu}, \overline{\delta}_{\mu}] \mu_n M_n g r_{Md} \operatorname{sgn}(\omega_m / k_{belt}) \\ &+ [\underline{\delta}_{k_s}, \overline{\delta}_{k_s}] k_{s,n} \int (\frac{\omega_m}{k_{belt}} - \omega_{Ld}) dt + [\underline{\delta}_{R_s}, \overline{\delta}_{R_s}] R_{s,n} (\frac{\omega_m}{k_{belt}} - \omega_{Ld}) \end{aligned} \right) \end{aligned} \quad (3.46)$$

Fig. 3.16 shows the residual profile under nominal conditions. Fig. 3.17 shows the effect of adding load (or frictional torque) in a discrete way on the system. ω_{Md} is controlled at 30 rad/s. Each time load is added, there is PI controller enabled compensation and it settles to the reference velocity. However, $-r_{2,n}(t)$ being sensitive to increase in current (and thus, voltage) decreases and settles to a new value. Saturation limit of input voltage is reached around t=65s

when the total load suspended is 1.6Kg. Thereafter, controller is unable to compensate the change in ω_{Md} . With addition of more load thereafter ($t > 65s$), motor disk speed decreases rapidly and stops at around $t = 70s$. For safety of the real system, disk is kept at stop condition only for few seconds after which the suspended load is removed, bringing back the controller action into play. It is clearly visible that residual captures the degradation of friction (variation of mass) while controller remains effective or otherwise.

The experiments involve only non-destructive procedures so that there is no degradation (wear) of the surfaces. In other words, μ is assumed constant. Experiments involve variation of suspended load mass M in a uniform way till the limit M_{fail} , is reached. $M(t)$ is treated as system parameter under degradation. The experiments were conducted in two distinct phases:

- Offline: In this phase, multiple tests were done with the load being added uniformly. As explained in Section 3.2.1, variations of $M(t)$ were obtained from the evolution of $r_{2,n}(t)$ found in (3.45). This provided the time dependent DM of the system parameter $M(t)$.
- Online health monitoring: The maximum limit of additive load mass M_{fail} was pre-decided keeping in mind the safety of the system. Load was varied until M_{fail} ; this was performed in the similar environment as of the offline phase. In real time, estimation of $M(t)$ and associated DPPs, and subsequent RUL predictions were obtained.

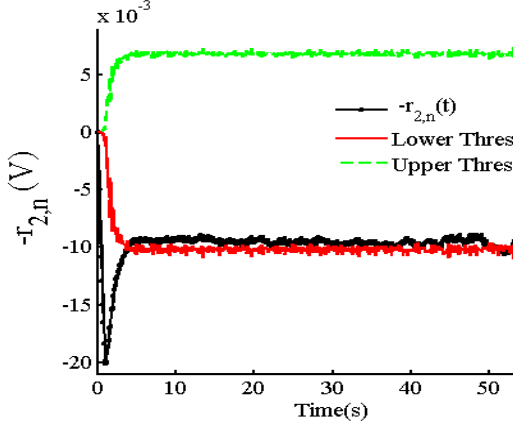


Fig. 3.16 Nominal residual $-r_{2,n}(t)$ under nominal conditions

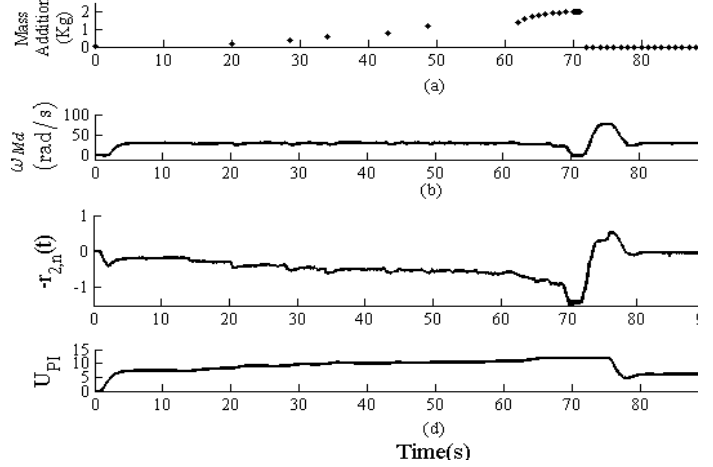


Fig. 3.17 (a) Addition of mass discretely to introduce degradation (b) Motor disk speed (c) Nominal residual $-r_{2,n}(t)$ (d) Input voltage (PI controlled)

3.7.1 Case I: Linear Variation of Load

Linear degradation models are frequently employed where incipient degradation does not accelerate subsequent degradation. Here, such a scenario is created through experiments and tested in real time.

3.7.1.1 Degradation Model

Load is varied in a continuous linear way. Ten experiments are carried out wherein; sand is poured with same environmental conditions to maintain the uniformity. With $g_2(\cdot)$ as the DM, $\theta^d = M(t)$ is the state variable and DPP vector $\gamma^d = \{\gamma^d\} = \gamma_2 v_{M_2}(t) \sim \mathcal{N}(0, \sigma_{M_2}^2)$,

$$\begin{aligned} M(t) &= g_2(\gamma_2, t) + v_{M_2}(t) \\ &= \gamma_2 \times t + v_{M_2}(t) \end{aligned} \quad (3.47)$$

Fig. 3.18 shows the experimental data and the data mean found at each instant. A linear fit over data mean is obtained using linear regression and an approximate $\gamma_2^* = 0.005$ Kg/s is obtained. Sum of squared errors provides an approximate standard deviation for process noise $v_M, \sigma_{M_2} = 1 \times 10^{-3}$ Kg.

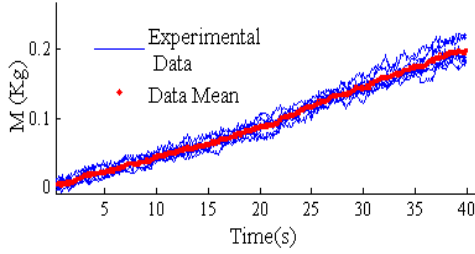


Fig. 3.18 Degradation Test Data (linear variation)

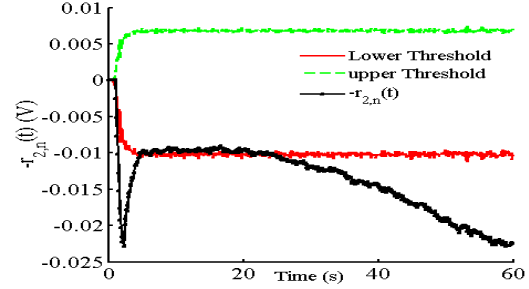


Fig. 3.19 Nominal residual $-r_{2,n}(t)$ while system is under degradation. (linear variation of mass)

3.7.1.2 Fault Model

The tuple $(g_2, M(t), \gamma_2)$ is formulated in state space as in (3.48), with $\xi_{2,k} \sim \mathcal{N}(0, \sigma_{\xi_2}^2)$ as the additive random walk noise.

$$\begin{aligned} M_k &= M_{k-1} + \gamma_{2,k-1} \times \Delta t + v_{M_{2k-1}} \\ \gamma_{2,k} &= \gamma_{2,k} + \xi_{2,k} \end{aligned} \quad (3.48)$$

Residual based state measurement is obtained from the observation equation formed by using the Nominal Part of I-ARR $[\underline{R}, \bar{R}]_2$, $r_{2,n}(t)$ as in (3.49) and (3.50) with $w_{2,k} \sim \mathcal{N}(0, \sigma_{w_2}^2)$ and σ_{w_2} is determined from $r_{2,n}(t)$ values during degradation tests of Fig. 3.18.

$$0 = r_{2,n}(t) + (M(t) - M_n) \cdot \frac{\partial(r_{2,n}(t))}{\partial(M)} \quad (3.49)$$

$$y_{2,k} = -r_{2,n,k} + w_{2,k}(t) = (M_k - M_n) \left(-\frac{\mu_n g r_{Md} \operatorname{sgn}(\omega_{Md,k})}{k_{belt}} \right) + w_{2,k} \quad (3.50)$$

For the experiment, load mass is varied until $M(t) = M_{fail} = 1.5 \text{ Kg}$. Fig. 3.19 shows the nominal residual profile under degradation.

3.7.1.3 Estimation of Degradation State

The estimation and prediction module is triggered at $t=20s$ and is performed with $N=50$ particles, $\Delta t=0.1s$, initial $\sigma_{\xi_2, k=0}^2=1 \times 10^{-6}$, $\sigma_{M_2}=1 \times 10^{-3} \text{ Kg}$, $\sigma_{w_2}=5 \times 10^{-3} \text{ V}$. For estimation, particle filter assumes measurement noise variance 9 times that of measurement variance $\sigma_{w_2}^2$ to counter sample *impoverishment* problem during the experimentation. Estimation of M is shown in Fig. 3.20 (a). Note that true M^* is the residual based measurement of $M(t)$, as described in Section 3.2.1, (cf. (3.3)) and is used for comparison purpose. The mass variation is estimated very accurately with $RMSE_M = 3.98\%$.

Estimation of DPP γ_2 is shown in Fig. 3.20 (b). Here, reference RMAD is set as $v^{\xi_2^*} = 5\%$, proportional gain $P=0.007$, true DPP interval $[\gamma_{2,l}^*, \gamma_{2,u}^*] = [3 \times 10^{-3}, 7 \times 10^{-3}] \text{ Kg/s}$ around the approximately true $\gamma_2^* = 0.005 \text{ Kg/s}$. It should be noted that in the practice, γ_2^* is not guaranteed to remain constant. From the DM, only an idea of the magnitude order is obtained. Fig. 3.20 (b) shows the estimation with large initial variance, due to a large value of initial random walk variance, set for quick convergence. The estimation spread is reduced effectively starting from $t=40s$ after which, the estimation mean remains around γ_2^* with RMAD around 6%.

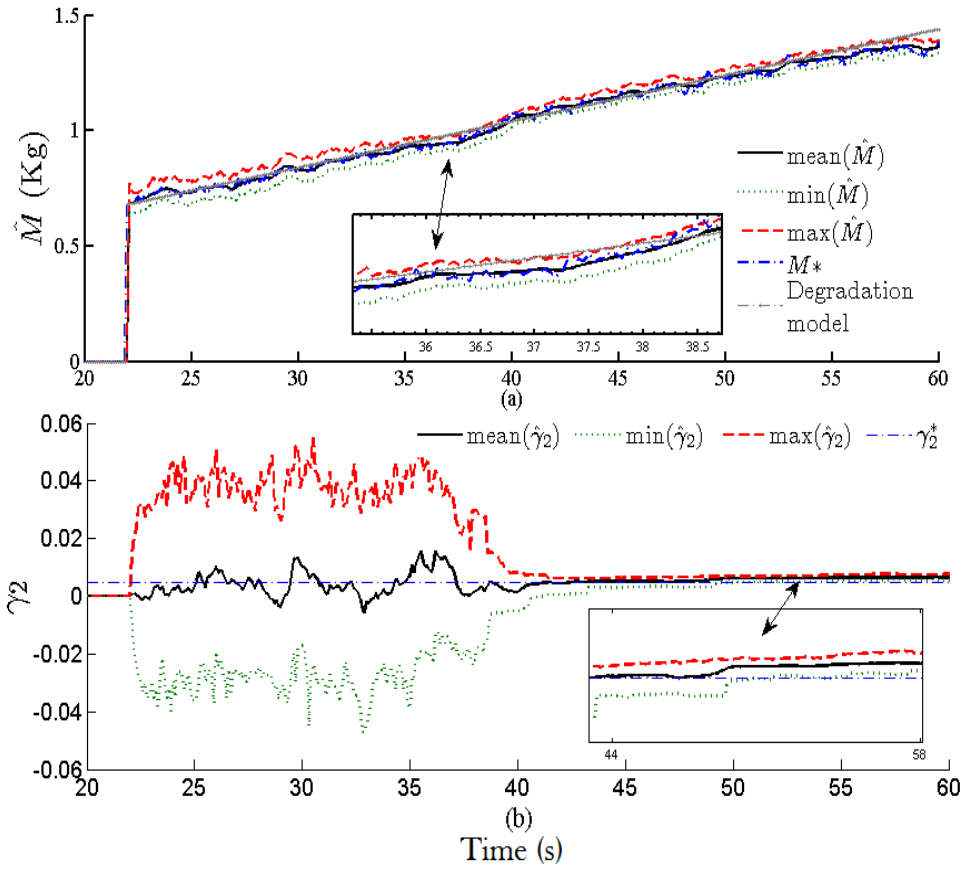


Fig. 3.20 (a). Estimation of M (b) Estimation of γ_2

3.7.1.4 RUL Prediction

Prediction of RUL is shown in Fig. 3.21. with $\alpha = 0.2$ and $\beta = 0.5$. The initial predictions have a very large spread due to large corresponding spread in $\hat{\gamma}_2$ and thus, a poor utility. However, after $t=35s$, the RUL obtained is within the $(1 \pm \alpha)RUL^*$ bounds with $\overline{RA} = 98.64\%$, $\overline{RMAD}_{RUL} = 9.4\%$. During last 3 seconds of experimentation, the sand inflow is stopped gradually (and not abruptly) bringing in certain non-uniformity. As such, RUL predictions at $t=58s$, $59s$ and $60s$, do not fall under the $(1 \pm \alpha)RUL^*$ bounds that are based upon the ideally uniform (linear) degradation model.

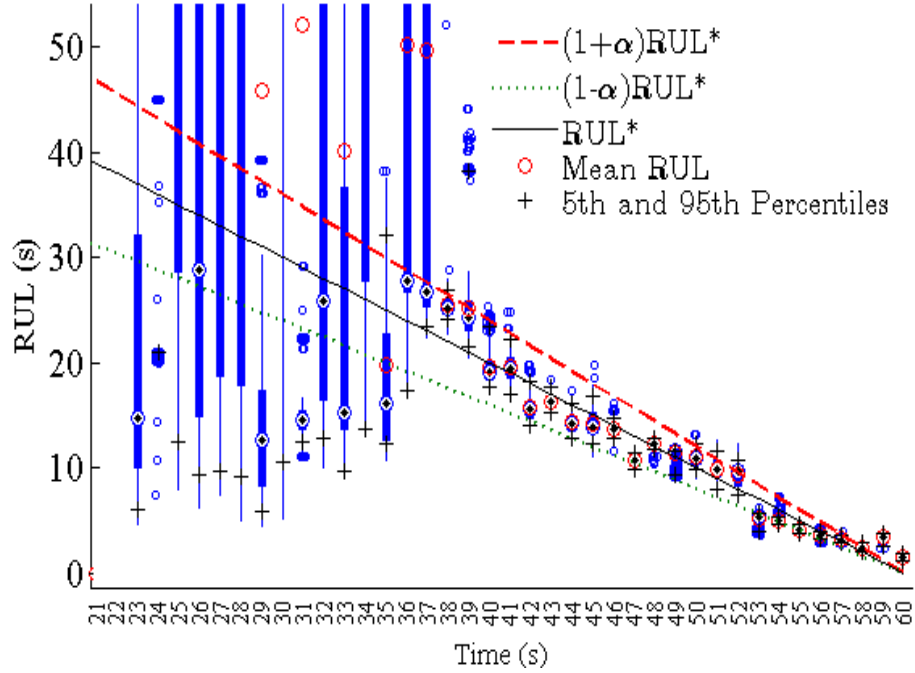


Fig. 3.21 RUL prediction in experimental case: Linear variation of mass

3.7.2 Case II: Exponential Variation of Load

Load is varied in an exponential way. Eight experiments are carried out in total. The DM for varying mass $M(t)$ is given in (3.51) where $g_3(\cdot)$ is the DM, $\theta^d = M(t)$, DPP vector $\gamma^d = \{\gamma^d\} = \gamma_3$ and $v_{M3}(t) \sim \mathcal{N}(0, \sigma_{M3}^2)$.

$$\begin{aligned}
 b_{Md}(t) &= g_3(M, \gamma_3) + v_{M3} \\
 &= M_n e^{\gamma_3(t)} + v_{M3}
 \end{aligned} \tag{3.51}$$

Fig. 3.22 (a) shows the experimental data and Fig. 3.22 (b) shows the exponential fit over the experimental data mean from which, the approximate value of DPP, $\gamma_3^* = 0.05$ Kg/s is obtained. Regression residuals provide process noise v_{M3} , $\sigma_{M3} = 8 \times 10^{-4}$ Kg.

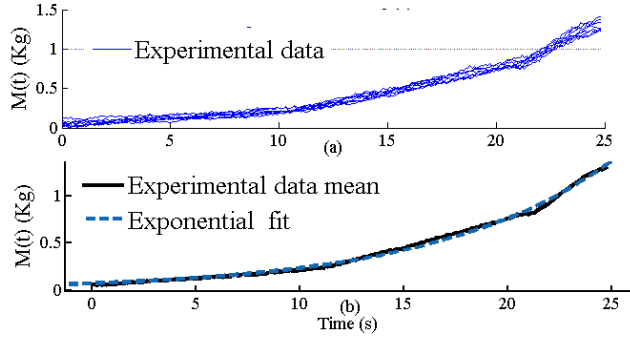


Fig. 3.22 Exponential variation of mass. (a) experimental data (b). Exponential fit over experimental data mean

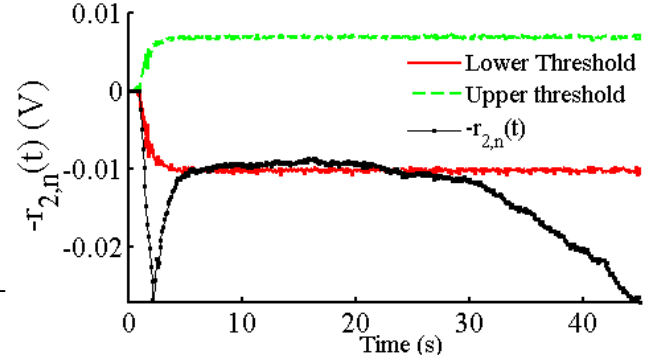


Fig. 3.23 Nominal residual $-r_{2,n}(t)$ while system is under degradation (exponential case)

3.7.2.1 Fault Model

The tuple $(g_3, M(t), \gamma_3)$ is formulated in state space as,

$$\begin{aligned}
 M_k &= M_{k-1} \cdot e^{\gamma_{3,k-1} \Delta t} + v_{M3,k-1} \\
 \gamma_{3,k} &= \gamma_{3,k-1} + \xi_{3,k-1} \\
 y_{3,k} &= -r_{2,n,k} + w_{3,k}(t) = (M_k - M_n) \left(-\frac{\mu_n g r_{Md} \operatorname{sgn}(\omega_{Md,k})}{k_{belt}} \right) + w_{3,k}
 \end{aligned} \tag{3.52}$$

where $\xi_{3,k} \sim \mathcal{N}(0, \sigma_{\xi_3}^2)$, $w_{3,k} \sim \mathcal{N}(0, \sigma_{w_3}^2)$ and the approximation of σ_{w_3} is determined from $r_{2,n}(t)$ values during degradation tests. The structure of the observation equation remains same as in (3.50). For the experiment, load mass is varied until $M(t) = M_{fail} = 1.8 \text{Kg}$. Fig. 3.23 shows the profile of nominal residual under exponential degradation.

3.7.2.2 Health Estimation and RUL Prediction

The estimation and prediction module is triggered at $t=20$ s. It is performed with $N=50$, $\Delta t = 0.1$ s, initial $\sigma_{\xi_3, k=0}^2 = 4 \times 10^{-6}$, $\sigma_{w_3} = 5 \times 10^{-3}$ V. For estimation, particle filter assumes measurement noise variance 9 times that of measurement variance $\sigma_{w_3}^2$ to counter sample *impoverishment* problem during the experimentation. As shown in Fig. 3.24 (a), state of parameter is estimated accurately with $RMSE_M = 3.78\%$. Fig. 3.24 (b) shows the DPP γ_3 estimation with reference RMAD set as $v^{\xi_3^*} = 10\%$, proportional gain $P=0.003$, true DPP interval $[\gamma_{3,l}^*, \gamma_{3,u}^*] = [1 \times 10^{-2}$,

9×10^{-2}] Kg/s. Estimation is achieved with $RMSE_{\gamma_3} = 7.6\%$. It must be noted that in real experiments γ_3^* cannot be claimed to be the accurate true value of γ_3 . Fig. 3.24 (c) shows the RUL prediction with $\alpha = 0.2, \beta = 0.5$. Ignoring the initial predictions until $t = 32$ s (due to large spread), $\overline{RMAD}_{RUL} = 9.4\%$ and $\overline{RA} = 97.02\%$. In fact, the EOL at $M = 1.8$ Kg is achieved slightly before than that predicted by DM.

It should be noted that $RMSE_{\gamma}$ in real time experiments is higher than that obtained in simulations. It is because γ^* does not remain perfectly constant in real cases. Also, lesser number of particles are used so that RUL predictions may be achieved in real time without data loss. This leads to worse estimation performance. However, overall prediction and estimation performances are very good and satisfactory.

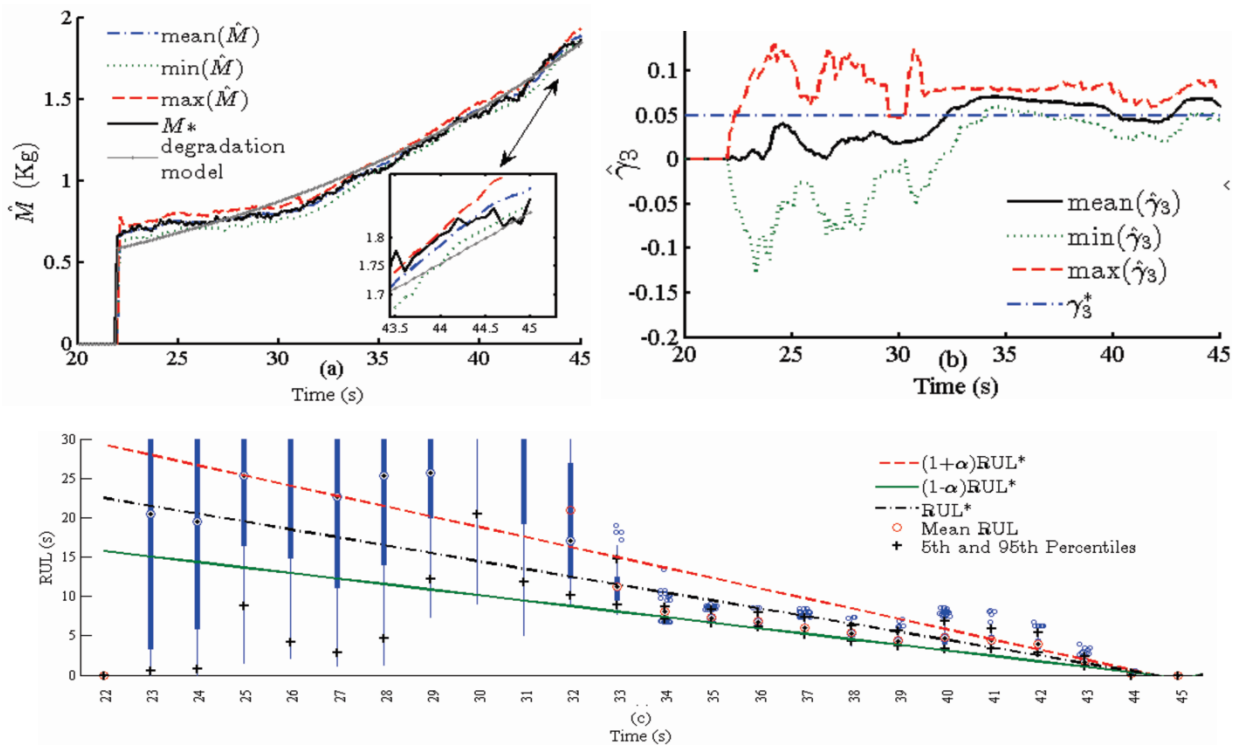


Fig. 3.24 (a) State estimation for Trail 1 (b) Estimation of DPP γ_3 (c) RUL prediction for case II

3.8 Conclusions and Contributions

It has been successfully demonstrated through simulation and experimental studies that the nominal part of Interval Valued Analytical Redundancy Relations (I-ARRs) derived from the Bond Graph (BG) model of the uncertain system can be used for detection of system parameter's degradation. Subsequent estimation of the state of health and associated degradation progression parameter(s), and prediction of the remaining useful life of the prognostic candidate can be obtained using particle filtering algorithms. This leads to an efficient integration of the benefits of BG modeling framework and Monte Carlo framework. The uncertain part of the I-ARRs is used for robust threshold generation over the nominal part. This enables efficient detection of the degradation commencement, robust to parametric uncertainty. Further, the same nominal residual can be used for obtaining the measurements of state variables in the fault model while the observation equation is developed from the nominal part of the I-ARR. For the latter, a novel algebraic approach is proposed so that the robust detection of degradation and further estimation of state variables of the fault model can be achieved using the same nominal residual in a unified framework. Being sensitive to the control inputs, nominal residual is able to capture the parametric degradation profile even while the system outputs remain in feedback closed loop regime. This makes the approach effective for system level health management. Approximation of the distribution of noise present in residuals can be difficult or impossible, due to presence of derivative or integral terms in the arguments. As such, employed Particle filter algorithms form the best choice in this regard, supporting non-Gaussian noises. The novel variance adaptation scheme leads to very good estimation results and involves less complexity in terms of tuning of the involved factors. In future, the latter will be developed further and exploited for similar purposes. Through simulations, this approach has the capability of generating long term and very long term predictions.

Through experiments, capability of obtaining RUL predictions in real time has been shown, although, in very short time window. The associated computational complexity prevents the long and very long-term RUL predictions in real time.

Various novel contributions of this work are as follows:

- Integration of BG modelling framework and Monte Carlo framework for estimation of state of health and prediction of RUL.
- Exploitation of nominal part of I-ARRs derived in (BG framework) for detection of degradation beginning and prognosis of incipient parametric degradation in Monte Carlo framework using PF.
- Obtaining the observation equation from the concerned nominal residual and construction of local fault model such that state of prognostic candidate and RUL prediction is achieved while system outputs are feedback controlled or otherwise.
- Proportional control type variance control algorithm with novel feedback condition that ensures a sustained convergence with low estimation variance (spread).

The work developed in this chapter has led to the development of following:

Jha, M.S., Dauphin-Tanguy,G., Ould-Bouamama,B., *Particle Filter Based Hybrid Prognostics for Health Monitoring of Uncertain Systems in Bond Graph Framework*, **in review process**, Mechanical systems and Signal Processing, Elsevier.

4. Hybrid Prognostics of Proton Exchange Membrane Fuel Cell

This chapter develops a holistic solution towards the prognostics of industrial Proton Exchange Membrane Fuel Cell (PEMFC). It involves the utilization of an efficient multi-energetic BG model suited for diagnostics and prognostics. The methodology of hybrid prognostics developed in Chapter 3 is applied over the PEMFC system. However, unlike Chapter 3 where an uncertain BG with interval valued uncertainties and interval thresholds is employed for robust detection of degradation; here, a BG-LFT model of the EE part is used for generation of robust adaptive thresholds. The issue of prognostics is addressed for the electrical-electrochemical (EE) part wherein, BG-LFT model of the latter is developed. Parametric uncertainty over global electrical resistance is considered. The benefits of Particle Filters (PF) is integrated with the BG-LFT model derived Analytical Redundancy Relations (ARRs). For the state equation, a statistical degradation model of the global resistance and limiting current is considered. The observation equation is obtained from ARRs. Using PF algorithms, estimation of state of health (SOH) is obtained along with the estimation of the associated hidden time-varying parameters that influence the degradation progression. This in turn is used for prediction of Remaining Useful Life (RUL) of the EE part of PEMFC, based on real degradation data sets, under constant and dynamic load current profile. The SOH estimation and RUL prediction is obtained with high accuracy and precise confidence bounds.

Various motivations propelling the development of this work are:

- There are very few existing model-based works that propose efficient prognostic solutions for PEMFC. (Wang, Y. et al., 2011) proposes physics based Degradation Model (DM) of the Electro-Chemical Active Surface Area (ECSA), used for damage tracking and prediction using Unscented Kalman Filter. ECSA being one of the several factors that influences the damage progression, efficient approaches are needed for a comprehensive study involving other factors. Only recently, (Jouin et al., 2014) proposed

a method employing statistical log-linear Degradation Model (DM) and PF for SOH estimation and RUL prediction. However, operation conditions are not considered and the DM lacks the insight into the physics of the phenomenon. (Chen, H. et al., 2015) proposed a rapid lifetime prediction formula to estimate the voltage drop rate. However, with only a linear DM employed, it required further investigation.

- The issue of PEMFC prognostics in BG framework has not even been touched. For instance, although (Saisset et al., 2006) and (Peraza et al., 2008) develop a detailed PEMFC BG model, they are not suited for diagnostics or prognostics. (Ouldbouamama et al., 2013) develops Signed BG model of PEMFC, but for diagnostics purposes only.

4.1 Description of a PEMFC

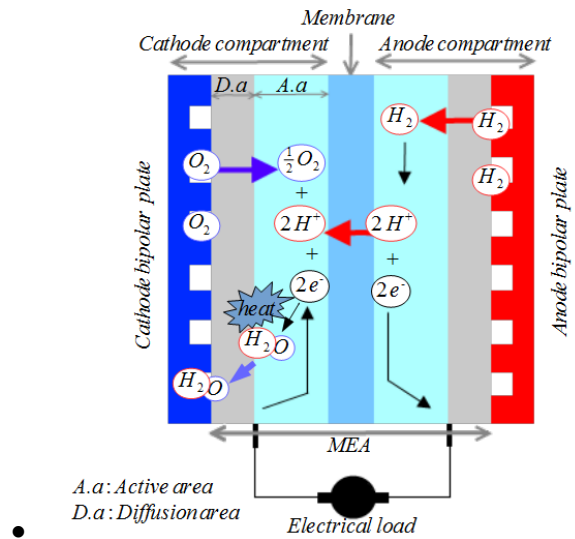
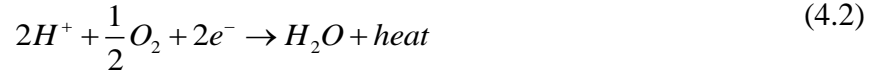


Fig. 4.1 Principle of operation of a PEMFC

A PEMFC (see Fig. 4.1) is an electrochemical converter which converts the chemical energy of hydrogen and oxygen into DC electricity that flows in an external electrical load. It is based on the reverse principle of electrolysis. At the anode, the hydrogen provided through the channels of the bipolar plates is diffused through the Gas Diffusion Layer (GDL) to the electrolyte, where the reaction occurs as,



The proton exchange membrane is designed to transport the H^+ ions to the cathode. The transfer of the other species is limited. The oxygen necessary for the exothermic reaction shown in (4.2), is brought to the reaction interface by the cathode compartment through the GDL.



Both of the reactions (c.f.(4.1),(4.2)) create a potential difference between the two electrodes (usually covered with platinum catalyst). This thermodynamic potential is a resultant of the Gibbs free energy ΔG , and is calculated based on the chemical affinity of the species as,

$$E = -\frac{\Delta G}{nF} \quad (4.3)$$

where, F is the Faraday number and n is the number of electron moles exchanged. This potential is corrected in temperature and pressure by the Nernst equation:

$$E = E_0 + \frac{RT}{2F} \ln \left(\frac{P_{H_2} \cdot P_{O_2}^{0.5}}{P_{H_2O}} \right) \quad (4.4)$$

This is the maximum theoretical potential that a PEMFC can reach. However, the kinetics of reaction generates an over-voltage named activation loss which is subtracted from the theoretical potential (c.f.(4.4)). Furthermore, the resistivity of the membrane electrode assembly (MEA) decreases the operational potential due to the Ohmic effect. The resistance value depends on the degree of humidification of the membrane and on the temperature. Finally, species are consumed and imply a loss of partial pressure on the reaction surfaces, thereby reducing the Nernst potential significantly, especially at high currents. This phenomenon is called diffusion / concentration losses.

These losses and the chemical reactions generate heat that must be evacuated by means of a cooling system. Moreover, during transients, one can observe an electron accumulation along the membrane electrode interface. It is the double layer capacitance effect. It is important to note that most of the phenomenon described above depends on one another (e.g. the over-potentials depend on the temperature, and the temperature depends on the heat created by the losses and also on the behavior of the cooling circuit).

4.2 Bond Graph Model of PEMFC

Bond Graph models of fuel cells have been developed in the past. Few of the significant works can be referred here: PEMFC related (Saisset et al., 2006),(Peraza et al., 2008); solid oxide fuel cell related : (Vijay et al., 2008, 2009). The extensively developed basic chemistry of PEMFC is omitted here and can be found in (Larminie et al., 2003). Instead, on the physical level, the BG model developed in derivative causality is presented in Fig. 4.2. The global system is decomposed into various subsystems where the input and output for each are the exchanged powers represented by two conjugated power variables: effort and flow (graphically shown by a half-arrow). As the initial conditions are not fully known in a real process, the derivative causality (suited for diagnostic and prognostic) is preferred.

4.2.1 Hydrogen Inlet

Source of hydrogen is represented by $Se : P_{H_2}$ where the corresponding pressure P_{H_2} , is a known quantity. The valve represented by a resistive BG element $R : Rh_n$ (where sub-script n denotes the nominal value) regulates the flow of hydrogen (measured by $SSf : F_{H_2}$). The pressure on the anode compartment is measured by the pressure sensor $SSe : P_{an}$. The hydraulic dynamics (storage of gases) is represented with the capacitive elements $C : C_{H_2}$ for anode. To transform the mass flow (kg/s) into a molar flow (mole/s), a transformer element $TF_{1/M}$ is used where M is the modulus representing the molar mass (kg/mole). Flow sensor $SSf : F_{H_2}$ measures the mass flow rate \dot{m}_{H_2} . Non-linear Bernoulli equation links the pressure across the valve P_{Rh} , and the flow \dot{m}_{H_2} through the valve, as:

$$P_{Rh} = R_{hn} (\dot{m}_{H_2})^2 \quad (4.5)$$

4.2.2 Oxygen Inlet.

In the similar fashion, $Sf : F_{O_2}$ represents the source of oxygen inlet flow, pressure sensor $SSe : P_{O_2}$ measures the pressure on the anode compartment, the hydraulic dynamics (storage of

gases) is represented by the capacitive BG elements $C : C_{O_2}$ for cathode, a transformer element

$TF_{(R,T,P_0)}$ transforms the mass flow(kg/s) into a molar flow (mole/s).

4.2.3 Chemical Part

The reduction-oxidation reaction (driven by the chemical affinity) is modeled using the Gibbs free energy ΔG in the 1_b junction as,

$$\Delta G = A_1 + A_2 - A_3 \quad (4.6)$$

$$A_1 = \mu_{H_2}, \quad A_2 = \frac{1}{2} \mu_{O_2}, \quad A_3 = \mu_{H_2O} \quad (4.7)$$

$$\mu_{H_2} = \mu_0^{H_2} + RT_{H_2} \ln(P_{H_2}) \quad (4.8)$$

$$\mu_{O_2} = \mu_0^{O_2} + RT_{O_2} \ln(P_{O_2}) \quad (4.9)$$

$$\mu_{H_2O} = \mu_0^{H_2O} \quad (4.10)$$

where R is the perfect gas constant, μ_x is the chemical potential of species x and the water is in liquid phase. The three transformer elements therein, $TF_{v_i}(i=1,2,3)$, have their respective modulus v_i , that represent the stoichiometric coefficients of the reactants ($v_1 = 1$ for hydrogen and $v_2 = 2$ for oxygen) and the product water with $v_3 = 1$.

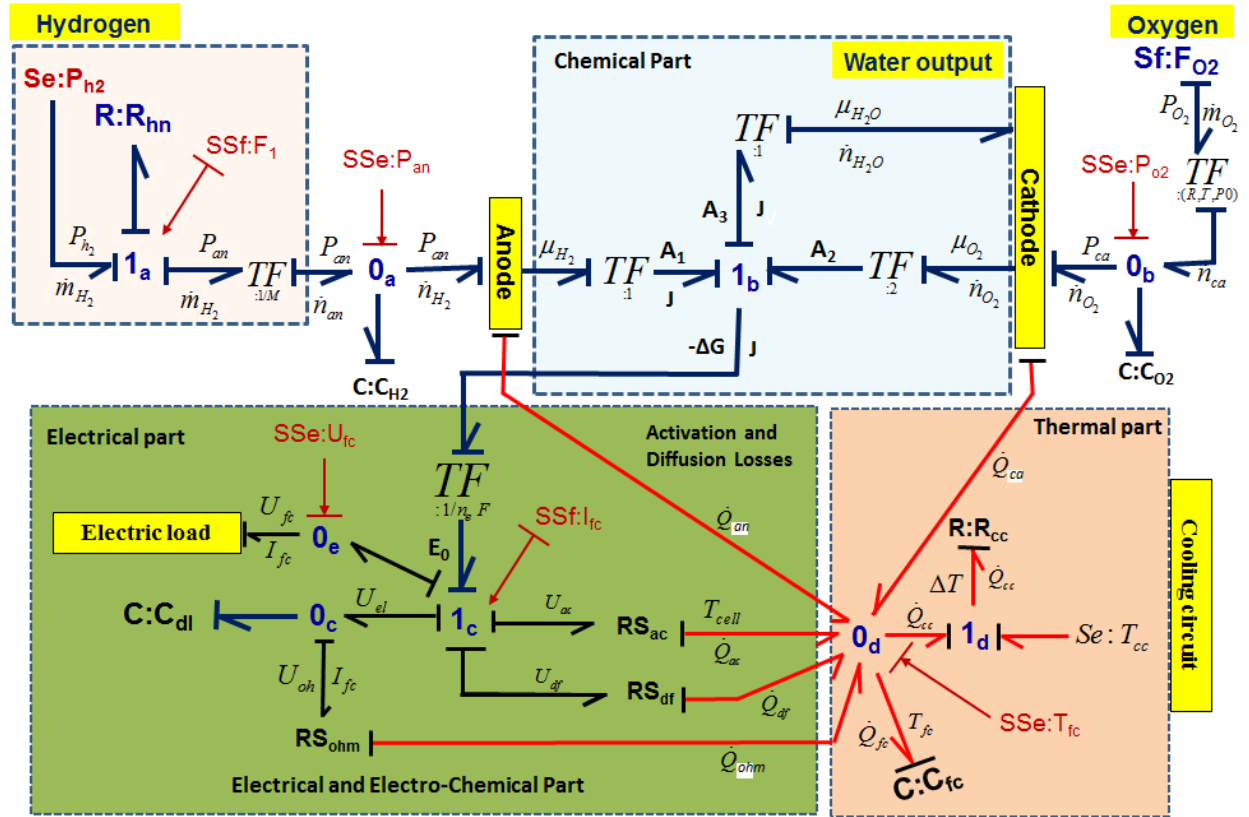


Fig. 4.2 Bond graph model of the PEMFC in preferred derivative causality

4.2.4 Electrical and Electro-Chemical (EE) Part

The EE subsystem accounts for electrical part and activation-diffusion losses. The kinetics of reaction shown in (4.6) generates an over-voltage named activation loss. Furthermore, the resistivity of the membrane electrode assembly decreases the operational potential due to the Ohmic effect. The resistance value depends on the degree of humidification of the membrane and on the temperature. Finally, consumption of species results in loss of partial pressure on the reaction surfaces, thereby reducing the Nernst potential significantly especially at high currents (Larminie et al., 2003). This phenomenon is called diffusion / concentration losses. Moreover, during transients, electron accumulation along the membrane electrode interface is observable. It is the double layer capacitance effect. Here, the EE subsystem and the chemical part are connected using the transformer $TF_{:1/n_e F}$. This results in obtaining the thermodynamic potential E_0 as,

$$E_0 = -\frac{\Delta G}{n_e F} = -\frac{A_1 + A_2 - A_3}{n_e F} \quad (4.11)$$

where n_e is the number of electron involved in the reaction and F is the number of Faraday. RS is an active two port dissipative (resistive) element that generates thermal energy. The two port thermal dissipative element RS_{ohm} models the Ohmic losses (membrane, electrodes and connectors). Similarly, the activation and the diffusion phenomenon are modeled by RS_{ac} and RS_{df} respectively. The associated power variables are related as,

$$U_{ac} = AT \ln\left(\frac{I_{fc}}{I_0}\right) \quad (4.12)$$

$$U_{df} = BT \ln\left(1 - \frac{I_{fc}}{I_L}\right) \quad (4.13)$$

where, A is the activation constant; $A = R / \chi nF$ and B is the diffusion constant; $B = -R / \chi nF$ with χ as the transfer coefficient, I_0 is the exchanged current, I_{fc} is the load current and I_L is the limiting current i.e. maximal current the fuel cell is able to provide. The double layer capacitance phenomenon is modeled by a capacitor element $C : C_{dl}$ and imposes the dynamics of the activation phenomena. U_{dl} is expressed at the junction $\mathbf{0}_C$, as the solution of the equation:

$$I_{fc} = \frac{U_{el}}{R_{ohm}} + C_{dl} \frac{dU_{el}}{dt} \quad (4.14)$$

where, R_{ohm} is the global resistance (membrane and connectors).

4.2.5 Thermal Part

The active elements and the chemical reaction being exothermic, generate heat that needs to be evacuated by means of a cooling system. The thermal resistance of the PEMFC and cooling circuit is modeled by the passive resistive element $R : R_{cc}$ (representing the thermal resistance). The thermal dynamics is fixed by the thermal capacitance $C : C_{fc}$ which depends on the fuel cell temperature (measured by the temperature sensor $SSe : T_{fc}$) and the ambient temperature is represented by an effort source $Se : T_{cc}$. The various power variables are related as,

$$\dot{Q}_{ca} = \Delta S_{H_2O} \dot{n}_{H_2O} - \Delta S_{O_2} \dot{n}_{O_2} \quad (4.15) \quad \dot{Q}_{cc} = R_{cc} (T_{fc} - T_{cc}) \quad (4.19)$$

$$\dot{Q}_{an} = -\Delta S_{H_2} \dot{n}_{H_2} \quad (4.16) \quad \dot{Q}_{df} = (R_{df})^2 I_{fc} \quad (4.20)$$

$$\dot{Q}_{ohm} = R_{ohm} U_{fc} \quad (4.17) \quad \dot{Q}_{ac} = (R_{ac})^2 I_{fc} \quad (4.21)$$

$$\dot{Q}_{fc} = C \frac{dT_{cc}}{dt}$$

where \dot{n}_x is the molar flow and $\Delta S_x = \Delta S_{x_0} + \int_{298}^T \frac{C_p}{\theta} d\theta$ is the flow of entropy of the specie x .

4.3 Generation of Deterministic ARR and Robust Thresholds

The deterministic ARRs are derived through energetic assessment at the junctions of BG model in preferred derivative causality of Fig. 4.2, as demonstrated for DC motor model in Section 1.4.3.2. The BG-LFT model of the system or the concerned EE subsystem can be used to derive ARRs in presence of additive or multiplicative uncertainties, which are decoupled into nominal and uncertain parts as discussed in Appendix B.

4.3.1 Derivation of Deterministic ARRs of PMFC

In Fig. 4.2, from the junction $\mathbf{1}_a$ (associated with flow sensor $SSf : F_{H_2}$), the ARR candidate is deduced from the conservative law equation, sum of efforts is equal to zero :

$$ARR_1 : P_{H_2} - P_{an} - P_{Rh} = 0 \quad (4.22)$$

Based on covering causal paths, using (4.5) and known variables, $P_{H_2} = Se : P_{H_2}$, $P_{an} = SSe : P_{an}$ and $\dot{m}_{H_2} = SSf : F_{H_2}$, (4.22) is expressed as,

$$ARR_1 = SSe : P_{H_2} - SSe : P_{an} + R_{hm} (F_{H_2})^2 \quad (4.23)$$

This ARR can be used to monitor the flooding (such as valve blockage) in the channels of the PEMFC which does not form the interest here. The second ARR is deduced from junction $\mathbf{1}_c$:

$$ARR_2 : n_s (E_0 - U_{ac} - U_{df} - U_{el}) - U_{fc} = 0 \quad (4.24)$$

where n_s is number of cells in a stack . Obviously here, $n_s=1$. From (4.8)-(4.13) and(4.14), the unknown variables can be eliminated using causal paths and known electro-chemical relations such that, ARR_2 is expressed as,

$$ARR_2 = n_s \left(\begin{array}{l} \mu_0^{H_2} + RT_{H_2} \ln(P_{H_2}) + \frac{1}{2} [\mu_0^{O_2} + RT_{O_2} \ln(P_{O_2})] - \mu_0^{H_2O} \\ - R_{ohm} I_{fc} - AT \ln\left(\frac{I_{fc}}{I_0}\right) - BT \ln\left(1 - \frac{I_{fc}}{I_l}\right) \end{array} \right) - SSe : U_{fc} \quad (4.25)$$

Note that due to fast electrical dynamics (4.14) has been approximated as (De Bruijn et al., 2008),

$$U_{el} = R_{ohm} \cdot I_{fc} \quad (4.26)$$

ARR_2 is sensitive to drying, flooding and to aging of the fuel cell and attracts the main focus of the work developed here. The third ARR is derived from junction $\mathbf{0}_d$ in the thermal field:

$$ARR_3 : \dot{Q}_{ac} + \dot{Q}_{df} + \dot{Q}_{an} + \dot{Q}_{ca} + \dot{Q}_{ohm} - \dot{Q}_{cc} - \dot{Q}_{fc} = 0 \quad (4.27)$$

From(4.15)-(4.21), the unknown variables are eliminated to express (4.27) as,

$$ARR_3 = (R_{ac})^2 I_{fc} + (R_{df})^2 I_{fc} - R_{cc} (T_{fc} - T_{cc}) - C \frac{dT_{cc}}{dt} + R_{ohm} U_{fc} - \Delta S_{H_2} \dot{n}_{H_2} + \Delta S_{H_2O} \dot{n}_{H_2O} - \Delta S_{O_2} \dot{n}_{O_2} \quad (4.28)$$

This ARR can be used to monitor a fault in the cooling system, which is out of the scope of this work.

4.3.2 Generation of Robust Adaptive Thresholds

As the interest of this work does not lie in diagnosis of PEMFC *per se*, BG-LFT model of PEMFC is not developed here. Instead, for robust detection of degradation, BG-LFT model of EE subsystem is formed. The latter is investigated for prognostic purposes where the robust thresholds are exploited for detection of degradation beginning (see Section 4.5.2). Consider BG-LFT model of EE subsystem wherein, the resistance element $R : Rh_{ohm}$ is considered uncertain as shown in (4.29), with multiplicative uncertainty $\delta_{Rh_{ohm}}$ related to additive uncertainty ΔRh as shown in (4.30).

$$Rh_{ohm} = Rh_{ohm,n} (1 + \delta_{Rh_{ohm}}) \quad (4.29)$$

$$\delta_{Rh_n} = \pm \Delta Rh / Rh_n \quad (4.30)$$

Consider ARR_2 (c.f.(4.25)) derived from energetic interaction present in the electrochemical subsystem, ARR_2 can be decoupled into nominal part $r_{2,n}(t)$ and uncertain part $r_{2,unc}$ as,

$$\begin{aligned} ARR_2 &= r_{2,n}(t) + r_{2,unc}(t) \\ &= n_s \underbrace{\left(E_0 - (R_{ohm,n}) I_{fc} - AT \ln \left(\frac{I_{fc}}{I_0} \right) - BT \ln \left(1 - \frac{I_{fc}}{I_l} \right) \right)}_{r_{2,n}(t)} - \underbrace{SSe : U_{fc} - n_s \left(\delta_{Rh_{ohm}} Rh_{ohm,n} I_{fc} \right)}_{r_{2,unc}(t)} \end{aligned} \quad (4.31)$$

The uncertain part is used to form the thresholds as,

$$-a < r_{2,n}(t) < a \quad (4.32)$$

$$a = |w_{R_{ohm}}| = n_s \left| \delta_{Rh_{ohm}} Rh_{ohm,n} I_{fc} \right| \quad (4.33)$$

The passive BG-LFT robust fault detection technique is employed to detect the beginning of degradation of the isolated faulty component. Once the degradation is detected, the estimators are triggered which produce the current state of health and RUL prediction. The associated pseudo algorithm is given in Table 4-I.

Table 4-I Detection of Degradation

Algorithm 1: Detection of Degradation

Input: $r_n^d(k), \sum |w_i(t)|$

Output: *degradation detection*

if $r^i(k) \geq -\sum |w_i(t)|$ **and** $r^i(k) \leq \sum |w_i(t)|$

degradation detection \leftarrow **false**

else

degradation detection \leftarrow **true**

end if

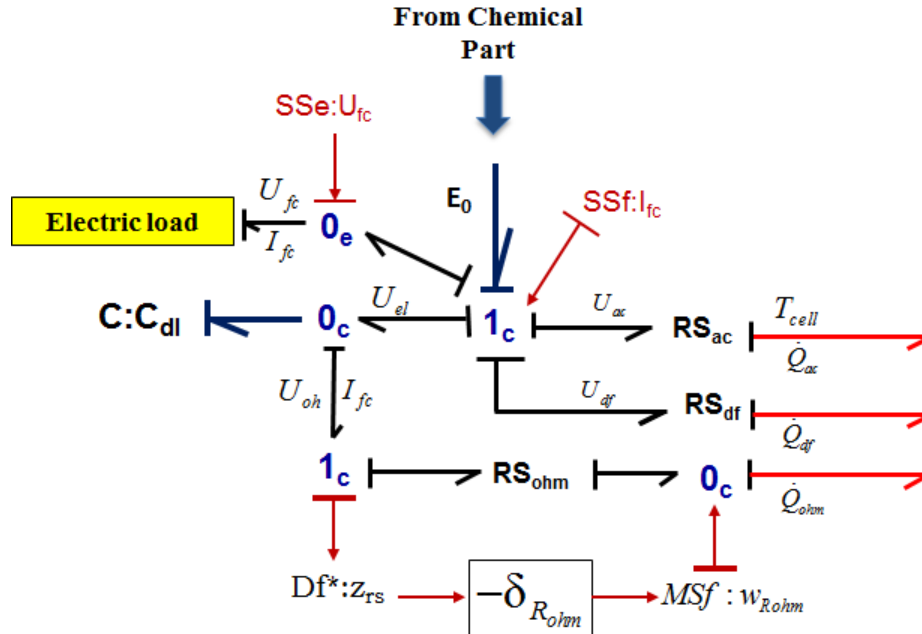


Fig. 4.3. BG-LFT model of Electrical-Electrochemical subsystem

4.4 Experimental Setup

Degradation tests are carried out on a 10kW test bench as shown in Fig. 4.4, that regulates the temperature (by means of a cooling system (c)), the moisture content (through boilers (b)), the anode and cathode pressures (through the air and hydrogen supplies (a)), the electrical load (d) and the test bench adjusts the gas flow rates accordingly. The stack voltages are recorded continuously (through the acquisition unit (e)) during the test with a one-hour sampling period.

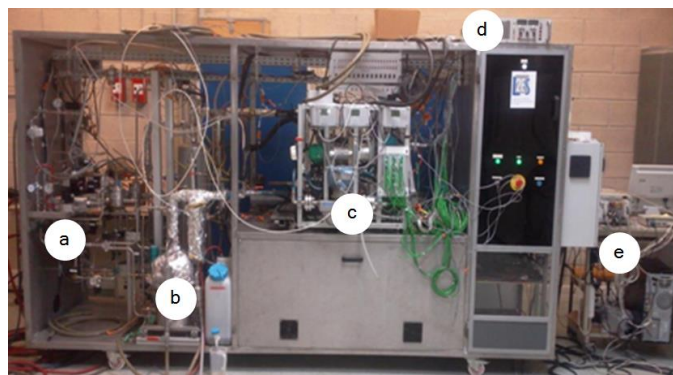


Fig. 4.4. 10kW in-lab test bench, (a) air and hydrogen supplies, (b) humidifiers, (c) cooling system (the PEMFC is located behind), (d) electrical load, (e) control and acquisition unit.

4.4.1 Degradation Tests

Two kinds of degradation tests were performed:

- **Constant Load Test** (referred to as FC1): This test is done for about 800 hours, on a commercially available stack of 5 cells, surface of 100 cm² and a nominal current I_{nom} of 70A. This corresponds to the fuel cell one (FC1).
- **Variable Load Test** (referred to as FC2): This test is done on a 8-cells stack PMFC with a surface of 220 cm², provided by the French Atomic Energy and Alternative Energy Commission (CEA). It is subjected to a μ -CHP profile (Combined Heat and Power) for a period of 900 hours. This profile is designed to simulate the energy consumption of a building along a year and follows the seasons:

Winter: I_{max} for about 250 hours.

Spring: 7 cycles of 24 hours between I_{nom} and $I_{nom} / 2$, followed by $I_{nom} / 2$ until 500 hours.

Summer: $I_{nom} / 2$ for 100 hours, followed by 9 cycles of 24 hours between $I_{nom} / 2$ and null power demand until t=800 hours.

Autumn: $I_{nom} / 2$ until the end of the test.

The operating conditions of these two PEMFC are summarized in Table 4-II.

Table 4-II Operating conditions

Parameter	FC1	FC2
Number of cells, n_s	5	8
Surface	100 cm ²	220 cm ²
Temperature, T	60°C	80°C
Anode and cathode stoichiometry ratios	1.5-2	1.5-2
Absolute pressure anode/cathode, P_{H_2} & P_{O_2}	1.5 bar	1.5 bar
Relative humidity anode/cathode	50 %	50%
Nominal current, I_{nom}	70 A	100 A
Maximal current I_{max}	140 A	170 A

4.4.2 Degradation Model

Periodically throughout the life of the fuel cell, the static response is measured with a polarization curve (voltage as a function of the current) as shown in (4.34). Note that ARR_2 derived in (4.25) is nothing but the polarization curve of (4.34), such that voltage sensor U_{fc} therein, is dualized as $SSe : U_{fc}$ to derive the ARR_2 of (4.25). Thus, ARR_2 expression is used to obtain the polarization curve as,

$$U_{fc} = n_s \left(E_0 - R_{ohm} I_{fc} - AT \ln \left(\frac{I_{fc}}{I_0} \right) - BT \ln \left(1 - \frac{I_{fc}}{I_L} \right) \right) \quad (4.34)$$

For each characterization time, a Levenberg-Marquardt method is used to extract the parameters of (4.34). The algorithm is initiated with a set of parameters whose values are chosen from the literature (Laffly et al., 2007; Larminie et al., 2003). The algorithm extracts: the Open Circuit Voltage (OCV) E_0 at nominal pressure and temperature, the global resistance R_{ohm} (membranes, connectors, end plates, etc.), the exchange current I_0 and the limiting current I_L .

4.4.2.1 Constant Load Tests (FC1)

With nominal current of 70 A, the recorded stack voltage U_{fc} (at sampling period of one Hour) is shown in Fig. 4.5.

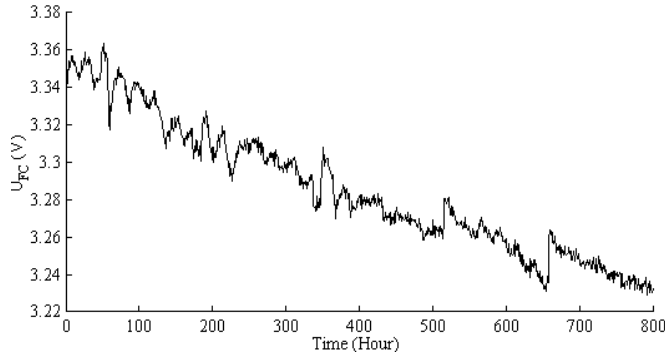


Fig. 4.5 Recorded voltage for FC1

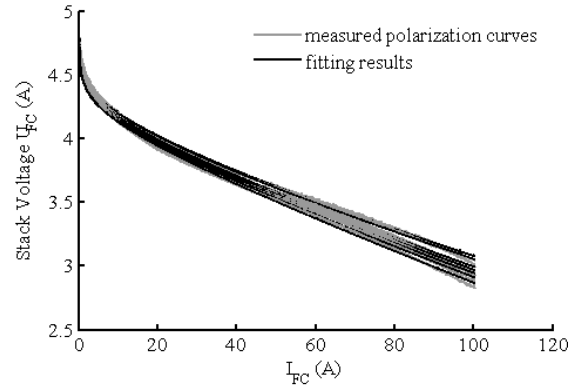


Fig. 4.6 Polarization Curve and fitting result during ageing for FC1

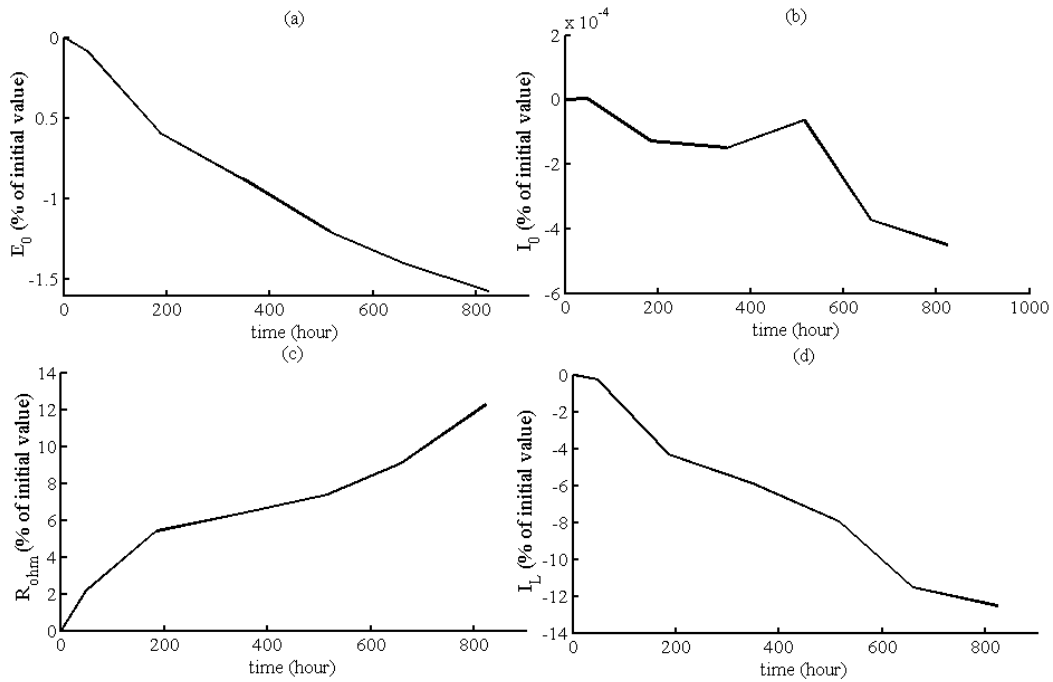


Fig. 4.7 Deviation of the parameters values (%) during aging (FC1)

The resulting model fitting of the measured polarization curves (during aging) is shown in Fig. 4.6. Fig. 4.7 shows the evolution of the parameter value with respect to the initial one (in

percentage). From the four chosen parameters, only two show significant deviations: the overall resistance R_{ohm} increases by more than 12% while the limit current I_L decreases by 13%.

4.4.2.2 Variable Load (FC2)

The current load profile and corresponding recorded voltage for FC2 is shown in Fig. 4.8. and the corresponding polarization curve is shown in Fig. 4.9.

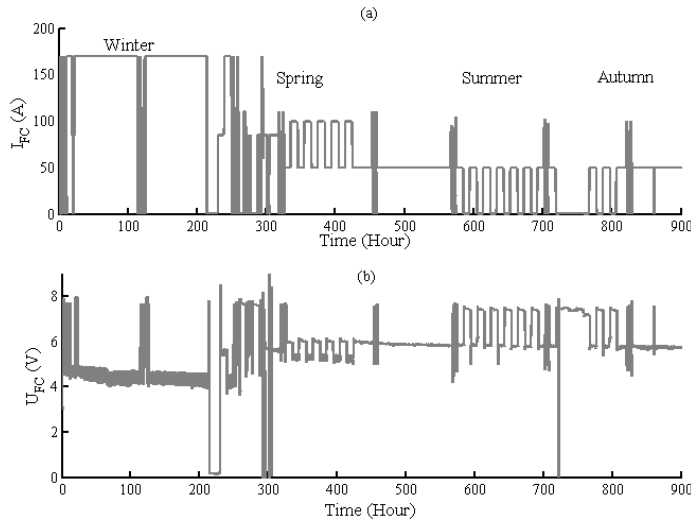


Fig. 4.8 Recorded profile for FC2 (a) Current (Load) Profile (b) Recorded Voltage

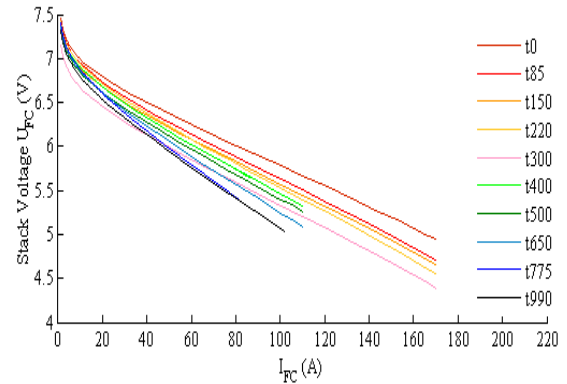


Fig. 4.9 Polarization curves during aging for FC2

The evolution of extracted parameters is shown in Fig. 4.10. Significant deviations are visible in the overall resistance R_{ohm} that increases by more than 70% and the limit current I_L that decreases by 60%.

As observed for FC1 and FC2, only two parameters R_{ohm} and I_L show significant degradations (deviation). Change in R_{ohm} is mainly due to degradation/dehydration of the polymer membrane and the corrosion of the carbon support for the resistance (Fowler et al., 2002). The limit current decreases due to the ripening of the catalyst particles, an insufficient evacuation of the water (due to changes in the surface) and the compression of the GDL .

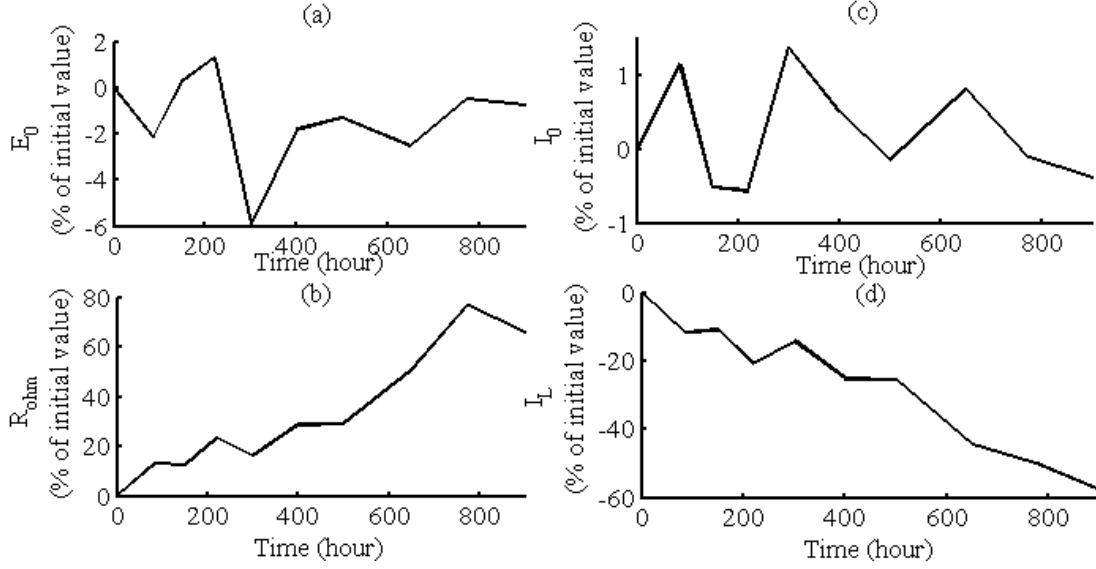


Fig. 4.10 Derivation of the parameters values (%) during aging (FC2)

There is no significant evolution in the value of the OCV and the exchange current I_0 , compared to the other parameters. Thus, the former parameters are considered constant in this paper.

For a given operating condition, since only the stack voltage is measured, it is impossible to separate the mutual coupling of global resistance and limiting current i.e. the loss due to both are not observable simultaneously. Moreover, although not perfectly, both R_{ohm} and I_L seem to evolve in an approximate linear manner. Therefore, the variations in the latter are parametrized with a single parameter α , a State of Health (SOH) indicator. The variation is expressed with as linear equation (since the parameters value seems to follow a linear relation). Thus, the model of degradation is expressed as,

$$R_{ohm}(t) = R_{ohm,n} (1 + \alpha(t)) \quad (4.35)$$

$$I_L(t) = I_{L,n} (1 - \alpha(t)) \quad (4.36)$$

$$\alpha(t) = \beta \times t \quad (4.37)$$

where β explains the approximately constant rate-change of α and sub-script n denotes the nominal value. Very recently, the similar approach is followed for construction of state equation in (Bressel et al., 2015), and has led to satisfactory results.

4.5 Prognostics of the Electrical-Electrochemical Part

Here, the particle filter based hybrid prognostics methodology developed in Chapter 0 is adapted for the prognostics of the EE part of the PEMFC.

As shown in Fig. 4.11, the basic architecture of the methodology in this work, remains similar to the one in Chapter 0 (see Fig. 3.2). However, unlike Chapter 3 where an uncertain BG with interval valued uncertainties and interval thresholds is employed for robust detection of degradation; here, a BG-LFT model of the EE part is used for generation of robust adaptive thresholds. Also, the observation equation needed for construction of the fault model is extracted from the nominal part of the BG-LFT derived ARR.

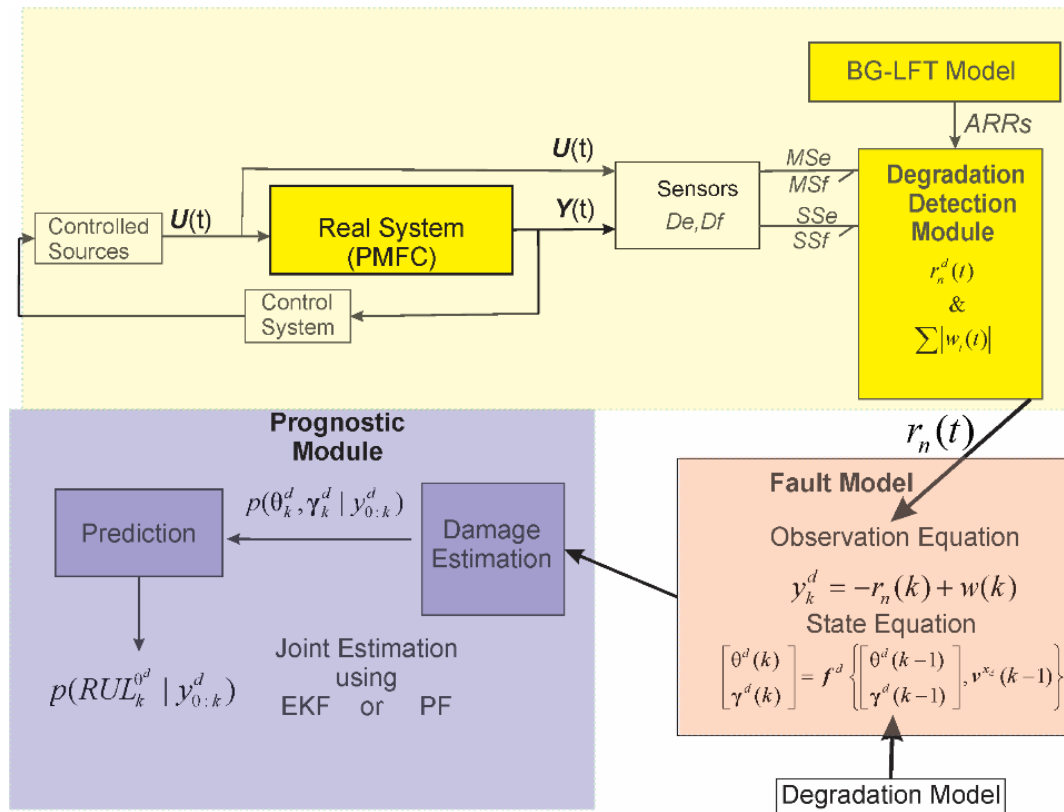


Fig. 4.11 Schematic of the Prognostic Methodology for PEMFC

4.5.1 Fault Model

Considering the fault model construction introduced in Chapter 0, (see Section 3.3.2), the same approach is followed to estimate the SOH indicated by $\alpha(t)$, which is chosen to assess the

parameter evolution, and make RUL predictions. State equation is formed such that $\alpha(t)$ becomes the chosen state parameter $\theta^d(t)$ undergoing degradation, and $\beta(t)$ is the associated *degradation progression parameter* γ^d modelled as a random walk process. As discussed in Chapter 0 (see section 3.3.2), state equation is formed as,

$$\alpha_k = \alpha_{k-1} + \beta_{k-1} \times \Delta t + v_{k-1} \quad (4.38)$$

$$\beta_k = \beta_{k-1} + \xi_{k-1} \quad (4.39)$$

where, $v_k \sim \mathcal{N}(0, \sigma_v^2)$ is the associated process noise $\xi_k \sim \mathcal{N}(0, \sigma_\xi^2)$ is a random walk noise and Δt is the sample time.

4.5.1.1 Observation Equation

The observation equation is obtained from the nominal part $r_n^d(t)$ of the ARR derived from the BG-LFT model that is sensitive to the prognostic candidate $\theta^d(t)$. The objective rests in exploitation of same ARR for estimation of (θ^d, γ^d) , apart from its usage for robust detection of degradation beginning. To achieve the same, following is proposed.

Proposition 4.1: Under the single degradation hypothesis, assuming that the nominal part $r_n^d(t)$ of an ARR derived from the BG-LFT model, can be expressed as a linear combination of non-linear functions of prognostic candidate parameter $\theta^d(t)$, the measurement of the $\theta^d(t)$ can be obtained from $r_n^d(t)$.

Proof: Let $\theta^d(t)$ be the prognostic candidate and $\theta' = \theta \setminus \theta^d(t)$. Assuming the nominal part $r_n^d(t)$ can be expressed as,

$$r_n^d(t) = \Xi \left(\theta'_n, \mathbf{S}\mathbf{S}\mathbf{e}(t), \mathbf{S}\mathbf{S}\mathbf{f}(t), \mathbf{S}\mathbf{e}(t), \mathbf{S}\mathbf{f}(t) \right) + \mathbf{A}^T \boldsymbol{\varphi}(\theta_n^d) \quad (4.40)$$

where $\forall i \mid i = 1, 2 \dots m$, $\mathbf{A}^{m \times 1} = [a_1 \ a_2 \dots a_m]^T$ is a vector of known (measured system variables) with $a_i = \phi_i(\theta'_n, \mathbf{S}\mathbf{S}\mathbf{e}(t), \mathbf{S}\mathbf{S}\mathbf{f}(t), \mathbf{S}\mathbf{e}(t), \mathbf{S}\mathbf{f}(t))$ and $\boldsymbol{\varphi}^{m \times 1}(\theta^d(t)) = [\varphi_1(\theta^d(t)), \varphi_2(\theta^d(t)), \dots, \varphi_m(\theta^d(t))]^T$ is the vector of non-linear functions of $\theta^d(t)$. Then, $\forall t \geq 0$ power conservation at the BG *junction* where the corresponding ARR is derived leads to,

$$ARR : r^d(t) = \Xi \left(\theta'_n, SSe(t), SSf(t), Se(t), Sf(t) \right) + A^T \boldsymbol{\varphi}(\theta^d(t)) = 0 \quad (4.41)$$

or,

$$\begin{aligned} r^d(t) &= \Xi \left(\theta'_n, SSe(t), SSf(t), \sum Se, \sum Sf, \right) + A^T \boldsymbol{\varphi}(\theta_n^d) + \left(A^T \boldsymbol{\varphi}(\theta^d(t)) - A^T \boldsymbol{\varphi}(\theta_n^d) \right) = 0 \\ r^d(t) &= r_n^d(t) + A^T \left(\boldsymbol{\varphi}(\theta^d(t)) - \boldsymbol{\varphi}(\theta_n^d) \right) = 0 \\ -A^T \left(\boldsymbol{\varphi}(\theta^d(t)) - \boldsymbol{\varphi}(\theta_n^d) \right) &= r_n^d(t) \end{aligned} \quad (4.42)$$

Thus, degradation state $\theta^d(t)$ can be linked implicitly to the measurements of $r_n^d(t)$.

Observation equation can be formed as,

$$y^d(t) = r_n^d(t) = -A^T \left(\boldsymbol{\varphi}(\theta^d(t)) - \boldsymbol{\varphi}(\theta_n^d) \right) \quad (4.43)$$

In this work, the noise is considered additive, *independent and identically distributed* (i.i.d.) drawn from a zero mean normal distribution and is assumed uncorrelated to $\mathbf{x}^d(t)$. Thus from (3.14), observation equation is formed as,

$$y^d(t) = h^d \left(\mathbf{x}^d(t) \right) + w^d(t) \quad (4.44)$$

where $h^d(\cdot)$ is a nonlinear observation function obtained from (3.14) and $w^d(t) \sim \mathcal{N}(0, \sigma_{w^d}^2)$. The standard deviation σ_{w^d} , is approximated from residual measurements during degradation tests.

□

Applying the **Proposition 4.1** in the context of uncertain EE part, the measurement of the state health can be obtained implicitly from ARR_2 , which is derived from the energetic interaction found in electro-chemical subsystem (see(4.24),(4.25)). With R_{ohm} and I_L under degradation, ARR_2 can be expressed as,

$$ARR_2 : r_2(t) = n_s \left(E_0 - \left(R_{ohm,n} (1 + \alpha(t)) \right) I_{fc} - AT \ln \left(\frac{I_{fc}}{I_0} \right) - BT \ln \left(1 - \frac{I_{fc}}{I_{L,n} (1 - \alpha(t))} \right) \right) - SSe : U_{fc} \quad (4.45)$$

$$\begin{aligned}
r_2(t) &= n_s \left(E_0 - (R_{ohm,n}) I_{fc} - AT \ln \left(\frac{I_{fc}}{I_0} \right) - BT \ln \left(1 - \frac{I_{fc}}{I_{L,n}} \right) \right) - SSe : U_{fc} \\
&+ n_s \left(-R_{ohm,n} \alpha(t) I_{fc} - BT \ln \left(1 - \frac{I_{fc}}{I_{L,n} (1 - \alpha(t))} \right) + BT \ln \left(1 - \frac{I_{fc}}{I_{L,n}} \right) \right) \\
&= r_{2,n}(t) + n_s \left(-R_{ohm,n} \alpha(t) I_{fc} - BT \ln \left(1 - \frac{I_{fc}}{I_{L,n} (1 - \alpha(t))} \right) + BT \ln \left(1 - \frac{I_{fc}}{I_{L,n}} \right) \right)
\end{aligned} \tag{4.46}$$

$\forall t > 0$, power conservation in ARR dictates,

$$r_{2,n}(t) + n_s \left(-R_{ohm,n} \alpha(t) I_{fc} - BT \ln \left(1 - \frac{I_{fc}}{I_{L,n} (1 - \alpha(t))} \right) + BT \ln \left(1 - \frac{I_{fc}}{I_{L,n}} \right) \right) = 0 \tag{4.47}$$

Thus, measurement of $\alpha(t)$ is acquired from $r_{2,n}(t)$. In discrete time k , observation equation is,

$$y^d(k) = r_{2,n}(k) = n_s \left(R_{ohm,n} \alpha_k I_{fc} + BT \ln \left(1 - \frac{I_{fc}}{I_{L,n} (1 - \alpha_k)} \right) - BT \ln \left(1 - \frac{I_{fc}}{I_{L,n}} \right) \right) + w_k^d \tag{4.48}$$

where $w_k^d \sim \mathcal{N}(0, \sigma_{w^d}^2)$ models the noise associated with measurement acquisition and is approximated as Gaussian in nature. σ_{w^d} is approximated from residual measurements during degradation tests.

4.5.2 State of Health Estimation and RUL Prediction

The prognostic approach described in Chapter 0 (see Section 3.3.3) is followed to estimate the SOH. Parameters in PF are set so as to obtain the best possible estimation of $\alpha(t)$, $\beta(t)$ with least possible error in measurement estimation $RMSE_{y^d}$, so that obtained estimations of $\alpha(t)$ and $\beta(t)$ are suitable for a viable RUL prediction. The pseudo-algorithm is given in Table 4-III. As it is clear from the pseudoalgorithm, there is no employment of variance adaptation scheme for the estimation of SOH in this work.

The RUL prediction technique detailed in Chapter 0 (see Section 3.3.4) is used here to make the RUL prediction with respect to the evolving estimate of $\alpha(t)$. The pseudo-algorithm is given in Table 4-IV.

Table 4-III Estimation using SIR filter

Algorithm 2: Estimation using SIR filter

Inputs: $\{(\alpha_{k-1}^i, \beta_{k-1}^i), w_{k-1}^i\}_{i=1}^N, y_k^d$

Output: $\{(\alpha_k^i, \beta_k^i), w_k^i\}_{i=1}^N$

for $i=1$ **to** N **do**

$\beta_k^i \sim p(\beta_k^i | \beta_{k-1}^i)$

$w_k^i \sim p(y_k^d | \alpha_k^i, \beta_k^i)$

end for

$W \leftarrow \sum_{i=1}^N w_k^i$

for $i=1$ **to** N **do**

$w_k^i \leftarrow w_k^i / W$

end for

$\{(\alpha_k^i, \beta_k^i), w_k^i\}_{i=1}^N \leftarrow \text{RESAMPLE} \{(\alpha_{k-1}^i, \beta_{k-1}^i), w_{k-1}^i\}_{i=1}^N$

Table 4-IV RUL Prediction using PF

Algorithm 3: RUL Prediction using PF

Inputs: $\{(\alpha_k^i, \beta_k^i), w_k^i\}_{i=1}^N$

Variable: l

Outputs: $\{RUL_k^{\alpha^i}, w_k^i\}_{i=1}^N$

for $i=1$ **to** N **do**

$l=0$

while $\alpha_{k+l}^i \leq \alpha_{fail}$ **do**

$\beta_{k+1}^i \sim p(\beta_{k+1}^i | \beta_k^i)$

$\alpha_{k+1}^i \sim p(\alpha_{k+1}^i | \alpha_k^i, \beta_{k+1}^i)$

$l \leftarrow l + 1$

end while

$RUL_k^{\alpha^i} \leftarrow l$

end for

4.5.2.1 Constant Load (FC1)

Motivated from Fig. 4.7, $\alpha_{fail} = 0.12$ signifies end of life of FC1 at 12% deviation on initial value. Moreover, the true value of α , α_{true} is considered to evolve in a perfect linear way with true value of slope β , $\beta_{true} = 1.3 \times 10^{-4}$ so that, α_{fail} is reached at 900 hours. Also, the value of the measurement noise variance $\sigma_{w^d}^2$ is obtained from square of the standard deviation of the nominal residual $r_{2,n}$ recorded during degradation tests, as $\sigma_{w^d}^2 = 10^{-6}$.

Estimation performance by PF as shown in Fig. 4.12, is realized with $N=2000$ particles. The measurement noise variance in PF is set as 100 times that of residual measurement variance $\sigma_{w^d}^2$. This is done to ensure a good estimation of the noisy measurement throughout. The initial

random walk noise variance is set as, $\sigma_{\xi}^2 = 10^{-10}$ for a quick convergence. A good value for process noise variance is found through successive tuning as $\sigma_v^2 = 10^{-6}$.

As shown in Fig. 4.12. (c), degradation is detected at $t=58$ hours by thresholds triggering the prognostic module. The thresholds a and $-a$, are sensitive to 2% uncertainty over nominal Rh_{ohm} i.e. $\delta_{Rh_{ohm}} = \pm 2\% Rh_{ohm}$ and the constant I_{fc} (see (4.33)). The measurement signal $r_{2,n}(t)$ is estimated with $RMSE_{r_{2,n}} = 4.2\%$ such that local non-linearity therein, is estimated very accurately. Fig. 4.12 (a) shows the estimation of approximately linear α with $RMSE_{\alpha} = 23.56\%$. Approximately constant β is estimated accurately with $RMSE_{\beta} = 9.3\%$.

Fig. 4.13 shows the box plot of RUL prediction obtained at time interval of 25 hours (for the sake of clarity). For all the time points, prediction performance is assessed by α - λ metric (see Section 3.5) with $\alpha=0.4$ and $\beta=0.4$ (not to be confused with SOH indicator $\alpha(t)$). The latter implies the requirement of 40% of RUL probability mass containment within 40% of true RUL value.

Percentage of probability mass falling within the accuracy cone is indicated against each box plot. Starting from $t=200$ hours, almost all the predictions are *true* (acceptable), except the ones at the last four prediction-points. The latter arise mainly because of characterizations performed at $t=800$ hours; as such, an insufficient recovery-effect occurs on the stack voltage while the latter is being recorded.

Over all, starting from $t= 350$ hours, the prediction performance is very good with $\overline{RA} = 96.07\%$.

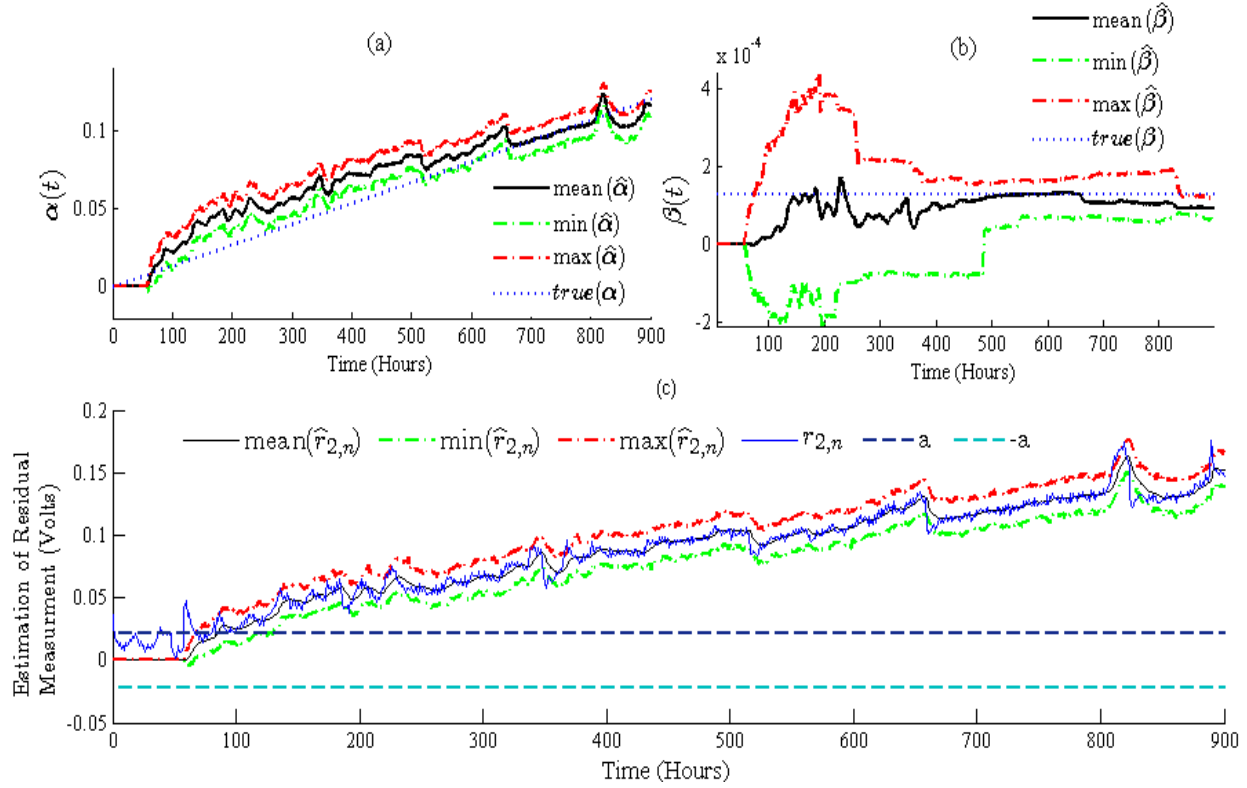


Fig. 4.12 Estimation performance in PF for FC1 (a). Estimation of α (b) Estimation of β (c) Measurement via. residual and its estimation

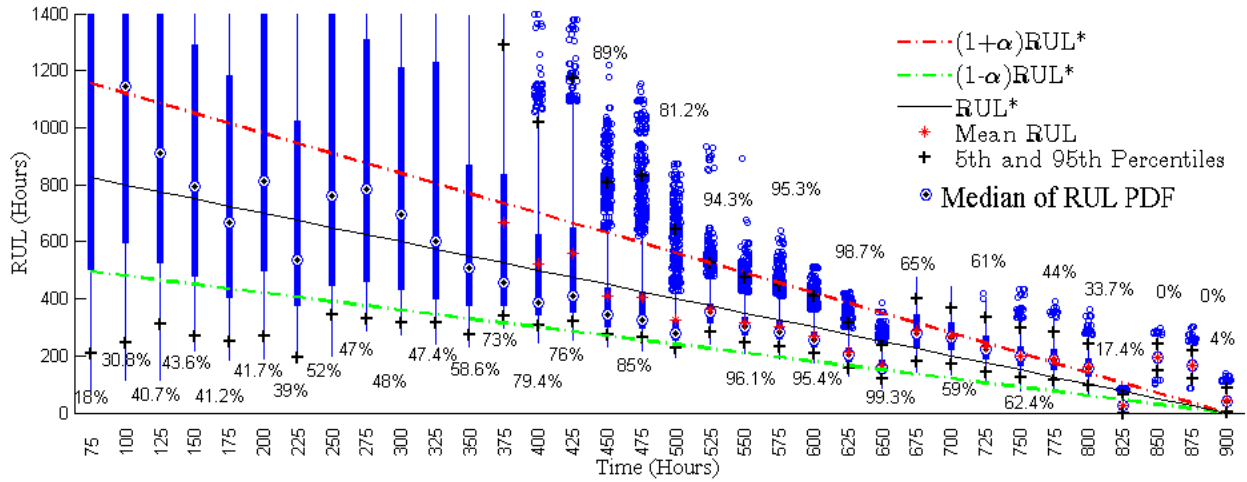


Fig. 4.13 RUL prediction in PF for FC1

Table 4-V Estimation-Prediction Performance Under With Different Number of Particles

N	$RMSE_{r_{2,n}}$	$RMSE_{\alpha}$	$RMSE_{\beta}$	\overline{RA}	Computation Time Taken for First Prediction Step	Total Computational Time for Prediction
100	9.03%	31.43%	22.3%	68.54%	14.56 Seconds	6.45 Minutes
500	7.56%	28.67%	17.78%	76.56%	1Minute 34 Seconds	1 Hour 34 Minutes
1000	6.84%	25.43%	11.44%	89.43%	2 Minutes 28 Seconds	3 Hours 31 Minutes
2000	4.2%	23.56%	9.3%	96.07%	4 Minutes 5 Seconds	6 Hours 48 Minutes

As detailed in Table 4-V, given that other PF related factors are kept same, an increase in the number of PF particles N , results in efficient measurement estimation and prediction accuracy. This justifies the choice of $N=2000$. During RUL prediction, each of the particles is propagated into future. As seen in Chapter 0, computational complexity is directly related to number of particles used and inversely related to the time instant (from start) at which RUL prediction is made. It also depends upon estimation values of hidden DPPs (see Section 3.6.9). The latter is reflected in Table 4-V. Computational time per sample step usually decreases as the time of prediction nears the EOL. In fact, higher the number of particles employed, higher is the estimation efficiency, RUL prediction efficiency and the total computational time consumed. Being run on over 900 Hours of data on an Intel Core i7 Processor, 16 GB RAM and 2.30GHz clock frequency, total time taken for prediction was 6 Hours 48 Minutes.

Discussion: In reality, α_{true} is only approximately linear and β_{true} is never perfectly constant. As such, $RMSE_{\alpha}$ and $RMSE_{\beta}$ cannot be regarded as reliable metrics for evaluation of estimation performance. However, $RMSE_{r_{2,n}}$ indicates the accuracy of measurement estimation. Moreover, prediction performance is accurately judged by \overline{RA} metric as the speed of degradation is uniform (constant loading regime). Recently in Bressel et al. (Bressel et al., 2015), the estimation approach is followed on the similar degradation test data and the polarization curve, employing the Extended Kalman Filter (EKF)(Celaya et al., 2011; Haykin, 2004). For the purpose of comparison, the methodology developed here is replaced with EKF as the estimator and outputs

are shown in Fig. 4.14. Note that therein, the bounds on RUL are obtained using the Inverse First Order Reliability Method (IFORM) (not detailed here)(Hohenbichler et al., 1987), which is used to estimate unknown parameters (for instance, the RUL) for a specified failure probability level.

As seen in Table 4-VI, although the sub-optimal EKF gives a manageable *RMSE*, the associated \overline{RA} (considering the mean of RUL's pdf) is comparatively very low. However, there is a huge difference in the computation time and EKF may be employed where computation time is the major concern.

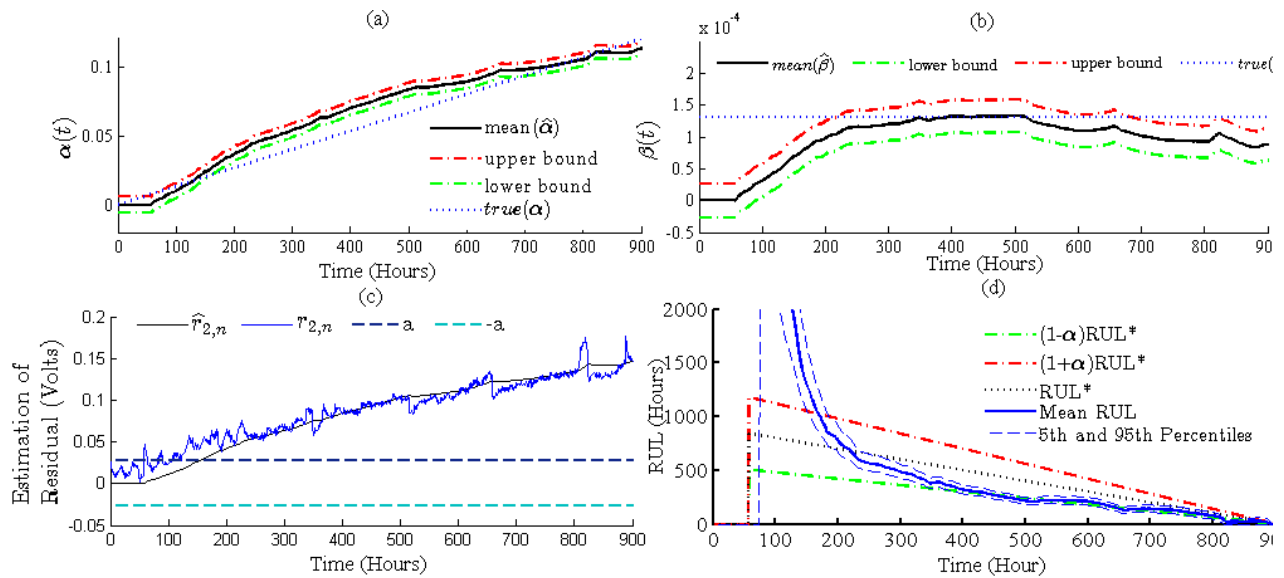


Fig. 4.14 Estimation and RUL prediction by EKF for FC1 (a) Estimation of α (b) Estimation of β (c) Measurement via residual and its estimation (d) RUL Prediction

As prognostic issues are majorly dealt in an offline manner, PF outperforms EKF and promises better prognostic outputs. Moreover, being a sub-optimal estimator, EKF may not be the best choice of the estimator when degradation models are highly non-linear (like crack propagation etc.). The latter, however, can be well taken care by PF.

Table 4-VI Performance comparison with Extended Kalman Filter

Estimator	$RMSE_{r_{2,n}}$	\overline{RA}	Total Computational Time for Prediction
PF ($N=2000$)	4.20%	96.07%	6 Hours 48 Minutes
EKF	9.86%	38.16%	Around 5 seconds

4.5.2.2 Variable Load (FC2)

Motivated from Fig. 4.8, $\alpha_{fail} = 0.6$ signifies EOL of FC2 at 60% deviation on initial value. In the variable load regime, the varying current profile (see Fig. 4.8) mimics the usage in different seasons and affects the speed of degradation significantly. As such, α_{true} seems to evolve in a piece wise linear way (see Fig. 4.10 (b) and (d)). Thus, α_{true} and β_{true} are un-observable in reality. Moreover, the actual measurement in form of residual $r_{2,n}$ is severely affected by the characterizations (see Fig. 4.8 (b) and Fig. 4.15. (c)). This phenomenon is mainly due to the re-standardization of the conditions of temperature and evacuation of liquid water in the PEMFC. However, the non-uniformity brought in by the latter is followed by recovery effect that enables a good SOH estimation.

Estimation results are shown in Fig. 4.15 which is realized with $N=2000$. The initial measurements $r_{2,n}$, being sensitive to stack voltage and current load, are highly corrupted with noise. As such, the detection of degradation using BG-LFT thresholds is not viable. For this reason, the estimations are made to be triggered from initial time $t=0$ Hour. Value of the measurement noise variance $\sigma_{w^d}^2$ is obtained from square of the standard deviation of the nominal residual $r_{2,n}$ for different time regimes, as listed in Table 4-VII. The measurement noise variance in PF is set as 100 times that of residual measurement variance $\sigma_{w^d}^2$. This is done to ensure a good estimation throughout. The $RMSE_{r_{2,n}}$ for different time regimes are listed in Table 4-VII. It should be noted that a different setting in PF may lead to a lesser $RMSE_{r_{2,n}}$, non-smooth estimations of $\alpha(t)$ and $\beta(t)$ with very large spread and consequently, non-viable RUL predictions.

In absence of reliable ground truths for evaluation of $RMSE_{\alpha}$ and $RMSE_{\beta}$, quantitative comparative study of estimation performance for $\alpha(t)$ and $\beta(t)$ cannot be found. However, results are very satisfactory qualitatively, as the estimated α reaches the true α_{fail} at EOL. The initial random walk noise variance is set as $\sigma_{\xi}^2 = 10^{-10}$, for a quick convergence. A good value for process noise variance is found through successive tuning to be $\sigma_v^2 = 10^{-5}$. This enables a smooth and desirable estimation performance.

Table 4-VII Estimation Performance

Time	Standard Deviation of Measurement (Residual $r_{2,n}$)	$RMSE_{r_{2,n}}$
100<t<300 h	0.156 V	42.56%
300<t<570 h	0.0532 V	19.56%
570<t<820 h	0.0145 V	6.85%
820<t< t_{EOL} h	0.0136 V	1.54%

Box plots of RUL predictions are shown in Fig. 4.16. Note that unlike Fig. 4.13, where the prediction accuracy is gauged by RUL^* , α - λ metric and \overline{RA} metric, the same metrics cannot be used here due to the non-uniform speed of degradation. In Fig. 4.16, the predictions obtained until $t=475$ Hours are virtually useless owing to their huge median value and large spread. This can be attributed to the very large corresponding $RMSE_{r_{2,n}}$. However, after $t=475$ Hours, useful predictions are obtained with very small spread. This is mainly due to the less and lesser $RMSE_{r_{2,n}}$ obtained, leading to better estimations of $\alpha(t)$ and $\beta(t)$. The accuracy of RUL predictions is reflected by the fact that it converges to 0 Hours at its true EOL of 900 Hours. Moreover, RUL seems to converge to zero at $t=800$ Hours. The latter is in accordance with the corresponding estimation of $\alpha(t)$ which seems to reach α_{fail} at $t=800$ Hours. This is mainly due to the corresponding evolution of measurement $r_{2,n}$, which undergoes recovery of SOH near $t=800$ Hours before characterization is performed (see Fig. 4.15. (c)), followed by the recovery of SOH until EOL is reached at 900 Hours. Overall the global method is able to assess the RUL

distribution with high accuracy and precise confidence bounds. Being run on the computer of same configuration as FC1, the RUL prediction took around 4 Hours 28 minutes of computation time in total.

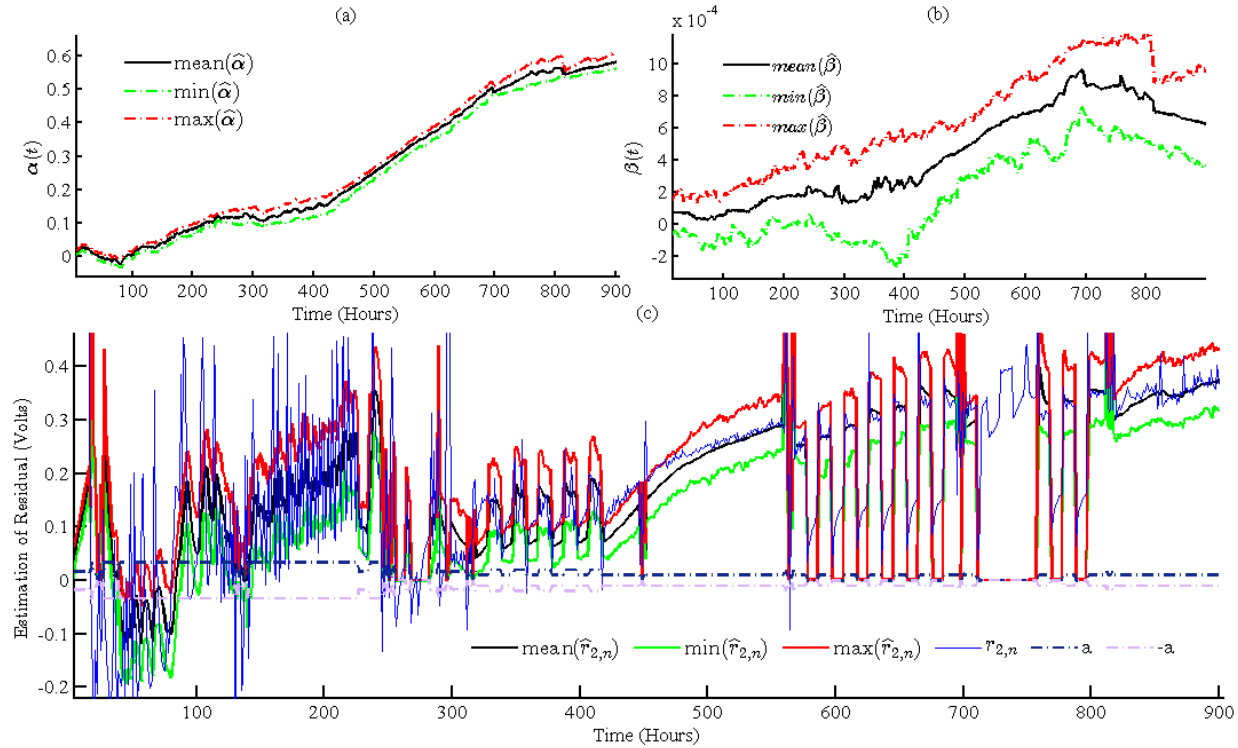


Fig. 4.15 Estimation performance in PF for FC2 (a). Estimation of α (b) Estimation of β (c) Measurement and its estimation

4.6 Conclusions and Contributions

Through real degradation data sets, the SOH and predict the RUL predictions are obtained with a very high accuracy and precise confidence bounds. Thus, the proposed methodology exploits the benefits of BG and PF for an efficient functional decomposition of PEMFC and accurate SOH estimation and RUL prediction. Using the same approach, the BG model that has been utilized here for prognostics of EE part, can be used for prognostics of other sub-systems (hydraulic, thermal etc.) with the availability of degradation data. The results obtained for FC1 is very satisfactory where PF outperforms EKF. For FC2, the accuracy of obtained estimations and RUL predictions is also satisfactory. The accuracy of results obtained here, demonstrates the viability and reliability of the method for prognostics. As such, this work forms a reliable reference for

related future works and a significant contribution towards efficient prognostics in BG framework. The various novel contributions of this chapter are listed as follows.

- BG model of PEMFC with efficient functional decomposition is utilized for the purpose of prognostics. BG-LFT model of electrical-electrochemical part ensures efficient robust detection of parametric degradation.

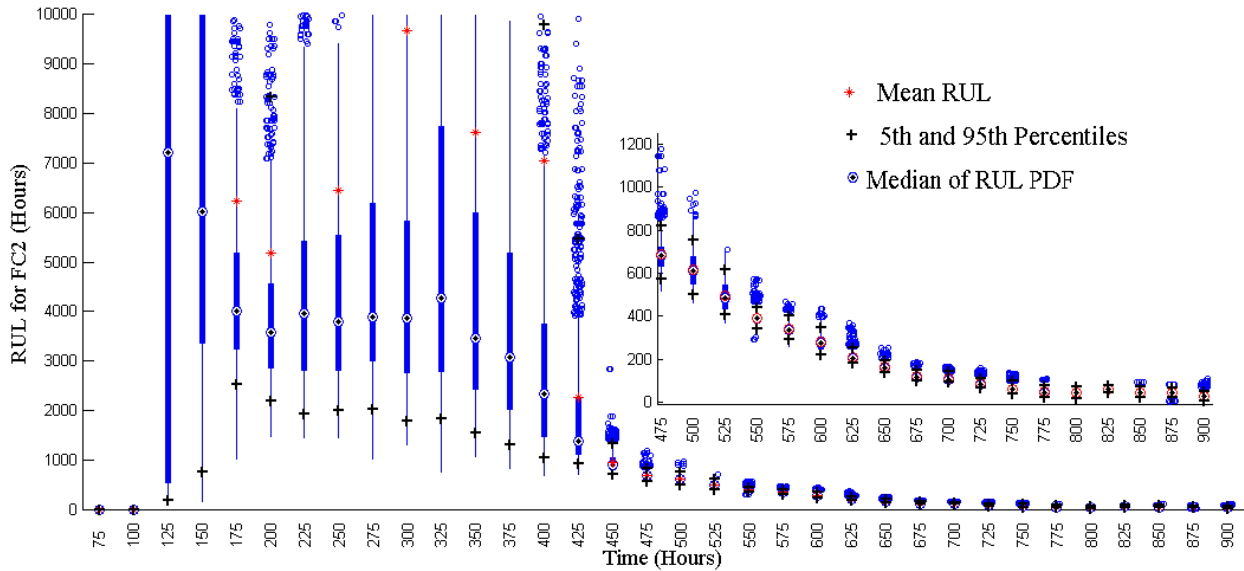


Fig. 4.16 RUL prediction in PF for FC2

- The Hybrid prognostic approach is proposed in Chapter 3 is successfully validated over real degradation data sets. Here, benefits of BG modelling framework and Monte Carlo framework are integrated for estimation of SOH and RUL prediction of degradation in the EE part of PEMFC.
- Novel technique is proposed to obtain observation equation from the nominal part of ARR derived in BG-LFT framework.
- Application of the developed methodology to EE part of PEMFC under both constant current load profile and variable load profile, using real degradation data sets. The performance of PF is discussed and analyzed. It is also compared with Extended Kalman Filter (EKF) for constant load case.

The work presented in this chapter has led to development of followings:

Mayank Shekhar Jha, Mathieu Bressel, Belkacem Ould-Bouamama, Genevieve Dauphin-Tanguy, Mickael Hilaret and Daniel Hissel, *Particle Filter Based Prognostics of PEM Fuel Cell in Bond Graph Framework*, **Selected for Presentation and Publication in 3^{ème} Conférence Internationale des Energies Renouvelables (CIER-2015)**, Sousse - Tunisie, Décembre 21-23, 2015.

Mayank Shekhar Jha, Mathieu Bressel, Belkacem Ould-Bouamama, Genevieve Dauphin-Tanguy, Mickael Hilaret and Daniel Hissel, *Particle Filter Based Hybrid Prognostics of Proton Exchange Membrane Fuel Cell in Bond Graph Framework*, **Submitted** to Applied Energy, Elsevier.

4.7 Acknowledgements

Work presented in Section 4.4.2.1 and Section 4.4.2.2 has been carried out by Mr. Mathieu Bressel, supported by the project ANR PROPICE (ANR-12-PRGE-0001) and by the project LABEX ACTION (ANR-11-LABX-01-0) both funded by the French National Research Agency. The author is grateful to Mathieu for providing the data collected during the degradation tests for the development of this work. Additionally, the details of associated projects and data-sets may be found on: <http://eng.fclab.fr/ieee-phm-2014-data-challenge/> & <https://propice.ens2m.fr/> .

5. General Conclusions and Perspectives

In Chapter 2, the methodology of modelling parametric uncertainties and measurements in interval form, on Bond Graph (BG) models is presented. It is a novel contribution and forms the initial step towards integrating interval analysis based capabilities in BG framework for fault detection and health monitoring of uncertain systems. Methodology to generate Interval valued Analytical Redundancy Relations (I-ARRs) and corresponding robust thresholds over the *nominal residual* is presented which are derived directly from the BG junctions utilizing the structural and causal properties of the uncertain BG. The interval valued *uncertain residual interval function* (URIF) can be directly obtained from the uncertain BG. The method of modeling uncertainties in interval form alleviates the limitation of quantifying the uncertainties with symmetric bounds (equal limits on the left and right side of nominal value) associated with BG-LFT method. In fact, this leads to the generation of adaptive thresholds which are not necessarily symmetric with respect to the nominal residual. Moreover, it is shown that BG-LFT enabled robust FDI is only a special case when interval valued uncertainties have symmetric interval bounds/limits. The proposed methodology is applied and validated over uncertain steam generator system and its usefulness over the previously used BG-LFT generated thresholds in fault detection is shown via real experimental results.

However, in this work, the overestimation incurred due to multi-incidence of interval variables in the I-ARR expression, has not been studied. This forms an interesting perspective. Modal Intervals can be used for such a purpose. There are well developed techniques in the realm of Modal Intervals that could be exploited in this context. Given the obvious betterment in diagnosis, the novel methodology carries the potential of being utilized as diagnostic module for all diagnostic related analysis in BG framework and health monitoring of uncertain systems. Also, the thesis work motivates the integration of set based bounding approaches in BG framework for health monitoring purposes in future, utilizing the formalism proposed in this work.

In Chapter 3, it has been successfully demonstrated that under single degradation hypothesis, the nominal part of Interval Analytical Redundancy Relation derived from Bond Graph model of globally uncertain system, can be used for detection of system parameter's degradation, estimation of the state of health, associated degradation progression parameter and a subsequent prediction of the remaining useful life of the parameter using particle filtering algorithms. Thus, the benefits of Bond graph modelling technique and Monte Carlo techniques are integrated.

However, this work revolves around the single fault hypothesis and considers only one system parameter exhibiting progressive degradation. The technique developed here can be extended in a straight forward manner, while there is single fault mode affecting several system parameters. Moreover, the method can be extended in case of multiple parametric degradations. The latter forms a potential future work.

The employed Particle filter algorithms form the best choice in this regard, supporting non-Gaussian noises and allowing their prior/online tuning. The methodology presented, uses local fault models and as such, does not suffer from scalability problems of large systems. This aspect can be analyzed in a detailed manner. The method presented here can be extended and developed for large scaled systems. Moreover, a detailed comparative study involving various Bayesian estimators can be exercised.

Through experiments, capability of obtaining RUL predictions in real time has been shown, although, in very short time windows. The associated computational complexity prevents the long and very long-term RUL predictions in real time. In future, additional ways to obtain the same in sliding time windows will be explored. The method will be extended to achieve very long term predictions in multiple stages, comprising of small time windows, in real time. Although, robustness of the methodology has not been analyzed quantitatively, a qualitative analysis has been presented which helps in an efficient tuning of the PF parameters.

In Chapter 4, through real degradation data sets, the proposed methodology is able to successfully assess the SOH and predict the RUL of the Electrical and Electro Chemical Part of an industrial Proton Exchange Membrane Fuel Cell (PEMFC), with a very high accuracy and precise confidence bounds. The proposed methodology thus, exploits the benefits of BG and PF for an efficient functional decomposition of PEMFC and accurate SOH estimation and RUL

prediction. Using the same approach, the developed model can be used for prognostics of other sub-systems (hydraulic, thermal etc.) with the availability of degradation data. The latter forms a potential future work. The results obtained for FC1 is very satisfactory where PF outperforms EKF. For FC2, the accuracy of obtained estimations and RUL predictions is very satisfactory. The initial RUL predictions can be ameliorated through online standard deviation calculation of residual, adapting the random walk noise variance, and PF measurement variance etc. which may be taken up as future work.

However, the results obtained in this work strongly depend upon the assumption associated with the choice of the health indicator. The assumption that the health indicator evolves linearly is based upon the available data sets. However, it is highly probable that such an assumption may not hold true in general. Thus, the work can be extended and adapted suitably with the availability of more data sets.

The methodology applied here on PEMFC, has the potential to be applied over any multi-energetic system. The accuracy of results obtained here demonstrates the viability of the method for prognostics. As such, this work forms a reliable reference for related future works and a significant contribution towards efficient prognostics in BG framework.

In fact, as this work can be extended to several subsystems within the global system of interest, post-prognostics maintenance strategies may be developed using the RULs obtained for various subsystems.

Appendix A Bond Graph Generalities

The BG is a unified modeling language for multiple physical domains, such that power variables associated with the bonds differ in accordance with energetic type of the system. The type of energy exchanged is defined by the power variables. A description of these variables is displayed in Table A-1.

Table A-1 Effort and Flow variables in different physical Domains

Physical Domain	Effort	Flow
Mechanical (Translational)	Force (F)	Velocity (v)
Mechanical (Rotational)	Torque (T)	Angular Velocity (ω)
Electrical	Voltage (V)	Current (i)
Hydraulic	Pressure (P)	Volume Flow Rate (Q)
Thermal	Temperature (T)	Entropy Flow rate (\dot{s})

Moreover, in the BG modelling framework, the physical system/component is divided into Active, Passive, and Multi-port elements. A schematic decomposition of the BG elements is given in Fig. A-1.

Active Elements: These are sources that supply power to the system (Sources of effort (Se), and flow (Sf)). The bond orientation always goes out of the source (see Fig. A-2).

- Source of Effort (Se): Give effort to the system e , $e = Se$
- Source of Flow (Sf): Gives the flow to the system f , $f = Sf$.

Passive elements: There are three types of basic passive elements: *Inertial* element I , *Capacitor* element C and *Resistor* element R . The representation of either of them is done by directing the bond onto these elements as shown in Fig. A-3

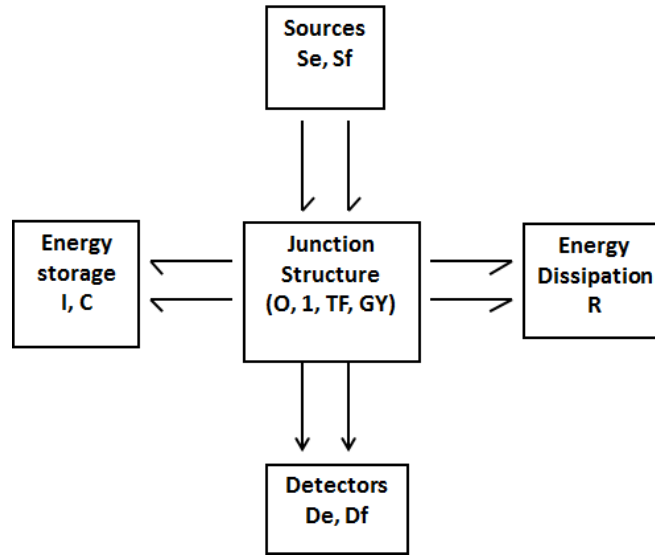


Fig. A-1: Various elements in Bond graph modelling

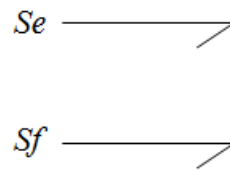


Fig. A-2 Active Elements: Sources of Effort and Flow

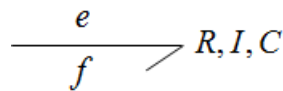


Fig. A-3 Representation of Passive Elements

Inertial Element- (I): This element models the phenomenon of energy storage defined by the constitutive equation that relates the flow $f(t)$ and integral of effort $e(t)$: $\Phi_I(f(t), \int e(t) dt) = 0$
 Examples of some components modelled as I elements are: electrical inductance, mass, inertial components etc.

Capacitor Element- (C): This element models the phenomenon of energy storage defined by the constitutive equation that relates the integral flow $f(t)$ and effort $e(t)$: $\Phi_C(e(t), \int f(t) dt) = 0$.
 Examples of some components modelled as C elements are: spring, hydraulic reservoir, electrical capacitance etc.

Resistor Element- (R): Resistor element models the phenomenon of energy dissipation and is defined by the constitutive equation that relates the flow $f(t)$ and effort $e(t) : \Phi_R(f(t), e(t)) = 0$. Examples of some components modelled as R elements are: electrical resistance, mechanical friction, dissipative forces etc.

The set of *behavioural equations* (C_B) can be derived for each of these elements as follows:

$$\begin{aligned}
 C_B &= \{C_R\} \cup \{C_C\} \cup \{C_I\} \\
 C_R &= \Phi_R(f_R(t), e_R(t)) = 0, \\
 C_C &= \Phi_C(e_C(t), \int f_C(t) dt) = 0, \\
 C_I &= \Phi_I(f_I(t), \int e_I(t) dt) = 0.
 \end{aligned}
 \tag{A.1}$$

Junction elements: Junction elements are power conservative in nature. They are used to depict and model the energy transfer in the system.

Transformer Element- (TF): is used to connect two subsystems where output effort of one subsystem is proportional to the input effort of the other subsystem (see Fig. A-4). Obviously, due to power conservation, the respective flows also remain proportional to each other. The constitutive relation associated to a TF element are : $e_1 = me_2$ and $f_2 = mf_1$ where m is the coefficient of the transformer element. Some of the examples include hydraulic cylinders, gear pairs, wheels etc.

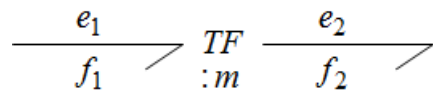


Fig. A-4 Representation of TF element

Gyrator Element (GY) : This element is used for connection of two subsystems where the output effort (input flow) is proportional to the input flow (output effort) of the other subsystem (see Fig. A-5). The associated constitutive equations are: $e_1 = kf_2$ and $e_2 = kf_1$ with k being the coefficient gyration. Some examples include gyroscopes, electric motors etc.

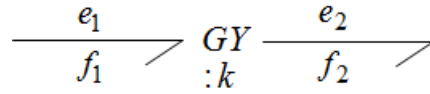


Fig. A-5 Representation of GY element

0 (1) Junction: is used to connect the elements with common effort (common flow). The equations that are derived from the junctions are termed as structural equations. Fig. A-6 illustrates the **0-Junction** and structural equations that may be derived from the latter are given in (A.2).

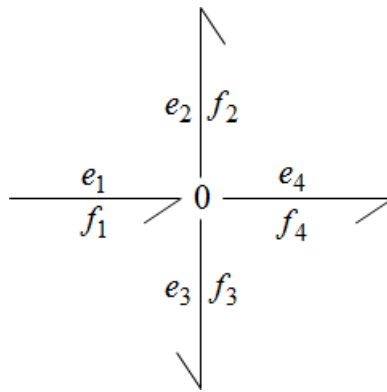


Fig. A-6 BG representation of 0 Junction

$$e_1 = e_2 = e_3 = e_4 \quad (\text{A.2})$$

$$\sum f_i = 0; f_1 - f_2 - f_3 - f_4 = 0$$

The **1-Junction** is illustrated in Fig. A-7. Structural equations derived from latter are shown in (A.3).

$$f_1 = f_2 = f_3 = f_4 \quad (\text{A.3})$$

$$\sum e_i = 0; e_1 - e_2 - e_3 - e_4 = 0$$

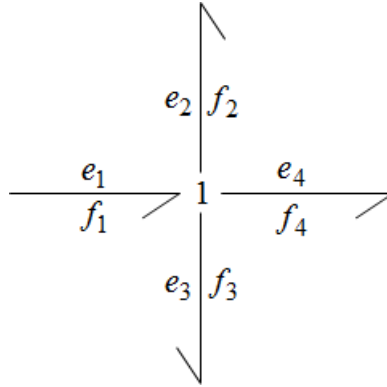


Fig. A-7 BG representation of 1 Junction

Finally, the system architecture is complete with the definitions of the measurement set. Detector of effort (flow) is represented by De (Df) elements. These elements are not connected by power bonds with junctions as there is no exchange of the energy between them. These elements are represented by a full arrow and represent the exchange of information. As discussed before, $\mathbf{0}$ ($\mathbf{1}$) junction connects BG elements with common effort (flow) and thus, a De (Df) element is used at these junctions to measure the common effort ($flow$). Common examples of De include voltmeter, pressure sensors etc. For Df , one can cite example as flow rate meter, ampere meter etc. The representation of De (Df) is shown in Fig. A-8.

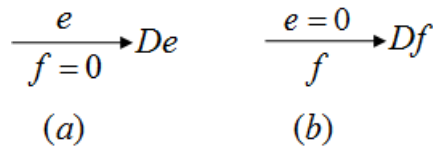


Fig. A-8 (a) BG representation of De element (b) BG representation of Df element

A.1. Causality

Causality enables the definition of cause and effect relationship among the different components of the system. The causality assigned to I and C elements determine whether integration or a differentiation with respect to time is required. For the storage element I , the

causal strokes in preferred integral causality representation is shown in Table A-2. For inertial element it implies acceptance of effort variable as input and production of flow as the output.

On the other hand, for the capacitor element in preferred integral causality, input flow is integrated to produce the output effort. The derivative causality implies that capacitor element C , accepts an input effort and produces output flow as shown in Table A-3.

 Table A-2 BG representation of I element

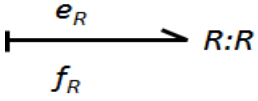
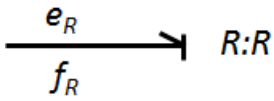
Causality	Constitutive relation	Representation	Block Diagram
Integral Causality	$\Phi_I : f_I(t) = \frac{1}{I} \int e_I(t) dt$		
Derivative Causality	$\Phi_I : e_I(t) = I \frac{d}{dt} f_I(t)$		

 Table A-3 BG representation of C element

Causality	Constitutive relation	Representation
Integral Causality	$\Phi_C : e(t) = \frac{1}{C} \int f(t) dt$	
Derivative Causality	$\Phi_C : f(t) = C \frac{d}{dt} e(t)$	

For R element, either of the representations may be followed according to the constitutive relation dominating the dynamics of component of interest. In other words, both the representations is acceptable for either of the causalities. Table A-4 shows the representation of R element.

Table A-4 BG representation of R element

Constitutive relation	Representation
$\Phi_R : e(t) = R f(t)$	
$\Phi_R : f(t) = \frac{1}{R} e(t)$	

A systematic procedure for causality assignment is given as (Mukherjee & Samantaray, 2006):

1. The sources and the nonlinear R elements are assigned with the required causality. Implications are extended through the graph as far as possible, using the constraint elements (O , I , TF , GY)
2. A preferred integral causality is assigned to the I and C –elements and the implications are extended through the graph.
3. Linear R -elements are then assigned the causality.
4. In case of causality conflict at a junction, the I - or C -elements are searched for possible conflicts. They are assigned with a derivative causality. Step 3 is repeated.

Appendix B Bond Graph in Linear Fractional Transformation

Linear Fractional Transformations (LFT) as shown in Fig. B-1 are generic objects, widely used for uncertain systems modeling. Genericity of the LFT is due to the fact that any rational expression can be written under this form. It is used for stability analysis and for control law synthesis using the m-analysis and synthesis principles, by separating the nominal part of the model from its uncertain part as shown in Fig. B-1. The nominal values are grouped in an augmented matrix denoted M , supposed proper and all uncertainties (structured and unstructured uncertainties, measurement noise ...) are gathered in a matrix D with a diagonal structure. In the linear case, this standard form leads to a state-space representation of form shown in (B.1) with $x \in R^n$ the state vector of the system, $u \in R^m$ the vector gathering the control inputs of the system, $y \in R^p$ the vector gathering the measured outputs of the system, $w \in R^l$ et $z \in R^l$ include respectively, the auxiliary inputs and outputs. n, m, l et p are positive integers. Les matrices $A, B_1, B_2, C_1, C_2, D_{11}, D_{12}, D_{21}, D_{22}$ are matrices of appropriate dimensions.

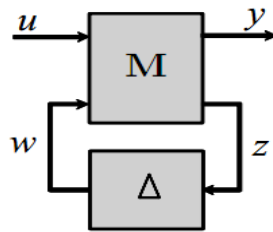


Fig. B- 1(a) LFT Representation

$$\begin{cases} \dot{x} = A.x + B_1.w + B_2.u \\ z = C_1.x + D_{11}.w + D_{12}.u \\ z = C_2.x + D_{21}.w + D_{22}.u \end{cases} \quad (\text{B.1})$$

BG-LFT is an efficient and systematic way of parametric uncertainty representation in BG framework. An uncertainty on a parameter value θ can be introduced under either an additive form or a multiplicative one, as given respectively in (B.2) and (B.3):

$$\theta = \theta_n \pm \Delta\theta; \quad \Delta\theta \geq 0 \quad (\text{B.2})$$

$$\theta = \theta_n (1 \pm \delta_\theta); \quad \delta_\theta = \frac{\Delta\theta}{\theta_n} \quad (\text{B.3})$$

where $\Delta\theta$ and δ_θ are respectively, the absolute and relative deviations around the nominal value θ_n . When the element characteristic law is written in terms of $\frac{1}{\theta}$, (B.1) becomes:

$$\frac{1}{\theta} = \frac{1}{\theta_n} \cdot (1 + \delta_{1/\theta}); \quad \delta_{1/\theta} = \frac{-\Delta\theta}{\theta_n + \Delta\theta} \quad (\text{B.4})$$

Consider R-element in resistance (imposed flow) causality. The characteristic law corresponding to R-element in the linear case (Fig. B- 2-(a)) is given as follows

$$e_R = R \cdot f_R \quad (\text{B.5})$$

In case of uncertainty on R, (B.5) becomes

$$e_R = R_n (1 + \delta_R) \cdot f_R = R_n \cdot f_R + \delta_R \cdot R_n \cdot f_R = e_{Rn} + e_{Runc} \quad (\text{B.6})$$

Constitutive equation (B.5) can be represented by the LFT BG of uncertain R-element in Fig. B- 2 (b) by introducing a modulated source MSe associated with auxiliary input w_R and a virtual effort sensor associated with auxiliary output z_R .

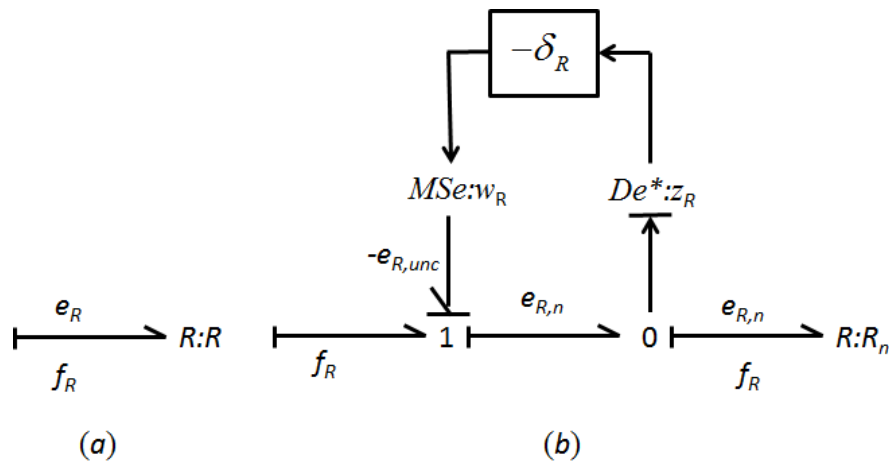


Fig. B- 2(a): R-element in resistance causality. (b): uncertain R-element in resistance causality in LFT form.

For a R-element in conductance (imposed effort) causality, the procedure is the same.

$$f_R = \frac{1}{R} \cdot e_R \quad (\text{B.7})$$

It can be written as shown in (B.8). The BG representation is shown in Fig. B- 3.

$$f_R = \frac{1}{R_n} (1 + \delta_{1/R}) \cdot e_R = \frac{e_R}{R_n} + \frac{e_R \cdot \delta_{1/R}}{R_n} = f_{R_n} + f_{R_{unc}} \quad (\text{B.8})$$

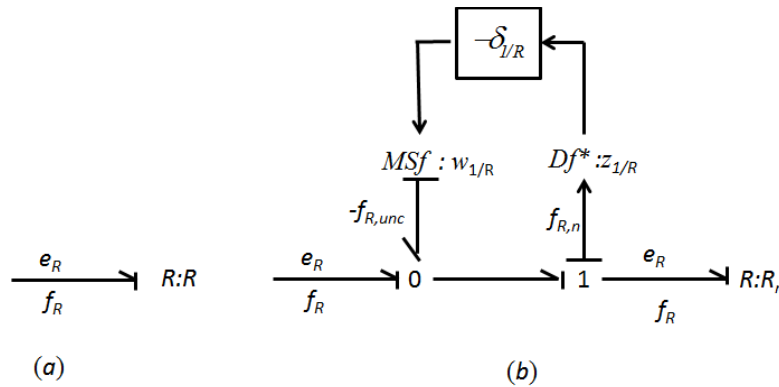


Fig. B- 3 (a): R-element in conductance causality. (b): uncertain R-element in conductance causality in LFT form

It must be noted that the (-) sign that appears in the BG representation in Fig. B- 2 and Fig. B- 3 is due to the power conservative convention followed. Moreover, the symbols De^* and Df^* represent virtual detectors. The virtual detectors are used to represent the information exchange/transfer. Also, the modulated sources $MSe : w_R$ ($MSf : w_{1/R}$) is added to represent the introduction of an additional effort (flow) generated by the uncertainty δ_R ($\delta_{1/R}$), on the system.

Similarly, parametric uncertainty on the other passive elements can be represented. Fig. B- 4 shows the BG-LFT representation of I and C elements while they are in derivative causality. Derivative causality is the preferred choice for diagnostic purposes (ARR generation). Thus, it is chosen for illustration of BG-LFT representation. A detailed summary of BG-LFT representation of various BG elements in either causalities can be found in the work of Borutzky (Borutzky, Wolfgang, 2009a).

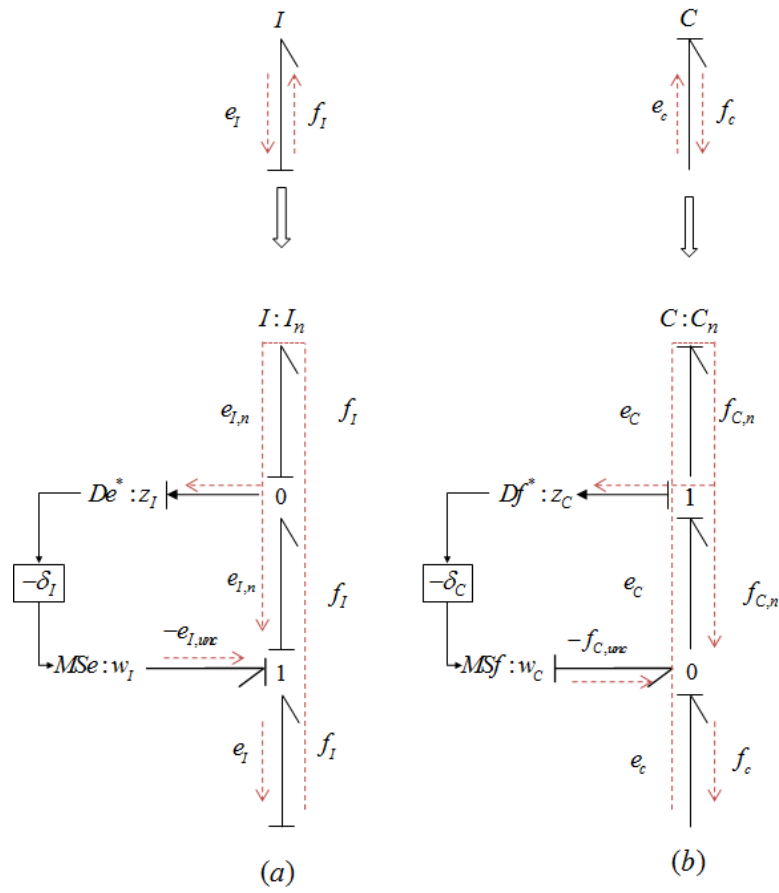


Fig. B- 4 BG-LFT representation of parametric uncertainty on I and C elements in derivative causality: (a) BG-LFT representation of I element (b) BG-LFT representation of C element

Fig. B- 5 illustrates the BG-LFT representation for TY element and Fig. B- 6 does the same for GY element.

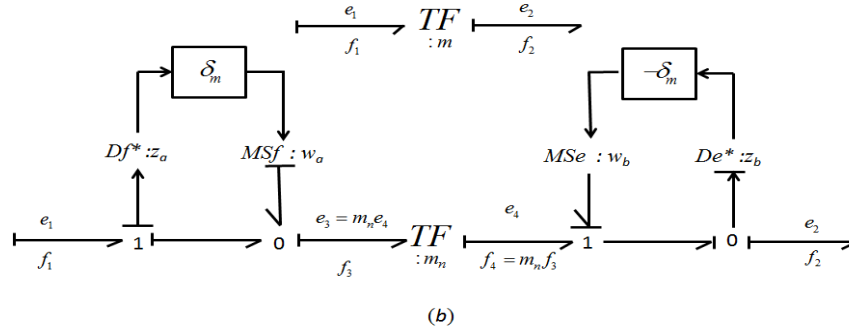
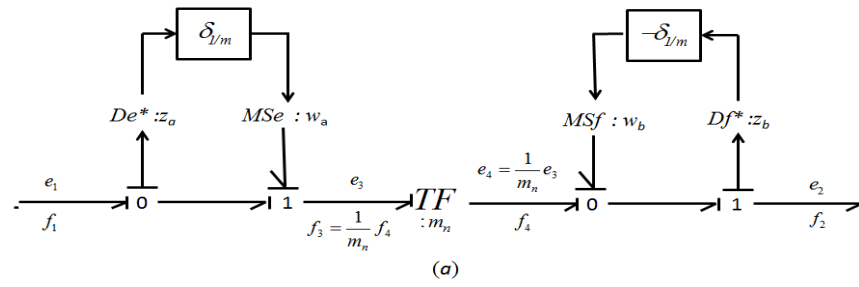


Fig. B- 5 BG-LFT representation of parametric uncertainty on *TF* element.

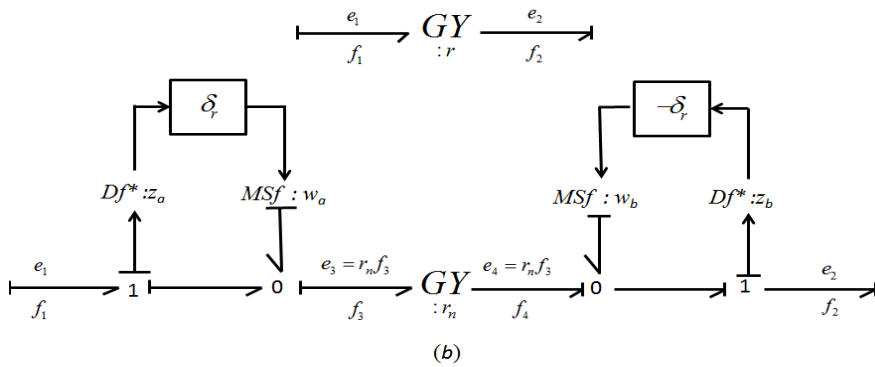
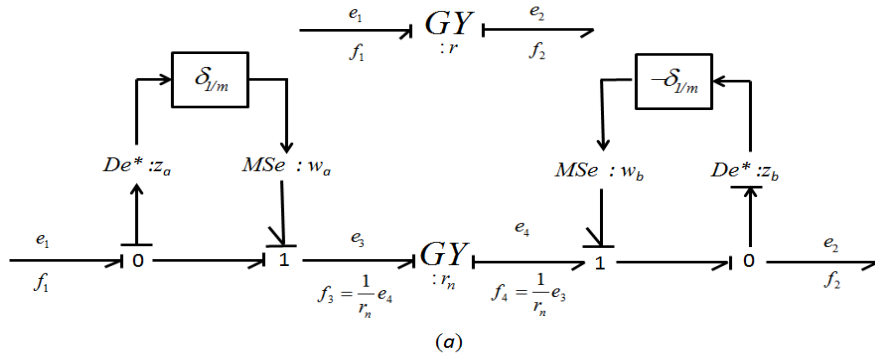


Fig. B- 6 BG-LFT representation of parametric uncertainty on *GY* element.

B.1. BG-LFT based Robust Fault Detection

Fault diagnosis in BG-LFT framework is mainly dependent upon ARR generation (Djeziri, Mohand Arab et al., 2007). The description in this section has been adapted from Djeziri et al. (Djeziri, Mohand Arab et al., 2007) and Borutzky et al. (Borutzky, Wolfgang, 2011).

Generation of Uncertain ARRs

The generation of robust analytical redundancy relations from an observable bond graph model is explained by the following steps:

1st *Step*: Preferred derivative causality is assigned to the nominal model and detectors De (Df) are dualized to SSe (SSf); wherever possible.

2nd *Step*: The LFT BG model is built.

3rd *Step*: The candidate ARRs are generated from “1” or “0” junction, where power conservation equation dictates that sum of efforts or flows, respectively, is equal to zero, as:

- for 0-junction:

$$\sum s_i \cdot f_{i,n} + \sum Sf + \sum s_i w_i = 0 \quad (\text{B.9})$$

- for 1-junction:

$$\sum s_i \cdot e_{i,n} + \sum Se + \sum s_i w_i = 0 \quad (\text{B.10})$$

with s being the sign rendered to the *bond* due to energy convention.

4th *Step*: The unknown effort or flow variables are eliminated using covering causal paths from unknown variables to known (measured) variables (dualized detectors), to obtain the ARRs which are sensitive to contain only known variables as,

$$R = \Phi \left\{ \sum Se, \sum Sf, SSe, SSf, R_n, C_n, I_n, TF_n, GY_n, RS_n, \sum w_i \right\} \quad (\text{B.11})$$

where subscript n represents the nominal value of the corresponding BG element.

Generation of Adaptive Thresholds

The ARR derived in (B.11) consists of two perfectly separable parts due to the properties of the BG-LFT model: a nominal part noted r shown in (B.12) and an uncertain part noted $b = \sum w_i$ shown in (B.13).

$$r = \Phi \{Se, Sf, SSe, SSf, R_n, C_n, I_n, TF_n, GY_n, RS_n\} \quad (\text{B.12})$$

$$b = \sum w_i$$

$$w_i = \Phi \{Se, Sf, SSe, SSf, R_n, C_n, I_n, TF_n, GY_n, RS_n, \delta_R, \delta_I, \delta_C, \delta_{TF}, \delta_{GY}, \delta_{RS}\} \quad (\text{B.13})$$

The uncertain part generates the adaptive threshold over the nominal part. From (B.11), (B.12) and (B.13), following may be obtained:

$$r + b = 0 \quad (\text{B.14})$$

$$r = -b = -\sum w_i$$

The thresholds are formed in form of envelop as:

$$-a < r < a \quad (\text{B.15})$$

where

$$a = \sum |w_i| \quad (\text{B.16})$$

The use of absolute values to generate the thresholds of normal operation ensures the robustness of this algorithm to false alarms.

Appendix C Non-Linear Bayesian Filtering using Particle Filters

Consider a dynamic system whose state at time step t_k is represented by the vector \mathbf{x}_k . The evolution of the system state is described by a state-space model,

$$\mathbf{x}_k = \mathbf{f}_k(\mathbf{x}_{k-1}, \mathbf{v}_{k-1}) \quad (\text{C.1})$$

$$\mathbf{y}_k = \mathbf{h}_k(\mathbf{x}_k, \mathbf{w}_k) \quad (\text{C.2})$$

where

- $\mathbf{f}_k : \mathbb{R}^{n_x} \times \mathbb{R}^{n_w} \rightarrow \mathbb{R}^{n_x}$ is a possibly non-linear the state transition function.
- $\mathbf{h}_k : \mathbb{R}^{n_x} \times \mathbb{R}^{n_w} \rightarrow \mathbb{R}^{n_y}$ is the measurement or observation function describing the sequence of measurements \mathbf{y}_k , obtained sequentially at successive time steps t_k .
- $\mathbf{v}_k \in \mathbb{R}^{n_v}$ is the process noise sequence of known distribution and is independently identically distributed (i.i.d).
- $\mathbf{w}_k \in \mathbb{R}^{n_w}$ is the i.i.d measurement noise sequence of known distribution.

Equations (C.1) and (C.2) can be equivalently represented as,

$$\mathbf{x}_k = \mathbf{f}_k(\mathbf{x}_{k-1}, \mathbf{v}_{k-1}) \leftrightarrow p(\mathbf{x}_k | \mathbf{x}_{k-1}) \quad (\text{C.3})$$

$$\mathbf{y}_k = \mathbf{h}_k(\mathbf{x}_k, \mathbf{w}_k) \leftrightarrow p(\mathbf{y}_k | \mathbf{x}_{k-1}) \quad (\text{C.4})$$

where $p(\mathbf{x}_k | \mathbf{x}_{k-1})$ represents the state transition probability and the function $p(\mathbf{y}_k | \mathbf{x}_{k-1})$ is the likelihood function that signifies the probability of the observation of \mathbf{y}_k , given the current estimate of \mathbf{x}_k .

Objective of filtering procedure is to obtain estimates of \mathbf{x}_k , based upon all of the available measurements $\mathbf{y}_{1:k} = \{\mathbf{y}_k, k = 1, 2, \dots, k\}$. From Bayesian perspective, the objective remains in recursively calculating the distribution of the state \mathbf{x}_k , given the set of observations $\mathbf{y}_{1:k}$ up to

time t_k , with some degree of belief. Construction of PDF $p(\mathbf{x}_k | \mathbf{y}_{1:k})$, known as the filtered *posterior state* PDF, provides all the information about \mathbf{x}_k , inferred from the measurements $\mathbf{y}_{1:k}$ and the initial state PDF $p(\mathbf{x}_0)$. The latter $p(\mathbf{x}_0)$ is assumed known.

Given $p(\mathbf{x}_{k-1} | \mathbf{y}_{0:k-1})$ at time t_{k-1} , theoretically, the posterior state is estimated in a recursive way through two sequential steps: *prediction* and *update*.

- *Prediction*: The estimation of *prior* state PDF $p(\mathbf{x}_k | \mathbf{y}_{1:k-1})$, is achieved by utilizing Chapman-Kolmogorov equation at time t_k from $p(\mathbf{x}_{k-1} | \mathbf{y}_{1:k-1})$ at time $k-1$,

$$\begin{aligned} p(\mathbf{x}_k | \mathbf{y}_{1:k-1}) &= \int p(\mathbf{x}_k | \mathbf{x}_{k-1}, \mathbf{y}_{1:k-1}) p(\mathbf{x}_{k-1} | \mathbf{y}_{1:k-1}) \\ &= \int p(\mathbf{x}_k | \mathbf{x}_{k-1}) p(\mathbf{x}_{k-1} | \mathbf{y}_{1:k-1}) d\mathbf{x}_{k-1} \end{aligned} \quad (\text{C.5})$$

where $p(\mathbf{x}_k | \mathbf{x}_{k-1})$ is to be obtained from (C.1), with system following 1st order Markovian assumption.

- *Update*: Bayes rule is used to *update* the *prior* as the new measurement \mathbf{y}_k arrives, to obtain the *posterior* distribution of \mathbf{x}_k as,

$$p(\mathbf{x}_k | \mathbf{y}_{1:k}) = p(\mathbf{x}_k | \mathbf{y}_{1:k-1}) p(\mathbf{y}_k | \mathbf{x}_k) / p(\mathbf{y}_k | \mathbf{y}_{1:k-1}) \quad (\text{C.6})$$

with the normalizing constant being,

$$p(\mathbf{y}_k | \mathbf{y}_{1:k-1}) = \int p(\mathbf{x}_k | \mathbf{y}_{1:k-1}) p(\mathbf{y}_k | \mathbf{x}_k) d\mathbf{x}_k \quad (\text{C.7})$$

The exact Bayesian solution can be obtained from recurrence relations (C.5) and (C.6), that form the basis of optimal Bayesian solution. This procedure produces best results but for few cases such as linear Gaussian state space models and in general, optimal solutions for non-linear systems with non-Gaussian noises, cannot be analytically determined using the same. For Gaussian state space models, the above procedure leads to the classical Kalman filter. For non-

linear state space models but with additive Gaussian noises, sub-optimal Extended Kalman filter (EKF) has been developed.

C.1. Particle Filters

Particle filtering, also known as Sequential Monte Carlo (SMC) methods (Doucet et al., 2001), is a technique for implementing a recursive Bayesian filter via Monte Carlo simulations. The basic principle of particle filtering is to represent the posterior state PDF by a set of random samples or “particles”, each with an associated weight, and to compute estimates based on these samples and weights (Doucet et al., 2009). One of the most commonly used particle filter algorithms is the *sequential importance sampling* (SIS) particle filter. The SIS particle filter approximates the posterior state PDF $p(\mathbf{x}_{0:k} | \mathbf{y}_{1:k})$ by a set S of N number of weighted particles (Arulampalam et al., 2002),

$$\{(\mathbf{x}_{0:k}^i), w_k^i\}_{i=1}^N \quad (\text{C.8})$$

where, $\mathbf{x}_{0:k} = \{\mathbf{x}_j, j=0, \dots, k\}$ is the set of all states up to time k , $\{\mathbf{x}_{0:k}^i, i=1, \dots, N\}$ is the set of particles representing the state value, with importance weights associated as $\{w_{0:k}^i, i=1, \dots, N\}$. The weights are the approximations of the relative posterior probabilities of the particles and are normalized so that,

$$\sum_i w_{0:k}^i = 1 \quad (\text{C.9})$$

The posterior PDF is approximated as,

$$p(\mathbf{x}_{0:k} | \mathbf{y}_{1:k}) \approx \sum_{i=1}^N w_k^i \cdot \delta(\mathbf{x}_{0:k} - \mathbf{x}_{0:k}^i) \quad (\text{C.10})$$

where δ denotes the Dirac delta function. This gives discrete weighted approximation to the true posterior state distribution $p(\mathbf{x}_{0:k} | \mathbf{y}_{1:k})$. As the number of samples/particles becomes very large, the Monte Carlo characterization becomes an equivalent representation to the usual functional description of the posterior state PDF, and the filter approaches the optimal Bayesian solution

C.2. Importance Sampling

It is impossible to sample from the posterior state $p(\mathbf{x}_{0:k} | \mathbf{y}_{1:k})$ without a closed form describing its distribution. To resolve this issue, principle of *importance sampling* is used (Arulampalam et al., 2002), where a PDF $q(x)$ is chosen such that it is easy to sample from $q(x)$ and $p(x) \propto q(x)$. Set of samples $x^i \sim q(x), i = 1, \dots, N$ are generated from the proposal distribution $q(\cdot)$, known as *importance density* so that a weighted approximation to the density $p(\cdot)$ given as,

$$p(x) \approx \sum_{i=1}^N w^i \cdot \delta(x - x^i) \quad (\text{C.11})$$

where the normalized weight is given as,

$$w^i \approx \frac{p(x^i)}{q(x^i)} \quad (\text{C.12})$$

For a set of samples $\{\mathbf{x}_{0:k}^i, i = 1, \dots, N\}$, this translates to the weights being defined as,

$$w_k^i \propto \frac{p(\mathbf{x}_{0:k} | \mathbf{y}_{1:k})}{q(\mathbf{x}_{0:k} | \mathbf{y}_{1:k})} \quad (\text{C.13})$$

For online implementation, recursive estimation is needed. In other words, distribution $p(\mathbf{x}_{0:k} | \mathbf{y}_{1:k})$ at time t_k must be estimated from $p(\mathbf{x}_{0:k-1} | \mathbf{y}_{1:k-1})$ at time t_{k-1} . To achieve it, constraint on *importance density* is placed to factorize it as,

$$q(\mathbf{x}_{0:k} | \mathbf{y}_{1:k}) = q(\mathbf{x}_k | \mathbf{x}_{0:k-1}, \mathbf{y}_{1:k}) q(\mathbf{x}_{0:k-1} | \mathbf{y}_{1:k-1}) \quad (\text{C.14})$$

Then, new sets of samples $\mathbf{x}_{0:k}^i \sim q(\mathbf{x}_{0:k} | \mathbf{y}_{1:k})$, are obtained by appending onto existing samples $\mathbf{x}_{0:k-1}^i \sim q(\mathbf{x}_{0:k-1} | \mathbf{y}_{1:k-1})$, the new state $\mathbf{x}_{0:k}^i \sim q(\mathbf{x}_k | \mathbf{x}_{0:k-1}, \mathbf{y}_{1:k})$. The particles weights are updated too, by first factorizing the posterior state PDF as,

$$p(\mathbf{x}_{0:k} | \mathbf{y}_{1:k}) = p(\mathbf{x}_{0:k-1} | \mathbf{y}_{0:k-1}) \frac{p(\mathbf{y}_k | \mathbf{x}_k) p(\mathbf{x}_k | \mathbf{x}_{k-1})}{p(\mathbf{y}_k, \mathbf{y}_{1:k-1})} \quad (\text{C.15})$$

Then, using (C.13), (C.14) and (C.15), particles are updated recursively as,

$$\begin{aligned}
w_k^i &\propto \frac{p(\mathbf{x}_{0:k} | \mathbf{y}_{1:k})}{q(\mathbf{x}_{0:k} | \mathbf{y}_{1:k})} \\
&\propto \frac{p(\mathbf{x}_{0:k-1} | \mathbf{y}_{0:k-1}) p(\mathbf{y}_k | \mathbf{x}_k) p(\mathbf{x}_k | \mathbf{x}_{k-1})}{q(\mathbf{x}_k | \mathbf{x}_{0:k-1}, \mathbf{y}_{1:k}) q(\mathbf{x}_{0:k-1}, \mathbf{y}_{1:k-1})} \\
&\propto w_{k-1}^i \frac{p(\mathbf{y}_k | \mathbf{x}_k) p(\mathbf{x}_k | \mathbf{x}_{k-1})}{q(\mathbf{x}_k | \mathbf{x}_{0:k-1}, \mathbf{y}_{1:k})}
\end{aligned} \tag{C.16}$$

With $q(\mathbf{x}_k^i | \mathbf{x}_{0:k-1}^i, \mathbf{y}_{1:k}) = q(\mathbf{x}_k^i | \mathbf{x}_{k-1}^i, \mathbf{y}_k)$, the importance density becomes dependent only upon \mathbf{x}_{k-1} and \mathbf{y}_k . Note that this is desirable and suitable for online implementation. Thus, only filtered estimate $p(\mathbf{x}_k | \mathbf{y}_{1:k})$ is required at each step, calling for storage of \mathbf{x}_k^i and $\mathbf{y}_{1:k}$; and discarding the previous state path up to $\mathbf{x}_{0:k-1}^i$. Thus, update step can be modified as,

$$w_k^i \propto w_{k-1}^i \frac{p(\mathbf{y}_k | \mathbf{x}_k^i) p(\mathbf{x}_k^i | \mathbf{x}_{k-1}^i)}{q(\mathbf{x}_k^i | \mathbf{x}_{0:k-1}^i, \mathbf{y}_{1:k})} \tag{C.17}$$

Then, the posterior filtered PDF $p(\mathbf{x}_k | \mathbf{y}_{1:k})$ is approximated as,

$$p(\mathbf{x}_k | \mathbf{y}_{1:k}) \approx \sum_{i=1}^N w_k^i \delta(\mathbf{x}_{0:k} - \mathbf{x}_{0:k}^i) \tag{C.18}$$

Substitution of priori state $p(\mathbf{x}_k | \mathbf{x}_{k-1})$ for importance density in (C.17) leads to a simplified update of particle weight as,

$$w_k^i \propto w_{k-1}^i p(\mathbf{y}_k | \mathbf{x}_k^i) \tag{C.19}$$

This simplified algorithm can be used for recursive estimation as the observations arrive sequentially. The likelihood functions of the new observations result in evaluation of weights of newly generated particles.

C.3. Particle Degeneracy and Resampling

While generating the estimate, the Monte Carlo procedure discussed above, ignores the state value of particles in state space (Ghahramani et al., 2002). During propagation step, the approximation density is adjusted through re-weighting of the particles. As a consequence, the approximation density is adjusted through re-weighting of the particles. After a few iterations, the weight concentrates on few particles only. This results in most of the particles having

negligible weight leading to the problem of namely, *sample degeneracy* (Doucet et al., 2001). It is an inherent default in SIS particle filters. to resolve this issue, the standard SIS is accompanied by a *resampling* step (referred to as Sampling-Importance resampling SIR) (Arulampalam et al., 2002). Here, the particles are forced in the region of high likelihood by multiplying high weighted particles and abandoning low weighted particles. In other words, *resampling* step involves elimination of those particles that have small weights so that focus shifts on the particles with large weight. This step results in generation of new set of particles $\{(\mathbf{x}_{0:k}^{i*}), w_k^i\}_{i=1}^N$ by resampling, without replacement, N times from the discrete approximation of $p(\mathbf{x}_k | \mathbf{y}_{1:k})$ as,

$$p(\mathbf{x}_k | \mathbf{y}_{1:k}) \approx \sum_{i=1}^N w_k^i \cdot \delta_{(\mathbf{x}_{0:k}^i)}(d\mathbf{x}_{0:k}) \quad (\text{C.20})$$

such that $Pr(\mathbf{x}_k^{i*} = \mathbf{x}_k^i) = w_k^i$. The new set of particles represents i.i.d from (C.20) and thus, the particle weights are reset again as $w_k^i = 1/N$. Fig. C-1 illustrates the principle of SIR particle filters.

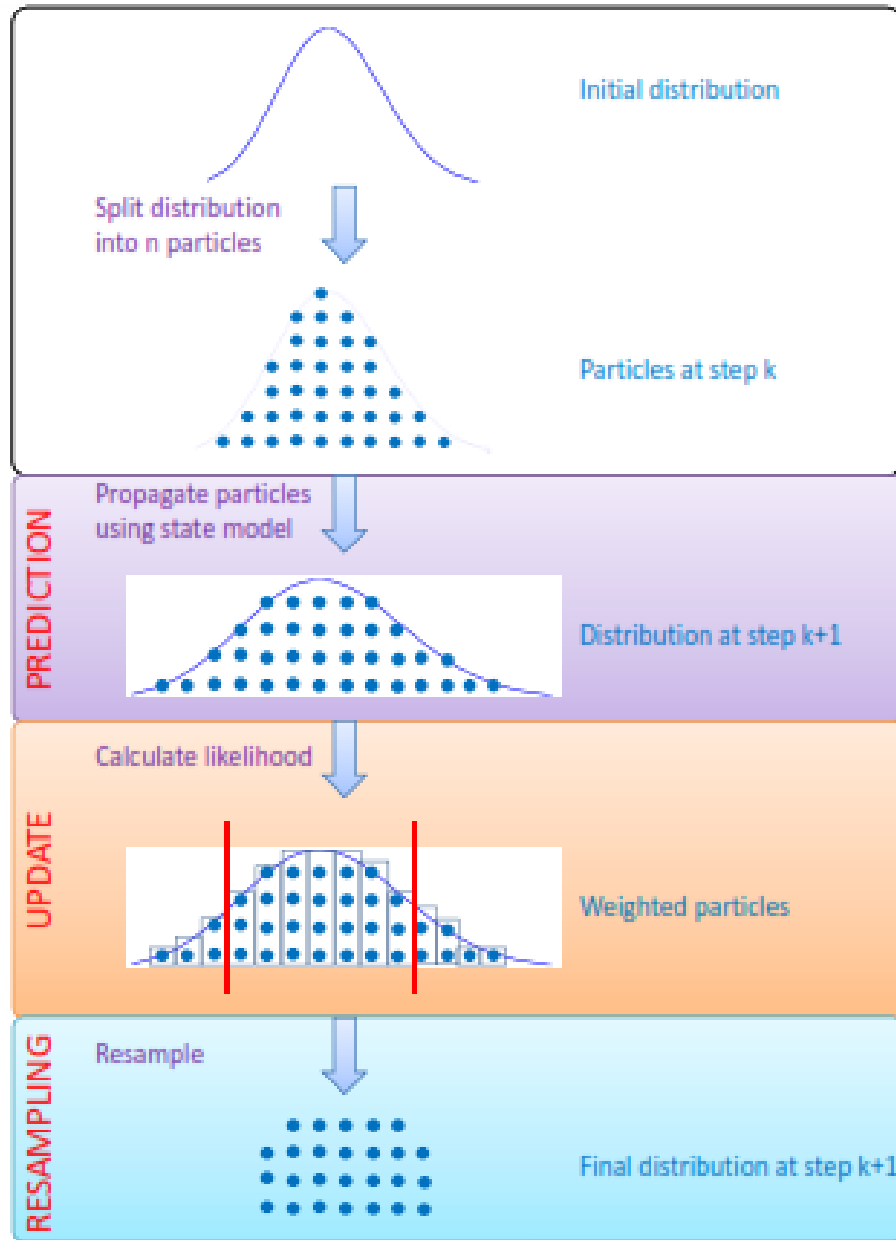


Fig. C-1 Principle of SIR particle filters (Jouin et al., 2014)

Appendix D Matlab and Simulink Code

Here, the SIMULINK interface and programation done in Matlab for execution of the various algorithms detailed in Chapter 3 and 4, are given.

D.1. Programation Code in Chapter 3

The interface of the Simulink model used for estimation of state of health and RUL prediction is shown in Fig. D-1. The Matlab code used for estimation of state of health and RUL prediction is written in the *Matlab Function Block*. Note that in the code given below, **x** represents the state variable of the fault model and **alpha** represents the degradation progression parameter. The code is given below:

```
function
[mean_x,max_x,min_x,x_para,alpha_para,RUL,rad_a,rmad_a,sigma_a,mean_alpha,prm
se_alpha,mean_RUL,max_alpha,min_alpha]
= fcn(start,u,condition,time)
%#codegen

persistent x alpha k v21

coder.extrinsic('prctile');
%coder.extrinsic('normpdf'); %normpdf cant be used in real time exwcution
%as it is not supported for the same in Matlab2013
%coder.extrinsic('tic');
%coder.extrinsic('toc');

%intializing the various variables at start
alpha_true=....;
np=500;
step_size=0.1;
w1=; % noise of the residual assumed by particle filter
v1=; %process noise
v2=; % artificial random walk noise
PP=; %intial proportional constant for variance control

mad_a=0;rmad_a=0;sigma_a=0;mean_alpha=0;

q=1;

RUL=zeros(1,np);
mean_RUL=0;
prmse_alpha=0;
```



```

lower_true_alpha=; %lower limit of true value of alpha is pre-decided
higher_true_alpha=; %higher limit of true value of alpha is pre-decided

if isempty(v21)
    v21=v2;
end

cdf=zeros(1,np);
x_para=zeros(1,np);
alpha_para=ones(1,np);

if isempty(x)
    x= 0*[1:np];
end

if isempty(alpha)
    alpha=zeros(1,np);
end

if isempty(k)
    k=0;
end

k=k+1;

mean_alpha=mean(alpha);
min_alpha=min(alpha);
max_alpha=max(alpha);

mean_x=mean(x_para);
min_x=min(x_para);
max_x=max(x_para);

if start==1 %detection of degradation

mad_a=median(abs(alpha-median(alpha)));
sigma_a=1.4826*mad_a;
rmad_a=100.*(mad_a./median(alpha));

% variance control scheme
if condition > lower_true_alpha && condition < higher_true_alpha

    v21=v21*(1+(PP*(10-rmad_a)/10));

else
    v21=v2;
end

% predictor step : the fault model is simulated one step to predict the
% value of state at the next step

```

```

x=x+(step_size.*alpha)+(v1.*randn(size(x)));
%x=x.*(exp(step_size.*alpha)+(v1.*randn(size(x)))); this can be used when
%the fault model follows the exponential dynamics
alpha=alpha+(v21.*randn(size(alpha)));

% likel=normpdf(u,x,w1); here normpdf can't be used as it is not
%not supported for the real time excution in Matlab2013.
% thus, the pdf function is created using supported functionalities.
% such a use of normpdf is supported in Matlab2015

likel=zeros(1,np);

u1=u.*(ones(1,np));
w11=w1.*(ones(1,np));

%.....
a=2*((w11).^2);
b=(u1-x).^2;

c=(a.*pi);
c1=c^(1/2);
c2=1./(c1);

d=(-1./a);
d1=(d.*b);
d2=exp(d1);

%.....
likel=c2.*d2;
%.....

% resampling step

for i=1:np;
    cdf(i)=sum(likel(1:i));
end;

cdf=cdf./max(cdf);

for i=1:np;
    u=rand;
    loca=find(cdf >= u);
    x_para(:,i)=x(:,loca(1));
    alpha_para(:,i)=alpha(:,loca(1));
end;

```

```

        %state variables are updated
x=x_para;
alpha=alpha_para;

mean_alpha=mean(alpha);

x_test=x_para;
alpha_test=alpha_para;

mean_x=mean(x_para);
min_x=min(x_para);
max_x=max(x_para);

mean_alpha=mean(alpha);
min_alpha=min(alpha);
max_alpha=max(alpha);
%%
%PRMSE metric
prmse_alpha=((mean(alpha_para)-alpha_true)./(alpha_true))^2;
%%

perc_x=prctile(x_para,50);
perc_alpha=prctile(alpha_para,50);

sort_alpha=sort(alpha_para);
sorted=sort_alpha(:,50);

%RUL prediction step
.....

tic %to record the computational time
thres=; % threshold value is pre-decided
for i=1:np;
    q=0;
    while x_test(:,i)<=thres ;
        % x_test=x_test.*(exp(step_size.*alpha_test));
        x_test(:,i)=x_test(:,i)+(step_size.*alpha_test(:,i));

        q=q+1;

        end
    RUL(:,i)=q*step_size;

end

```

```
mean_RUL=mean(RUL);
toc

else
    x_para=zeros(1,np);
    % x_para=0.16.*ones(1,np);
    alpha_para=zeros(1,np);
    perc_x=0;
    perc_alpha=0;

    mean_alpha=mean(alpha);
    min_alpha=min(alpha);
    max_alpha=max(alpha);

    RUL=zeros(1,np);
    mean_RUL=0;

    mean_x=mean(x_para);
    min_x=min(x_para);
    max_x=max(x_para);

    mad_a=0;rmad_a=0;sigma_a=0;mean_alpha=0;

    prmse_alpha=0;
end
end
```

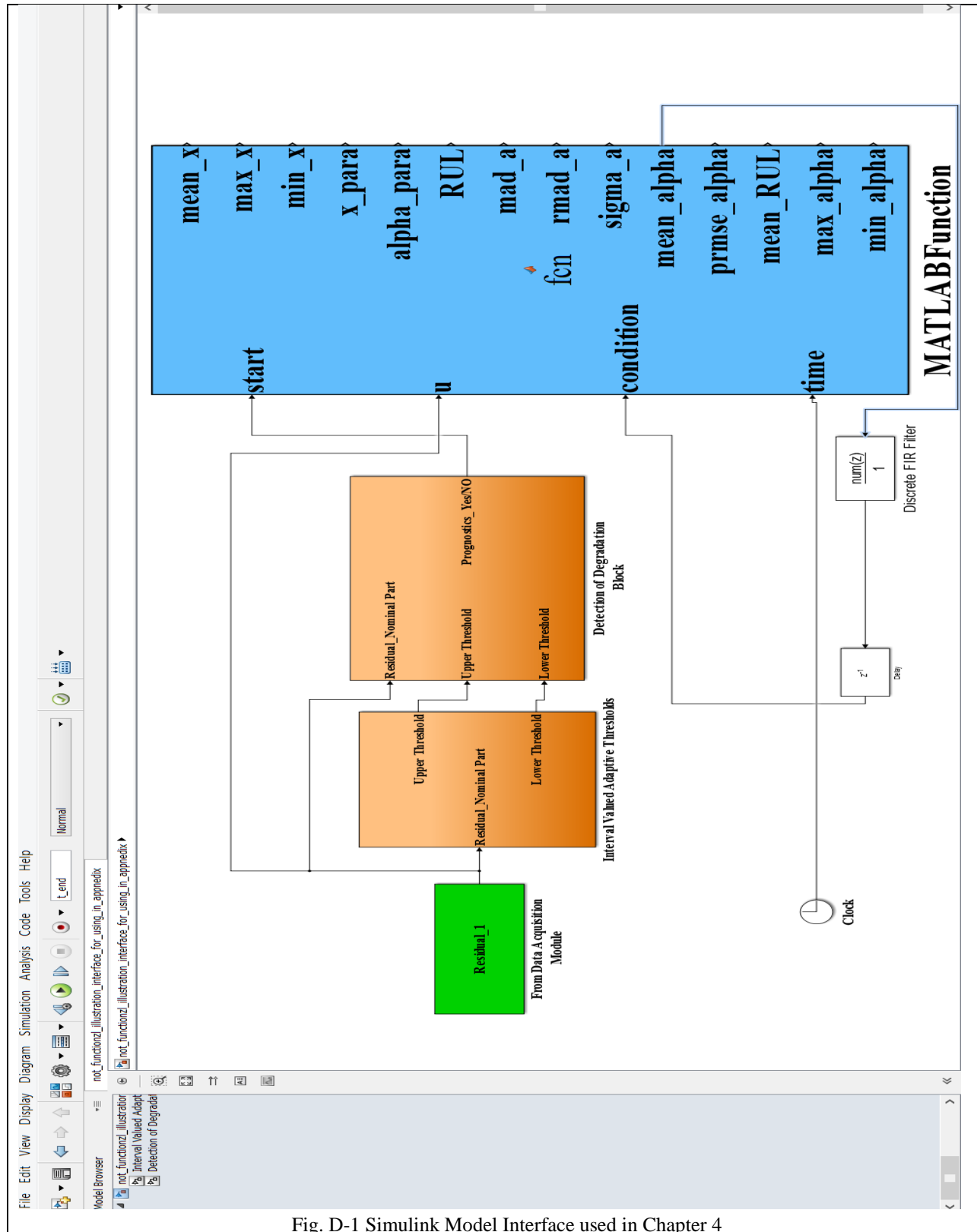



Fig. D-1 Simulink Model Interface used in Chapter 4

D.2. Programation code in Chapter 4

The Simulink model interface utilized in Chapter 4 is shown in Fig. D-2. The Matlab code used for estimation of state of health and RUL prediction is written in the *Matlab Function Block*. It is given below:

```
function
[alpha_para,mean_alpha,max_alpha,min_alpha,mean_beta,max_beta,min_beta,est_re
s,min_est_residual,max_est_residual,RUL,mean_RUL,max_RUL,min_RUL,elapsed_time
,beta_para]
= fcn(residual,I_fc,B,T,IL0,R0,n,time,start)
%#codegen

persistent alpha k beta

coder.extrinsic('prctile');
coder.extrinsic('normpdf');
coder.extrinsic('tic');
coder.extrinsic('toc');

% intializing the variables at the start

elapsed_time=0; % to record Computaitonal time

np=2000; % Number of PARTICLES
step_size=1; % step size

w1=.....; % residual noise
v1=.....; %process noise
v2=.....; % artificial noise

RUL=zeros(1,np);
max_RUL=max(RUL);
min_RUL=min(RUL);
mean_RUL=mean(RUL);

est_res=0.0;
min_est=min(est_res);
max_est=max(est_res);

cdf=zeros(1,np);

alpha_para=zeros(1,np);
beta_para=zeros(1,np);

% prmse_alpha=0;

if isempty(beta)
```

```

%   alpha=0*[1:np];
    beta=0.*ones(1,np);
end

if isempty(alpha)
%   alpha=0*[1:np];
    alpha=0.*ones(1,np);
end

if isempty(k)
%   alpha=0*[1:np];
    k=0;
end
k=k+1;

max_alpha=max(alpha);
min_alpha=min(alpha);

max_beta=max(beta);
min_beta=min(beta);

if start==1 % the estimation and prediction of RUL starts
                %when the residual is detected outside the LFT thresholds

% fault model is simulated to predict the next state

alpha=alpha+beta.*1+(v1.*randn(size(alpha)));

beta=beta+(v2.*randn(size(beta)));

% a condition is out so that logarithmic argument is never negative
if (min(IL0.*(1-alpha))-im <5;
    im=min((IL0.*(1-alpha))-20;
else
    im=im;
end

% update step
gg=n.*((im*R0.*alpha)+(B*T*log(1-(im./(IL0.*(1-alpha)))))-(B*T*log(1-
(im/IL0))));
likel=normpdf(u,gg,w1);

% resampling step

for i=1:np;
    cdf(i)=sum(likel(1:i));
end;

```



```

cdf=cdf./max(cdf);

    for i=1:np;
        u=rand;
        loca=find(cdf >= u);
        alpha_para(:,i)=alpha(:,loca(1));
        beta_para(:,i)=beta(:,loca(1));
    end;

    %variables are updated with the estimated value
alpha=alpha_para;
beta=beta_para;

mean_alpha=mean(alpha);
max_alpha=max(alpha);
min_alpha=min(alpha);

mean_beta=mean(beta);
max_beta=max(beta);
min_beta=min(beta);

alpha_test=alpha_para;
beta_test=beta_para;

est_res=mean(gg);
min_est=min(gg);
max_est=max(gg);

% RUL prediction step
thres=0.12; %theshold is decided beforehand
tic % computational time is recorded

% the fault model is simulated and particles are projected in future

for i=1:np;
    q=0;
while alpha_test(:,i)<=thres && alpha_test(:,i)>0;
    alpha_test(:,i)=alpha_test(:,i)+(step_size.*beta_test(:,i));

    q=q+1;
end

RUL(:,i)=q*step_size;
end

```

```
%rul variables are updated
max_RUL=max(RUL);
min_RUL=min(RUL);
mean_RUL=mean(RUL);

% computational time is stored
elapsed_time= toc;
%%
else

alpha_para=zeros(1,np);
beta_para=zeros(1,np);

RUL=zeros(1,np);
max_RUL=max(RUL);
min_RUL=min(RUL);
mean_RUL=mean(RUL);

mean_alpha=0;
max_alpha=max(alpha);
min_alpha=min(alpha);

mean_beta=0;
max_beta=max(beta);
min_beta=min(beta);

elapsed_time=0;
end
```

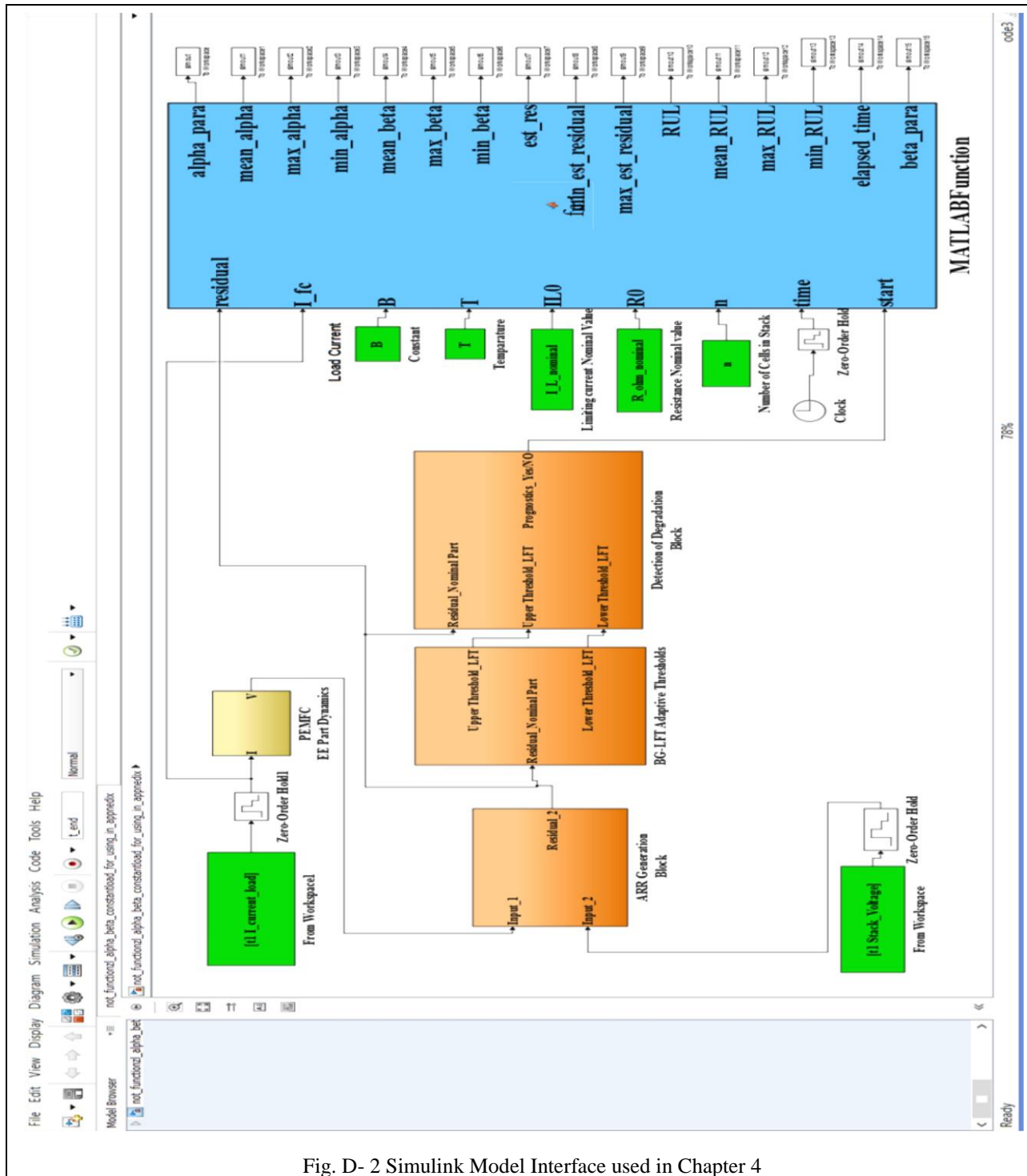


Fig. D- 2 Simulink Model Interface used in Chapter 4

References

- Abbas, M., Ferri, A. A., Orchard, M. E., & Vachtsevanos, G. J. (2007). *An intelligent diagnostic/prognostic framework for automotive electrical systems*. Paper presented at the Intelligent Vehicles Symposium, 2007 IEEE.
- An, D., Choi, J.-H., & Kim, N. H. (2013). Prognostics 101: A tutorial for particle filter-based prognostics algorithm using Matlab. *Reliability Engineering & System Safety*, *115*(0), 161-169.
- An, D., Kim, N. H., & Choi, J.-H. (2015). Practical options for selecting data-driven or physics-based prognostics algorithms with reviews. *Reliability Engineering & System Safety*, *133*, 223-236.
- Armengol, J., Vehí, J., Travé-Massuyès, L., & Sainz, M. Á. (2001). Application of modal intervals to the generation of error-bounded envelopes. *Reliable Computing*, *7*(2), 171-185.
- Armengol Llobet, J. (2000). *Application of Modal Interval Analysis to the simulation of the behaviour of dynamic systems with uncertain parameters*: Universitat de Girona.
- Arogeti, S. A., Danwei, W., Chang Boon, L., & Ming, L. (2013). Energy-Based Mode Tracking of Hybrid Systems for FDI. *Systems, Man, and Cybernetics: Systems, IEEE Transactions on*, *43*(1), 14-28.
- Artes, M., Del Castillo, L., & Perez, J. (2003). *Failure prevention and diagnosis in machine elements using cluster*. Paper presented at the Proceedings of the Tenth International Congress on Sound and Vibration, Stockholm, Sweden.
- Arulampalam, M. S., Maskell, S., Gordon, N., & Clapp, T. (2002). A tutorial on particle filters for online nonlinear/non-Gaussian Bayesian tracking. *Signal Processing, IEEE Transactions on*, *50*(2), 174-188.
- Baraldi, P., Cadini, F., Mangili, F., & Zio, E. (2013a). Model-based and data-driven prognostics under different available information. *Probabilistic Engineering Mechanics*, *32*, 66-79.
- Baraldi, P., Mangili, F., & Zio, E. (2013b). Investigation of uncertainty treatment capability of model-based and data-driven prognostic methods using simulated data. *Reliability Engineering & System Safety*, *112*(0), 94-108.
- Baruah, P., & Chinnam*, R. B. (2005). HMMs for diagnostics and prognostics in machining processes. *International Journal of Production Research*, *43*(6), 1275-1293.
- Basseville, M., & Nikiforov, I. V. (1993). *Detection of abrupt changes: theory and application* (Vol. 104): Prentice Hall Englewood Cliffs.
- Bechhoefer, E. (2008). *A method for generalized prognostics of a component using Paris law*. Paper presented at the Annual Forum Proceedings-American Helicopter Society.
- Bengtsson, M. (2004). Condition based maintenance system technology—Where is development heading. *Condition Based Maintenance Systems—An Investigation Of Technical Constituents And Organizational Aspects*, 55.
- Benmoussa, S., Bouamama, B. O., & Merzouki, R. (2014). Bond Graph Approach for Plant Fault Detection and Isolation: Application to Intelligent Autonomous Vehicle. *Automation Science and Engineering, IEEE Transactions on*, *11*(2), 585-593.
- Biagetti, T., & Sciubba, E. (2004). Automatic diagnostics and prognostics of energy conversion processes via knowledge-based systems. *Energy*, *29*(12), 2553-2572.

- Blanke, M., Kinnaert, M., Lunze, J., Staroswiecki, M., & Schrder, J. (2010). *Diagnosis and fault-tolerant control*: Springer Publishing Company, Incorporated.
- Blanke, M., Staroswiecki, M., & Wu, N. E. (2001). *Concepts and methods in fault-tolerant control*. Paper presented at the American Control Conference, 2001. Proceedings of the 2001.
- Blischke, W. R., & Murthy, D. P. (2011). *Reliability: modeling, prediction, and optimization* (Vol. 767): John Wiley & Sons.
- Borutzky, W. (2009a). *Bond graph methodology: development and analysis of multidisciplinary dynamic system models*: Springer Science & Business Media.
- Borutzky, W. (2009b). Bond graph model-based fault detection using residual sinks. *Proceedings of the Institution of Mechanical Engineers, Part I: Journal of Systems and Control Engineering*, 223(3), 337-352.
- Borutzky, W. (2011). *Bond Graph Modelling of Engineering Systems*: Springer.
- Borutzky, W. (2014). Bond graph model-based system mode identification and mode-dependent fault thresholds for hybrid systems. *Mathematical and Computer Modelling of Dynamical Systems*(ahead-of-print), 1-32.
- Borutzky, W. (2015). Failure Prognosis for Hybrid Systems Based on ARR Residuals *Bond Graph Model-based Fault Diagnosis of Hybrid Systems* (pp. 221-233): Springer.
- Borutzky, W., & Dauphin-Tanguy, G. (2004). Incremental bond graph approach to the derivation of state equations for robustness study. *Simulation Modelling Practice and Theory*, 12(1), 41-60.
- Borutzky, W., & Granda, J. (2001). Determining sensitivities from an incremental true bond graph. *SIMULATION SERIES*, 33(1), 3-8.
- Borutzky, W., & Granda, J. (2002). Bond graph based frequency domain sensitivity analysis of multidisciplinary systems. *Proceedings of the Institution of Mechanical Engineers, Part I: Journal of Systems and Control Engineering*, 216(1), 85-99.
- Bouamama, B. O., Biswas, G., Loureiro, R., & Merzouki, R. (2014). Graphical methods for diagnosis of dynamic systems: Review. *Annual Reviews in Control*, 38(2), 199-219.
- Bouamama, B. O., Samantaray, A., Staroswiecki, M., & Dauphin-Tanguy, G. (2003). Derivation of constraint relations from bond graph models for fault detection and isolation. *SIMULATION SERIES*, 35(2), 104-109.
- Box, G. E., Jenkins, G. M., & Reinsel, G. C. (2011). *Time series analysis: forecasting and control* (Vol. 734): John Wiley & Sons.
- Bressel, M., Hilairet, M., Hissel, D., & Ould-Bouamama, B. (2015). Extended Kalman Filter for Prognostic of Proton Exchange Membrane Fuel Cell. *Submitted to Applied Energy*.
- Broenink, J. F. (1997). Modelling, simulation and analysis with 20-sim. *Journal A*, 38(3), 22-25.
- Byington, C. S., & Roemer, M. J. (2002). *Prognostic enhancements to diagnostic systems for improved condition-based maintenance [military aircraft]*. Paper presented at the Aerospace Conference Proceedings, 2002. IEEE.
- Cadini, F., Zio, E., & Avram, D. (2009). Monte Carlo-based filtering for fatigue crack growth estimation. *Probabilistic Engineering Mechanics*, 24(3), 367-373.
- Caesarendra, W., Widodo, A., & Yang, B.-S. (2010). Application of relevance vector machine and logistic regression for machine degradation assessment. *Mechanical Systems and Signal Processing*, 24(4), 1161-1171.

- Calderón-Espinoza, G., Armengol, J., Vehí, J., & Gelso, E. R. (2007). Dynamic diagnosis based on interval analytical redundancy relations and signs of the symptoms. *AI Communications*, 20(1), 39-47.
- Celaya, J., Kulkarni, C., Biswas, G., Saha, S., & Goebel, K. (2011). A model-based prognostics methodology for electrolytic capacitors based on electrical overstress accelerated aging.
- Chang Boon, L., Danwei, W., Arogeti, S., & Jing Bing, Z. (2010). Causality Assignment and Model Approximation for Hybrid Bond Graph: Fault Diagnosis Perspectives. *Automation Science and Engineering, IEEE Transactions on*, 7(3), 570-580.
- Chang, I.-C., Yu, C.-C., & Liou, C.-T. (1994). Model-based approach for fault diagnosis. 1. Principles of deep model algorithm. *Industrial & engineering chemistry research*, 33(6), 1542-1555.
- Chen, H., Pei, P., & Song, M. (2015). Lifetime prediction and the economic lifetime of Proton Exchange Membrane fuel cells. *Applied Energy*, 142, 154-163.
- Chen, J., & Patton, R. (1999). Robust Model-based Fault Diagnosis for Dynamic Systems.
- Chen, J., & Patton, R. J. (2012a). *Robust model-based fault diagnosis for dynamic systems* (Vol. 3): Springer Science & Business Media.
- Chen, J., & Patton, R. J. (2012b). *Robust model-based fault diagnosis for dynamic systems*: Springer Publishing Company, Incorporated.
- Chisci, L., Garulli, A., & Zappa, G. (1996). Recursive state bounding by parallelotopes. *Automatica*, 32(7), 1049-1055.
- Chow, E. Y., & Willsky, A. S. (1984). Analytical redundancy and the design of robust failure detection systems. *Automatic Control, IEEE Transactions on*, 29(7), 603-614.
- Cordier, M.-O., Dague, P., Dumas, M., Lévy, F., Montmain, J., Staroswiecki, M., & Travé-Massuyes, L. (2000). *A comparative analysis of AI and control theory approaches to model-based diagnosis*. Paper presented at the ECAI.
- Daigle, M., & Goebel, K. (2009). *Model-based prognostics with fixed-lag particle filters*. Paper presented at the Conference of the PHM Society.
- Daigle, M., & Goebel, K. (2010). *Model-based prognostics under limited sensing*. Paper presented at the Aerospace Conference, 2010 IEEE.
- Daigle, M., Saha, B., & Goebel, K. (2012). *A comparison of filter-based approaches for model-based prognostics*. Paper presented at the Aerospace Conference, 2012 IEEE.
- Daigle, M. J., Bregon, A., & Roychoudhury, I. (2014). Distributed prognostics based on structural model decomposition.
- Daigle, M. J., & Goebel, K. (2011a). A Model-Based Prognostics Approach Applied to Pneumatic Valves. *International Journal of Prognostics and Health Management*, 2(2).
- Daigle, M. J., & Goebel, K. (2011b). A model-based prognostics approach applied to pneumatic valves. *International Journal of Prognostics and Health Management Volume 2 (color)*, 84.
- Daigle, M. J., & Goebel, K. (2013). Model-based prognostics with concurrent damage progression processes. *Systems, Man, and Cybernetics: Systems, IEEE Transactions on*, 43(3), 535-546.
- Dauphin-Tanguy, G., & Kam, C. S. (1999). *How to model parameter uncertainties in a bond graph framework*. Paper presented at the Simulation in Industry, 11th European Simulation Symposium, ESS.
- De Bruijn, F., Dam, V., & Janssen, G. (2008). Review: durability and degradation issues of PEM fuel cell components. *Fuel cells*, 8(1), 3.

- de Kleer, J., Hamsher, W., & Console, L. (1992). Readings in model-based diagnosis. *Readings in model-based diagnosis, chapter Diagnosing multiple faults*, 100-117.
- de Kleer, J., & Kurien, J. (2004). *Fundamentals of model-based diagnosis*. Paper presented at the Proc. 5th IFAC Symposium on Fault Detection, Supervision, and Safety of Technical Processes (Safeprocess).
- De Kleer, J., & Williams, B. C. (1987). Diagnosing multiple faults. *Artificial intelligence*, 32(1), 97-130.
- Djeziri, M., Ananou, B., & Ouladsine, M. (2013a). *Data driven and model based fault prognosis applied to a mechatronic system*. Paper presented at the Power Engineering, Energy and Electrical Drives (POWERENG), 2013 Fourth International Conference on.
- Djeziri, M., Toubakh, H., & Ouladsine, M. (2013b). *Fault prognosis based on fault reconstruction: Application to a mechatronic system*. Paper presented at the Systems and Control (ICSC), 2013 3rd International Conference on.
- Djeziri, M. A., Merzouki, R., & Bouamama, B. O. (2009a). Robust Monitoring of an Electric Vehicle With Structured and Unstructured Uncertainties. *Vehicular Technology, IEEE Transactions on*, 58(9), 4710-4719.
- Djeziri, M. A., Merzouki, R., Bouamama, B. O., & Dauphin-Tanguy, G. (2007). Robust fault diagnosis by using bond graph approach. *Mechatronics, IEEE/ASME Transactions on*, 12(6), 599-611.
- Djeziri, M. A., Ould Bouamama, B., & Merzouki, R. (2009b). Modelling and robust FDI of steam generator using uncertain bond graph model. *Journal of Process Control*, 19(1), 149-162.
- Doucet, A., De Freitas, N., & Gordon, N. (2001). *An introduction to sequential Monte Carlo methods*: Springer.
- Doucet, A., & Johansen, A. M. (2009). A tutorial on particle filtering and smoothing: Fifteen years later. *Handbook of Nonlinear Filtering*, 12, 656-704.
- Dragomir, O. E., Gouriveau, R., Zerhouni, N., & Dragomir, F. (2007). *Framework for a distributed and hybrid prognostic system*. Paper presented at the 4th IFAC Conference on Management and Control of Production and Logistics, MCPL'2007.
- El Harabi, R., Ould-Bouamama, B., Gayed, M. K. B., & Abdelkrim, M. N. (2010). *Pseudo bond graph for fault detection and isolation of an industrial chemical reactor part I: bond graph modeling*. Paper presented at the Proceedings of the 2010 Spring Simulation Multiconference.
- Emami-Naeini, A., Akhter, M. M., & Rock, S. M. (1988). Effect of model uncertainty on failure detection: the threshold selector. *Automatic Control, IEEE Transactions on*, 33(12), 1106-1115.
- Engel, S. J., Gilmartin, B. J., Bongort, K., & Hess, A. (2000). *Prognostics, the real issues involved with predicting life remaining*. Paper presented at the Aerospace Conference Proceedings, 2000 IEEE.
- Fowler, M. W., Mann, R. F., Amphlett, J. C., Peppley, B. A., & Roberge, P. R. (2002). Incorporation of voltage degradation into a generalised steady state electrochemical model for a PEM fuel cell. *Journal of Power Sources*, 106(1), 274-283.
- Frank, P. M. (1990). Fault diagnosis in dynamic systems using analytical and knowledge-based redundancy: A survey and some new results. *Automatica*, 26(3), 459-474.
- Fugate, M. L., Sohn, H., & Farrar, C. R. (2001). Vibration-based damage detection using statistical process control. *Mechanical systems and signal processing*, 15(4), 707-721.

- Garga, A. K., McClintic, K. T., Campbell, R. L., Yang, C.-C., Lebold, M. S., Hay, T., & Byington, C. S. (2001). *Hybrid reasoning for prognostic learning in CBM systems*. Paper presented at the Aerospace Conference, 2001, IEEE Proceedings.
- Ghahramani, Z., & Rasmussen, C. E. (2002). *Bayesian monte carlo*. Paper presented at the Advances in neural information processing systems.
- Goebel, K., Saha, B., & Saxena, A. (2008). *A comparison of three data-driven techniques for prognostics*. Paper presented at the 62nd meeting of the society for machinery failure prevention technology (mfpt).
- Guo, H., & Liao, H. (2015). *Practical Approaches for Reliability Evaluation Using Degradation Data*. Paper presented at the Annual Reliability and Maintainability Symposium.
- Hamelin, F., & Sauter, D. (2000). Robust fault detection in uncertain dynamic systems. *Automatica*, 36(11), 1747-1754.
- Hansen, E., & Walster, G. W. (2003). *Global optimization using interval analysis: revised and expanded* (Vol. 264): CRC Press.
- Haykin, S. (2004). *Kalman filtering and neural networks* (Vol. 47): John Wiley & Sons.
- Heimes, F. O. (2008). *Recurrent neural networks for remaining useful life estimation*. Paper presented at the Prognostics and Health Management, 2008. PHM 2008. International Conference on.
- Helton, J. C. (1993). Uncertainty and sensitivity analysis techniques for use in performance assessment for radioactive waste disposal. *Reliability Engineering & System Safety*, 42(2), 327-367.
- Heng, A., Tan, A. C., Mathew, J., Montgomery, N., Banjevic, D., & Jardine, A. K. (2009). Intelligent condition-based prediction of machinery reliability. *Mechanical systems and signal processing*, 23(5), 1600-1614.
- Herrero, P., Calm, R., Vehí, J., Armengol, J., Georgiou, P., Oliver, N., & Tomazou, C. (2012). Robust fault detection system for insulin pump therapy using continuous glucose monitoring. *Journal of diabetes science and technology*, 6(5), 1131-1141.
- Herzog, M. A., Marwala, T., & Heyns, P. S. (2009). Machine and component residual life estimation through the application of neural networks. *Reliability Engineering & System Safety*, 94(2), 479-489.
- Hess, A., Calvello, G., Frith, P., Engel, S., & Hoitsma, D. (2006). *Challenges, issues, and lessons learned chasing the "Big P": real predictive prognostics Part 2*. Paper presented at the Aerospace Conference, 2006 IEEE.
- Hohenbichler, M., Gollwitzer, S., Kruse, W., & Rackwitz, R. (1987). New light on first-and second-order reliability methods. *Structural safety*, 4(4), 267-284.
- Hu, C., Youn, B. D., Wang, P., & Yoon, J. T. (2012). Ensemble of data-driven prognostic algorithms for robust prediction of remaining useful life. *Reliability Engineering & System Safety*, 103, 120-135.
- Hu, Y., Baraldi, P., Di Maio, F., & Zio, E. (2015). A particle filtering and kernel smoothing-based approach for new design component prognostics. *Reliability Engineering & System Safety*, 134, 19-31.
- Isermann, R. (2005). Model-based fault-detection and diagnosis—status and applications. *Annual Reviews in control*, 29(1), 71-85.
- ISO13381-1. (2004). Condition Monitoring And Diagnostics Of Machines –Prognostics - Part 1: General Guidelines *Mechanical systems and signal processing*.

- Janati-Idrissi, H., Adrot, O., Ragot, J., & Kratz, F. (2002). *Fault detection of uncertain models using polytope projection*. Paper presented at the 15th IFAC World Congress on Automatic Control.
- Jardine, A. K., Lin, D., & Banjevic, D. (2006). A review on machinery diagnostics and prognostics implementing condition-based maintenance. *Mechanical systems and signal processing*, 20(7), 1483-1510.
- Jaulin, L., & Walter, E. (1993). Set inversion via interval analysis for nonlinear bounded-error estimation. *Automatica*, 29(4), 1053-1064.
- Jouin, M., Gouriveau, R., Hissel, D., Péra, M.-C., & Zerhouni, N. (2014). Prognostics of PEM fuel cell in a particle filtering framework. *International Journal of Hydrogen Energy*, 39(1), 481-494.
- Kam, C. S., & Dauphin-Tanguy, G. (2005). Bond graph models of structured parameter uncertainties. *Journal of the Franklin Institute*, 342(4), 379-399.
- Kapur, K. C., & Pecht, M. (2014). *Reliability engineering*: John Wiley & Sons.
- Karim, J., Jauberthie, C., & Combacau, M. (2008). *Model-based fault detection method using interval analysis: Application to an aeronautic test bench*. Paper presented at the 19th International Workshop on Principles of Diagnosis DX.
- Karnopp, D. C., Margolis, D. L., & Rosenberg, R. C. (2012). *System Dynamics: Modeling, Simulation, and Control of Mechatronic Systems*: Wiley.
- Katipamula, S., & Brambley, M. R. (2005). Review article: methods for fault detection, diagnostics, and prognostics for building systems—a review, Part I. *HVAC&R Research*, 11(1), 3-25.
- Kinnaert, M. (1999). Robust fault detection based on observers for bilinear systems. *Automatica*, 35(11), 1829-1842.
- Kleijn, C. (2011). Torsion Bar 2.0 Reference Manual. from http://www.20sim.com/downloads/files/Torsion_Bar_2.0_Reference_Manual.pdf
- Kleijn, C., Differ H.G. (2013). 20-SIM 4C 2.1 Reference Manual. from <http://www.20sim.com/downloads/files/20sim4C21.pdf>
- Klutke, G.-A., Kiessler, P. C., & Wortman, M. (2003). A critical look at the bathtub curve. *IEEE Transactions on Reliability*, 52(1), 125-129.
- Korbicz, J., Koscielny, J. M., Kowalczyk, Z., & Cholewa, W. (2012). *Fault diagnosis: models, artificial intelligence, applications*: Springer Science & Business Media.
- Krantz, S. G., & Parks, H. R. (2012). *The implicit function theorem: history, theory, and applications*: Springer Science & Business Media.
- Kuehl, R. W. (2010). Using the Arrhenius equation to predict drift in thin film resistors. *CARTS Europe*, 121-133.
- Kulkarni, C. S., Celaya, J. R., Goebel, K., & Biswas, G. (2012). Physics based electrolytic capacitor degradation models for prognostic studies under thermal overstress.
- Kumar, S., Torres, M., Chan, Y., & Pecht, M. (2008). *A hybrid prognostics methodology for electronic products*. Paper presented at the Neural Networks, 2008. IJCNN 2008.(IEEE World Congress on Computational Intelligence). IEEE International Joint Conference on.
- Laffly, E., Péra, M.-C., & Hissel, D. (2007). *Polymer electrolyte membrane fuel cell modelling and parameters estimation for ageing consideration*. Paper presented at the 2007 IEEE International Symposium on Industrial Electronics.
- Larminie, J., Dicks, A., & McDonald, M. S. (2003). *Fuel cell systems explained* (Vol. 2): Wiley New York.

- Lebold, M. S., Reichard, K. M., Ferullo, D., & Boylan, D. (2003). Open Systems Architecture For Condition-Based Maintenance: Overview And Training Manual. Penn State University/Applied Research Laboratory.
- Lee, J., Ni, J., Djurdjanovic, D., Qiu, H., & Liao, H. (2006). Intelligent prognostics tools and e-maintenance. *Computers in industry*, 57(6), 476-489.
- Li, T., Sun, S., Sattar, T. P., & Corchado, J. M. (2014). Fight sample degeneracy and impoverishment in particle filters: A review of intelligent approaches. *Expert Systems with applications*, 41(8), 3944-3954.
- Liao, L., & Kottig, F. (2014). Review of hybrid prognostics approaches for remaining useful life prediction of engineered systems, and an application to battery life prediction. *Reliability, IEEE Transactions on*, 63(1), 191-207.
- Liao, S.-H. (2005). Expert system methodologies and applications—a decade review from 1995 to 2004. *Expert systems with applications*, 28(1), 93-103.
- Lin, Y., & Stadtherr, M. A. (2007). Validated solutions of initial value problems for parametric ODEs. *Applied Numerical Mathematics*, 57(10), 1145-1162.
- Loureiro, R., Benmoussa, S., Touati, Y., Merzouki, R., & Ould Bouamama, B. (2014). Integration of Fault Diagnosis and Fault-Tolerant Control for Health Monitoring of a Class of MIMO Intelligent Autonomous Vehicles. *Vehicular Technology, IEEE Transactions on*, 63(1), 30-39.
- Lu, J.-C., Park, J., & Yang, Q. (1997). Statistical inference of a time-to-failure distribution derived from linear degradation data. *Technometrics*, 39(4), 391-400.
- Maricau, E., & Gielen, G. (2009). *A methodology for measuring transistor ageing effects towards accurate reliability simulation*. Paper presented at the On-Line Testing Symposium, 2009. IOLTS 2009. 15th IEEE International.
- Medjaher, K. (2011). A bond graph model-based fault detection and isolation. *Maintenance Modelling and Applications. Chapter 6: Fault Diagnostics.*, 503-512.
- Medjaher, K., Samantaray, A. K., Ould Bouamama, B., & Staroswiecki, M. (2006). Supervision of an industrial steam generator. Part II: Online implementation. *Control Engineering Practice*, 14(1), 85-96.
- Medjaher, K., & Zerhouni, N. (2009). *Residual-based failure prognostic in dynamic systems*. Paper presented at the 7th IFAC International Symposium on Fault Detection, Supervision and Safety of Technical Processes, SAFE PROCESS'09.
- Medjaher, K., & Zerhouni, N. (2013). Hybrid prognostic method applied to mechatronic systems. *The International Journal of Advanced Manufacturing Technology*, 69(1-4), 823-834.
- Merzouki, R., Medjaher, K., Djeziri, M. A., & Ould-Bouamama, B. (2007). Backlash fault detection in mechatronic system. *Mechatronics*, 17(6), 299-310.
- Milanese, M., Norton, J., Piet-Lahanier, H., & Walter, É. (2013). *Bounding approaches to system identification*: Springer Science & Business Media.
- Milanese, M., & Vicino, A. (1996). Optimal estimation theory for dynamic systems with set membership uncertainty: an overview *Bounding Approaches to System Identification* (pp. 5-27): Springer.
- Ming, Y., Danwei, W., Ming, L., & Lei, H. (2011). Prognosis of Hybrid Systems With Multiple Incipient Faults: Augmented Global Analytical Redundancy Relations Approach. *Systems, Man and Cybernetics, Part A: Systems and Humans, IEEE Transactions on*, 41(3), 540-551.

- Moore, R. E. (1979). *Methods and applications of interval analysis* (Vol. 2): SIAM.
- Moore, R. E., Kearfott, R. B., & Cloud, M. J. (2009). *Introduction to interval analysis*: Siam.
- Mukherjee, A., & Samantaray, A. K. (2006). *Bond graph in modeling, simulation and fault identification*: IK International Pvt Ltd.
- Nam, D. S., Han, C., Jeong, C. W., & Yoon, E. S. (1996). Automatic construction of extended symptom-fault associations from the signed digraph. *Computers & chemical engineering*, *20*, S605-S610.
- Neerukatti, R. K., Liu, K. C., Kovvali, N., & Chattopadhyay, A. (2014). Fatigue life prediction using hybrid prognosis for structural health monitoring. *Journal of Aerospace Information Systems*, *11*(4), 211-232.
- Niu, G., Zhao, Y., Defoort, M., & Pecht, M. (2014). Fault diagnosis of locomotive electro-pneumatic brake through uncertain bond graph modeling and robust online monitoring. *Mechanical Systems and Signal Processing*.
- Niu, G., Zhao, Y., Defoort, M., & Pecht, M. (2015). Fault diagnosis of locomotive electro-pneumatic brake through uncertain bond graph modeling and robust online monitoring. *Mechanical systems and signal processing*, *50*, 676-691.
- Orchard, M., Kacprzynski, G., Goebel, K., Saha, B., & Vachtsevanos, G. (2008). *Advances in uncertainty representation and management for particle filtering applied to prognostics*. Paper presented at the Prognostics and health management, 2008. phm 2008. international conference on.
- Orchard, M. E. (2007). *A particle filtering-based framework for on-line fault diagnosis and failure prognosis*. Georgia Institute of Technology.
- Ould-Bouamama, B., El Harabi, R., Abdelkrim, M. N., & Ben Gayed, M. (2012). Bond graphs for the diagnosis of chemical processes. *Computers & Chemical Engineering*, *36*, 301-324.
- Ould Bouamama, B., Medjaher, K., Samantaray, A. K., & Staroswiecki, M. (2006). Supervision of an industrial steam generator. Part I: Bond graph modelling. *Control Engineering Practice*, *14*(1), 71-83.
- Ouldbouamama, B., Chatti, N., & Gehin, A. (2013). *Signed Bond Graph for health monitoring of PEM fuel cell*. Paper presented at the 5th International Conference of Development of Fuel Cells, Karlsruhe, Germany.
- Paynter, H. (1961). *Analysis and Design of Engineering Systems*: M.I.T. Press.
- Peraza, C., Diaz, J. G., Arteaga-Bravo, F. J., Villanueva, C., & Gonzalez-Longatt, F. (2008). *Modeling and simulation of PEM fuel cell with bond graph and 20sim*. Paper presented at the American Control Conference, 2008.
- Plett, G. L. (2004). Extended Kalman filtering for battery management systems of LiPB-based HEV battery packs: Part 3. State and parameter estimation. *Journal of Power Sources*, *134*(2), 277-292.
- Pouliezos, A., & Stavrakakis, G. S. (2013). *Real time fault monitoring of industrial processes* (Vol. 12): Springer Science & Business Media.
- Qin, S. J. (2012). Survey on data-driven industrial process monitoring and diagnosis. *Annual Reviews in control*, *36*(2), 220-234.
- Rambeaux, F., Hamelin, F., & Sauter, D. (2000). Optimal thresholding for robust fault detection of uncertain systems. *International Journal of Robust and Nonlinear Control*, *10*(14), 1155-1173.

- Rausand, M., & Høyland, A. (2004). *System reliability theory: models, statistical methods, and applications* (Vol. 396): John Wiley & Sons.
- Redheffer, R. (1960). On a certain linear fractional transformation. *J. Math. Phys.*, 39(0960), 269-286.
- Rinner, B., & Weiss, U. (2004). Online monitoring by dynamically refining imprecise models. *Systems, Man, and Cybernetics, Part B: Cybernetics, IEEE Transactions on*, 34(4), 1811-1822.
- Roychoudhury, I., & Daigle, M. (2011). *An integrated model-based diagnostic and prognostic framework*. Paper presented at the Proceedings of the 22nd International Workshop on Principle of Diagnosis (DX'11). Murnau, Germany.
- Rump, S. M. (1999). *INTLAB—interval laboratory*: Springer.
- Saha, B., & Goebel, K. (2009a). *Modeling Li-ion battery capacity depletion in a particle filtering framework*. Paper presented at the Proceedings of the annual conference of the prognostics and health management society.
- Saha, B., Goebel, K., & Christophersen, J. (2009b). Comparison of prognostic algorithms for estimating remaining useful life of batteries. *Transactions of the Institute of Measurement and Control*.
- Saha, B., Goebel, K., Poll, S., & Christophersen, J. (2009c). Prognostics methods for battery health monitoring using a Bayesian framework. *Instrumentation and Measurement, IEEE Transactions on*, 58(2), 291-296.
- Sainz, M. A., Armengol, J., Calm, R., Herrero, P., Jorba, L., & Vehi, J. (2014). Modal Interval Analysis. *Lecture Notes in Mathematics*, 2091.
- Saisset, R., Fontes, G., Turpin, C., & Astier, S. (2006). Bond Graph model of a PEM fuel cell. *Journal of Power Sources*, 156(1), 100-107.
- Samantaray, A. K., & Bouamama, B. O. (2008). *Model-Based Process Supervision*: Springer.
- Samantaray, A. K., Medjaher, K., Bouamama, B. O., Staroswiecki, M., & Dauphin-Tanguy, G. (2006a). Diagnostic bond graphs for online fault detection and isolation. *Simulation Modelling Practice and Theory*, 14(3), 237-262.
- Samantaray, A. K., Medjaher, K., Ould Bouamama, B., Staroswiecki, M., & Dauphin-Tanguy, G. (2006b). Diagnostic bond graphs for online fault detection and isolation. *Simulation Modelling Practice and Theory*, 14(3), 237-262.
- Saxena, A., Celaya, J., Saha, B., Saha, S., & Goebel, K. (2010). Metrics for offline evaluation of prognostic performance. *International Journal of Prognostics and Health Management Volume 1 (color)*, 4.
- Shi, Z., Gu, F., Lennox, B., & Ball, A. (2005). The development of an adaptive threshold for model-based fault detection of a nonlinear electro-hydraulic system. *Control Engineering Practice*, 13(11), 1357-1367.
- Sié Kam, C., & Dauphin-Tanguy, G. (2005). Bond graph models of structured parameter uncertainties. *Journal of the Franklin Institute*, 342(4), 379-399.
- Sikorska, J., Hodkiewicz, M., & Ma, L. (2011). Prognostic modelling options for remaining useful life estimation by industry. *Mechanical systems and signal processing*, 25(5), 1803-1836.
- Smith, A. E., Coit, D. W., & Liang, Y.-C. (2003). A neural network approach to condition based maintenance: case study of airport ground transportation vehicles. *IMA Journal of Management Mathematics on Maintenance, Replacement and Reliability*.

- Sohn, H., Worden, K., & Farrar, C. R. (2002). Statistical damage classification under changing environmental and operational conditions. *Journal of Intelligent Material Systems and Structures*, 13(9), 561-574.
- Sorsa, T., & Koivo, H. N. (1993). Application of artificial neural networks in process fault diagnosis. *Automatica*, 29(4), 843-849.
- Sueur, C., & Dauphin-Tanguy, G. (1989). Structural controllability/observability of linear systems represented by bond graphs. *Journal of the Franklin Institute*, 326(6), 869-883.
- Sun, B., Zeng, S., Kang, R., & Pecht, M. G. (2012). Benefits and challenges of system prognostics. *Reliability, IEEE Transactions on*, 61(2), 323-335.
- Swanson, D. C., Spencer, J. M., & Arzoumanian, S. H. (2000). Prognostic modelling of crack growth in a tensioned steel band. *Mechanical Systems and Signal Processing*, 14(5), 789-803.
- Tagina, M., Cassar, J. P., Dauphin-Tanguy, G., & Staroswiecki, M. (1995). *Monitoring Of Systems Modelled By Bond Graph*. Paper presented at the ICBGM'95. International conference on bond graph modeling Las Vegas.
- Tarasov, E., Sueur, C., Bouamama, B. O., & Dauphin-Tanguy, G. (2014). *Flat control of a torsion bar with unknown input estimation*. Paper presented at the Control Applications (CCA), 2014 IEEE Conference on.
- Tartakovsky, A., Nikiforov, I., & Basseville, M. (2014). *Sequential analysis: Hypothesis testing and changepoint detection*: CRC Press.
- Thoma, J., & Bouamama, B. O. (2000). *Modelling and simulation in thermal and chemical engineering: A bond graph approach*: Springer.
- Tian, Z. (2012). An artificial neural network method for remaining useful life prediction of equipment subject to condition monitoring. *Journal of Intelligent Manufacturing*, 23(2), 227-237.
- Tobon-Mejia, D. A., Medjaher, K., Zerhouni, N., & Tripot, G. (2012). A data-driven failure prognostics method based on mixture of gaussians hidden markov models. *Reliability, IEEE Transactions on*, 61(2), 491-503.
- Touati, Y., Merzouki, R., & Ould Bouamama, B. (2012a). *Bond graph model based for fault estimation and isolation*. Paper presented at the Fault Detection, Supervision and Safety of Technical Processes.
- Touati, Y., Merzouki, R., & Ould Bouamama, B. (2012b). Robust diagnosis to measurement uncertainties using bond graph approach: Application to intelligent autonomous vehicle. *Mechatronics*, 22(8), 1148-1160.
- Triki, S., Mekki, T., & Kamoun, A. (2014). Modeling Switched Behavior with Hybrid Bond Graph: Application to a Tank System. *arXiv preprint arXiv:1402.2925*.
- Tsui, K. L., Chen, N., Zhou, Q., Hai, Y., & Wang, W. (2015). Prognostics and Health Management: A Review on Data Driven Approaches. *Mathematical Problems in Engineering*, 2015.
- Uckun, S., Goebel, K., & Lucas, P. J. (2008). *Standardizing research methods for prognostics*. Paper presented at the Prognostics and Health Management, 2008. PHM 2008. International Conference on.
- Vachtsevanos, G., Lewis, F., Roemer, M., Hess, A., & Wu, B. (2007). *Intelligent Fault Diagnosis and Prognosis for Engineering Systems*. New Jersey: John Wiley & Sons, Inc.

- Vachtsevanos, G., & Wang, P. (2001). *Fault prognosis using dynamic wavelet neural networks*. Paper presented at the AUTOTESTCON Proceedings, 2001. IEEE Systems Readiness Technology Conference.
- Venkatasubramanian, V., Rengaswamy, R., & Kavuri, S. N. (2003a). A review of process fault detection and diagnosis: Part II: Qualitative models and search strategies. *Computers & Chemical Engineering*, 27(3), 313-326.
- Venkatasubramanian, V., Rengaswamy, R., Kavuri, S. N., & Yin, K. (2003b). A review of process fault detection and diagnosis: Part III: Process history based methods. *Computers & Chemical Engineering*, 27(3), 327-346.
- Vijay, P., Samantaray, A., & Mukherjee, A. (2008). Bond graph model of a solid oxide fuel cell with a C-field for mixture of two gas species. *Proceedings of the Institution of Mechanical Engineers, Part I: Journal of Systems and Control Engineering*, 222(4), 247-259.
- Vijay, P., Samantaray, A., & Mukherjee, A. (2009). A bond graph model-based evaluation of a control scheme to improve the dynamic performance of a solid oxide fuel cell. *Mechatronics*, 19(4), 489-502.
- Wang, P., & Vachtsevanos, G. (2001). Fault prognostics using dynamic wavelet neural networks. *AI EDAM*, 15(04), 349-365.
- Wang, Y., Chen, K. S., Mishler, J., Cho, S. C., & Adroher, X. C. (2011). A review of polymer electrolyte membrane fuel cells: technology, applications, and needs on fundamental research. *Applied Energy*, 88(4), 981-1007.
- Widodo, A., & Yang, B.-S. (2011). Application of relevance vector machine and survival probability to machine degradation assessment. *Expert Systems with applications*, 38(3), 2592-2599.
- Wu, W., Hu, J., & Zhang, J. (2007). *Prognostics of machine health condition using an improved arima-based prediction method*. Paper presented at the Industrial Electronics and Applications, 2007. ICIEA 2007. 2nd IEEE Conference on.
- Yoon, S., & MacGregor, J. F. (2001). Fault diagnosis with multivariate statistical models part I: using steady state fault signatures. *Journal of Process Control*, 11(4), 387-400.
- Yu, M., Wang, D., Luo, M., & Huang, L. (2011). Prognosis of hybrid systems with multiple incipient faults: augmented global analytical redundancy relations approach. *Systems, Man and Cybernetics, Part A: Systems and Humans, IEEE Transactions on*, 41(3), 540-551.
- Zhang, H., Kang, R., & Pecht, M. (2009). *A hybrid prognostics and health management approach for condition-based maintenance*. Paper presented at the Industrial Engineering and Engineering Management, 2009. IEEM 2009. IEEE International Conference on.
- Zio, E. (2012). Prognostics and health management of industrial equipment. *Diagnostics and Prognostics of Engineering Systems: Methods and Techniques*, 333-356.
- Zio, E., & Di Maio, F. (2012). Fatigue crack growth estimation by relevance vector machine. *Expert Systems with applications*, 39(12), 10681-10692.
- Zio, E., & Peloni, G. (2011). Particle filtering prognostic estimation of the remaining useful life of nonlinear components. *Reliability Engineering & System Safety*, 96(3), 403-409.

Diagnostic et Pronostic de Systèmes Dynamiques Incertains dans un contexte Bond Graph

Résumé Cette thèse développe des approches pour le diagnostic et le pronostic de systèmes dynamiques incertains en utilisant la technique de modélisation Bond Graph (BG).

Tout d'abord, une représentation par intervalles des incertitudes paramétriques et de mesures est intégrée à un modèle BG-LFT (Linear Fractional Transformation). Une méthode de détection robuste de défaut est développée en utilisant les règles de l'arithmétique d'intervalle pour la génération de seuils robustes et adaptatifs sur les résidus nominaux. La méthode est validée en temps réel sur un système de générateur de vapeur. Deuxièmement, une nouvelle méthodologie de pronostic hybride est développée en utilisant les Relations de Redondance Analytique déduites d'un modèle BG et les Filtres Particulaires. Une estimation de l'état courant du paramètre candidat pour le pronostic est obtenue en termes probabilistes. La prédiction de la durée de vie résiduelle est atteinte en termes probabilistes. Les incertitudes associées aux mesures bruitées, les conditions environnementales, etc. sont gérées efficacement. La méthode est validée en temps réel sur un système mécatronique incertain. Enfin, la méthodologie de pronostic développée est mise en œuvre et validée pour le suivi efficace de la santé d'un sous-système électrochimique d'une pile à combustible à membrane échangeuse de protons (PEMFC) industrielle à l'aide de données de dégradation réelles.

Mots-clefs : Diagnostic, Pronostic, Systèmes Incertain, Durée de vie résiduelle, Bond Graph, Relations de Redondance Analytique, Filtres Particulaires, Pile à combustible à membrane échangeuse de protons.

Diagnostics and Prognostics of Uncertain Dynamical Systems in a Bond Graph Framework

Abstract: This thesis develops the approaches for diagnostics and prognostics of uncertain dynamic systems in Bond Graph (BG) modeling framework. Firstly, properties of Interval Arithmetic (IA) and BG in Linear Fractional Transformation, are integrated for representation of parametric and measurement uncertainties on an uncertain BG model. Robust fault detection methodology is developed by utilizing the rules of IA for the generation of adaptive interval valued thresholds over the nominal residuals. The method is validated in real time on an uncertain and highly complex steam generator system. Secondly, a novel hybrid prognostic methodology is developed using BG derived Analytical Redundancy Relationships and Particle Filtering algorithms. Estimations of the current state of health of a system parameter and the associated hidden parameters are achieved in probabilistic terms. Prediction of the Remaining Useful Life (RUL) of the system parameter is also achieved in probabilistic terms. The associated uncertainties arising out of noisy measurements, environmental conditions etc. are effectively managed to produce a reliable prediction of RUL with suitable confidence bounds. The method is validated in real time on an uncertain mechatronic system. Thirdly, the prognostic methodology is validated and implemented on the electrical electro-chemical subsystem of an industrial Proton Exchange Membrane Fuel Cell. A BG of the latter is utilized which is suited for diagnostics and prognostics. The hybrid prognostic methodology is validated, involving real degradation data sets.

Keywords: Diagnostics, Prognostics, Remaining useful life, Bond graphs, Analytical Redundancy Relations, Particle Filters, Proton Exchange Membrane Fuel Cell, Interval Arithmetic